

**Labeling Stem Cells and Macrophages
with Gold and Iron Oxide Nanoparticles for Tracking Applications**

**Dissertation
zur Erlangung des Doktorgrades
an der Fakultät für Mathematik, Informatik und Naturwissenschaften
Fachbereich Physik
der Universität Hamburg**

vorgelegt von

Xing Sun

Hamburg

2019

Gutachter/innen der Dissertation:

Prof. Dr. Wolfgang Parak

Zusammensetzung der Prüfungskommission:

Prof. Dr. Wolfgang Hansen

Prof. Dr. Florian Grüner

Prof. Dr. Viacheslav Nikolaev

Prof. Dr. Gabriel Bester

Vorsitzende/r der Prüfungskommission:

Prof. Dr. Wolfgang Parak

Datum der Disputation:

08.08.2019

Vorsitzender Fach-Promotionsausschusses PHYSIK:

Prof. Dr. Michael Potthoff

Leiter des Fachbereichs PHYSIK:

Prof. Dr. Wolfgang Hansen

Dekan der Fakultät MIN:

Prof. Dr. Heinrich Graener

Table of contents

List of abbreviations	2
Zusammenfassung.....	3
Abstract	5
1. Introduction	7
2. Nanomaterials	9
2.1 Synthesis and development of AuNPs.....	9
2.2 Synthesis and development of IONPs	11
3. Surface modification of NPs	15
4. Biocompatibility of NPs	17
5. Factors affecting the labeling of cells with NP	21
5.1 Influencing factors of NPs for cell labeling.....	21
5.2 Influencing factors from cells	25
5.2.1 Cell properties	25
5.2.2 Pathways for NP uptake.....	29
6. Methods for cell tracking	31
6.1 CT.....	31
6.2 MRI	33
Conclusions.....	36
Perspectives	38
Reference	39
List of publications.....	47
Bibliography.....	49
Acknowledgements.....	50
Declaration on oath.....	51

List of abbreviations

Au	Gold
Fe	Iron
CHCl ₃	Chloroform
HAuCl ₄	Hydrogen tetrachloroaurate (III) hydrate
NP(s)	Nanoparticle(s)
NR(s)	Nanorod(s)
PEG	Polyethylene glycol
AuNPs	Gold nanoparticles
IONPs	Iron oxide nanoparticles
PMA	Poly (isobutylene–alt–maleic anhydride)–graft–dodecylamine
THF	Tetrahydrofuran
DDA	Dodecylamine
Gd	Gadolinium
SCs	Stem cells
MSCs	Mesenchymal stem cells
HCA	Hierarchical cluster analysis
LSM	Laser scanning microscopy
PET	Positron emission tomography
SPECT	Single photon emission tomography
CT	Computed tomography
MRI	Magnetic resonance imaging
ICP-MS	Inductively coupled plasma mass spectrometry
MTT	3-(4,5-Dimethylthiazol-2-yl)-2,5-diphenyltetrazolium bromide
PI	Propidium Iodide
EdU	5-ethynyl-2'-deoxyuridine
LDH	Lactate dehydrogenase

Zusammenfassung

Diese kumulative Dissertation zielt darauf ab, die optimalen Markierungsbedingungen für mesenchymale Stammzellen (humane Stammzellen, Hundestammzellen und Pferdestammzellen) sowie für alveolare Mausmakrophagen mit einer Bibliothek aus Gold- und Eisenoxid-Nanopartikeln zu bestimmen. Diese Zellen verfügen über die intrinsische Tumor-Homing-Fähigkeit, wodurch sie gute Voraussetzungen für den Einsatz in der Krebsdiagnose und -therapie bieten. Deshalb wurden in dieser Doktorarbeit die Bedingungen zur Markierung mit verschiedenen großen und unterschiedlich geformten Gold- (AuNPs) und Eisenoxidnanopartikeln (IONPs) detailliert diskutiert. Darüber hinaus wurde der Einfluss der Zellmerkmale Zelltyp, Zelloberfläche, Wachstumsrate und der entsprechende Exozytose-Effekt gründlich untersucht. Um ihr Potenzial für die In-vivo-Verfolgung zu untersuchen, wurden die markierten Zellen mittels Computertomographie (CT) und Magnetresonanztomographie (MRI) nachgewiesen, welche gute Kontraste in In-vitro-Studien zeigten. Um diese Ziele zu erreichen, wurden in dieser Studie mehrere Verfahren angewendet:

Zunächst wurden verschiedene Arten von AuNPs und IONPs synthetisiert, nämlich 5 nm AuNPs, 25 nm AuNPs, 50 nm AuNPs, 100 nm AuNPs, 40 nm AuNRs, 100 nm AuNRs, 4 nm IONPs bzw. 8 nm IONPs,. Dann wurden verwandte Oberflächenmodifikationen wie PEGylation und PMA-Polymerbeschichtung durchgeführt, um die kolloidale Stabilität und Biokompatibilität für die anschließenden Anwendungen zu verbessern. Auf diese Weise wurden alle NP mit derselben Oberflächenchemie modifiziert.

Als zweites wurde der Einfluss der oben genannten Nanopartikel auf die Zellviabilität der verschiedenen MSCs (humane Stammzellen (humane MSCs), Hundestammzellen (dog MSCs), Pferde-Stammzellen (horse MSCs) und murine Alveolarmakrophagen (MHS)) anhand eines Resazurin-basierten Zelllebensfähigkeitstests und einem EdU-basierten Zellproliferationsassay untersucht. Darauf basierend wurden die kompatiblen Dosen für die Zellmarkierung bestimmt.

Drittens wurden Zellaufnahmestudien an verschiedenen Zelltypen mit allen oben erwähnten Nanopartikeln durchgeführt, um zu bestätigen, welche NPs unter welchen Bedingungen am stärksten innerhalb der Zellen akkumulierten oder die optimalen Markierungsbedingungen aufweisen. Darüber hinaus wurden Einflussfaktoren wie Zelltyp, Zelloberfläche, Wachstumsrate, Sedimentationseffekte der Nanopartikel, Zellviabilität und auch die Exozytose gemeinsam mit den Daten der Aufnahmestudien diskutiert. Infolgedessen wurden die dominierenden Kennzeichnungsfaktoren vollständig bestimmt.

Schließlich wurden die Zellen, die später für die CT- und MRI-Bildgebung verwendet wurden, unter optimalen Bedingungen mit AuNPs und IONPs markiert. Gleichzeitig wurden die

Vorhersagewerte basierend auf der NPs-Standardkurve und den Aufnahmewerten der Zellen erstellt. Diese beiden Ergebnisse zeigten gute Übereinstimmungen, wodurch die Möglichkeit für den Einsatz von AuNPs und IONPs in Zellmarkierungsanwendungen erhöht wird.

Wie diese Studie zeigt, die Größe oder das Molekulargewicht der Nanopartikel als auch der Zelltyp spielen eine dominierende Rolle bei der Aufnahme in Zellen. Genauer gesagt, akkumulieren größere NPs (d. H. 100 nm AuNPs) in den Zellen mehr als kleinere NPs (d. H. 5 nm AuNPs) unter den gleichen experimentellen Bedingungen. Gleichzeitig neigen Zellen mit großer Zelloberfläche, langsamerem Zellwachstum und Exozytoserate zu einer höheren Anhäufung von NPs. Schließlich lassen sich sowohl mit AuNPs als auch mit IONPs markierte Stammzellen und Makrophagen mittels CT und MRI gut nachweisen, was einen Beweis dafür liefert, dass sie als vielversprechende Vektoren in biologische Anwendungen dienen können.

Abstract

This cumulative dissertation aims to establish the optimal labeling condition for mesenchymal stem cells (human stem cells, dog stem cells, and horse stem cells), as well as murine alveolar macrophages with a library of gold and iron oxide nanoparticles (AuNPs and IONPs). These cells were reported with intrinsic tumor-homing ability, which offers them a good opportunity in cancer diagnosis and therapy. Therefore, in this Ph.D. study their labeling condition with different sized and shaped AuNPs and IONPs were discussed in detail. Furthermore, the influence of the cell characteristics such as cell types, cell surface area, cell growth rates, and corresponding exocytosis effects was investigated thoroughly. Meanwhile, to explore the potential of NPs for in vivo tracking, the labeled cells were detected by means of computed tomography (CT) and magnetic resonance imaging (MRI), which showed good contrasts in in vitro trials. To achieve these goals, several procedures were performed in this study:

Firstly, several different types of AuNPs and IONPs, namely 5 nm AuNPs, 25 nm AuNPs, 50 nm AuNPs, 100 nm AuNPs, 40 nm AuNRs, 100 nm AuNRs, 4 nm IONPs, and 8 nm IONPs, were synthesized respectively. Then, the surface modifications such as PEGylation and PMA polymer coating were conducted to improve their colloidal stability and biocompatibility for the following applications. In this way, all of NPs were modified with the same surface chemistry.

Secondly, the influence of the above-mentioned NPs on the cell viability of human stem cells (human MSCs), dog stem cells (dog MSCs), horse stem cells (horse MSCs), and murine alveolar macrophages (MHS) were evaluated by resazurin-based cell viability assay and EdU-based cell proliferation assay. Based on this, the compatible doses for cell labeling were obtained.

Thirdly, in order to evaluate the optimal conditions to label the cells with NPs, cellular uptake studies were performed in different cells types, different NPs at different exposure conditions. Furthermore, the influence factors, such as cell type, cell surface area, cell growth rate, NP sedimentation effects, cell viability and also exocytosis, were discussed together with the uptake data. As a result, the dominating labeling factors were fully discussed.

Finally, the cells were then labeled with AuNPs and IONPs at the optimal conditions, which were later used for CT and MRI imaging. At the same time, the predicted imaging values were made based on the NPs standard curve and the cellular uptake values. These two sets of results exhibit good agreements with each other, which suggest the possible use of AuNPs and IONPs for cell labeling applications both in vitro and in vivo.

Herein, this study shows that the size of the NPs and the type of cells have an important role on the cellular uptake. Indeed, at the same experimental conditions (same Au concentration), bigger

and dense NPs (i.e.100 nm AuNPs),which contain more gold elements in one NP, are enable to accumulate into the cells with higher amount of elements than the smaller NPs (i.e. 5 nm AuNPs). Meanwhile, cells with big cell surface area, slower cell growth and exocytosis rate tend to retain or accumulate more gold. Finally, both AuNPs and IONPs labeled stem cells and macrophages can be detected well by means of CT and MRI, which offers good evidence that they could act as promising materials for cell tracking applications.

1. Introduction

Cell-based therapies, which employ living cells as delivery systems or medicines, offer an attractive alternative to the traditional therapeutics.^[1] At present, stem cells and macrophages, because of their great potentials for dealing with numerous diseases and disorders, are two main types of cells chosen as potential therapeutic cell agents.^[2, 3]

With regard to stem cells, which are endowed with the intrinsic ability to home to the injury and/or inflammation sites enabling site-specific delivery and secrete therapeutic factors^[4], have shown great potential for applications in the fields of regenerative medicine, cardiology, neurology, oncology and muscular regeneration (Figure 1). Owing to this ability, stem cells can also be used as a vehicle to transport NPs. In this case, stem cells can firstly be loaded with NPs and then administered in vivo, where they can migrate towards malignancies and deposit the loaded NPs close to the tumor.^[5] Combining NP based therapeutics with stem cell delivery is a nascent partnership that warrants further investigation for the treatment of cancer. Furthermore, stem cells can also be modified to stably express and release various anticancer agents, thereby circumventing the short half-lives that many chemotherapeutic agents exhibit.^[6]

Alternatively, macrophages are one of the most essential members of the immune system, which play an important role in host defense, such as removing the dead cells, debris and pathogens by phagocytosis, shaping the inflammatory response by secreting cytokines, enzymes and other factors and modulating adaptive immunity by presenting antigens to lymphocytes.^[7, 8] During inflammation, macrophages are recruited to the wound sites, where they display impressive plasticity in that they can express a polarization of classic and alternative activation phenotypes. Notably, macrophages are also present in the microenvironment of solid tumors, which is known as tumor-associated macrophages (TAMs). Most evidence suggests that TAMs have a tumor-promoting phenotype. TAMs affect most aspects of tumor cell biology and drive pathological phenomena including tumor cell proliferation, tumor angiogenesis, invasion and metastasis, immunosuppression, and drug resistance.^[9, 10] Hence, macrophages have become recognized as an attractive target in cancer therapy.

As promising as it may seem, introducing cell-based therapy from bench to bedside still reminds a challenge.^[11] The major obstacle in clinical translation is the inconsistency of outcomes seen in preclinical and clinical studies. While some patients exhibit some major improvements, some others exhibit minimal or no improvements.^[12] These inconsistencies are remaining puzzles, which are needed to be solved urgently. As a consequence, it is required to collect sufficient data on the fate of the injected cells. Currently, however, the most used methods for assessing the success or failure of treatment is by evaluating symptom improvements, which can only be done

weeks after treatment. In this way, the best time for treatment may be delayed, and in turn the medical costs will be increased. Therefore, to realize faster and more accurate diagnosis and treatment, the fate of the injected cells had better be assessed in real time. This requires a reliable, noninvasive cell imaging and tracking technique, which can provide the information of the labeled cells in real time after injection.^[13] With the advent and fast development of nanotechnology, biocompatibility NPs may serve as promising contrast agents for the cell based therapy.

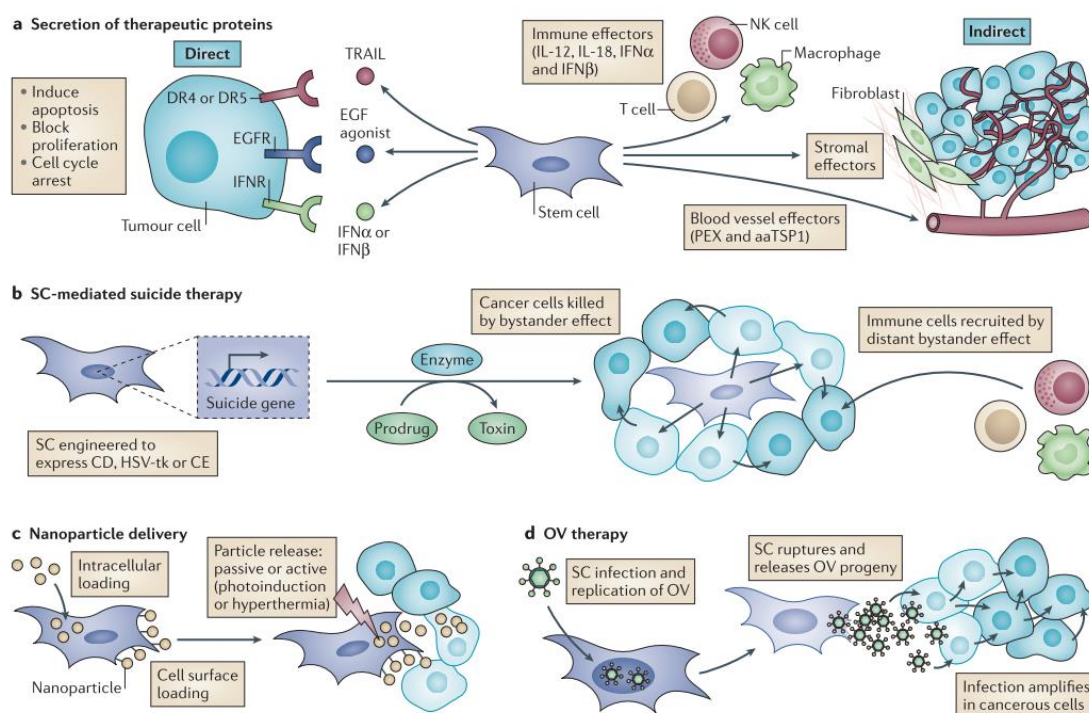


Figure 1. Using SCs to promote tumor cell death. SCs can be modified in various ways to generate antitumor capabilities. Ref 3 copyright 2014 Nature Publishing Group.

At present, much attention has been paid to the stem cells and macrophage labeling with various kinds of materials.^[14, 15] In clinics, the most widely used reagents are compounds with small molecular weight, such as Iohexol for CT and gadolinium for MRI. However, these reagents show low labeling efficiency, and the low sensitivity of detection approaches remain problems waiting ahead. NPs have been proved good candidates for cell labeling and many groups have reported their trails in stem cell and macrophage labeling with bismuth ferrite harmonic NPs (BFO HNPs)^[14], AuNPs^[16], superparamagnetic iron oxide NPs (SPIONs)^[15] and further imaging by means of near infred (NIR) multiphoton microscopy, CT, and MRI. However, much more efforts still needed to improve the labeling condition for further tracking applications.

2. Nanomaterials

Materials are the bases in the building of the world. When it comes to the nano sizes, the resulting physical-chemical properties of these materials are neither those of bulk nor those of molecular compounds, but strongly depend on the particle size, nature of the particle shell, and shape etc. In the past decades, a huge burst of nanomaterials, such as noble metal NPs, semiconductor quantum dots, carbon-based nanomaterials, rare earth NPs etc. have come into the horizons of material researchers.

NPs, because of their ultra-small sizes, they are endowed with various excellent physicochemical properties, such as fluorescence^[17, 18], electronics^[19, 20], catalysis^[21, 22], photothermal properties^[23], and magnetic properties^[24], which make NPs attractive for a wide range of applications, including medicine^[25-28]. Indeed, AuNPs and IONPs are promising materials to be used for the in vivo diagnosis and therapy in the future. Therefore, these NPs for cell labeling need to be discussed detailed in this section.

2.1 Synthesis and development of AuNPs

The preparation and application of AuNPs is not a new concept, which can date back to the Roman Empire and early Chinese dynasties.^[29] The most well-known example is the Lycurgus Cup made in the 4th century, even when the knowledge of the nanotechnology was still not clear.

However, the vast development of the AuNPs originated from the facile synthesis method modified by Brust, which was the well-known Brust-Schiffrin method^[30]. This work was published in 1994, has had a considerable impact on the overall field in less than a decade, because it allowed the facile synthesis of thermally stable and air-stable AuNPs of reduced dispersity and controlled size for the first time (ranging in diameter between 1.5 and 5.2 nm). However, the NPs obtained from this method always showed wide distribution, sometimes cannot meet the demand for applications. Further modified methods like Ostwald rippling and digestive rippling^[31] were developed to optimized the synthesis pathways. In this way, monodisperse NPs can form superlattice structures^[32], provide ideal systems to study the effects of sizes without being affected by the complexity of particle size distribution^[31].

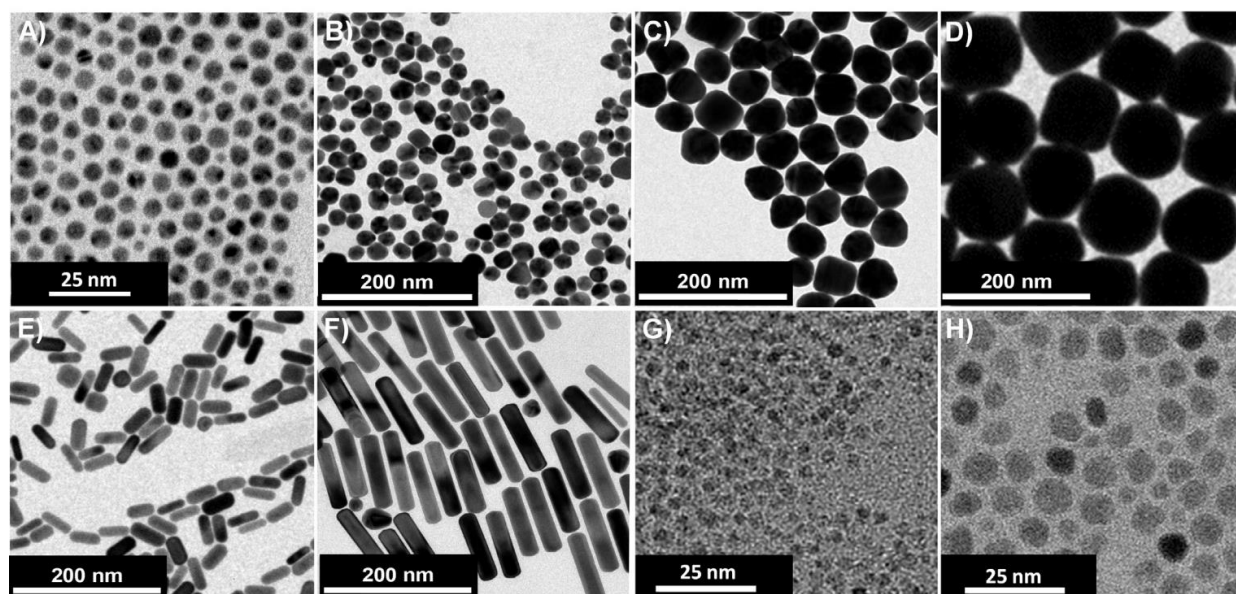


Figure 2. (A) Transmission electron microscopy (TEM) images of the NP library used in the study: (A) 5 nm AuNPs, (B) 25 nm AuNPs, (C) 50 nm AuNPs, (D) 100 nm AuNPs, (E) 40 nm AuNRs, (F) 100 nm AuNRs, (G) 4 nm IONPs, and (H) 8 nm IONPs. Ref 33 copyright 2019 Elsevier.

In the case of the bigger sized spherical AuNPs, because of their excellent practical properties, such as higher electronic contrast^[34], intense visible absorption^[35], increased the number density of molecules being delivered in biological systems, and related distribution and toxicity effects of different sized NPs^[36-38], their corresponding synthesis method, as a result, were later on developed and optimized^[39-41]. This method was a technical development of Turkevich/Frens method.^[42-44] In this routine, generally a nucleation and growth mechanism occurred in this process. Precisely, by relying on the kinetic control of NPs growth process by careful controlling the reaction conditions, in detail, temperature, pH level, and seed concentration, the secondary nucleation was dramatically inhibited during the homogeneous growth process, leading to the enlargement of pre-synthesized AuNPs via the surface-catalyzed reduction of Au³⁺ by sodium citrate. Consequently, it produced particles of high monodispersity, allowed smaller particles to be grown into larger particles, and led to higher AuNP concentrations relative to the Frens method (from 3×10^{12} NPs/mL, 8.5 nm to 5×10^9 NPs/mL, 180.5 nm)^[39].

AuNPs, in the past decades, have experienced extensive advancements.^[29] As a consequence, not only spherical shaped NPs were obtained, various shapes, such as rod^[45, 46]-, prism^[47]-, star^[48]-, bipyramid^[49]- and flower^[50]- like NPs have been successfully synthesized with excellent quality as well, which makes the family of gold diverse (Figure 2). Particularly, among all of the possible shapes, gold nanorods (AuNRs) are of the greatest interest as they offer strong plasmonic fields while exhibiting excellent tunability and biocompatibility.^[51]

AuNRs, as one member of anisotropic metal NPs, also provide access to shape dependent optical phenomena, which are not seen in spherical NPs.^[52, 53] One of these most striking features in the UV–vis–NIR absorption spectrum of AuNRs is the emergence of multiple plasmon bands (one band for the transverse plasmon and the other for the longitudinal plasmon). Unlike spherical AuNPs whose plasmon absorbances have similar energies across 4–200 nm AuNP diameters, the energy of the AuNR longitudinal plasmon is strongly influenced by the aspect ratio of the AuNRs. These shape-dependent properties have frequently been taken advantage of over the past decade to enable sensing applications, plasmon-enhanced spectroscopies, biomedical imaging, and photothermal therapy for cancer.^[18] Maximizing AuNR performance in these applications requires access to AuNRs that have precisely designed physiochemical properties.

The fabrication of colloidal AuNRs, however, unlike spherical AuNPs, emerged only during the past decade^[54]. Even though faced with a late birth, nanorods with high yield, quality and uniformity have achieved great advancement under the efforts of material researchers^[45, 46, 55]. Up till now, there are three most popular AuNR seeded growth syntheses: (i) the three-step seeded growth synthesis, (ii) the one-step silver-assisted seeded growth synthesis, and (iii) the silver-assisted “seedless” approach to AuNR synthesis. In addition, AuNRs of small sizes, compared to the larger ones, have larger absorption cross sections and higher photothermal efficiency. Therefore, the demand for small nanorods is becoming urgent. Chang et. al. have reported the methods for small nanorods^[56].

Even though the universal utility of the AuNRs, many key features of AuNR growth mechanisms thus far remain poorly understood, still tremendous challenges exist in the synthesis. Despite these difficulties, mechanistic investigations have led to significant advances in synthesis of AuNRs over the past several years, including the development of more reproducible syntheses, access to an extended range of aspect ratios, the ability to tune AuNR dimensions independently of aspect ratio, and the development of gram-scale syntheses for AuNRs. Given recent instrumental advances, such as the application of SAXS and liquid-cell TEM, in the study of metal NP growth mechanisms, we expect that significant advances in our mechanistic understanding of AuNR growth will occur with increasing regularity, and this will be quickly followed by further synthetic improvements.

2.2 Synthesis and development of IONPs

IONPs have emerged as promising tools with increasing applications in detection^[57], drug delivery^[58], hyperthermia therapy^[59], and tissue repair^[60]. Their development has been intensively pursued, not only for their fundamental scientific interests, but also for many

technological applications. As a result, huge efforts have been made in fabricating stable colloidal iron oxide solutions with superior magnetic properties, good dispersibility, and biocompatibility.

For IONPs, they have a size-dependent magnetization as shown in Figure 3. When the particle size is smaller than ~ 20 nm, the magnetization of IONPs is randomized by thermal energy so that they become superparamagnetic. These IONPs have been intensively investigated as T2 MRI contrast enhancement agents. And when the particle size of IONPs decreases to smaller than 3 nm, most of their magnetic spins are canted and consequently they exhibit nearly paramagnetic behavior.^[61]

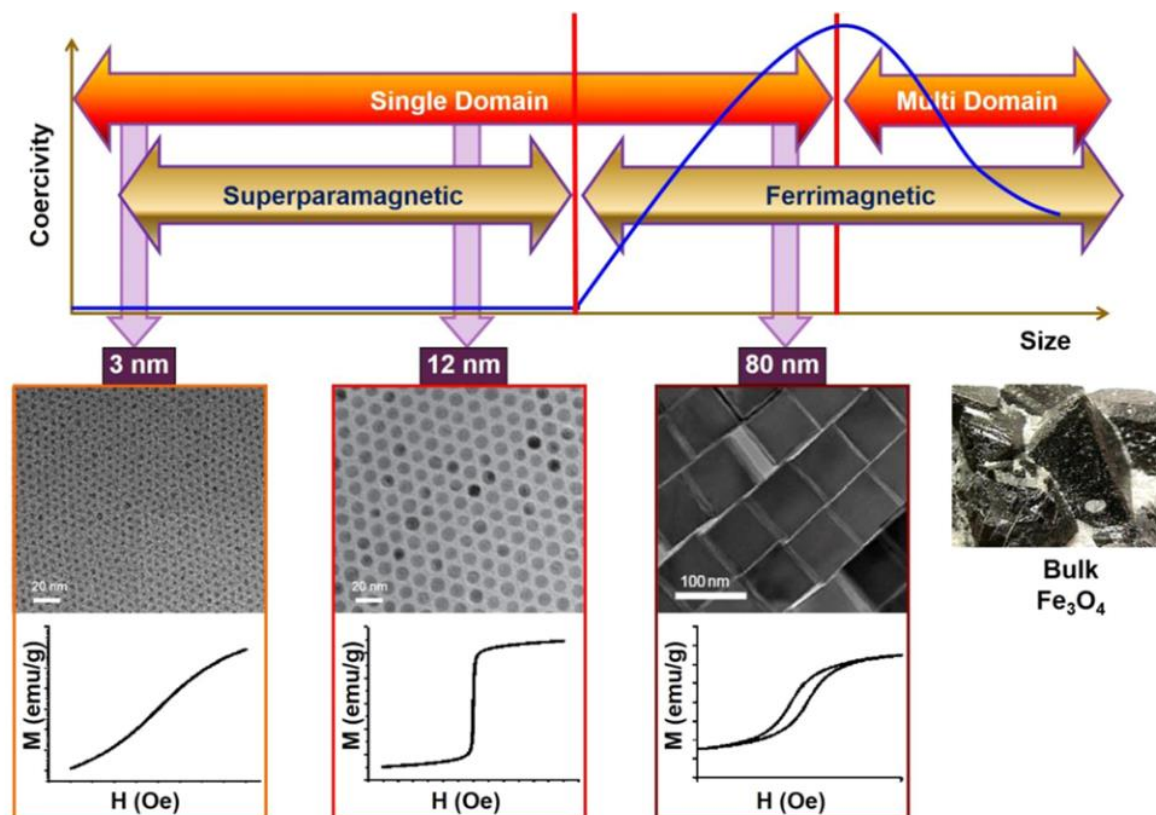


Figure 3. Size-dependent magnetic properties of IONPs. Inset TEM images and magnetization curves of magnetic NPs were reproduced with permission from refs 61 and 62. Copyright 2011 and 2008 American Chemical Society. And ref 66. Copyright 2004 Nature Publishing Group.

In addition, iron is one of the most abundant metallic elements in living organisms and is also essential for various biological processes, including oxygen transport by hemoglobin and cellular respiration by redox enzymes. IONPs, therefore, are known to be biologically well tolerated and benign. The toxicity, metabolism, and pharmacokinetics of intravenously injected IONPs have been well studied.^[62] In a rodent model, no adverse effect was observed up to 100 mg Fe per kg, and even an injection of 600 mg Fe per kg was not fatal.^[63] Injected IONPs are cleared by macrophages in the reticuloendothelial system (RES) and subsequently degraded in the

lysosomes. The degraded iron ions are incorporated into ferritin and/or hemosiderin as an iron pool and finally employed in biological functions such as red blood cell production.

Apart from their superior biocompatibility, IONPs exhibit greater sensitivity in the micromolar or nanomolar range than gadolinium complexes, so they can be used as T2 MRI contrast agents.^[64] Thus far, several IONPs have even been approved for clinical use. For example, Feridex is approved by FDA for the detection of liver lesions, and Combidex entered into phase III clinical trials for imaging of lymph node metastases. Thus, current development of IONPs is expected to yield advanced MRI contrast agents having high relaxivity and improved surface coating for targeted imaging and prolonged circulation. Such tailored IONPs can provide opportunity for ultrasensitive imaging of specific cells and biological molecules as well as accurate diagnosis based on detailed anatomic information.

The past 10 years have witnessed enormous advances in the synthesis of various IONPs via thermal decomposition processes.^[65] It is now possible to synthesize uniformly sized IONPs ranging in size from a few nanometers to tens of nanometers.^[66] These NPs have better crystallinity and magnetic properties than the NPs obtained by conventional co-precipitation methods. The tailored synthesis and modification of NPs enable fine control of the MRI contrast effect (Table 1).

Name	Magnetic core material	Surface	Core diameter/nm	Hydrodynamic diameter/nm	Magnetization/ emu g ⁻¹	Relaxivity/mM ⁻¹ s ⁻¹			Ref.
						r ₁ ^a	r ₂ ^a	B ₀ ^a /T	
Ferumoxide (Feridex)	Fe ₃ O ₄ , γ-Fe ₂ O ₃	Dextran	4.96	160	45	10.1	120	1.5	10
MION	Fe ₃ O ₄	Dextran	4.6	20	68	16.5	34.8	0.47	11
WSIO	Fe ₃ O ₄	DMSA ^b	12		120		218	1.5	21
FION	Fe ₃ O ₄	DSPE-mPEG 2000 ^b	58		132.1 ^a		324	1.5	22
ESION	γ-Fe ₂ O ₃	PEG	3	15		4.77	29.2	3	24
MnMEIO	MnFe ₂ O ₄	DMSA ^b	12		110		358	1.5	26
CoMEIO	CoFe ₂ O ₄	DMSA ^b	12		99		172	1.5	26
NiMEIO	NiFe ₂ O ₄	DMSA ^b	12		85		152	1.5	26
Zn-doped ferrite	Zn _{0.4} Mn _{0.6} Fe ₂ O ₄	DMSA ^b			175		860	4.5	27
Cannonball	Fe/Fe ₃ O ₄ core/shell	DMSA ^b	16		139		312	1.5	29
Fe@MFe ₂ O ₄	Fe/MnFe ₂ O ₄ core/shell	DMSA ^b	16		149	11	356	0.47	30
MNP									
Fe/Fe ₃ O ₄ NP	bcc Fe/Fe ₃ O ₄ core/shell	PEG	15	40–45	164		220	3	31
Iron/iron oxide core/shell NP	α-Fe/FeO ₄ core/shell	DMSA ^b	16		140		324	9.4	32
DySiO ₂ -(Fe ₃ O ₄) _n	9 nm Fe ₃ O ₄	DMSA ^b	45 ^c				397	9.4	43
Fe ₃ O ₄ -MSN	8.5 nm Fe ₃ O ₄	PEG		93			76.2	1.5	44
SPIO-14	Fe ₃ O ₄	DSPE-mPEG 1000 ^b	13.8	28.6			385	0.47	46
SPIO-5	Fe ₃ O ₄	DSPE-mPEG 1000 ^b	4.8	14.8			130	0.47	46

^a r₁: longitudinal relaxivity; r₂: transverse relaxivity; B₀: magnetic field strength. ^b DMSA: 2,3-dimercaptosuccinic acid; DSPE-mPEG; 1,2-distearoyl-*sn*-glycero-3-phosphoethanolamine-*N*-[methoxy(polyethylene glycol)-2000]. ^c Multiple iron oxide nanoparticles are assembled on the surface of silica nanoparticles.

Table 1. Properties of iron based MRI contrast agents. Ref 66 copyright 2004 Nature Publishing Group.

Although numerous chemical methods have been developed for the synthesis of IONPs^[67, 68], the “heat-up” method, which was pioneered by the Hyeon group for the scalable synthesis of IONPs,

shows excellent quality.^[66] This method, which was chosen for this thesis, involves slow heating of a reaction mixture of precursors, surfactants, and high boiling solvent from room temperature to a high temperature. In addition to its simplicity, this method can also produce highly monodisperse IONPs without a separate size sorting process. This improvement is attributed to an intermediate step between the decomposition of the in situ generated iron-oleate complex and the formation of the final NPs.^[69] Consequently, these iron-oxo cluster intermediate species, rather than the iron-oleate complex itself, seem to act as monomers for the generation of iron oxide nanocrystals. The overall formation mechanism of the heat-up process consists of the following steps: the generation and accumulation of monomers, burst nucleation, and the diffusion controlled growth process, which are in accordance with the LaMer model for monodisperse microspheres.^[70] Since thermally stable intermediate species play an important role in the formation of uniform-sized NPs, it allows a wide range of precursors, including cheap and environmentally benign metal salts, to be used. This eventually led to the large scale synthesis of uniform iron oxide nanocrystals via an improved heat-up method using iron-oleate complex precursor, which was easily obtained from a simple reaction between iron chloride and sodium oleate.^[66]

IONPs obtained by the heat-up method show remarkable size uniformity. Moreover, the particle diameter can be readily controlled by using solvents with different boiling points. Iron-oleate complex could be synthesized by other routes including the reaction of either FeO(OH) with oleic acid^[71] or ferric and ferrous chlorides with oleic acid.^[72] More precise size control of the NPs in one nanometer scale was also achieved by the seed-mediated growth process using as-synthesized monodisperse iron NPs as seeds.^[73] More recently, matrix-assisted laser desorption/ionization time-of flight (MALDI-TOF) mass spectrometry (MS) was employed to characterize the size distribution of these ultrasmall-sized IONPs with very high accuracy and time efficiency compared to the conventional characterization methods such as transmission electron microscopy (TEM).^[74]

3. Surface modification of NPs

Because of the small sizes of nanomaterials, their surface energy are relatively high. As a result, small NPs have high tendency of agglomeration, aggregation and adsorption of molecules in the exposure system forming the so-called protein corona.^[75] In addition, the synthesis of NP in organic solvent is also a good way to obtain high quality of NPs. However, this kind of NPs is always hydrophobic, which make them unable to be applied into biological systems.

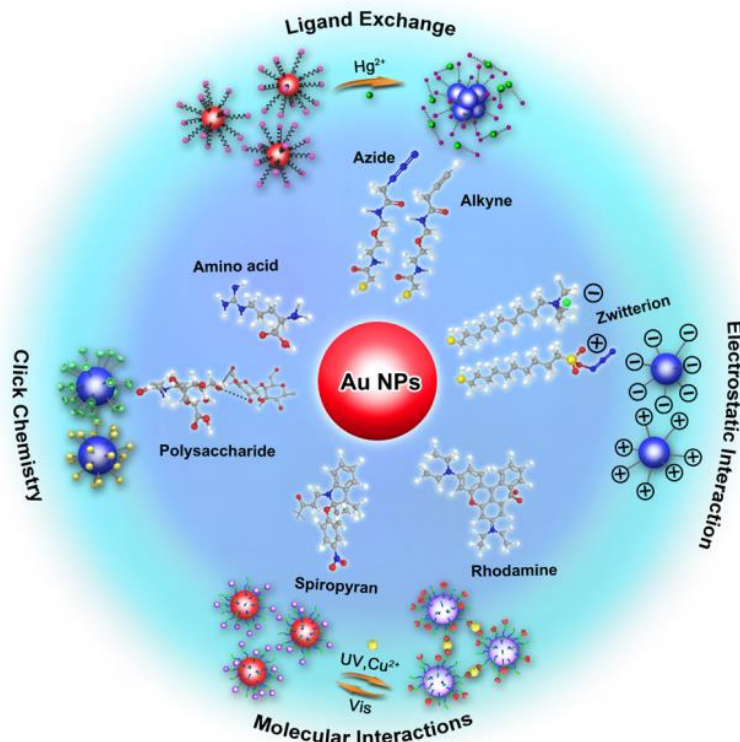


Figure 4. Strategies of surface chemistry for functionalization of AuNPs with small molecules and their application in biochemical analysis. Ref 76 copyright 2017 American Chemical Society.

To avoid these problems above, therefore, in the process of NP synthesis, some coupling ligands are well designed to passivate their surface to avoid NP aggregation and formation of protein corona. With regard to the hydrophobic NPs, by way of surface modification NPs can be transferred from organic phase into water phase broadening their application fields. Furthermore, apart from the improvement of the NPs' stability and water solubility, these approaches in turn also provides some possibilities for their surface modification or functionalization to achieve the practical purposes.^[76] For instance, the modified NPs can have better stability and bio-compatibility, faster signal transduction, higher signal intensity, and more convenient signal readout, which are as a result endowed with enhanced detection efficiency and broadened possible applications.^[77] Surface chemistry is an easy and useful strategy to introduce

the functional groups or molecules to the NPs via bioconjugation, electrostatic forces or ligand exchange, etc (Figure 4).^[78]

Among all of the surface modification strategies, utilizing amphiphilic polymers as coating agents so far have been proved one of the good choices.^[79-82] In general, the amphiphilic polymers consist of hydrophobic side chains for the linkage to the surface of NPs and a hydrophilic backbone that provides water solubility through charged groups and also acts as an anchor for the conjugation of biological molecules. This class of amphiphilic polymer coatings not only enables the phase transfer of the NPs from organic solvents to aqueous solution, but also serves as a versatile platform for chemical modification and bioconjugation of the particles.^[83, 84]

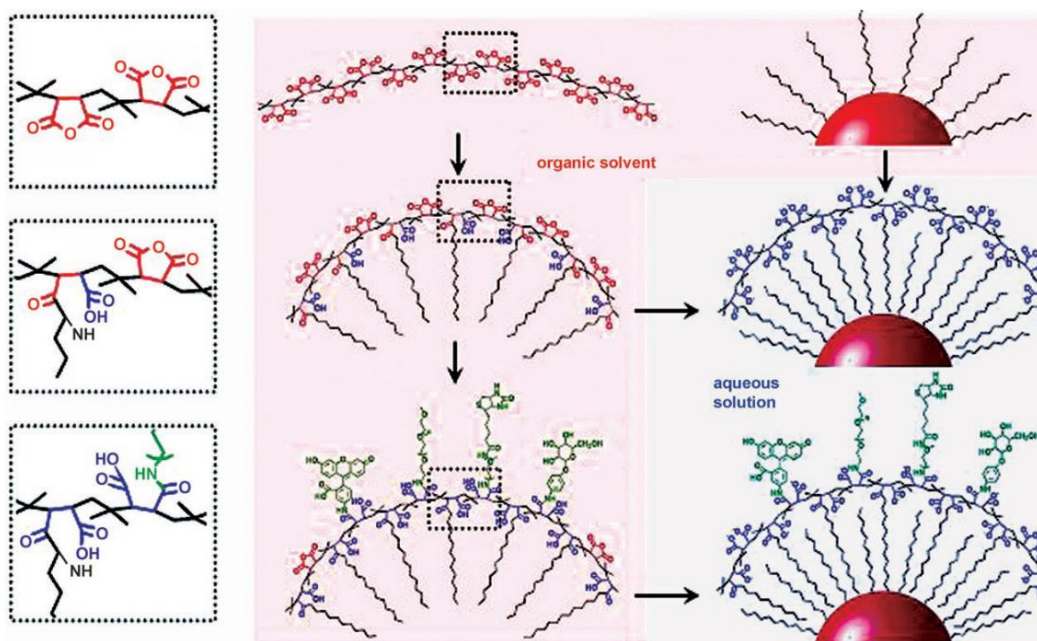


Figure 5. Scheme of the synthesis of the amphiphilic polymer and the coating of NPs. In the center column the synthesis of the amphiphilic polymer is shown. In the left column the amide linkage between the amino ligands and the anhydride rings is shown in detail. NPs with hydrophobic capping (right column, top line) are coated with the amphiphilic polymer by hydrophobic interaction between the alkyl chains of the polymer and the surfactant molecules on the NPs (middle line). Ref 83 copyright 2008 Wiley-VCH.

To be noted, the group of Parak has pioneered the strategy of surface polymer coating with dodecylamine (DDA) grafted poly(isobutylene-*alt*-maleic anhydride) (PMA), and achieved the versatile surface functionalization for several kinds of NPs, such as AuNPs, AuNRs, IONPs and CdSe/ZnS quantum dots (Figure 5).^[83-85] This type of polymer coated NPs showed great stability and offered a good platform to study further biological phenomenon, such as tracking the integrity of polymer coated NPs^[86] and exploring the influence of antibody number on tumor homing and therapeutic effect *in vivo*^[87].

4. Biocompatibility of NPs

NPs hold great promises for both industrial and biomedical applications. In the past decades, a series of NPs have been deeply investigated in various fields. Nanotechnology applied in commercially available products is becoming increasingly common. It has been reported that the production of NPs will experience a continuous increase from the estimated 2300 tons produced in 2008 to 58000 tons by 2020.^[88] Considering the sharp increase in manufacturing of NP-containing merchandise along with the constant new discovery in nanoscience, it is a pity that our knowledge on the toxic effects of NPs is still limited. Moreover, there are some findings reported the negative sides of the nanotechnology, which may jeopardize public perception of nanotechnology.^[89, 90] Therefore, toxicity or viability issues are a major concern and are important factors in the context of biological applications, especially for regenerative medicine and tissue engineering and it is increasingly necessary to verify the safety of NPs in advance.

When interpreting cytotoxicity, it is hard to make a clear definition, because even for the same cells exposed at the same experimental condition, there are a huge number of different types of NPs, which are composed of various components, such as carbon, silica, metals, polymers, rare earth elements, and semiconductor elements, let alone the cytotoxicity of NPs is always in a dose- and time- dependent manner, which increases the complexity for the overall assessment. It should be noted that to verify whether the NPs are toxic is never an easy and direct issue.

Assay	Targets
MTT assay	mitochondria
Resazurin assay	mitochondria
LDH assay	cell membrane
Trypan blue assay	cell membrane
Live/Dead assay	cell membrane
PI assay	DNA
EdU proliferation assay	DNA

Table 2. The assays used in the evaluation of cytotoxicity and targets in cells.

The evaluation in vitro studies usually includes the investigation of significant cytotoxic effects, i.e., decreased cell viability, induction of oxidative stress, mitochondrial activity, cytoskeleton dysfunction, cell membrane and DNA damage. Therefore, a correct assessment of NP-induced cytotoxicity should take into account the different aspects of toxicokinetics that may be targeted by NPs. The commonly used tests used for NP-mediated toxicity and cell viability are 3-(4,5-dimethylthiazol-2-yl)-2,5-diphenyltetrazolium bromide (MTT), resazurin, propidium iodide (PI), Live/Dead assay, trypan blue assay, EdU proliferation assay and lactate dehydrogenase (LDH)

assay et. al., shown in Table 2. Assessments via different methods should be considered respectively, because their sensitivity may be different. For instance, from the comparison between resazurin assay and EdU based proliferation, we can see that the EdU proliferation assay showed high sensitivity than the cell viability studies by the resazurin assay, Figure 7 and 8. This difference in sensitivity is because resazurin measures the activity of mitochondria, while EdU based proliferation the DNA synthesis in the nucleus. Therefore, this proliferation assay is a relatively more sensitive assay in the evaluation of cell viability.

In addition, with regard to stem cells, the stemness is one of the most characteristic property, which can be demonstrated by immunophenotype (surface marker expression), migration etc., Figure 6.^[91]

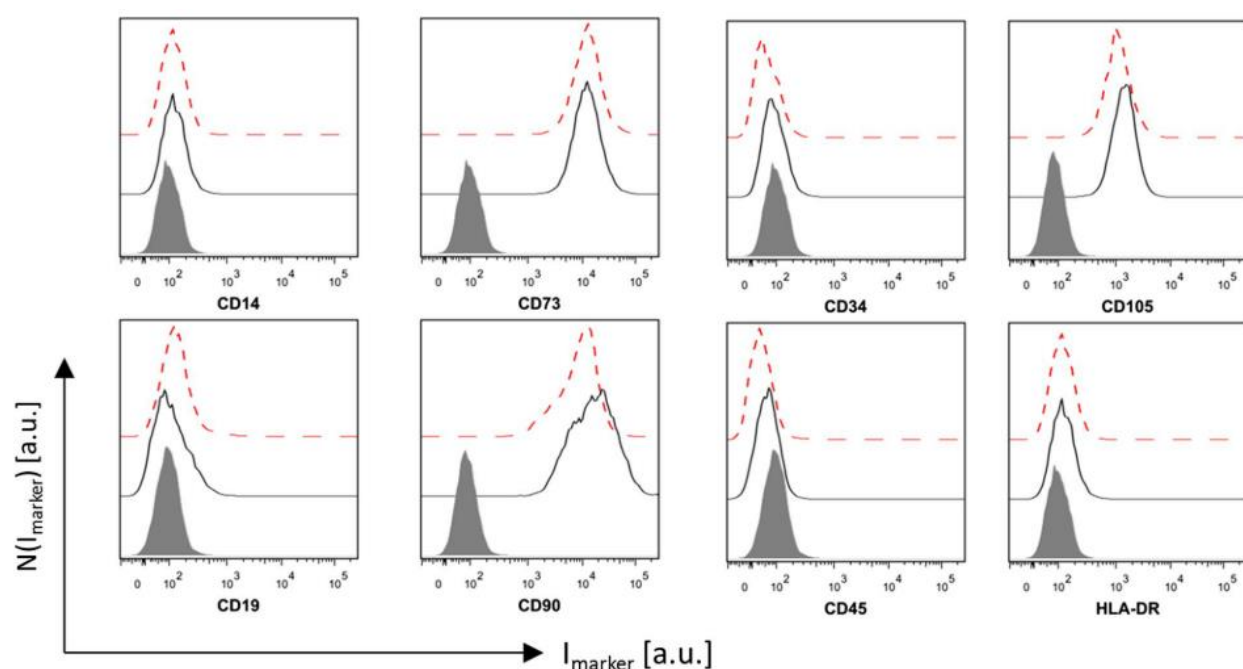


Figure 6. Surface marker expression of MSCs after 48hrs' incubation with 5nm AuNPs. Untreated MSCs (black solid line) and MSCs exposed to AuNPs at $C_{NP} = 10$ nM (red dashed line), the solid grey front curve represents the isotype control. Ref 91 copyright 2017 Wiley-VCH.

In general, the cytotoxicity of NPs has a time- and dose- dependent manner. It may come from the following aspects: 1) the release of toxic ions from NPs, 2) the high amount of NPs accumulated in cells impeding the normal function of the system in cells, 3) the catalytic effects of NPs that influence the reaction in cells due to their high surface activity. Therefore, when it comes to the biocompatibility of NPs, their characteristics such as size, shape, surface charge, core materials and so on should be taken into consideration. Basically, NPs with higher cytotoxicity are likely to be the ones with small sizes^[92], positive charge^[93], toxic components/elements^[94].

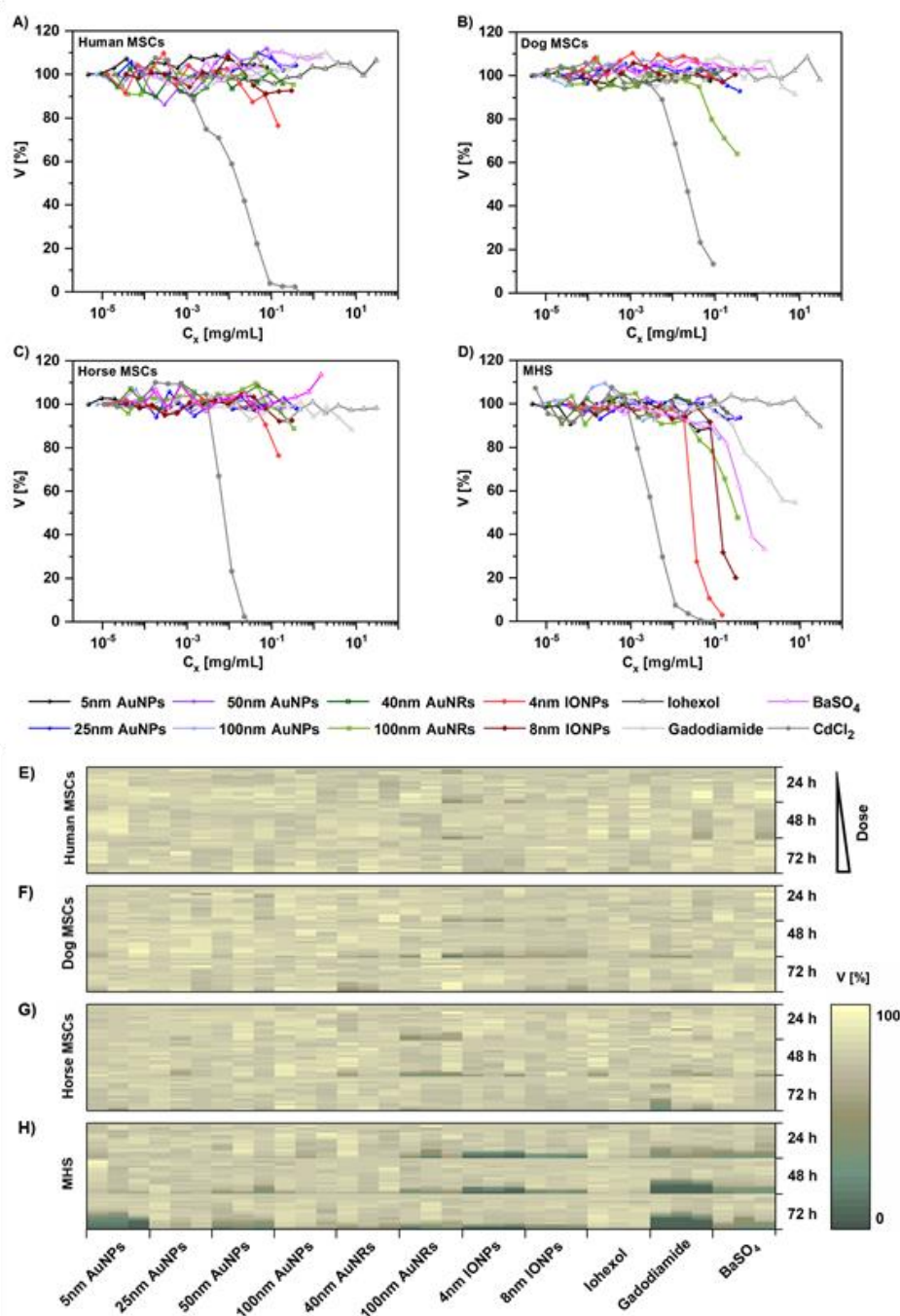


Figure 7. Cell viability (Resazurin assay) of MSCs and MHS macrophages after 24 h exposure to AuNPs and IONPs at different Au ($C_x = C_{Au}$) and Fe ($C_x = C_{Fe}$) concentrations, respectively. As control, cells were exposed to Iohexol, Gadodiamide, BaSO₄, and CdCl₂ at different I ($C_x = C_I$), Gd ($C_x = C_{Gd}$), Ba ($C_x = C_{Ba}$), and Cd ($C_x = C_{Cd}$) concentrations, respectively. Ref 33 copyright 2019 Elsevier.

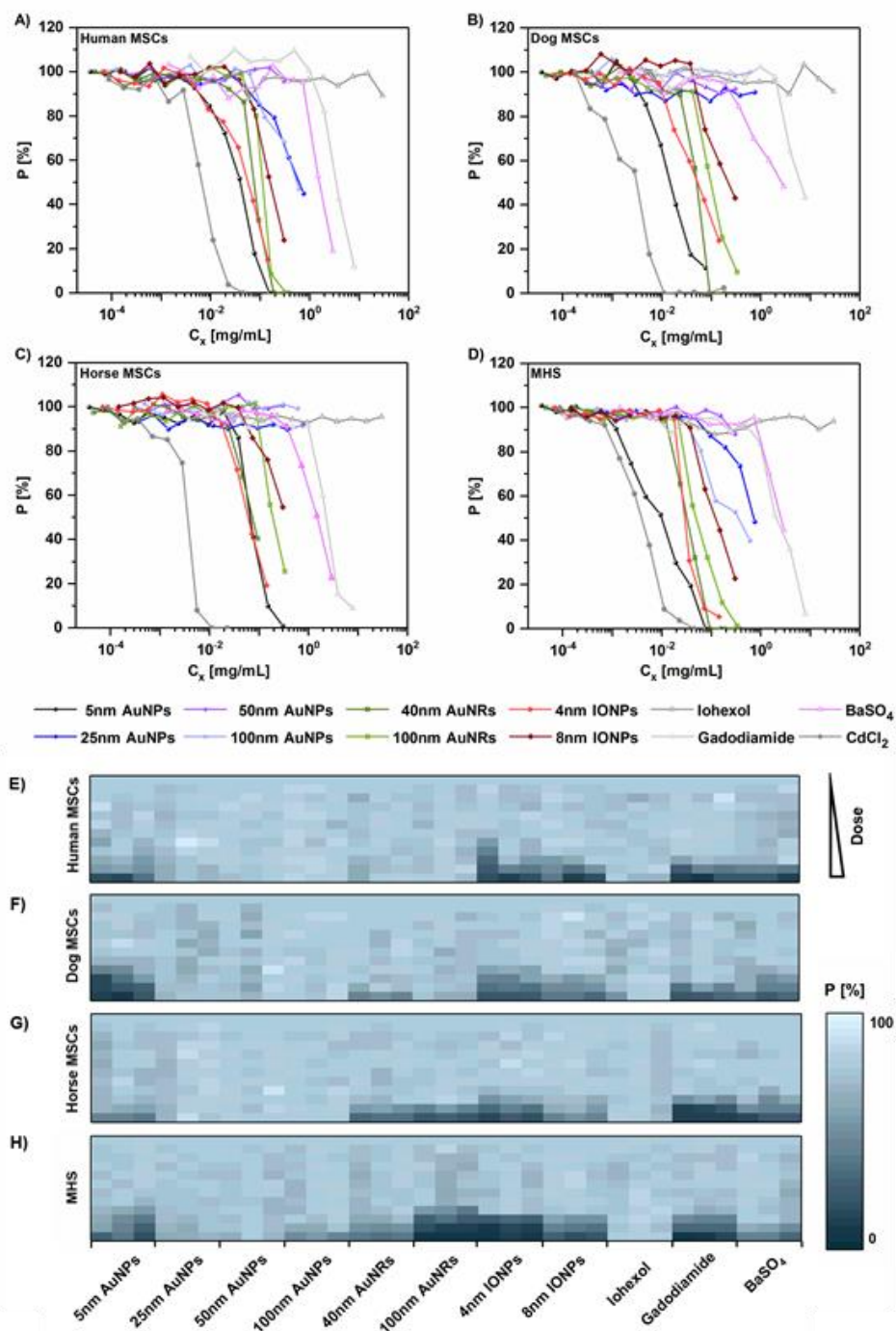


Figure 8. EdU based cell proliferation of MSCs and MHS macrophages after 24 h exposure to AuNPs and IONPs at different Au ($C_x = C_{Au}$) and Fe ($C_x = C_{Fe}$) concentrations. As control cells were exposed to Iohexol, Gadodiamide, BaSO₄, and CdCl₂ at different I ($C_x = C_I$), Ba ($C_x = C_{Ba}$), Gd ($C_x = C_{Gd}$), and Cd ($C_x = C_{Cd}$) concentrations, respectively. Ref 33 copyright 2019 Elsevier.

5. Factors affecting the labeling of cells with NP

The cell is the basic structural, functional, and biological unit of all known living organisms. A cell is the smallest unit of life, which is also known as the "building blocks of life". In terms of cell-based therapies, clearly tracking the fate of implanted cells in vivo, have a better understanding of their survival, migration, differentiation and regenerative behaviors in living subjects, may offer more reliable evidences for medical treatment.^[95] However, cells are always transparent and consequently hard to be distinguished from the uninterested host tissue cells. Therefore, efficient labeling cells strategies which allow the tracking and monitoring the cells after implantation in vivo noninvasively is of vital importance. Thus, NPs can be used as promising CA to label the cells.

Efficiency labeling the cells with NPs is not as straight forward, there are several aspects affecting including: the physic-chemical properties of NPs (e.g. size, colloidal stability, materials, cells type, toxicity, etc., Figure 9 showed possible factors affecting the labeling of cells with NPs.

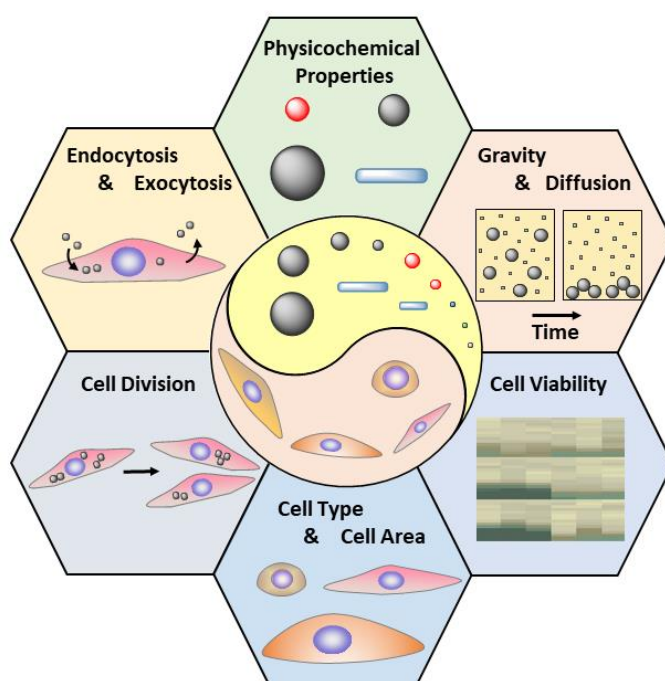


Figure 9. Factors that influences the cell labeling, which can be categorized into two groups. One is factors from NPs, such as size, shape, core materials, gravity and diffusion properties, the other is from cells: cell division, cell type, cell viability endocytosis and exocytosis. Ref 33 copyright 2019 Elsevier.^[33]

5.1 Influencing factors of NPs for cell labeling

NPs, as materials whose sizes are well-defined and can pass the biological barriers, enter and distribute within cells by some energy-dependent pathways, are considered as a primary vehicle

for targeted therapies. Therefore, NPs as a promising candidate for cell labeling have attracted increasing attention. So far, however, when it comes to the labeling efficiency of NPs, the properties of NPs always have strong influences on the whole labeling efficiency. Properties of NPs, such as the sizes^[96], shapes^[51, 97], charges^[98], surface chemistry^[99], stiffness^[100], etc. have already been discussed in the past years, however, some clear conclusions are so far hard to make.

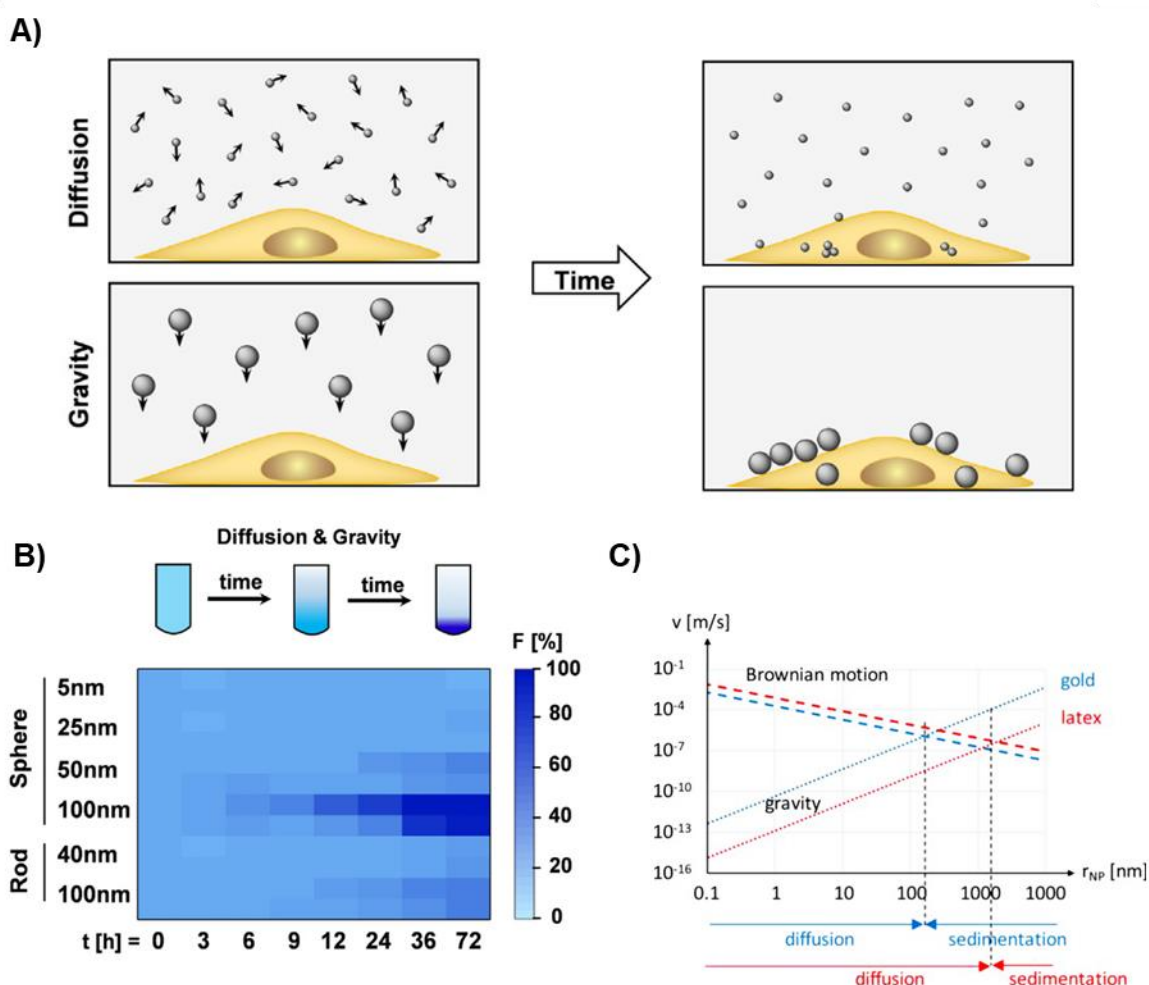


Figure 10. (A) Scheme illustrating the effects of basic colloidal properties of NPs on their cellular uptake. Knowing the colloidal properties of the NPs allows to consider the amount of NPs which will reach the cell surface in 2-dimensional (2D) in vitro cultures. (B) Sedimentation rate of the NPs dispersed in water and cell media containing 10% FBS over time, as quantified by the fraction F [%] of NPs which from an originally dispersed solution has sedimented after a time t to the bottom of the tube ($n=3$). (C) Sedimentation velocity v_G (dotted lines) and diffusion velocity v_{th} (dashed lines) for gold (blue) and latex (red) spheres of different NP diameter r_{NP} . Ref 33 copyright 2019 Elsevier. Ref 101 copyright 2017 American Chemical Society.

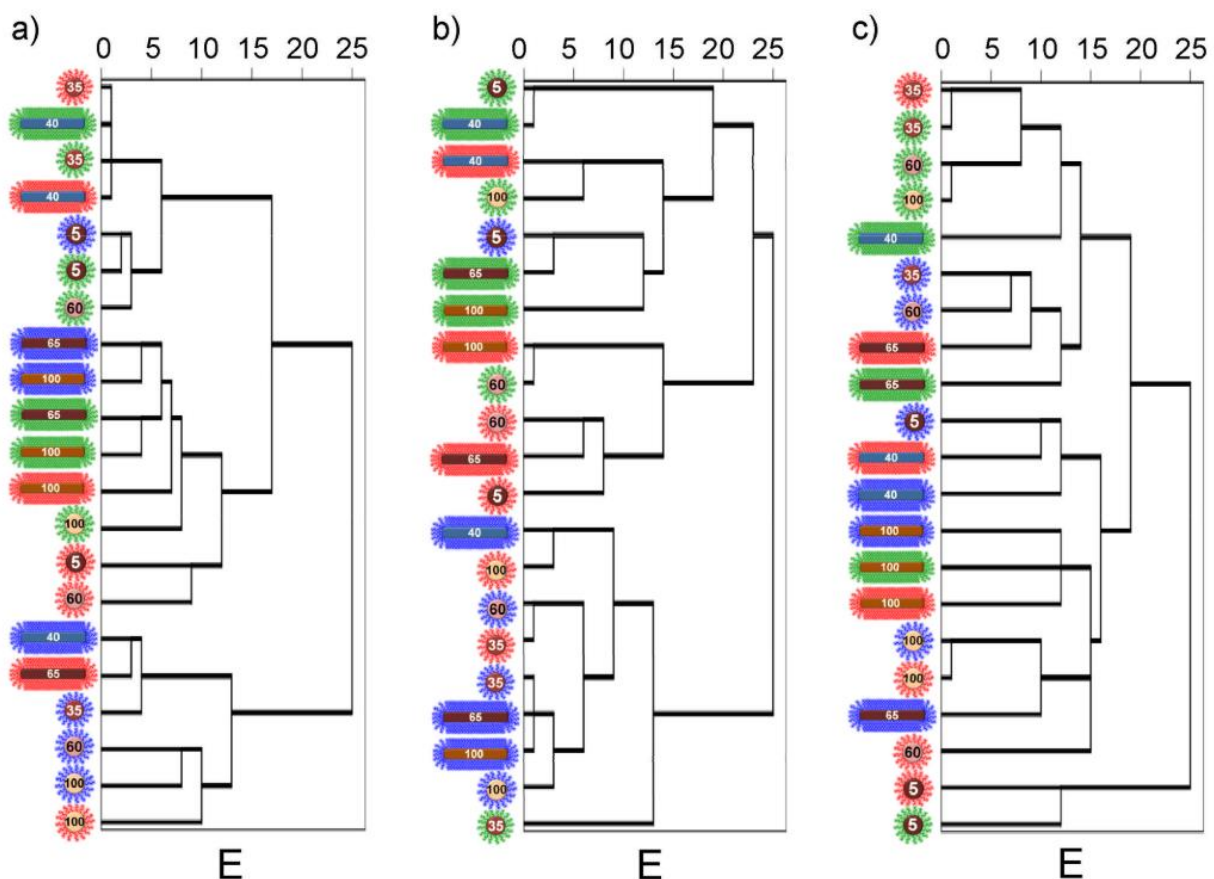


Figure 11. HCA analysis of different subsets of physicochemical properties, shown in terms of Euclidean distance E . (a) HCA of zeta-potentials, demonstrating that in particular the PEG coating (green) causes high similarity. (b) HCA of hydrodynamic diameters, resulting in dependence of similarity according to the type of NP core (diameter, shape). (c) HCA of hydrodynamic diameters, zeta-potentials, and electrophoretic mobilities, sorting the NPs remarkably well by their core volume ($V_c(100\text{-GNPs}) > V_c(60\text{-GNPs}) > V_c(100\text{-GNRs}) > V_c(35\text{-GNPs}) > V_c(65\text{-GNRs}) > V_c(40\text{-GNRs}) > V_c(5\text{-GNPs})$). Ref 103 copyright 2018 American Chemical Society.

Still, there is plenty of room at the bottom. When materials come into the nano sizes, it is generally assumed that this suspension is well-dispersed, which seemingly become a widely accepted awareness for in vitro experiments typically measuring the uptake of NPs by exposing cells at the bottom of a petri dish to a suspension of NPs. However, as the increase of the sizes, the influence of gravity on NPs also correspondingly increases. And with regard to small NPs, they can agglomerate in exposing condition, which changes the dispersibility of NPs. These effects, as a result, lead to the sedimentation of the NPs in exposed media, which means that the actual concentration of NPs around the cells on the bottom of petri dish may be higher than the initial bulk concentration, and in turn, this could lead to an enhanced uptake by cells (Figure 10). The schematic graph (Figure 10A), where the bigger NPs sediment near the cells and results in an enhanced uptake, while small NPs not. Build a model in Milli-Q water, the effect of Brownian motion and gravity (Figure 10C).^[101] Likewise, Cho et.al. also arised this issue, offering a new

insight into the cell labeling study, especially in the case where the sizes of the NPs are bigger than 50 nm^[102]. Based on this consideration, the understanding and modelling of the interactions between NPs and cells can be improved, and thus offer a better and more efficient way to apply NPs in various biomedical applications.

Alternatively, in biological systems the cell labeling efficiency with NPs is influenced by many parameters. Attempts to sort out the biological effect of NPs according to individual physicochemical parameter seems not reasonable.^[103] Put all of these factors that influence the labeling efficiency together, and build the hierarchical clusters according to relative relationship of all the factors. This method to analyze the multiple influencing data, which is called hierarchical cluster analysis (HCA), define which NPs are most closely related, (Figure 11). In HCA, the closer two types of NPs are in these “family trees”, the more their properties are related. Based on this analysis, the volume of the NP core and the surface coating around the NP core play an important role in cell labeling process.

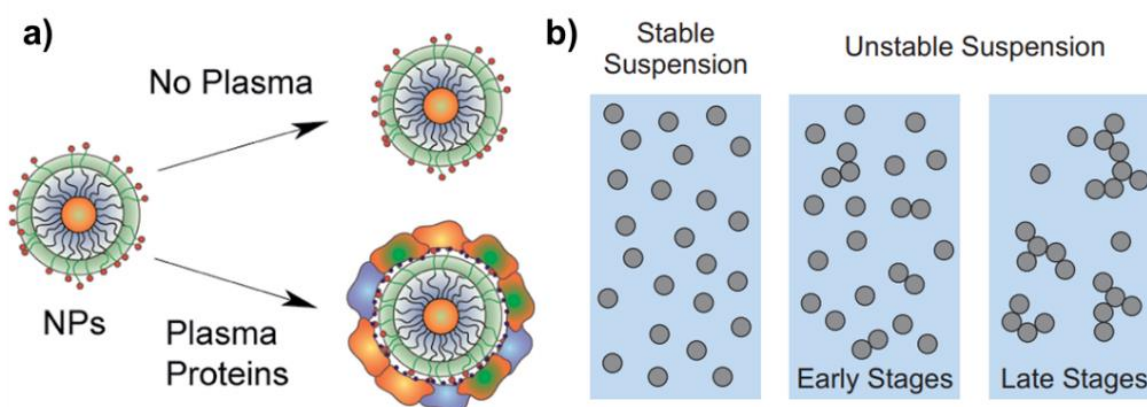


Figure 12. a) Protein corona formation around NPs, b) aggregation of AuNPs in biological environment. Ref 105 copyright 2013 American Chemical Society.

Apart from the properties of NPs and cell conditions, to study the cellular uptake normally a media, such as cell culture media or/and saline buffer, are always used as the medium between NPs and cells. In this occasion, the interaction between NPs and cells also include the interaction with the containing proteins, peptides, salts and so on. Therefore, these components contained in the medium increase the complexity of the system.

The components inside the medium also change the properties of the media, such as the pH value, medium density, viscosity and so on. Once the NPs are introduced into these systems, their properties, such as colloid stability, thermal movement, surface physico-chemical properties, are also changed correspondingly. As a result, the behavior of NPs maybe be not the same as characterized in the test tub .Thus the results obtained need to be discussed critically.

Interestingly, among them, the most debated influencing factors are the protein corona^[104] and NP aggregation (Figure 12). Ideally, when the NPs are introduced into a biological system, they will transport around until reach their destination, where the NPs will interact with the target sites. The fact, however, is another scenario. Because proteins in a biological environment can coat on the surface of a NP and affect its subsequent action.^[105] Meanwhile, the pH value and the salts included in the environment will change the stability of the NPs, afterwards leading to the agglomeration or aggregation.^[36] Based on these consideration above, the actual interaction between NPs and cells is not the same as the initial assumption. Thus when some studies to be made on this, these factors should be taken into consideration carefully.

5.2 Influencing factors from cells

Upon above consideration, the cell labeling efficiency depends heavily on the NP properties, on the other hand, the role of cell properties could not be negligible. The type and cell state affects the overall cell behaviors, which in turn influences the final outcomes of cell labeling with NPs.

5.2.1 Cell properties

Cell type, cell morphology, cell surface area, cell division, exocytosis and cell viability are also vital cell properties. When NPs interact with cells in different conditions, the final results will also different. Thus, much attention should be paid in the study of cell labeling with NPs.

Cell type

When talking about the cell types used in vitro studies, there comes the choice of primary cells and cell lines. Cell line is a population of cells which can proliferate indefinitely because of natural or intentional mutations. In many academic researches cells lines as they are generally highly proliferative, and easier to culture and transfect, therefore have been chosen as the most popular model in vitro.^[106] In some occasions, cell lines have been in culture for decades and have already well adapted to the two-dimensional culture condition. As a result, they often show different genetic behaviors and phenotypes as well as the altered morphology from their original tissues.

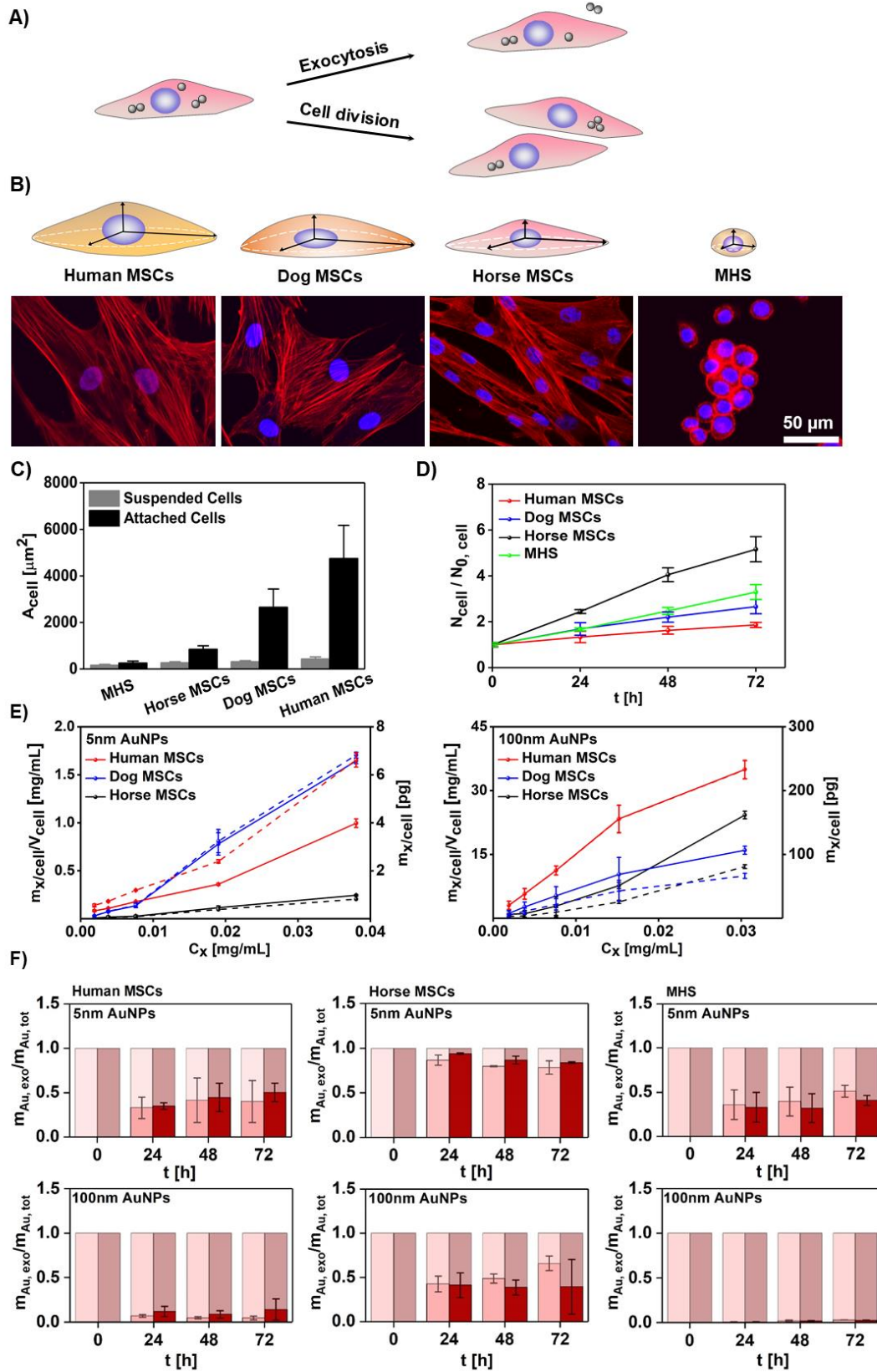


Figure 13. Factors that influence the NP labeling efficiency of cells. (A) Scheme illustrating the effects of cell division and exocytosis on the retention of NPs in cells. (B) Sketch of the morphology of the MSCs and MHS cells, together with fluorescence microscopy images of stained cytoskeleton and nuclei of cells. The scale bar is 50 μm . (C) Cross-section area of adherent and trypsinized (i.e. suspended) cells (A_{cell}). (D) Cell division as described by the time-dependent number of cells in culture N_{cell} versus the initial amount of seeded cells $N_{0,\text{cell}}$ ($N_{\text{cell}}/N_{0,\text{cell}}$). (E) Amount of elemental Au ($m_{\text{x/cell}} = m_{\text{Au/cell}}$) found in MSCs after 24 h exposure to 5 nm and 100 nm AuNPs at different Au ($C_{\text{x}} = C_{\text{Au}}$) exposure concentrations. The uptake results are expressed in terms of Au per cell ($m_{\text{x/cell}}$ [pg], represented as slashed lines) and normalized to the respective cell volume ($m_{\text{x/cell}}/V_{\text{cell}}$ [mg/mL], represented as solid lines). (F) Percentage of exocytosed for 5 nm AuNPs and 100 nm AuNP in Human MSCs, Horse MSCs, and MHS macrophages expressed as $m_{\text{Au,exo}}/m_{\text{Au,tot}}$. $m_{\text{Au,tot}}$ is the total amount of internalized Au directly after removal of AuNPs from the extracellular medium. Ref 33 copyright 2019 Elsevier.

By contrast, primary cells which are isolated directly from tissues, have normal cell morphology and maintain many of the important markers and functions seen in vivo^[107, 108]. Furthermore, primary cells are extremely sensitive cells requiring additional nutrients not included in classical media. For these reasons, although primary cells have a limited lifespan and expansion capacity, they are more reasonable models for in vitro study and show better similarities to the actual cells in vivo and provide more effective information for the following studies.

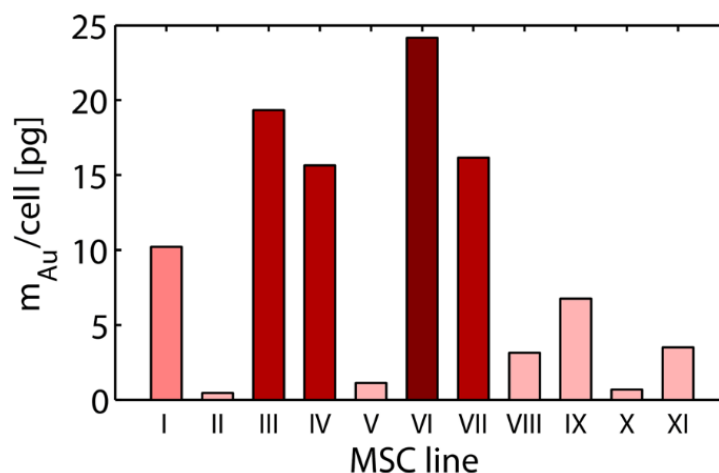


Figure 14. Donor dependence of AuNP uptake. MSCs in 3rd or 4th passage were labeled with 10 nM Au NPs for 48 h in vitro. Ref 91 copyright 2017 Wiley-VCH.

In addition, cells from different tissue origins may also differ in their behaviors, which show various properties like cell morphology, cell surface area, cell division velocity, exocytosis, etc., Figure 13. In the case of primary stem cells, internalized NPs may vary when stem cells from different donor are chosen, Figure 14.^[91] MHS is one cell line of macrophages that can protect the body by taking in and ingesting harmful foreign particles, bacteria, and dead or dying cells. For this reason, this kind of cells can internalize NPs in higher quantity, compared with other cell types. Particularly, as one important member of phagocytes, macrophages have also this ability. As a result, even with small cell sizes, which reduces the possibility to contact with NPs, the macrophage-labeling still shows a higher efficiency.

Exocytosis

Exocytosis is a significant pathway of cells to organize membrane proteins and lipids, excrete of essential molecules, and repair the cell membrane.^[109] In cell labeling, part of the internalized NPs by the cells are expelled into the extracellular environment via exocytosis. For this reason, it is also a vital process for NPs in cell labeling, which influences the overall amount of NPs accumulated inside cells. In the uptake study, our data suggest that smaller NPs (i.e. 5 and 25 nm AuNPs) are exocytosized from the cells in a higher amount, while bigger NPs (i.e. 100 nm AuNPs) less, as shown in Figure 13 (E). This difference may come from the slower transportation of big NPs than the small ones.

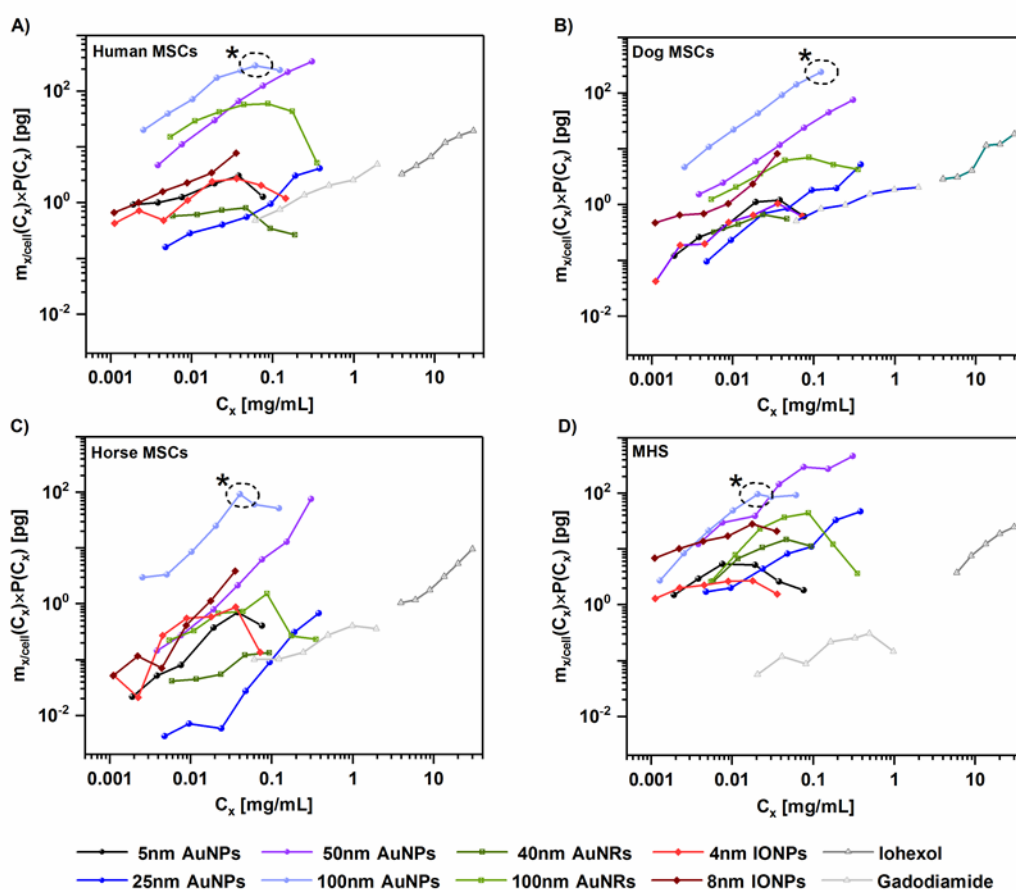


Figure 15. Amount of incorporated Au, Fe, I, and Gd multiplied with the cell proliferation after 24 h exposure of cells to AuNPs and IONPs at different Au ($C_x = C_{\text{Au}}$) and Fe ($C_x = C_{\text{Fe}}$) concentrations, respectively. As control cells were exposed to Iohexol and Gadodiamide at different I ($C_x = C_{\text{I}}$) and Gd ($C_x = C_{\text{Gd}}$) concentrations, respectively. (A) Human MSCs, (B) dog MSCs, (C) horse MSCs, and (D) MHS macrophages. For the 100 nm AuNPs the optimum exposure concentration C_x^* is indicated with a black star. Results were obtained from a minimum three independent experiments using cells from different donors or different cell passages. Ref 33 copyright 2019 Elsevier.

Cell viability

The cellular uptake of NPs is usually in a dose and time dependent manner, for instance, when incubating cells with higher doses of NPs for a longer time, the total amount of internalized NPs may increase. However, in this condition, the possibility of cytotoxicity from NPs maybe higher. Thus, their normal cell function may be impaired. Therefore, sufficient amount of NPs inside cells to achieve imaging by increasing exposure concentration for labeling together with the avoidance of cytotoxicity by decreasing the NP quantity will provide us a more reasonable way for the subsequent cell tracking. Based on this, the optimum labeling conditions can be determined by multiplying cell proliferation numbers with the cell uptake values, with which the curve can be plotted versus NP concentrations. From this curve a peak will show, the optimal labeling condition will be established, Figure 15.

5.2.2 Pathways for NP uptake

In the process of cell internalization, NPs may enter the cells via several different pathways, phagocytosis, macropinocytosis, clathrin-mediated endocytosis, caveolin-dependent endocytosis and simple diffusion (Figure 16).^[110]

Phagocytosis is primarily used to treat dead cells, cell debris, and pathogens in biological systems. This pathway can internalize bigger NPs up to micrometer scale. When NPs come into the vicinity, cells will form the cup-shaped membrane protrusions, which gradually surround and then internalize the particles.^[111] Macropinocytosis, as an actin-regulated process, can engulf of a large quantity of extracellular fluid. This pathway can also engulf NPs through plasma membrane ruffling.^[112]

There are two receptor-mediated endocytosis pathways, clathrin-mediated endocytosis and caveolin-mediated endocytosis. In clathrin-mediated endocytosis, the binding of NPs and receptor triggers the recruitment and formation of “coated pits” (clathrin) on the cell membrane. These pits locally wrap around NPs and then facilitate the endocytosis. The transportation of NPs is always via early endosomes to late endosomes and eventually to lysosomes.^[113] Caveolin-mediated endocytosis involves the assembly of the hairpin-like caveolin coats on the cytosolic side of the cell membrane, forming a flask-shaped caveolae of ~50-80 nm in diameter. It is generally known that clathrin- and caveolin-mediated endocytosis involves complex biochemical signaling cascades and both of them are energy consuming pathways.^[114] However, to some extent how is the entry of engineered NPs regulated by the biochemical signaling remains poorly understood.

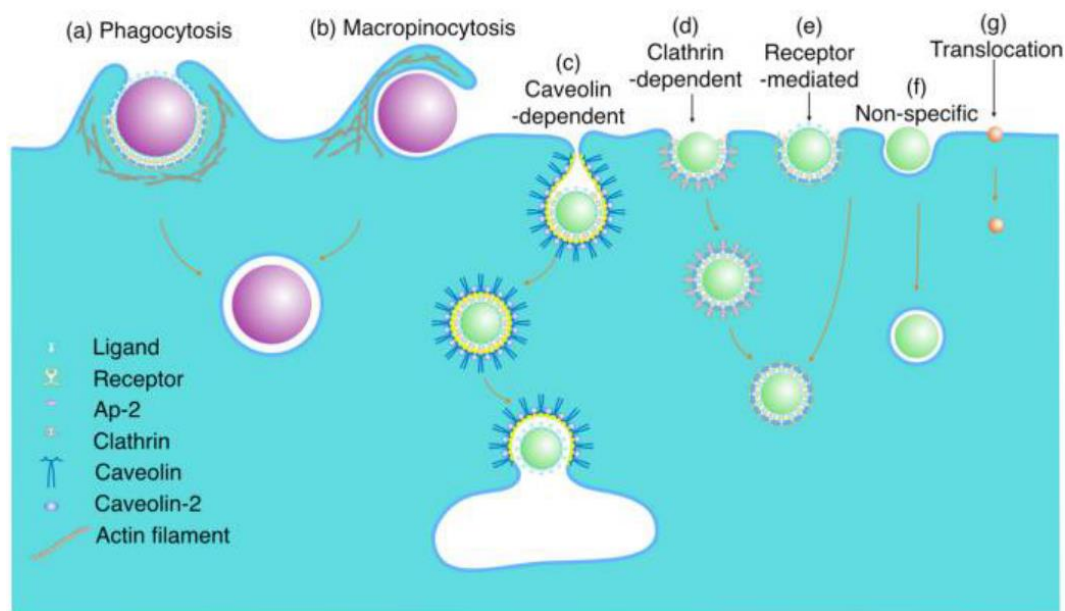


Figure 16. Possible internalization pathways of NPs. Ref 110 copyright 2015 American Chemical Society.

In addition, with regard to the NPs without conjugation ligands, non-specific interactions can also act as alternatives. For large NPs, if the interaction force is sufficiently large, the transmembrane penetration may occur.^[115] In the case of small NPs, especially when the NPs are smaller than 1 nm, they may enter the cells easily by simply diffusing across the lipid bilayer in cell membrane.

6. Methods for cell tracking

To satisfy the demand of diagnose and therapy in clinics, a great number of approaches combined with corresponding contrast agents have recently become available for cell imaging and tracking. These techniques include optical imaging techniques, ultrasound, positron-emission tomography (PET), single photon emission tomography (SPECT), CT and MRI and so on. Each of these approaches has its own advantages and also drawbacks with respect to sensitivity, temporal and spatial resolution, clinical safety, anatomical details, and functional information.

With respect to optical imaging techniques, target cells are usually either labeled with fluorescent materials such as organic dyes or some fluorescent NPs^[116] like quantum dots and nanoclusters, or even transfected with a reporter gene encoding the synthesis of a fluorescent protein detectable with fluorescence imaging^[117] or a luciferase enzyme, which are detectable with bioluminescence imaging. Although these optical techniques have the advantages of being reliable, inexpensive and fast, they are limited to preclinical studies which are mainly originated from the light penetration limits.^[118] Additional approaches like PET and SPECT with the use of radiolabeling, are clinically relevant and have excellent sensitivity. However, because of the fast radioisotope decay, they are not suitable for long-term cell tracking.^[119] In addition, radionuclide-based techniques are unable to provide anatomical imaging alone, and must be combined with anatomical imaging methods i.e., CT or MRI. Thus, their intensive applications are highly restricted. In contrast, CT and MRI are recently the most commonly used methods in clinics, which are introduced detailed in the following part.

6.1 CT

CT is an X-ray based imaging technology that can create detailed cross-sectional images of many different tissue types, which is at present one of the most widely used imaging techniques in the field of clinic applications, owing to its wide availability, high efficiency, low cost, and the development of novel hybrid imaging systems such as positron-emission tomography (PET)/CT and single-photon emission computed tomography (SPECT)/CT.^[120] It is typically accomplished by taking multiple X-rays from different angles to form image “slices” which can then be composited together to form a detailed set of cross-sectional images. Its resolution is relatively high, which falls in the range of submillimeter for clinical systems and the micrometer range for preclinical systems.^[7] Therefore, it is commonly used for imaging of the pelvis, head, abdomen and chest.^[121]

In the case of CT, unlike other imaging techniques, in order to absorb enough amount of X-ray for imaging, materials for contrast agents are normally with a relatively high number of atom mass, at the same time, a relatively high concentrations are also needed. Hence, only a few nanomaterials can act as CT imaging agents, namely iodine based nanomaterials^[122, 123] and

AuNPs^[13, 16, 124, 125]. At present the most employed materials for CT in clinics are iodine based contrast agents like Iohexol. However, due to their low labeling efficient and short retention time in vivo as well as the obvious signal fluctuation in different environment, their practical applications become relatively challenging.

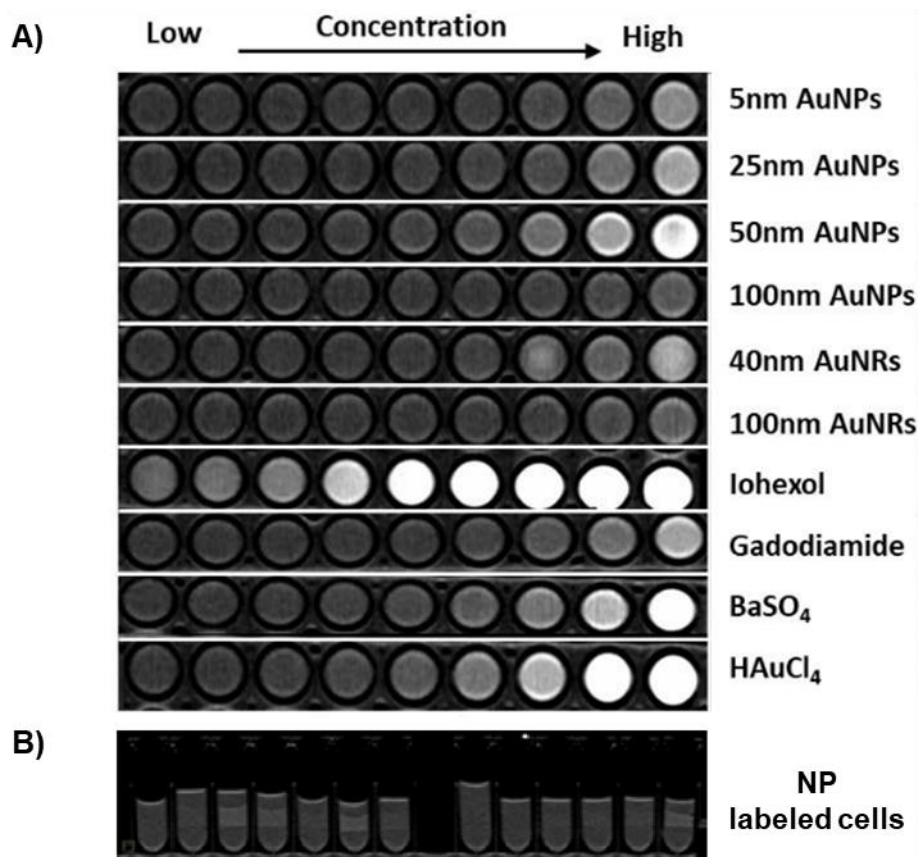


Figure 17. CT image of phantoms. A) in EP test tubes containing AuNPs, As control, commercial CAs, Iohexol, Gadodiamide, BaSO₄, and in addition gold salt (HAuCl₄) were used. From left to right dilution series of materials (dilution factor 1:2 between adjacent samples) are shown, i.e. the sample of the left has half of the dose of the sample on the right). B) in EP test tubes cells labeled with AuNPs and CAs embedded in agarose. Images were acquired in 1% agarose at 80 kV respectively. Ref 33 copyright 2019 Elsevier.

Therefore, to overcome the drawbacks above, AuNPs based contrast agents endowed with better features are emerging as a new generation of contrasts for CT imaging, generally providing greater contrast than iodinated contrast agents^[126], (Figure 17). In addition, AuNRs because of their easier clearance by phagocytes than spherical NPs, exhibiting longer circulation time^[127], have already been tried to be used as CT contrast agents for tumor imaging.^[128] What is more, for accurate diagnosis, multimodal imaging agents based on AuNPs have been developed. In this case, materials with different sensitivity of each imaging modality have been considered. For example,

based on the high atomic weight of platinum, FePt NPs were used for dual modal CT/MRI imaging^[129]. AuNPs coated with Gd-chelates were used as contrast agents for CT and MRI.^[130, 131]

6.2 MRI

MRI is one powerful and highly useful technique in soft-tissue imaging and diagnostics, its high temporal and spatial resolution, safe and non-invasive, which facilitate its highly effective property for tumor imaging as well as the real-time monitoring of drug delivery and bio-distribution in the targeted sites. In particular, it can also have the ability to visualize and track individual cells *in vivo*.

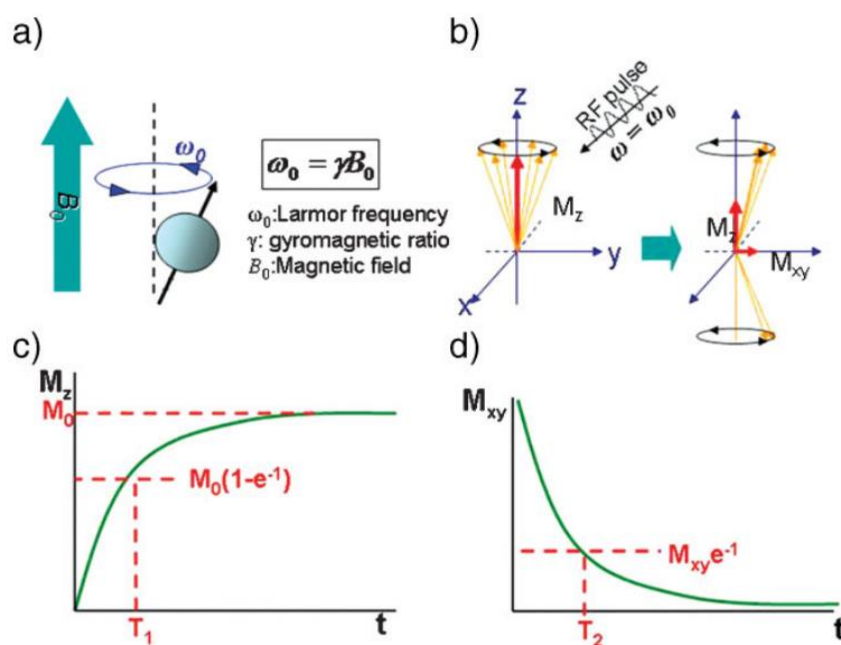


Figure 18. Principle of magnetic resonance imaging. a) Spins align parallel or antiparallel to the magnetic field and precess under Larmor frequency (ν_0). b) After induction of RF pulse, magnetization of spins changes. Excited spins take relaxation process of c) T1 relaxation and d) T2 relaxation. Ref 132 copyright 2009 Wiley-VCH.

In principle, MRI works by applying a strong external magnetic field to interact with the abundant water protons that are found in soft tissue. This applied external magnetic field will lead to the magnetic moments in the protons to align in the direction of the field. Therefore, when a radiofrequency (RF) pulse is sent through the tissue, the protons will precess in a specific direction at a certain frequency, and then the proton specific to the type of tissue happens to reside in. Upon removal of the RF pulse, the protons return to their ground state, this process is termed as relaxation. And the time for protons used to return to ground state is called relaxation time. There are two different relaxation pathways in this process. One called longitudinal or T1 relaxation,

involves the decreased net magnetization (M_z) recovering to the initial state (Figure. 17c). The other called transverse or T2 relaxation, involves the induced magnetization on the perpendicular plane (M_{xy}) disappearing by the dephasing of the spins (Figure. 18d).^[132] Later on through computer reconstruction of the values leads to contrast differences in the resulting composite detected relaxation signals, the tissue-dependent variation in the T1 and T2 images. A greater difference in relaxation time between two tissues will produce greater contrast on the MR image.

Similar as CT imaging, for many MRI applications, such as tumor diagnosis and cellular imaging and tracking, it is also crucial to improve the imaging capabilities by using contrast enhancing agents. Because of the relaxation processes in MRI, the contrast agents are classified as T1 and T2 contrast agents. With a different concept, contrast agents for MRI produce a more pronounced image by altering the relaxation times of water protons around them ^[133]. Thus by accumulating in specific tissues, the contrast agents will further enhance the visibility of various structures and lesions on an MR image.

Currently, contrast agents for MRI many clinically used contrast agents are based on Gadolinium (III) complexes. Gadolinium complexes are strongly paramagnetic; they have a large magnetic moment due to their unpaired electrons^[134]. These agents provide positive contrast, bright spots, on T1 weighted images. Although the gadolinium ions themselves are highly toxic, the proper choice of ligands can produce gadolinium chelates that are nontoxic and highly stable in the body during the period of administration. One of the most common chelates is Gd-DTPA (DTPA = diethylenetriamine pentaacetic acid), which has been used clinically as the contrast agent Magnevist[®]^[134].

Because of the size effects, NPs offer good characteristics for medical applications, such as a longer plasma-circulation time. The most commonly used and clinically relevant contrast agent is the IONPs. Even several commercial MRI contrast agents are based on IONPs, such as Feridex, Resovist, and Combidex. In principle, IONPs improve imaging by reducing the T2 producing visible signal voids – seen as dark spots – on T2-weighted images. The superparamagnetic property of IONPs is one of their most important characteristics for in vivo imaging applications, which only occurs when the individual particles are below 20 nm in size^[135]. This property is absent in bulk iron oxide, which is a ferromagnetic (permanently magnetized) material. When a strong magnetic field is applied, IONPs exhibit a stronger magnetic response than most paramagnetic materials ^[136], making them highly useful for imaging applications. The degree of MRI signal interference, and thus the contrast enhancement, provided by IONPs is proportional to their saturation magnetization (M_s) value, the point at which all the values bulk magnetite individual magnetic moments in a sample are uniformly aligned.

Owing to their unique size-dependent magnetic properties, IONPs become a single domain as the particle size decreases below ~ 100 nm, where coercivity is maximized, while as the particle size is smaller than ~ 20 nm, their magnetization is randomized by thermal energy so that in this condition they become superparamagnetic.^[137] As MRI contrast enhancement agents, IONPs have been intensively investigated. It should be noted that magnetic properties of IONPs depend on the particle size.^[61, 66, 72] For example, uniformly sized IONPs with the sizes of 4, 6, 9, and 12 nm exhibit saturation magnetization values of 25, 43, 80, and 120 emu/g Fe, respectively.^[138] This size-dependent magnetization of IONPs, in turn, affects the T2 contrast in MRI. Consequently, synthesis of uniformly sized IONPs is critical for their clinical applications as MRI contrast agents, (Figure 19).

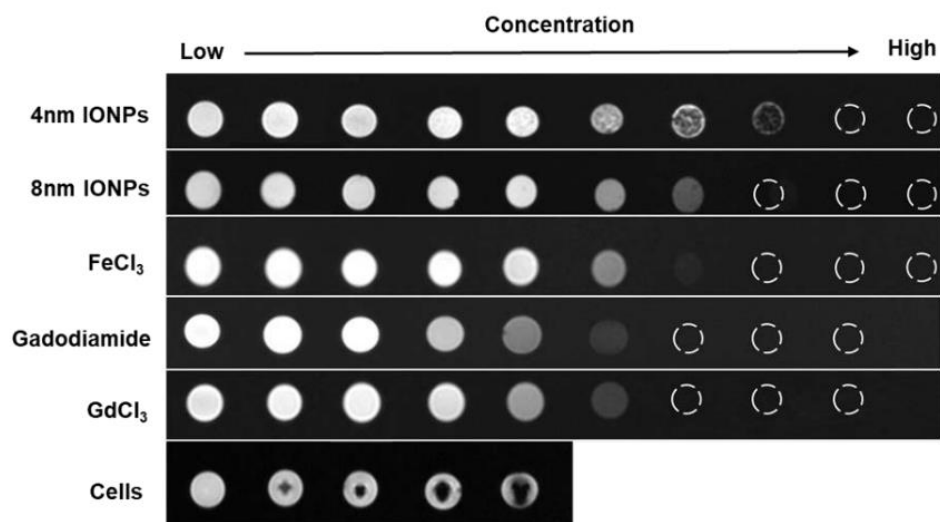


Figure 19. MRI image of phantoms with EP test tubes containing IONPs and contrast agents. A) 4 nm IONPs, B) 8 nm IONPs, C) FeCl_3 , D) Gadodiamide, E) GdCl_3 , F) Cells labeled with IONPs (from left to right: control cells, cells labeled with 633 nM of 4 nm IONPs, 317 nM of 4 nm IONPs, and 42 nM of 8 nm IONPs, and 21 nM of 8 nm IONPs). The highest concentration of the NPs/CAs starts from the right side. The dilution factor between adjacent samples is 2. Images were acquired in 1% agarose. Ref 33 copyright 2019 Elsevier.

Conclusions

To label stem cells and macrophages with NPs and explore their feasibility for in vivo tracking, best suited NPs in a library of AuNPs and IONPs and corresponding optimal labeling condition have been studied. In this work, we show that PMA coated AuNPs and IONPs have good biological compatibility, which are suitable for further applications. Subsequently, factors such as size, shape, surface chemistry, cell properties have been studied in the labeling of stem cells and macrophages with a library of NPs. What is more, the underlying reasons for the choices of best suited NPs and labeling condition have been elucidated in detail. To prove the potentials of NPs in practical applications, CT and MR imaging of NP labeled stem cells and macrophages have been tested, which offered good contrasts.

To be precise, the conclusions of this work are given as follows:

1. The motion of materials in small sizes are dominated by thermal movements. However, in nanosize, the effect of gravity in some cases should also be taken into consideration. Particularly, as the increase of size and/or density, especially when the sizes are bigger than 50 nm, the effect of gravity becomes obvious. Therefore, driven by gravity, bigger NPs have a great orientation towards the bottom in the exposure system, while the smaller NPs not. In our case, the 100 nm AuNPs sediment at the fastest speed, which is followed by the 50 nm AuNPs and 100 nm AuNRs, while the smaller NPs, i.e., 5 nm and 25 nm AuNPs, 4 nm and 10 nm IONPs, show no obvious trend of sedimentation. Thus in the investigation the uptake of the NPs, the sedimentation and Brownian movement of the bigger NPs should be considered;
2. Cells, even cultured in the same in vitro system, have different properties. In this work, we find out that different kinds of stem cells have different morphology, division cycles and exocytosis features. In our case, when cultured on the bottom of the flasks, the human MSCs grow at the slowest rate, but with biggest cell surface area, whereas the horse MSCs, grow the fastest and with smallest cell surface area. MHS, as another kind of cell, grow almost as fast as horse MSCs, but the smallest of the cell surface area as well as a different kind of cell uptake behaviors. These intrinsic features of cells have a synergistic influence on the cellular uptake of NPs;
3. In terms of cellular uptake, our data reveal that bigger NPs were internalized into cells with higher amount, i.e., 100 nm AuNPs accumulated in the human MSCs with the biggest quantity, while the 5 nm AuNPs the smallest in the horse MSCs. This not only results from the size effects between cells and NPs. Because the human MSCs have the largest cell surface area and lowest speed of cell division, and for 100 nm AuNPs they have high trend of sedimentation. So there are more chances of contacts and communications between bigger

NPs and cells with higher surface area. Therefore, in the cell labeling with NPs, there are the most amount of gold accumulated in human MSCs exposed with 100 nm AuNPs;

4. Based on the data of 21 different NPs concerning physicochemical characterization, protein corona formation, and in vitro as well as in vivo effects of the NPs, we find the correlation cannot be made only with one individual parameter, but that effects of different parameters are entangled. In vitro uptake of NPs and in vivo biodistribution of NPs are directly driven by the physicochemical properties as well as the corona and the in vitro/in vivo behavior. Surface properties of the NPs reveal a stronger impact on in vivo biodistribution than in vitro uptake of NPs in standard two-dimensional static cell cultures;
5. In the established optimal labeling condition, NPs labeled cells were observed under CT and MRI. Higher contrast signals can be obtained by labeling cells with bigger NPs than smaller NPs. Meanwhile, these signals from NPs labeled cells showed good agreements with that in the standard solution. Furthermore, compared with universal commercial contrast agents, NPs showed better resonance even exposed at relatively lower doses.

In summary, bigger NPs (normally larger than 50 nm), because of their characteristic of sedimentation, have tremendous advantages for cell labeling over smaller NPs. In terms of labeling efficiency, highly stretched cells with slower divided rates showed higher amount of NPs accumulation inside cells, which is beneficial for the CT and MR imaging. In general, NPs based imaging and therapy are still attractive and promising in the future, which will provide more possibility for the development of diagnosis and therapy in medical fields.

Perspectives

Cell based therapy, generally with the aid of stem cells and macrophages, shows promising possibilities to achieve the ultimate goal of overcoming the diseases such as cancer, heart diseases, and Parkinson. Even though there are clearly still many obstacles to overcome, it is of paramount significance that cell based therapy especially stem cell and macrophage based therapy is now conceivable. In the coming years, it is undoubtedly that more and more new investments and developments will be made in these fields owing to the increasing clinical demands.

Meanwhile, in recent decades, cell labeling techniques due to the vast development of nanotechnology, also witness tremendous advancements. Much efforts have been made in the exploration of new materials, as well as the comprehensive investigation the biological behaviors and/or advantages over existing materials. Accordingly, the deep and detailed understanding of the cell fates both in in vitro and in vivo scenario has been fully investigated. In this process, the optimal condition for cell labeling with various NPs has been well explored as well. Thus exciting opportunities lie ahead in combining cell therapy with nanotechnology for disease diagnostics and therapeutics.

To conclude, NPs have been proved to be promising candidates for cell labeling and tracking. In the coming future, there is no doubt that some breakthroughs will be made to overcome problems in clinics.

Reference

1. Barker, R.A., J. Drouin-Ouellet, and M. Parmar, *Cell-based therapies for Parkinson disease—past insights and future potential*. Nature Reviews Neurology, 2015. **11**(9): p. 492.
2. Phinney, D.G., M. Di Giuseppe, J. Njah, E. Sala, S. Shiva, C.M. St Croix, D.B. Stolz, S.C. Watkins, Y.P. Di, and G.D. Leikauf, *Mesenchymal stem cells use extracellular vesicles to outsource mitophagy and shuttle microRNAs*. Nature communications, 2015. **6**: p. 8472.
3. Srivastava, D. and K.N. Ivey, *Potential of stem-cell-based therapies for heart disease*. nature, 2006. **441**(7097): p. 1097.
4. Motaln, H., K. Gruden, M. Hren, C. Schichor, M. Primon, A. Rotter, and T.T. Lah, *Human mesenchymal stem cells exploit the immune response mediating chemokines to impact the phenotype of glioblastoma*. Cell transplantation, 2012. **21**(7): p. 1529-1545.
5. Auffinger, B., R. Morshed, A. Tobias, Y. Cheng, A.U. Ahmed, and M.S. Lesniak, *Drug-loaded nanoparticle systems and adult stem cells: a potential marriage for the treatment of malignant glioma?* Oncotarget, 2013. **4**(3): p. 378.
6. Stuckey, D.W. and K. Shah, *Stem cell-based therapies for cancer treatment: separating hope from hype*. Nature reviews Cancer, 2014. **14**(10): p. 683.
7. Weissleder, R., M. Nahrendorf, and M.J. Pittet, *Imaging macrophages with nanoparticles*. Nature materials, 2014. **13**(2): p. 125.
8. Mauriello, A., G. Sangiorgi, S. Fratoni, G. Palmieri, E. Bonanno, L. Anemona, R.S. Schwartz, and L.G. Spagnoli, *Diffuse and active inflammation occurs in both vulnerable and stable plaques of the entire coronary tree: a histopathologic study of patients dying of acute myocardial infarction*. Journal of the American College of Cardiology, 2005. **45**(10): p. 1585-1593.
9. Qian, B.-Z. and J.W. Pollard, *Macrophage Diversity Enhances Tumor Progression and Metastasis*. Cell, 2010. **141**(1): p. 39-51.
10. Mantovani, A., F. Marchesi, A. Malesci, L. Laghi, and P. Allavena, *Tumour-associated macrophages as treatment targets in oncology*. Nature Reviews Clinical Oncology, 2017. **14**: p. 399.
11. Bianco, P., *"Mesenchymal" stem cells*. Annual review of cell and developmental biology, 2014. **30**: p. 677-704.
12. Nguyen, P.K., D. Nag, and J.C. Wu, *Methods to assess stem cell lineage, fate and function*. Advanced drug delivery reviews, 2010. **62**(12): p. 1175-1186.
13. Meir, R. and R. Popovtzer, *Cell tracking using gold nanoparticles and computed tomography imaging*. Wiley Interdisciplinary Reviews: Nanomedicine and Nanobiotechnology, 2018. **10**(2): p. e1480.
14. Dubreil, L., I. Leroux, M. Ledevin, C. Schleder, L. Lagalice, C. Lovo, R. Fleurisson, S. Passemard, V. Kilin, S. Gerber-Lemaire, M.-A. Colle, L. Bonacina, and K. Rouger, *Multi-harmonic Imaging in the Second Near-Infrared Window of Nanoparticle-Labeled Stem Cells as a Monitoring Tool in Tissue Depth*. ACS nano, 2017. **11**(7): p. 6672-6681.
15. Andreas, K., R. Georgieva, M. Ladwig, S. Mueller, M. Notter, M. Sittinger, and J. Ringe, *Highly efficient magnetic stem cell labeling with citrate-coated superparamagnetic iron oxide nanoparticles for MRI tracking*. Biomaterials, 2012. **33**(18): p. 4515-4525.
16. Kim, T., N. Lee, D.R. Arifin, I. Shats, M. Janowski, P. Walczak, T. Hyeon, and J.W. Bulte, *In Vivo Micro - CT Imaging of Human Mesenchymal Stem Cells Labeled with Gold - Poly - I - Lysine Nanocomplexes*. Advanced functional materials, 2017. **27**(3): p. 1604213.
17. Alivisatos, A.P., *Semiconductor clusters, nanocrystals, and quantum dots*. science, 1996. **271**(5251): p. 933-937.

18. Eustis, S. and M.A. El-Sayed, *Why gold nanoparticles are more precious than pretty gold: noble metal surface plasmon resonance and its enhancement of the radiative and nonradiative properties of nanocrystals of different shapes*. Chemical Society Reviews, 2006. **35**(3): p. 209-217.
19. Li, Y., Y. Wu, and B.S. Ong, *Facile synthesis of silver nanoparticles useful for fabrication of high-conductivity elements for printed electronics*. Journal of the American Chemical Society, 2005. **127**(10): p. 3266-3267.
20. Mirkin, C.A., R.L. Letsinger, R.C. Mucic, and J.J. Storhoff, *A DNA-based method for rationally assembling nanoparticles into macroscopic materials*. nature, 1996. **382**(6592): p. 607.
21. Daniel, M.-C. and D. Astruc, *Gold nanoparticles: assembly, supramolecular chemistry, quantum-size-related properties, and applications toward biology, catalysis, and nanotechnology*. Chemical reviews, 2004. **104**(1): p. 293-346.
22. Gucci, L., G. Pető, A. Beck, K. Frey, O. Geszti, G. Molnár, and C. Daróczy, *Gold nanoparticles deposited on SiO₂/Si (100): Correlation between size, electron structure, and activity in CO oxidation*. Journal of the American Chemical Society, 2003. **125**(14): p. 4332-4337.
23. Huang, X., P.K. Jain, I.H. El-Sayed, and M.A. El-Sayed, *Plasmonic photothermal therapy (PPTT) using gold nanoparticles*. Lasers in medical science, 2008. **23**(3): p. 217.
24. Lu, A.H., E.e.L. Salabas, and F. Schüth, *Magnetic nanoparticles: synthesis, protection, functionalization, and application*. Angewandte Chemie International Edition, 2007. **46**(8): p. 1222-1244.
25. Niemeyer, C.M., *Nanoparticles, proteins, and nucleic acids: biotechnology meets materials science*. Angewandte Chemie International Edition, 2001. **40**(22): p. 4128-4158.
26. Daniel, M.-C. and D. Astruc, *Gold Nanoparticles: Assembly, Supramolecular Chemistry, Quantum-Size-Related Properties, and Applications toward Biology, Catalysis, and Nanotechnology*. Chemical reviews, 2004. **104**(1): p. 293-346.
27. Kim, D., Y.Y. Jeong, and S. Jon, *A drug-loaded aptamer– gold nanoparticle bioconjugate for combined CT imaging and therapy of prostate cancer*. ACS nano, 2010. **4**(7): p. 3689-3696.
28. Popovtzer, R., A. Agrawal, N.A. Kotov, A. Popovtzer, J. Balter, T.E. Carey, and R. Kopelman, *Targeted gold nanoparticles enable molecular CT imaging of cancer*. Nano letters, 2008. **8**(12): p. 4593-4596.
29. Lohse, S.E. and C.J. Murphy, *The Quest for Shape Control: A History of Gold Nanorod Synthesis*. Chemistry of Materials, 2013. **25**(8): p. 1250-1261.
30. Brust, M., M. Walker, D. Bethell, D.J. Schiffrin, and R. Whyman, *Synthesis of thiol-derivatised gold nanoparticles in a two-phase liquid–liquid system*. Journal of the Chemical Society, Chemical Communications, 1994(7): p. 801-802.
31. Lin, X., C. Sorensen, and K. Klabunde, *Digestive ripening, nanophase segregation and superlattice formation in gold nanocrystal colloids*. Journal of Nanoparticle Research, 2000. **2**(2): p. 157-164.
32. Wen, T. and S.A. Majetich, *Ultra-large-area self-assembled monolayers of nanoparticles*. ACS nano, 2011. **5**(11): p. 8868-8876.
33. Sun, X., M. Gamal, P. Nold, A. Said, I. Chakraborty, B. Pelaz, F. Schmied, K. von Pückler, J. Figiel, and Y. Zhao, *Tracking stem cells and macrophages with gold and iron oxide nanoparticles—The choice of the best suited particles*. Applied Materials Today, 2019. **15**: p. 267-279.
34. Sperling, R.A., P.R. Gil, F. Zhang, M. Zanella, and W.J. Parak, *Biological applications of gold nanoparticles*. Chemical Society Reviews, 2008. **37**(9): p. 1896-1908.
35. Alvarez-Puebla, R., L.M. Liz-Marzán, and F.J. García de Abajo, *Light concentration at the nanometer scale*. The Journal of Physical Chemistry Letters, 2010. **1**(16): p. 2428-2434.
36. Albanese, A. and W.C. Chan, *Effect of gold nanoparticle aggregation on cell uptake and toxicity*. ACS nano, 2011. **5**(7): p. 5478-5489.

37. Perrault, S.D., C. Walkey, T. Jennings, H.C. Fischer, and W.C. Chan, *Mediating tumor targeting efficiency of nanoparticles through design*. Nano letters, 2009. **9**(5): p. 1909-1915.
38. Pan, Y., S. Neuss, A. Leifert, M. Fischler, F. Wen, U. Simon, G. Schmid, W. Brandau, and W. Jahnen-Dechent, *Size-dependent cytotoxicity of gold nanoparticles*. Small, 2007. **3**(11): p. 1941-1949.
39. Bastús, N.G., J. Comenge, and V. Puntes, *Kinetically controlled seeded growth synthesis of citrate-stabilized gold nanoparticles of up to 200 nm: size focusing versus Ostwald ripening*. Langmuir, 2011. **27**(17): p. 11098-11105.
40. Piella, J., N.G. Bastús, and V. Puntes, *Size-Controlled Synthesis of Sub-10-nanometer Citrate-Stabilized Gold Nanoparticles and Related Optical Properties*. Chemistry of Materials, 2016. **28**(4): p. 1066-1075.
41. Hühn, J., C. Carrillo-Carrion, M.G. Soliman, C. Pfeiffer, D. Valdeperez, A. Masood, I. Chakraborty, L. Zhu, M. Gallego, and Z. Yue, *Selected standard protocols for the synthesis, phase transfer, and characterization of inorganic colloidal nanoparticles*. Chemistry of Materials, 2016. **29**(1): p. 399-461.
42. Turkevich, J., P.C. Stevenson, and J. Hillier, *A study of the nucleation and growth processes in the synthesis of colloidal gold*. Discussions of the Faraday Society, 1951. **11**: p. 55-75.
43. Enustun, B. and J. Turkevich, *Coagulation of colloidal gold*. Journal of the American Chemical Society, 1963. **85**(21): p. 3317-3328.
44. Frens, G., *Controlled nucleation for the regulation of the particle size in monodisperse gold suspensions*. Nature physical science, 1973. **241**(105): p. 20.
45. Ye, X., L. Jin, H. Caglayan, J. Chen, G. Xing, C. Zheng, V. Doan-Nguyen, Y. Kang, N. Engheta, and C.R. Kagan, *Improved size-tunable synthesis of monodisperse gold nanorods through the use of aromatic additives*. ACS nano, 2012. **6**(3): p. 2804-2817.
46. Ye, X., C. Zheng, J. Chen, Y. Gao, and C.B. Murray, *Using binary surfactant mixtures to simultaneously improve the dimensional tunability and monodispersity in the seeded growth of gold nanorods*. Nano letters, 2013. **13**(2): p. 765-771.
47. Shankar, S.S., A. Rai, B. Ankamwar, A. Singh, A. Ahmad, and M. Sastry, *Biological synthesis of triangular gold nanoprisms*. Nature materials, 2004. **3**(7): p. 482.
48. Nehl, C.L., H. Liao, and J.H. Hafner, *Optical properties of star-shaped gold nanoparticles*. Nano letters, 2006. **6**(4): p. 683-688.
49. Chen, H., X. Kou, Z. Yang, W. Ni, and J. Wang, *Shape-and size-dependent refractive index sensitivity of gold nanoparticles*. Langmuir, 2008. **24**(10): p. 5233-5237.
50. Xie, J., Q. Zhang, J.Y. Lee, and D.I. Wang, *The synthesis of SERS-active gold nanoflower tags for in vivo applications*. ACS nano, 2008. **2**(12): p. 2473-2480.
51. Yang, H., Z. Chen, L. Zhang, W.Y. Yung, K.C.F. Leung, H.Y.E. Chan, and C.H.J. Choi, *Mechanism for the cellular uptake of targeted gold nanorods of defined aspect ratios*. Small, 2016. **12**(37): p. 5178-5189.
52. Jain, P.K., X. Huang, I.H. El-Sayed, and M.A. El-Sayed, *Noble metals on the nanoscale: optical and photothermal properties and some applications in imaging, sensing, biology, and medicine*. Accounts of chemical research, 2008. **41**(12): p. 1578-1586.
53. Dreaden, E.C., A.M. Alkilany, X. Huang, C.J. Murphy, and M.A. El-Sayed, *The golden age: gold nanoparticles for biomedicine*. Chemical Society Reviews, 2012. **41**(7): p. 2740-2779.
54. Wiesner, J. and A. Wokaun, *Anisometric gold colloids. Preparation, characterization, and optical properties*. Chemical Physics Letters, 1989. **157**(6): p. 569-575.
55. Li, Z., S. Tang, B. Wang, Y. Li, H. Huang, H. Wang, P. Li, C. Li, P.K. Chu, and X.-F. Yu, *Metabolizable small gold nanorods: Size-dependent cytotoxicity, cell uptake and in vivo biodistribution*. ACS Biomaterials Science & Engineering, 2016. **2**(5): p. 789-797.

56. Chang, H.-H. and C.J. Murphy, *Mini gold nanorods with tunable plasmonic peaks beyond 1000 nm*. Chemistry of Materials, 2018. **30**(4): p. 1427-1435.
57. Gu, H., K. Xu, C. Xu, and B. Xu, *Biofunctional magnetic nanoparticles for protein separation and pathogen detection*. Chemical Communications, 2006(9): p. 941-949.
58. Piao, Y., J. Kim, H.B. Na, D. Kim, J.S. Baek, M.K. Ko, J.H. Lee, M. Shokouhimehr, and T. Hyeon, *Wrap–bake–peel process for nanostructural transformation from β -FeOOH nanorods to biocompatible iron oxide nanocapsules*. Nature materials, 2008. **7**(3): p. 242.
59. Sonvico, F., S. Mornet, S. Vasseur, C. Dubernet, D. Jaillard, J. Degrouard, J. Hoebeke, E. Duguet, P. Colombo, and P. Couvreur, *Folate-conjugated iron oxide nanoparticles for solid tumor targeting as potential specific magnetic hyperthermia mediators: synthesis, physicochemical characterization, and in vitro experiments*. Bioconjugate chemistry, 2005. **16**(5): p. 1181-1188.
60. Heymer, A., D. Haddad, M. Weber, U. Gbureck, P.M. Jakob, J. Eulert, and U. Nöth, *Iron oxide labelling of human mesenchymal stem cells in collagen hydrogels for articular cartilage repair*. Biomaterials, 2008. **29**(10): p. 1473-1483.
61. Kim, B.H., N. Lee, H. Kim, K. An, Y.I. Park, Y. Choi, K. Shin, Y. Lee, S.G. Kwon, and H.B. Na, *Large-scale synthesis of uniform and extremely small-sized iron oxide nanoparticles for high-resolution T 1 magnetic resonance imaging contrast agents*. Journal of the American Chemical Society, 2011. **133**(32): p. 12624-12631.
62. Bourrinet, P., H.H. Bengel, B. Bonnemain, A. Dencausse, J.-M. Idee, P.M. Jacobs, and J.M. Lewis, *Preclinical safety and pharmacokinetic profile of ferumoxtran-10, an ultrasmall superparamagnetic iron oxide magnetic resonance contrast agent*. Investigative radiology, 2006. **41**(3): p. 313-324.
63. Simonsen, C.Z., L. Østergaard, P. Vestergaard-Poulsen, L. Røhl, A. Bjørnerud, and C. Gyldensted, *CBF and CBV measurements by USPIO bolus tracking: reproducibility and comparison with Gd-based values*. Journal of Magnetic Resonance Imaging: An Official Journal of the International Society for Magnetic Resonance in Medicine, 1999. **9**(2): p. 342-347.
64. Bulte, J.W. and D.L. Kraitchman, *Iron oxide MR contrast agents for molecular and cellular imaging*. NMR in Biomedicine: An International Journal Devoted to the Development and Application of Magnetic Resonance In Vivo, 2004. **17**(7): p. 484-499.
65. Park, J., J. Joo, S.G. Kwon, Y. Jang, and T. Hyeon, *Synthesis of monodisperse spherical nanocrystals*. Angewandte Chemie International Edition, 2007. **46**(25): p. 4630-4660.
66. Park, J., K. An, Y. Hwang, J.-G. Park, H.-J. Noh, J.-Y. Kim, J.-H. Park, N.-M. Hwang, and T. Hyeon, *Ultra-large-scale syntheses of monodisperse nanocrystals*. Nature materials, 2004. **3**(12): p. 891.
67. Reddy, L.H., J.L. Arias, J. Nicolas, and P. Couvreur, *Magnetic nanoparticles: design and characterization, toxicity and biocompatibility, pharmaceutical and biomedical applications*. Chemical reviews, 2012. **112**(11): p. 5818-5878.
68. Ling, D. and T. Hyeon, *Chemical design of biocompatible iron oxide nanoparticles for medical applications*. Small, 2013. **9**(9-10): p. 1450-1466.
69. Hyeon, T., S.S. Lee, J. Park, Y. Chung, and H.B. Na, *Synthesis of highly crystalline and monodisperse maghemite nanocrystallites without a size-selection process*. Journal of the American Chemical Society, 2001. **123**(51): p. 12798-12801.
70. Kwon, S.G., Y. Piao, J. Park, S. Angappane, Y. Jo, N.-M. Hwang, J.-G. Park, and T. Hyeon, *Kinetics of monodisperse iron oxide nanocrystal formation by "heating-up" process*. Journal of the American Chemical Society, 2007. **129**(41): p. 12571-12584.
71. William, W.Y., J.C. Falkner, C.T. Yavuz, and V.L. Colvin, *Synthesis of monodisperse iron oxide nanocrystals by thermal decomposition of iron carboxylate salts*. Chemical Communications, 2004(20): p. 2306-2307.

72. Kim, D., N. Lee, M. Park, B.H. Kim, K. An, and T. Hyeon, *Synthesis of uniform ferrimagnetic magnetite nanocubes*. Journal of the American Chemical Society, 2008. **131**(2): p. 454-455.
73. Park, J., E. Lee, N.M. Hwang, M. Kang, S.C. Kim, Y. Hwang, J.G. Park, H.J. Noh, J.Y. Kim, and J.H. Park, *One - nanometer - scale size - controlled synthesis of monodisperse magnetic Iron oxide nanoparticles*. Angewandte Chemie, 2005. **117**(19): p. 2932-2937.
74. Kim, B.H., K. Shin, S.G. Kwon, Y. Jang, H.-S. Lee, H. Lee, S.W. Jun, J. Lee, S.Y. Han, and Y.-H. Yim, *Sizing by weighing: characterizing sizes of ultrasmall-sized iron oxide nanocrystals using MALDI-TOF mass spectrometry*. Journal of the American Chemical Society, 2013. **135**(7): p. 2407-2410.
75. Keller, A.A., H. Wang, D. Zhou, H.S. Lenihan, G. Cherr, B.J. Cardinale, R. Miller, and Z. Ji, *Stability and aggregation of metal oxide nanoparticles in natural aqueous matrices*. Environmental science & technology, 2010. **44**(6): p. 1962-1967.
76. Chen, Y., Y. Xianyu, and X. Jiang, *Surface Modification of Gold Nanoparticles with Small Molecules for Biochemical Analysis*. Accounts of chemical research, 2017. **50**(2): p. 310-319.
77. Xu, J.-J., W.-W. Zhao, S. Song, C. Fan, and H.-Y. Chen, *Functional nanoprobe for ultrasensitive detection of biomolecules: an update*. Chemical Society Reviews, 2014. **43**(5): p. 1601-1611.
78. Chen, W., S. He, W. Pan, Y. Jin, W. Zhang, and X. Jiang, *Strategy for the modification of electrospun fibers that allows diverse functional groups for biomolecular entrapment*. Chemistry of Materials, 2010. **22**(23): p. 6212-6214.
79. Wu, X., H. Liu, J. Liu, K.N. Haley, J.A. Treadway, J.P. Larson, N. Ge, F. Peale, and M.P. Bruchez, *Immunofluorescent labeling of cancer marker Her2 and other cellular targets with semiconductor quantum dots*. Nature biotechnology, 2003. **21**(1): p. 41.
80. Pellegrino, T., L. Manna, S. Kudera, T. Liedl, D. Koktysh, A.L. Rogach, S. Keller, J. Rädler, G. Natile, and W.J. Parak, *Hydrophobic nanocrystals coated with an amphiphilic polymer shell: a general route to water soluble nanocrystals*. Nano letters, 2004. **4**(4): p. 703-707.
81. Gao, X., Y. Cui, R.M. Levenson, L.W. Chung, and S. Nie, *In vivo cancer targeting and imaging with semiconductor quantum dots*. Nature biotechnology, 2004. **22**(8): p. 969.
82. Nikolic, M.S., M. Krack, V. Aleksandrovic, A. Kornowski, S. Förster, and H. Weller, *Tailor-Made Ligands for Biocompatible Nanoparticles*. Angewandte Chemie International Edition, 2006. **45**(39): p. 6577-6580.
83. Lin, C.A.J., R.A. Sperling, J.K. Li, T.Y. Yang, P.Y. Li, M. Zanella, W.H. Chang, and W.J. Parak, *Design of an amphiphilic polymer for nanoparticle coating and functionalization*. Small, 2008. **4**(3): p. 334-341.
84. Sperling, R.A., T. Pellegrino, J.K. Li, W.H. Chang, and W.J. Parak, *Electrophoretic separation of nanoparticles with a discrete number of functional groups*. Advanced functional materials, 2006. **16**(7): p. 943-948.
85. Soliman, M.G., B. Pelaz, W.J. Parak, and P. Del Pino, *Phase transfer and polymer coating methods toward improving the stability of metallic nanoparticles for biological applications*. Chemistry of Materials, 2015. **27**(3): p. 990-997.
86. Kreyling, W.G., A.M. Abdelmonem, Z. Ali, F. Alves, M. Geiser, N. Haberl, R. Hartmann, S. Hirn, D.J. de Aberasturi, K. Kantner, G. Khadem-Saba, J.-M. Montenegro, J. Rejman, T. Rojo, I.R. de Larramendi, R. Ufartes, A. Wenk, and W.J. Parak, *In vivo integrity of polymer-coated gold nanoparticles*. Nature nanotechnology, 2015. **10**: p. 619.
87. Colombo, M., L. Fiandra, G. Alessio, S. Mazzucchelli, M. Nebuloni, C. De Palma, K. Kantner, B. Pelaz, R. Rotem, F. Corsi, W.J. Parak, and D. Prospero, *Tumour homing and therapeutic effect of colloidal nanoparticles depend on the number of attached antibodies*. Nature communications, 2016. **7**: p. 13818.
88. Lewinski, N., V. Colvin, and R. Drezek, *Cytotoxicity of Nanoparticles*. Small, 2008. **4**(1): p. 26-49.

89. Wolinsky, H., *Nanoregulation: a recent scare involving nanotech products reveals that the technology is not yet properly regulated*. EMBO reports, 2006. **7**(9): p. 858-861.
90. Long, T.C., N. Saleh, R.D. Tilton, G.V. Lowry, and B. Veronesi, *Titanium dioxide (P25) produces reactive oxygen species in immortalized brain microglia (BV2): implications for nanoparticle neurotoxicity*. Environmental science & technology, 2006. **40**(14): p. 4346-4352.
91. Nold, P., R. Hartmann, N. Feliu, K. Kantner, M. Gamal, B. Pelaz, J. Hühn, X. Sun, P. Jungebluth, and P. Pino, *Optimizing conditions for labeling of mesenchymal stromal cells (MSCs) with gold nanoparticles: a prerequisite for in vivo tracking of MSCs*. Journal of nanobiotechnology, 2017. **15**(1): p. 24.
92. Pan, Y., S. Neuss, A. Leifert, M. Fischler, F. Wen, U. Simon, G. Schmid, W. Brandau, and W. Jahnen-Dechent, *Size-Dependent Cytotoxicity of Gold Nanoparticles*. Small, 2007. **3**(11): p. 1941-1949.
93. Connor, E.E., J. Mwamuka, A. Gole, C.J. Murphy, and M.D. Wyatt, *Gold Nanoparticles Are Taken Up by Human Cells but Do Not Cause Acute Cytotoxicity*. Small, 2005. **1**(3): p. 325-327.
94. He, H., X. Sun, X. Wang, and H. Xu, *Synthesis of highly luminescent and biocompatible CdTe/CdS/ZnS quantum dots using microwave irradiation: a comparative study of different ligands*. Luminescence, 2014. **29**(7): p. 837-845.
95. Bhirde, A., J. Xie, M. Swierczewska, and X. Chen, *Nanoparticles for cell labeling*. Nanoscale, 2011. **3**(1): p. 142-153.
96. Chithrani, B.D., A.A. Ghazani, and W.C. Chan, *Determining the size and shape dependence of gold nanoparticle uptake into mammalian cells*. Nano letters, 2006. **6**(4): p. 662-668.
97. Li, J., J. Zhang, X. Wang, N. Kawazoe, and G. Chen, *Gold nanoparticle size and shape influence on osteogenesis of mesenchymal stem cells*. Nanoscale, 2016. **8**(15): p. 7992-8007.
98. He, C., Y. Hu, L. Yin, C. Tang, and C. Yin, *Effects of particle size and surface charge on cellular uptake and biodistribution of polymeric nanoparticles*. Biomaterials, 2010. **31**(13): p. 3657-3666.
99. Del Pino, P., F. Yang, B. Pelaz, Q. Zhang, K. Kantner, R. Hartmann, N. Martinez de Baroja, M. Gallego, M. Möller, and B.B. Manshian, *Basic physicochemical properties of polyethylene glycol coated gold nanoparticles that determine their interaction with cells*. Angewandte Chemie International Edition, 2016. **55**(18): p. 5483-5487.
100. Hartmann, R., M. Weidenbach, M. Neubauer, A. Fery, and W.J. Parak, *Stiffness-dependent in vitro uptake and lysosomal acidification of colloidal particles*. Angewandte Chemie International Edition, 2015. **54**(4): p. 1365-1368.
101. Feliu, N., X. Sun, R.A. Alvarez Puebla, and W.J. Parak, *Quantitative particle-cell interaction: some basic physicochemical pitfalls*. Langmuir, 2017. **33**(27): p. 6639-6646.
102. Cho, E.C., Q. Zhang, and Y. Xia, *The effect of sedimentation and diffusion on cellular uptake of gold nanoparticles*. Nature nanotechnology, 2011. **6**(6): p. 385.
103. Xu, M., M.G. Soliman, X. Sun, B. Pelaz, N. Feliu, W.J. Parak, and S. Liu, *How Entanglement of Different Physicochemical Properties Complicates the Prediction of in vitro and in vivo Interactions of Gold Nanoparticles*. ACS nano, 2018.
104. Pelaz, B., P. del Pino, P. Maffre, R. Hartmann, M. Gallego, S. Rivera-Fernandez, J.M. de la Fuente, G.U. Nienhaus, and W.J. Parak, *Surface functionalization of nanoparticles with polyethylene glycol: effects on protein adsorption and cellular uptake*. ACS nano, 2015. **9**(7): p. 6996-7008.
105. Lundqvist, M., *Nanoparticles: tracking protein corona over time*. Nature nanotechnology, 2013. **8**(10): p. 701.
106. Lorsch, J.R., F.S. Collins, and J. Lippincott-Schwartz, *Fixing problems with cell lines*. Science, 2014. **346**(6216): p. 1452-1453.

107. Pan, C., C. Kumar, S. Bohl, U. Klingmueller, and M. Mann, *Comparative proteomic phenotyping of cell lines and primary cells to assess preservation of cell type-specific functions*. *Molecular & Cellular Proteomics*, 2009. **8**(3): p. 443-450.
108. Alge, C.S., S.M. Hauck, S.G. Priglinger, A. Kampik, and M. Ueffing, *Differential protein profiling of primary versus immortalized human RPE cells identifies expression patterns associated with cytoskeletal remodeling and cell survival*. *Journal of proteome research*, 2006. **5**(4): p. 862-878.
109. Wu, L.-G., E. Hamid, W. Shin, and H.-C. Chiang, *Exocytosis and endocytosis: modes, functions, and coupling mechanisms*. *Annual review of physiology*, 2014. **76**: p. 301-331.
110. Zhang, S., H. Gao, and G. Bao, *Physical Principles of Nanoparticle Cellular Endocytosis*. *ACS nano*, 2015. **9**(9): p. 8655-8671.
111. Swanson, J.A., *Shaping cups into phagosomes and macropinosomes*. *Nature reviews Molecular cell biology*, 2008. **9**(8): p. 639.
112. Mooren, O.L., B.J. Galletta, and J.A. Cooper, *Roles for actin assembly in endocytosis*. *Annual review of biochemistry*, 2012. **81**: p. 661-686.
113. Marsh, M. and A. Helenius, *Virus entry: open sesame*. *Cell*, 2006. **124**(4): p. 729-740.
114. Cavalli, V., M. Corti, and J. Gruenberg, *Endocytosis and signaling cascades: a close encounter*. *FEBS letters*, 2001. **498**(2-3): p. 190-196.
115. Ding, H.-m., W.-d. Tian, and Y.-q. Ma, *Designing nanoparticle translocation through membranes by computer simulations*. *ACS nano*, 2012. **6**(2): p. 1230-1238.
116. Wang, X., X. Sun, H. He, H. Yang, J. Lao, Y. Song, Y. Xia, H. Xu, X. Zhang, and F. Huang, *A two-component active targeting theranostic agent based on graphene quantum dots*. *Journal of Materials Chemistry B*, 2015. **3**(17): p. 3583-3590.
117. Turgeman, L. and D. Fixler, *Photon efficiency optimization in time-correlated single photon counting technique for fluorescence lifetime imaging systems*. *IEEE Transactions on Biomedical Engineering*, 2013. **60**(6): p. 1571-1579.
118. Jha, P., D. Golovko, S. Bains, D. Hostetter, R. Meier, M.F. Wendland, and H.E. Daldrup-Link, *Monitoring of natural killer cell immunotherapy using noninvasive imaging modalities*. *Cancer research*, 2010. **70**(15): p. 6109-6113.
119. Zhang, S.J. and J.C. Wu, *Comparison of imaging techniques for tracking cardiac stem cell therapy*. *Journal of Nuclear Medicine*, 2007. **48**(12): p. 1916-1919.
120. Schenkman, L., *Second thoughts about CT imaging*. 2011, American Association for the Advancement of Science.
121. Rosen, J., S. Yoffe, A. Meerasa, M. Verma, and F. Gu, *Nanotechnology and diagnostic imaging: new advances in contrast agent technology*. *J. Nanomed. Nanotechnol*, 2011. **2**(5): p. 1-12.
122. Aillon, K.L., N. El-Gendy, C. Dennis, J.P. Norenberg, J. McDonald, and C. Berkland, *Iodinated NanoClusters as an inhaled computed tomography contrast agent for lung visualization*. *Molecular pharmaceutics*, 2010. **7**(4): p. 1274-1282.
123. Hyafil, F., J.-C. Cornily, J.E. Feig, R. Gordon, E. Vucic, V. Amirbekian, E.A. Fisher, V. Fuster, L.J. Feldman, and Z.A. Fayad, *Noninvasive detection of macrophages using a nanoparticulate contrast agent for computed tomography*. *Nature medicine*, 2007. **13**(5): p. 636.
124. Mahmoudi, M., V. Serpooshan, and S. Laurent, *Engineered nanoparticles for biomolecular imaging*. *Nanoscale*, 2011. **3**(8): p. 3007-3026.
125. Cormode, D.P., E. Roessl, A. Thran, T. Skajaa, R.E. Gordon, J.-P. Schlomka, V. Fuster, E.A. Fisher, W.J. Mulder, and R. Proksa, *Atherosclerotic plaque composition: analysis with multicolor CT and targeted gold nanoparticles*. *Radiology*, 2010. **256**(3): p. 774-782.
126. Galper, M.W., M.T. Saung, V. Fuster, E. Roessl, A. Thran, R. Proksa, Z.A. Fayad, and D.P. Cormode, *Effect of computed tomography scanning parameters on gold nanoparticle and iodine contrast*. *Investigative radiology*, 2012. **47**(8): p. 475.

127. Huang, P., L. Bao, C. Zhang, J. Lin, T. Luo, D. Yang, M. He, Z. Li, G. Gao, and B. Gao, *Folic acid-conjugated silica-modified gold nanorods for X-ray/CT imaging-guided dual-mode radiation and photo-thermal therapy*. *Biomaterials*, 2011. **32**(36): p. 9796-9809.
128. Von Maltzahn, G., J.-H. Park, A. Agrawal, N.K. Bandaru, S.K. Das, M.J. Sailor, and S.N. Bhatia, *Computationally guided photothermal tumor therapy using long-circulating gold nanorod antennas*. *Cancer research*, 2009. **69**(9): p. 3892-3900.
129. Chou, S.-W., Y.-H. Shau, P.-C. Wu, Y.-S. Yang, D.-B. Shieh, and C.-C. Chen, *In vitro and in vivo studies of FePt nanoparticles for dual modal CT/MRI molecular imaging*. *Journal of the American Chemical Society*, 2010. **132**(38): p. 13270-13278.
130. Alric, C., J. Taleb, G. Le Duc, C. Mandon, C. Billotey, A. Le Meur-Herland, T. Brochard, F. Vocanson, M. Janier, and P. Perriat, *Gadolinium chelate coated gold nanoparticles as contrast agents for both X-ray computed tomography and magnetic resonance imaging*. *Journal of the American Chemical Society*, 2008. **130**(18): p. 5908-5915.
131. Sun, H., Q. Yuan, B. Zhang, K. Ai, P. Zhang, and L. Lu, *Gd III functionalized gold nanorods for multimodal imaging applications*. *Nanoscale*, 2011. **3**(5): p. 1990-1996.
132. Na, H.B., I.C. Song, and T. Hyeon, *Inorganic nanoparticles for MRI contrast agents*. *Advanced Materials*, 2009. **21**(21): p. 2133-2148.
133. Shapiro, E.M., S. Skrtic, K. Sharer, J.M. Hill, C.E. Dunbar, and A.P. Koretsky, *MRI detection of single particles for cellular imaging*. *Proc Natl Acad Sci U S A*, 2004. **101**(30): p. 10901-6.
134. Zhu, D., R.D. White, P.A. Hardy, N. Weerapreeyakul, K. Sutthanut, and M. Jay, *Biocompatible nanotemplate-engineered nanoparticles containing gadolinium: stability and relaxivity of a potential MRI contrast agent*. *J Nanosci Nanotechnol*, 2006. **6**(4): p. 996-1003.
135. Teja, A.S. and P.-Y. Koh, *Synthesis, properties, and applications of magnetic iron oxide nanoparticles*. *Progress in Crystal Growth and Characterization of Materials*, 2009. **55**(1): p. 22-45.
136. Sun, C., J.S. Lee, and M. Zhang, *Magnetic nanoparticles in MR imaging and drug delivery*. *Adv Drug Deliv Rev*, 2008. **60**(11): p. 1252-65.
137. Ling, D., N. Lee, and T. Hyeon, *Chemical synthesis and assembly of uniformly sized iron oxide nanoparticles for medical applications*. *Accounts of chemical research*, 2015. **48**(5): p. 1276-1285.
138. Jun, Y.-w., J.-w. Seo, and J. Cheon, *Nanoscaling laws of magnetic nanoparticles and their applicabilities in biomedical sciences*. *Accounts of chemical research*, 2008. **41**(2): p. 179-189.

List of publications

The described data in the previous chapters is based on my publications during my PhD study from 2015 to 2019, which are listed below. Each publication is briefly summarized and contributions to these publications are also described. The publications (published, submitted or in preparation) are attached in the Appendix.

1. **Sun, X.**, Soliman, M. G., Nold, P., Said, A. H., Chakraborty, I., Pelaz, B., Schmied, F., von Pückler, K., Figiel, J., Zhao, Y., Brendel, C., Hassan, M., Parak, W. & Feliu, N. (2019) Tracking stem cells and macrophages with gold and iron oxide nanoparticles - the choice of the best suited particles. *Applied Materials Today*. 15(2019)267–279.

In this paper a library of PMA coated NPs of different sizes, shapes and core materials were synthesized. The amount of NPs which can be delivered to different cells in relation to the physicochemical properties of the NPs was investigated. From the study we optimized the conditions to label stem cells and macrophages with a library of gold and iron oxide NPs of different sizes (5–100 nm core diameter) and shapes.

The author contributed to all of the experiments of NPs synthesis, cell experiment, data analysis, as well as to the writing and editing of the manuscript.

2. Xu, M., Soliman, M. G., **Sun, X.**, Pelaz, B., Feliu, N., Parak, W. J., & Liu, S. (2018). How Entanglement of Different Physicochemical Properties Complicates the Prediction of in vitro and in vivo Interactions of Gold Nanoparticles. *ACS Nano*, 12(10), 10104-10113.

In this paper a set of 21 different AuNPs were used to study protein corona formation, in vitro uptake, effect on cell viability and proliferation, and in vivo biodistribution of NPs. The results show that the physicochemical properties of AuNPs are mainly accounted for by their hydrodynamic diameter and their zeta-potential. The formation of the protein corona is determined by the pH-dependence of their zeta-potential.

The author contributed to the experiments of NPs synthesis, in vitro uptake, and cell viability assessment, as well as to the writing and editing of the manuscript.

3. Feliu, N., **Sun, X.**, Alvarez Puebla, R. A., & Parak, W. J. (2017). Quantitative particle–cell interaction: some basic physicochemical pitfalls. *Langmuir*, 33(27), 6639-6646.

In this paper the particle–cell interaction studies was discussed in relation of gravity, Brownian motion, and interparticle interactions. The actual in vitro scenario of NPs exposure was shown, which offers a deep insight of the between in vitro and in vivo experiment.

Meanwhile the underlying physic models were used for the explanations. From this study we know that the state of dispersion to some extent determine NP-cell interactions.

The author contributed to the discussion of the influence of dispersion state on the NP-cell interactions, as well as to the editing of the figures and manuscript.

4. Nold, P., Hartmann, R., Feliu, N., Kantner, K., Gamal, M., Pelaz, B., Hühn, J. **Sun, X.**, Jungebluth, P., del Pino, P., Hackstein, H., Macchiarini, P., P, Parak, W., and Brendel, C. (2017). Optimizing conditions for labeling of mesenchymal stromal cells (MSCs) with gold nanoparticles: a prerequisite for in vivo tracking of MSCs. *Journal of Nanobiotechnology*, 15(1), 24.

In this paper, the exocytosis versus endocytosis were studied in the process of cell labeling. Then the cell viability and migration of MSCs were discussed in the following. From this paper we established an optimized labeling strategy for human MSCs with AuNPs that preserves their migratory capacity in vivo. A gentle and efficient labeling strategy for human MSCs that is applicable in vivo was described, which paves the way for future clinical applications.

The author contributed to the experiments of NPs synthesis, cell viability assessment, and cell imaging as well as to the writing and editing of the manuscript.

5. **Sun, X.**, Feliu, N., & Parak, W. J. Uptake study of different sized and shaped gold nanoparticles in static and dynamic condition **[In preparation]**

In this work, a library of PMA coated NPs of different sizes and shapes were synthesized. The amount of NPs which can be delivered to different cells in relation to the physicochemical properties of the NPs was investigated. From the study we discussed the influence of static and dynamic conditions as well as the cycling fluid system on NP-cell interaction.

The author contributed to all of the experiments of NPs synthesis, cell experiment, data analysis, as well as to the writing and editing of the manuscript.

Bibliography

Personal Information

Name: Xing	Family name: Sun
Birthplace: Henan, China	Nationality: Chinese

Education

2015.09-2019.06	Hamburg University, AG Biophotonics (Prof. Wolfgang Parak) Doctor of Natural Sciences
2012.09-2015.06	China University of Petroleum (East China) Master in Chemistry
2008.09-2012.06	China University of Petroleum (East China) Bachelor in Chemistry

Acknowledgements

Here I write my thankfulness part of my thesis at the moment when my Ph.D. study is about to finish. When looking back to this journey, I have to say every Ph.D. degree is not easy to get, especially when this degree is got in another foreign country. One person alone, it is almost not possible to accomplish such a huge amount of work. With the help of the people surrounding and moving forward step by step, I get the chance to see the finishing line of this long run ahead. Full of gratefulness and thankfulness, maybe this is the reason why in every thesis, there is always one part named "Acknowledgements".

First of all, I want to thank my supervisor Wolfgang Parak. Because of him, I got the chance to spend some of my youth time in Germany. Because of him, I can get the chance to study in Germany and participate some interesting and promising projects, which give me a better and deep understanding into the nano science.

The second part, I want to thank my co-supervisor Neus Feliu, my mini boss. Her careful thinking and encouraging and humorous characteristics always motivate me and give me energy and hope to finish my hard project. Her good attitude makes me realize: many times it does not mean the work is too hard, only because we do not choose the right attitude to conquer them. Always be positive and optimistic, it will always be helpful to win a good game.

Thirdly, I would like to thank my parents and my brother. Even in a place far away, I can feel their encouragement. In a time of hardness and full of senses of failure, it is their hands to pull me out. I feel very lucky to be a member of a warm family.

Finally, I would like to all of the good friends come to my life in this period of time, they are like the shiny stars in the beautiful evening sky. They did not do any academic help for my Ph.D. study, but their accompany let me know there are beautiful scenery when I feel tired and just looking into the sky, there will be happiness I will get. Coming a little early or a little late, they are my valuable treasures I get here. Interestingly, I feel happy to build a friendly Hamburg zoo, the monkey, squirrel, giraffe, eagle, elephant, zebra, seal, unicorn, crocodile, bear, owl, mushroom etc. Funny...

It is really a long journey to finish the Ph.D., hard but also beautiful. Here I want to show all my thankfulness again to every interesting souls coming to me, thanks for your company, thanks for your encouragement and thanks for your special characters. Nothing could be better. Good!

Declaration on oath

"I hereby declare on oath, that I have written the present dissertation by my own and have not used other than the acknowledged resources and aids. The submitted written version corresponds to the version on the electronic storage medium. I hereby declare that I have not previously applied or pursued for a doctorate (Ph.D. studies)."

Date:

09.08.2019

Signature:

A handwritten signature in black ink, appearing to be 'Ling S', written in a cursive style.



Tracking stem cells and macrophages with gold and iron oxide nanoparticles – The choice of the best suited particles

Xing Sun^a, Mahmoud Gamal^b, Philipp Nold^c, Alaa Said^{b,d}, Indranath Chakraborty^a, Beatriz Pelaz^b, Franziska Schmied^e, Kerstin von Pückler^e, Jens Figiel^f, Ying Zhao^{g,h}, Cornelia Brendel^{c,f}, Moustapha Hassan^{g,h}, Wolfgang J. Parak^{a,b,i}, Neus Feliu^{a,g,*}

^a Center for Hybrid Nanostructures (CHyN), University of Hamburg, Hamburg, Germany

^b Department of Physics, Philipps-University of Marburg, Marburg, Germany

^c Department of Hematology, Oncology and Immunology, Philipps University Marburg, Marburg, Germany

^d Electronic and Nano Devices Lab, Faculty of Science, South Valley University, Qena, Egypt

^e Department of Veterinary Clinical Sciences, Clinic for Small Animal–Surgery, Faculty of Veterinary Medicine, Justus–Liebig–University Giessen, Giessen, Germany

^f Department of Diagnostic and Interventional Radiology, University Hospital Marburg, Philipps-University of Marburg, Marburg, Germany

^g Experimental Cancer Medicine (ECM), Department of Laboratory Medicine, Karolinska Institutet, Sweden

^h Clinical Research Centre (KFC), Karolinska University Hospital, Stockholm, Sweden

ⁱ CIC Biomagune, San Sebastian, Spain

ARTICLE INFO

Article history:

Received 14 November 2018

Accepted 4 December 2018

Keywords:

Nanoparticles

Cell Tracking

Stem Cell Labeling

Gold Nanoparticles

Biocompatibility

Contrast

Computed tomography

ABSTRACT

Nanoparticle (NP)-based cell imaging offers good potential for future diagnosis tools in medicine. Gold and iron oxide NPs can be used as contrast agents for imaging by computed tomography (CT) and magnetic resonance imaging (MRI), respectively. Thus, also cells which have been labeled with these NPs may be tracked. This may be important for *in vivo* tracking of administered or transplanted cells. In this work, we optimized the conditions to label stem cells and macrophages with a library of gold and iron oxide NPs of different sizes (5–100 nm core diameter) and shapes. We investigated the amount of NPs which can be delivered to different cells, as well as their related toxic effects, in relation to the physicochemical properties of the NPs. Our study revealed that in general, when cells are exposed to NPs at similar elemental concentration (e.g., Au or Fe), bigger NPs lead to higher internalized elemental amounts as compared to exposure with smaller sized NPs. While the exposure concentrations are limited concerning the onset of toxicity, bigger NPs lead to better labeling than small NPs, resulting in improved contrast for imaging with enhanced biocompatibility.

© 2018 Elsevier Ltd. All rights reserved.

1. Introduction

For future nanoparticle (NP)-based diagnostics and therapeutics, *in vivo* delivery to the target site, such as tumors, is of importance. In general, for targeted delivery to tumors still sufficient accumulation of the NPs is a challenge [1]. Therefore, to overcome this limitation alternative strategies are under development. There are reports showing that stem cells as well as macrophages possess homing capabilities. After systemic administration, those cells could be found in inflamed, injured, and cancerous tissues [2–4]. Thus, these cells might act as delivery sys-

tems. They could be used for example as shuttle vehicles to deliver NPs to target sites such as zones of inflammation or tumors [4–6], potentially minimizing the clearance rate and toxicity associated to the NPs themselves. In the context of imaging, once reaching the target site, NPs can be used to provide contrast, e.g., superparamagnetic NPs for magnetic resonance imaging (MRI) [3,7–13], NPs composed of high atomic weight elements for computed tomography (CT) [14], plasmonic NPs for photoacoustic imaging [15,16], fluorescent NPs for fluorescence imaging [17,18], etc. In addition, the NPs from isotopes which do not naturally exist in the human body could be analyzed by inductively coupled plasma mass spectrometry (ICP-MS) [19]. In the context of treatment, Choi et al. showed that mouse macrophages loaded with liposomal doxorubicin (LP-Dox) enabled a more effective therapy as compared to the conventional administration of the drug, thus suggesting that the cells were able to migrate to the target site and effectively delivered

* Corresponding author at: Center for Hybrid Nanostructures (CHyN), University of Hamburg, Hamburg, Germany.

E-mail address: nfeliu@physnet.uni-hamburg.de (N. Feliu).

the LP-Dox [20]. Also NPs once delivered by cells to the target site, could be used for other therapeutic purposes, e.g., photothermal heating [21,22], photodynamic therapy [23], etc.

Concerning regenerative medicine, a deeper understanding of the fate of transplanted cells, including their recruitment into the target site, or their interaction with the host environment after infusion, as well as additional studies underling their efficiency and potential benefits are needed [24]. However, one of the current limitation is to monitor the transplanted cells *in vivo*. There are several approaches used to detect cells after administration. The most common methods are (i) *ex vivo* techniques such as the real-time polymerase chain reaction (RT-PCR), histology, etc. (ii) the evaluation of transplanted cells in peripheral blood by conventional flow cytometry, and (iii) a variety of imaging systems which allow to monitor the cell homing *in vivo* [2]. Indeed, in the recent years, new imaging technologies have facilitated the possibility to noninvasively monitor the fate of transplanted cells *in vivo* [25]. However, there is still room for improvement and several limitations still remain a challenge. In this context, the current advances in nanotechnology allowed the development and production of distinct NP probes for cellular labeling, which enable the use of new imaging modalities [26]. To some extent, NPs could be used as a sensitive probe for labeling cells, with higher sensitivity than the current approaches, e.g., standard fluorescence labeling. Different NPs have been frequently used as contrast agents for cellular imaging as described above [27,28].

As outlined with the above-mentioned examples, NP labeling of cells offers applications in imaging, as well as in potential diagnosis and treatment. In the following the focus will be toward imaging, though the results of our study also apply to the other applications. As a rule of thumb, the more NPs have been loaded to a cell, the higher the contrast due to the NPs for imaging (or in case of treatment with photothermal therapy the higher the production of induced heat) will be. Thus, concerning contrast as many NPs as possible should be introduced *per cell*. However, the more NPs have been loaded *per cell*, the higher the probability is that this impairs the viability, proliferation, and homing capabilities of cells [19]. Concerning toxic effects, thus there should be as few NPs loaded *per cell* as possible. For this reason, the optimum for NP-loading has to be experimentally established. Conditions may be modified depending on the NPs' sizes and shapes, as endocytosis as well as toxicity may depend on these two parameters [29,30]. In order to achieve the same contrast with NP labeling below the toxic threshold, is it better to load cells with more smaller or fewer bigger NPs? While there is a whole body of work available in literature, a large comparative study outlining improved labeling protocols is missing, which is the objective of this report.

The goal of the present work is to find optimum conditions for stem cells and macrophage labeling with gold (Au) and iron oxide (IO) NPs toward CT and MRI imaging, respectively, while verifying that the NPs have no acute effect on cellular properties. In this case, optimum conditions refer to the maximum amount of NPs that can be loaded into cells without impairing their viability and proliferation. In the case of CT, the contrast is basically determined by the amount of elemental gold [31,32]. AuNPs of different sizes and shapes obviously contain different amounts of Au *per NP*. "Big" NPs contain more Au *per NP*, but the bigger the NPs, the fewer of them are incorporated by cells [29]. On the other hand, while "small" NPs are internalized to a higher amount, due to their enhanced surface-to-volume ratio also their toxicity (at the same amount of delivered elemental Au) maybe higher [33]. The question thus is which size of AuNPs are most suited for cellular labeling and what is the maximum amount of elemental Au that can be added to cells. For MRI contrast, due to superparamagnetic FeO_x-based NPs (SPIONs) is not directly related to the amount of delivered iron (Fe), but also in this case the more IONPs have been internalized by cells the higher the

contrast will be. The present work involves a comprehensive study, in which 6 types of AuNPs of different sizes and shapes (spherical → NP, rod-shaped → NR), together with Iohexol and BaSO₄ as standard contrast agents (CAs) for CT, and 2 types of IONPs of different sizes, together with Gadodiamide as standard CA for MRI, were used to label three different types of stem cells and one macrophage cell line. Concentration-dependent uptake of NPs, exocytosis, cell viability, and proliferation were measured after 24 h and/or up to 72 h of exposure of NPs in serum supplemented medium. For each combination, the maximum amount of elemental Au or Fe that can be introduced to cells without impairing cell viability was determined, thus indicating the best labeling conditions. Comparison of results between the 4 different types of cells, three primary stem cell types, from different species and sources, human, horse, and dog which are abbreviated as MSCs throughout the manuscript, as well as murine alveolar macrophages (MHS), allows for a solid database to discuss generality of the results. Finally, CT and MRI imaging capabilities of NPs, CAs and NP-labeled cells are shown. Based on the maximum amount of elemental Au or Fe that can be incorporated *per cell* (uptake studies as measured by ICP-MS) and the CT and MRI calibration curves, the maximum contrast *per cell* for imaging could be also calculated.

2. Results and discussion

A library of AuNPs and IONPs of different sizes and shapes were synthesized exclusively for this study, adopting protocols from previous reports [34,35], see Fig. 1. The synthesis details and the full characterization of the NPs is provided in Supplement Information (SI, Section SI-I and SI-II). Cells were exposed to the NPs, whereby the amount of NPs which reach the surface of cells, which is a requirement for subsequent endocytosis, depends on the colloidal properties of the NPs [36]. In the following the NP dose is provided in terms of mass concentrations C_{Au} and C_{Fe} [mg/mL] of elemental Au and Fe for the AuNPs and IONPs, respectively. The corresponding molar NP concentrations are provided in SI [35].

The amount of Au and Fe found *per cell* ($m_{Au/cell}$ and $m_{Fe/cell}$) after exposing primary human, dog, and horse MSCs as well as MHS for 4 h, 24 h, and 48 h to AuNPs and IONPs at concentration C_{Au} and C_{Fe} , respectively, was determined by ICP-MS and is shown in Fig. 2 and Fig. SI-VII.1–9. In all cases concentration-dependent uptake was observed, which increased upon increasing NP concentration. Only in case of very high NP uptake, such as for 100 nm diameter spherical AuNPs, saturation effects were observed, in particular in the case of horse MSCs. The mass-concentrations C_{Au} and C_{Fe} of elemental Au and Fe form a more different metrics than the NP concentrations, as with increasing diameter each NP will comprise more atoms [30]. Thus, in order to account for different metrics and different representation, the same uptake data are plotted *versus* the NP concentrations C_{AuNP} and C_{IONP} in SI (section SI-VII). Due to presentation issues, the data shown in Fig. 2, which are the mean values of 3 independent experiments, are shown without error bars. The full data set for all experiments is provided in SI (section SI-VII). Our results indicate that the order of uptake for all different types of NPs was similar for the 4 different types of cells. In all cases at the same exposure concentration, 100 nm diameter spherical AuNPs yielded the most Au *per cell*, and 25 nm diameter spherical AuNPs delivered the lowest amount of Au *per cell* (see Table SI-VII.2). In general, at equal exposure conditions (in terms of Au concentration (C_{Au})), the bigger spherical AuNPs are capable of delivering more Au to cells as compared to the smaller sized AuNPs. Indeed, 40 and 100 nm rod shaped AuNPs (AuNRs) had lower uptake than the spherical NPs. As AuNRs with a length corresponding to the diameter of spherical AuNPs have a lower volume and thus mass *per NP* as spherical NPs, this is most likely due to mass-dependent

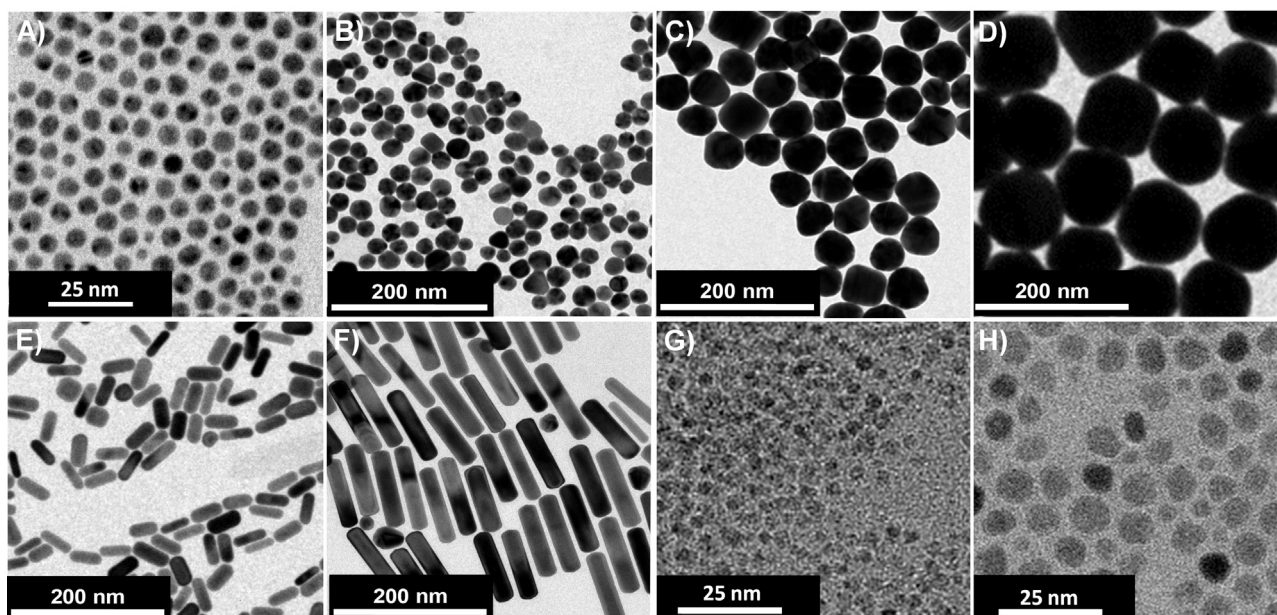


Fig. 1. (A) Transmission electron microscopy (TEM) images of the NP library used in the study: (A) 5 nm AuNPs, (B) 25 nm AuNPs, (C) 50 nm AuNPs, (D) 100 nm AuNPs, (E) 40 nm AuNRs, (F) 100 nm AuNRs, (G) 4 nm IONPs, and (H) 8 nm IONPs.

sedimentation [36] and not the size-dependent endocytosis [29]. Colloidal stability studies of spherical AuNPs in milliQ water and cell media supplemented with fetal bovine serum (FBS) were performed up to 72 h incubation, see Fig. 3A and SI (section II.4, Figs. SI-II.4.1.–4.3). As expected, the data indicated that 100 nm diameter spherical AuNPs followed by 50 nm diameter spherical AuNPs are the NPs with the highest percentage of sedimentation observed under our experimental conditions, which coincides with the highest amount of internalized Au found *per cell*, see Fig. 3B and C. Also for the IONPs the bigger NPs lead to (slightly) more internalized Fe *per cell*. In fact, enhanced uptake of big NPs in 2D cultures is driven by the local NP concentration at the cell surface, which depends on the sedimentation of the NPs, see Fig. 3D [36]. See SI for detailed information. It is important to have in consideration that NP suspensions may be subject to physicochemical transformations and thus the final NP dose delivered to the cells may be affected [37].

The uptake of NPs was time dependent. In general, both the NPs and CAs are internalized by cells in a time and concentration dependent manner. The uptake data after 4 h and 48 h of NP exposure, as well as CAs are shown in SI (section II.4). Indeed, for the desired doses, the uptake of NPs is higher than for the commercial CAs, even at lower doses (*i.e.* $C_{NP} \ll C_{CAs}$). For all the doses and time points evaluated, the human MSCs appear to internalize NPs at higher extent as compared to the other types of MSCs. On the other hand, for almost all conditions, the uptake of NPs by MHS macrophages is much higher than the uptake by MSCs. This is most probably due to the phagocytic properties of the macrophages MHS cells [38].

There are several factors influencing the labeling efficiency of cells. Living cells are dynamic entities, thus the NPs concentration within the cell will be altered by several cellular processes. Critical factors affecting the NP concentration within a cell will be the cell cycle, exocytosis, proliferation rate of the cells, *etc.*, see Fig. 4A [39,40]. In fact, we observed a variation in uptake concerning the 4 different types of cells (*cf.* Fig. 2, Section SI-VII). In the same exposure condition for the MSCs, the most Au was found in human MSCs, while the lowest in horse MSCs. Apart from detailed “biological” differences between different cell types, uptake of NPs by cells may be affected by the surface area of cells and by their proliferation rate,

as well as by other factors. For being delivered to cells, the NPs first have to come into contact with the cell surface, before they can be endocytosed. Therefore, one may hypothesize that the bigger the surface area of cells, the more NPs are likely to be internalized *per cell*. Upon cell division, incorporated NPs are distributed between the daughter cells [39], so the amount of internalized NPs *per cell* is diluted [41]. Thus, one may hypothesize that cells with a high proliferation rate thus should have less NPs *per cell* internalized. In order to probe both hypotheses, for each of the 4 cell types, their cross section area A_{cell} and their average time interval to cell division $T_{1/2,cell}$ were experimentally determined, see Table 1, Fig. 4B–D, and SI. Results show that, the human MSCs have the largest surface area A_{cell} and cell volume V_{cell} , followed by the dog MSCs, horse MSCs and MHS macrophages.

In general, the MHS macrophages whose cross-section surface ($A_{cell,sus}$) is around 2.7 times lower than the one of the human MSCs, have a higher NP uptake rate. This is probably due to their phagocytic capacity in contrast to the MSCs. Within the 3 different types of MSCs indeed the amount of NPs found inside each cells depends on the cellular cross-section area. In order to visualize this the amount of Au found *per cell* ($m_{Au/cell}$) can be normalized to the cell volume ($m_{Au/cell}/V_{cell}$), see Fig. 4E and F and SI §VII. The $m_{Au/cell}$ data indicate for example, that in the case of 100 nm AuNPs dog and horse MSCs incorporate much less AuNPs *per cell* than human MSCs (Fig. 3E). However, when normalizing to the cell volume, the $m_{Au/cell}/V_{cell}$ data indicate that this is in part due to the fact that the dog and horse MSCs are smaller than the human MSCs. We clearly need to state that there is no direct linear correlation between the amount of internalized NPs and the cross section area of cells, but that in the present data set MSCs with bigger surface often incorporate more NPs *per MSCs* than those with smaller surface area. As stated above, for dividing cells, the labeling efficiency or internalization of NPs also should be normalized to cell growth or proliferation rate, as the NPs are diluted upon each cell division. In Fig. 4G and H and SI §VII normalization concerning the proliferation rate is shown, in which the normalized amount of internalized NPs is given as $m_{Au/cell}/T_{1/2,cell}$. While again there is no direct correlation, data show that in MSCs faster proliferation leads to a lower mean number of internalized NPs *per cell*. At least part of the different uptake

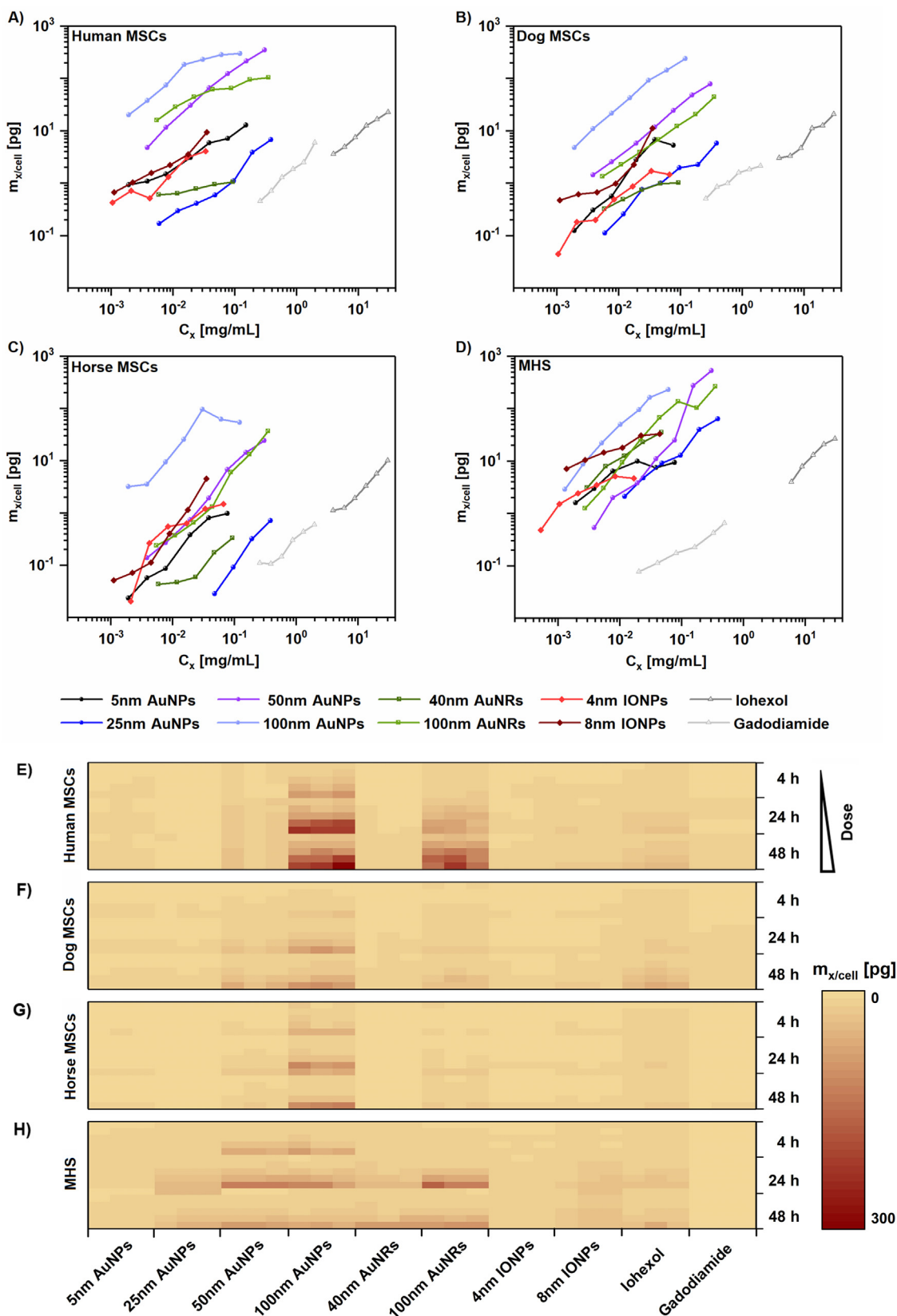


Fig. 2. Amount of elemental Au ($m_{x/cell} = m_{Au/cell}$) and Fe ($m_{x/cell} = m_{Fe/cell}$) found in MSCs and MHS macrophages after 24 h exposure to AuNPs and IONPs at different Au ($C_x = C_{Au}$) and Fe ($C_x = C_{Fe}$) concentrations, respectively. As control, cells were exposed to Iohexol and Gadodiamide at different I ($C_x = C_I$) and Gd ($C_x = C_{Gd}$) concentrations, and the amount of incorporated iodine ($m_{x/cell} = m_{I/cell}$) and gadolinium ($m_{x/cell} = m_{Gd/cell}$) per cell was determined, respectively. Data are shown for: (A) human MSCs, (B) dog MSCs, (C) horse MSCs, and (D) MHS macrophages. (E–H) Heat map representing the internalization studies of different cells conducted at 4 h, 24 h and 48 h (same data as displayed in A–D). The amount of incorporated NPs/contrast agents was determined as mass of elemental Au, Fe, I, Gd per cell by ICP-MS. The exposure is quantified as mass of added elemental Au, Fe, I, Gd per volume of solution, and not as mass of added NPs (which for example in case of IONPs also comprises the mass of oxygen and the surface coating/CAs). The results represent the mean value from minimum three independent experiments using cells from different donors or different cell passages. The error bars are omitted for clarity, see SI.

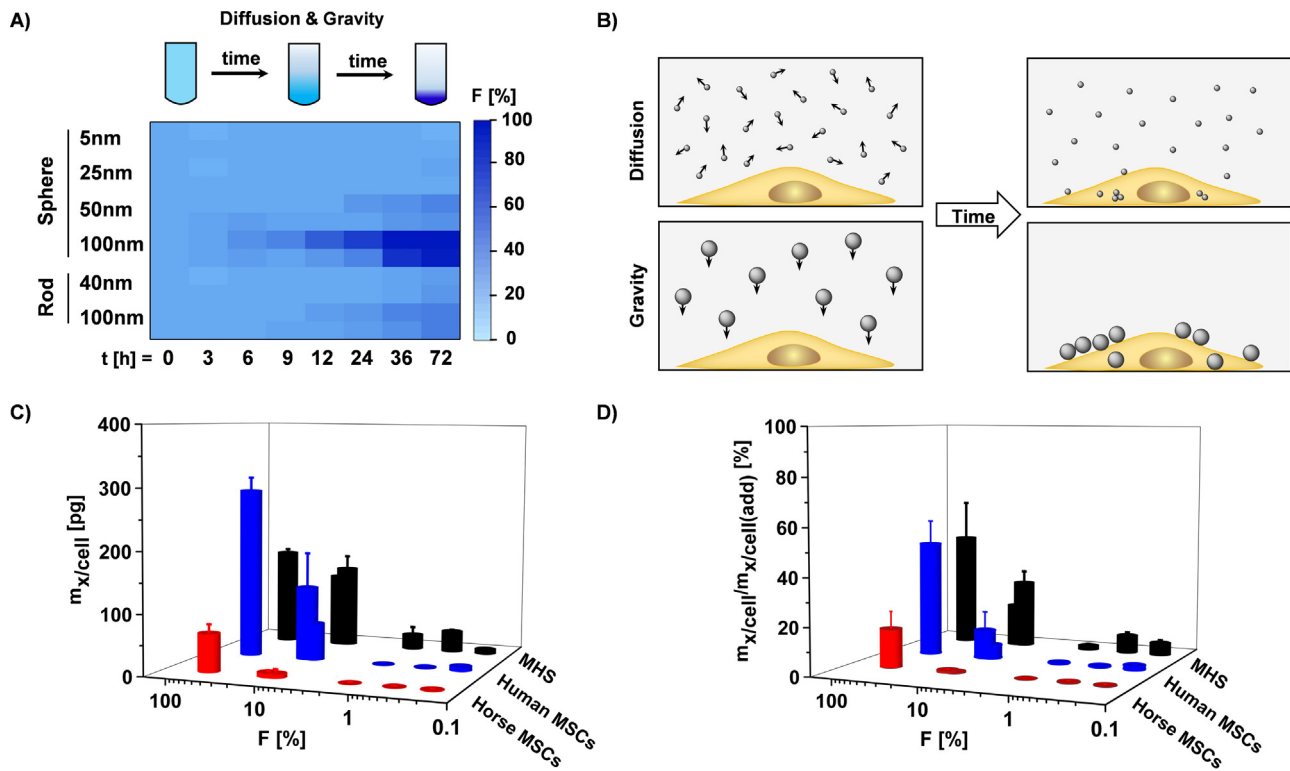


Fig. 3. (A) Sedimentation rate of the NPs dispersed in milliQ and complete cell media containing 10% FBS over time, as quantified by the fraction F [%] of NPs which from an originally dispersed solution has sedimented after a time t to the bottom of the tube ($n=3$). (B) Scheme illustrating the effects of basic colloidal properties of NPs on their cellular uptake. Knowing the colloidal properties of the NPs allows to consider the amount of NPs which will reach the cell surface in 2-dimensional (2D) *in vitro* cultures [36]. (C) Amount of internalized Au per cell ($m_{x/cell} = m_{Au/cell}$) in dependence of the fraction F of sedimented NPs. (D) Amount of internalized Au per cell ($m_{x/cell} = m_{Au/cell}$) normalized to the amount of Au which has been added to cells $m_{x/cell(added)} = C_x \cdot V_{medium} / N_{cell}$, whereby $C_x = C_{Au}$ is the concentration of Au in the AuNP solution of volume V_{medium} which has been added to N_{cell} cells. From left to right, bars representing the 100 nm AuNPs, 50 nm AuNPs, 100 nm AuNRs, 40 nm AuNRs, 25 nm AuNPs and 5 nm AuNPs, respectively. The results represent the mean value from three independent experiments using cells from different donors or different cell passages. See the SI for details.

Table 1

Basic characteristics of the investigated cell types comprising the cross section area A_{cell} as determined from suspended (“sus”) and attached (“att”) cells, the cell volume V_{cell} , and the average time to cell division $T_{1/2,cell}$. Here V_{cell} is obtained from the $A_{cell,sus}$ data with the approximation that suspended cells are spheres. Consequently, the radius of suspended cells was experimentally determined and volume was obtained.

	Human MSCs	Dog MSCs	Horse MSCs	MHS
$A_{cell,sus}$ [μm^2]	427 ± 96	310 ± 42	270 ± 44	158 ± 40
$A_{cell,att}$ [μm^2]	4740 ± 1431	2650 ± 784	846 ± 156	254 ± 85
V_{cell} [μm^3]	6650 ± 710	4150 ± 200	3340 ± 220	1500 ± 200
$T_{1/2,cell}$ [h]	81 ± 7	41 ± 5	16 ± 2	33 ± 6

results in-between different MSCs thus can be ascribed to basic parameters such as cell cross-section area and proliferation rate.

While uptake is governed by endocytosis, the amount of internalized NPs is also influenced by exocytosis, which counteracts endocytosis [42–44]. Thus, NP retention studies are an important factor to be evaluated. We found that for all cells studied, the exocytosis rate of the small NPs was higher than the exocytosis rate of NPs of bigger size, *i.e.* results were independent of the exposure dose, internalization rate and proliferation, see Fig. 5B and C and Fig. SI-VIII.3. Furthermore, enhanced exocytosis was found in those cells which divided faster, *i.e.* cells with lower $T_{1/2}$ (see Fig. 5A, and Fig. SI-VIII.1 and VIII.3). The exocytosis rate was not directly depending on the percentage of internalized NPs and cell proliferation ($T_{1/2,cell}$). The extend of exocytosis was rather associated to the size and the exposure dose of the NPs (see Fig. 5). A summary of the uptake study pointing out the influence of the different parameters is shown in Fig. 5B and C.

While so far, the loading of cells with NPs was discussed, high NP doses of internalized NP may also impair cells. Thus, in addition, further biocompatibility studies were conducted. For the cells exposed to the different NPs and CAs the cell viability V was measured after 24 h (see Fig. 6), 48 h, and 72 h (see SI) by the standard resazurin assay [19,45]. Exposure to CdCl_2 was used as positive control. Data indicate that for the used NP concentrations (at higher concentrations some of the NPs are no longer colloidal stable) most NPs and CAs did not reduce cell viability in MSCs (*cf.* Fig. 6). Analysis of surface markers also demonstrated that the human MSCs kept their phenotype after exposure to NPs for 24 h (see SI section VI). In contrast, concentration-dependent reduction of viability was observed for the macrophage cell line under high exposure conditions. Viability was as expected more impaired after 48 h or 72 h exposure than after 24 h (see SI). There is an earlier onset of reduction in cell viability in terms of mass concentration C_x for the IONPs than for the AuNPs. This, however, is partly due to the metrics, as one atom of iron has less mass than one atom of Au ($M_{Fe}/M_{Au} = (55.845 \text{ g/mol}) / (196.967 \text{ g/mol}) = 0.283$). Reduction of cell viability upon exposure to rod-shaped AuNRs of 100 nm length may be due to the fact that their internalization to cells is high and that they had been initially grown in toxic cetyltrimethylammonium bromide (CTAB) [46], which maybe has not been completely removed before the polymer surface chemistry was applied [47].

Also, the proliferation of the different cells upon exposure for 24 h (see Fig. 7) to the NPs and CAs was recorded. As expected, longer incubation time had more effects on reducing the proliferation. In general, at the same exposure dose, MHS cells and human MSCs are more sensitive than the dog and horse MSCs to

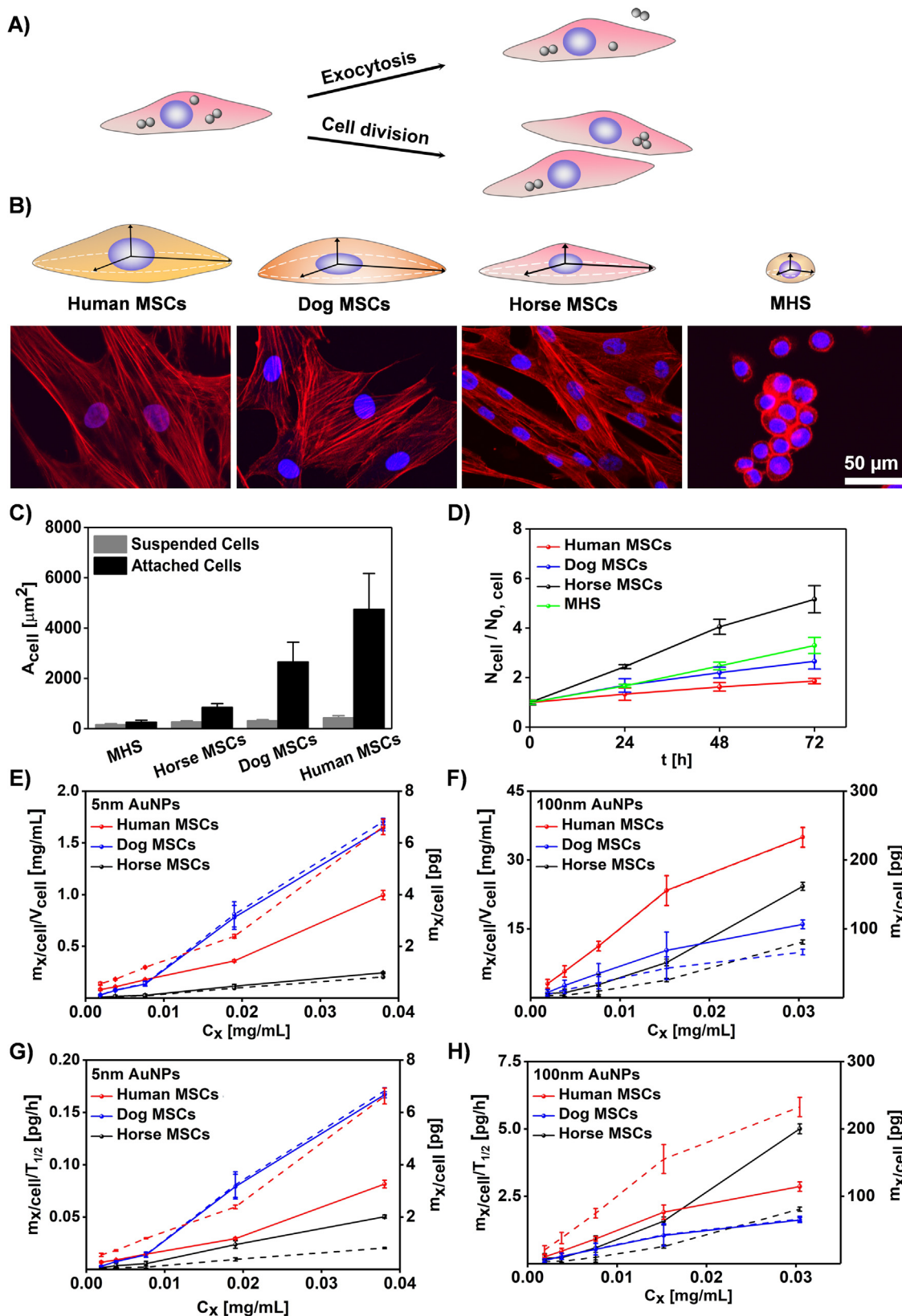


Fig. 4. Overview of factors influencing the NP labeling efficiency of cells. (A) Scheme illustrating the effects of cell division and exocytosis on the retention of NPs within a cell. (B) Sketch of the morphology of the MSCs and MHS cells, together with fluorescence microscopy images of stained cytoskeleton and nuclei of cells. The scale bar corresponds to 50 μm . The scale bar is the same for all the images. (C) Cross-section area of adherent and trypsinized (i.e. suspended) cells (A_{cell}). (D) Cell division as described by the time-dependent number of cells in culture N_{cell} versus the initial amount of seeded cells $N_{0,\text{cell}}$ ($N_{\text{cell}}/N_{0,\text{cell}}$). (E and F) Amount of elemental Au ($m_{\text{x}/\text{cell}} = m_{\text{Au}/\text{cell}}$) found in MSCs after 24 h exposure to 5 nm and 100 nm AuNPs at different Au ($C_{\text{x}} = C_{\text{Au}}$) exposure concentrations. The uptake results are expressed in terms of Au per cell ($m_{\text{x}/\text{cell}}$ [pg], represented as slashed lines) and normalized to the respective cell volume ($m_{\text{x}/\text{cell}}/V_{\text{cell}}$ [mg/mL], represented as solid lines). (G and F) Amount of elemental Au ($m_{\text{x}/\text{cell}} = m_{\text{Au}/\text{cell}}$) found in MSCs after 24 h exposure to 5 nm and 100 nm AuNPs at different Au ($C_{\text{x}} = C_{\text{Au}}$) exposure concentrations. The uptake results are expressed in terms of Au per cell ($m_{\text{x}/\text{cell}}$ [pg], represented as slashed lines) and normalized to the respective proliferation time ($m_{\text{x}/\text{cell}}/T_{1/2,\text{cell}}$ [pg/h], represented as solid lines).

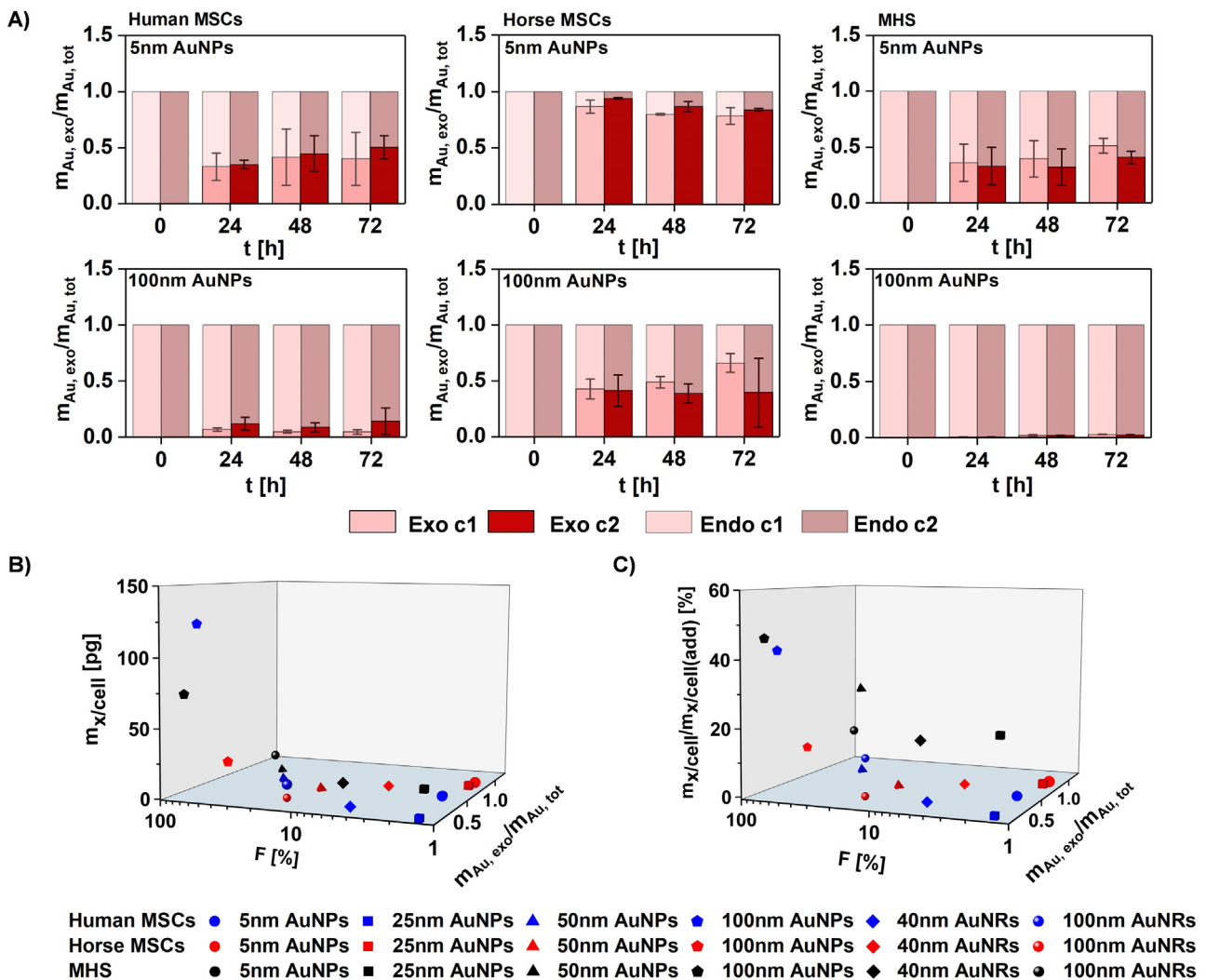


Fig. 5. (A) Percentage of exocytosed for 5 nm AuNPs and 100 nm AuNP in Human MSCs, Horse MSCs, and MHS macrophages expressed as $m_{Au,exo}/m_{Au,tot}$. $m_{Au,tot}$ is the total amount of internalized Au directly after removal of AuNPs from the extracellular medium. Upon exocytosis this is split into the amount of Au which remains inside cells (m_{Au}) and the amount of exocytosed Au ($m_{Au,exo}$): $m_{Au,tot} = m_{Au} + m_{Au,exo}$. The C_{AuNP} values used in the experiment are summarized in the SI (Table SI-VIII.1): 5 nm AuNPs $c_1 = 50$ nM, $c_2 = 100$ nM, 100 nm AuNPs $c_1 = 1.6$ pM, $c_2 = 3.3$ pM. Endocytosis values are named “Endo” and exocytosis values “Exo”. Results are obtained from a minimum three independent experiments using cells from different donors or different cell passages. (B and C) Compilation of uptake results. The AuNP concentrations C_{AuNP} used for the data points presented here are summarized in the SI (Table SI-VIII.1): 5 nm AuNPs: 100 nM, 25 nm AuNPs: 0.5 nM, 50 nm AuNPs: 0.5 nM, 100 nm AuNPs: 3.3 pM, 40 nm AuNRs: 0.5 nM, and 100 nm AuNRs: 0.12 nM.

the exposure of NPs and CAs. In agreement with a previous study, proliferation is a more sensitive indicator than viability to the onset of cytotoxic effects of NPs [48]. Our results indicate that at similar elemental exposure dose C_x [mg], small spherical AuNPs are more toxic than big spherical AuNPs. However, the 100 nm AuNPs impair macrophages but not human MSC (probably due to their high phagocytic capacity). In addition, for AuNRs, at similar dose, bigger AuNRs impair proliferation more than smaller AuNRs. Furthermore, IONPs showed similar toxicity as the AuNPs of similar size. As the visualization of results such as cell viability, proliferation, uptake, etc. depends on the exposure metrics [49], in SI all the metrics used in this study and the corresponding conversions are provided.

For cellular labeling, the amount of intracellular Au or Fe should be as high as possible, but without impairing cells. The higher the exposure concentration C_x , the more label inside cells ($m_x/cell(C_x)$), see Fig. 2. On the other hand, the higher the exposure concentration, the more the cell proliferation $P(C_x)$ may be reduced (the same is true for viability, but proliferation is a more sensitive indicator). Thus, in order to find the optimum labeling conditions both curves

were convoluted. In Fig. 8 the $m_x/cell(C_x) \times P(C_x)$ versus C_x data are shown. The data typically lead to a maximum-type curve. For low exposure concentrations, still more NPs can be incorporated and thus $m_x/cell(C_x) \times P(C_x)$ raises. For high exposure concentrations, there is an onset of toxicity and thus $m_x/cell(C_x) \times P(C_x)$ declines. The maximum of the $m_x/cell(C_x) \times P(C_x)$ curve gives the exposure concentration C_x^* at which the maximum amount of Au or Fe can be loaded to the cells without impairing them. From Fig. 2 then the maximum mass of delivered Au or Fe can be determined as $m_x/cell(C_x^*)$. In some cases, the $m_x/cell(C_x) \times P(C_x)$ curves are steadily raising. In this case, it was not possible to reach exposure concentrations at which proliferation starts to be reduced (due to onset of agglomeration of the NPs). The optimum exposure concentration C_x^* then is the maximum concentration which was possible to be added to the cells. The obtained results are enlisted in Table 2.

Overall, from our results we could conclude that the spherical 50 nm and 100 nm AuNPs are the best NP candidates for labeling MSCs and MHS cells with regard to labeling efficacy, exocytosis, viability, and maintenance of proliferation. Indeed, similar exposure doses of 100 nm AuNPs (in terms of C_x [mg/mL]) lead to higher

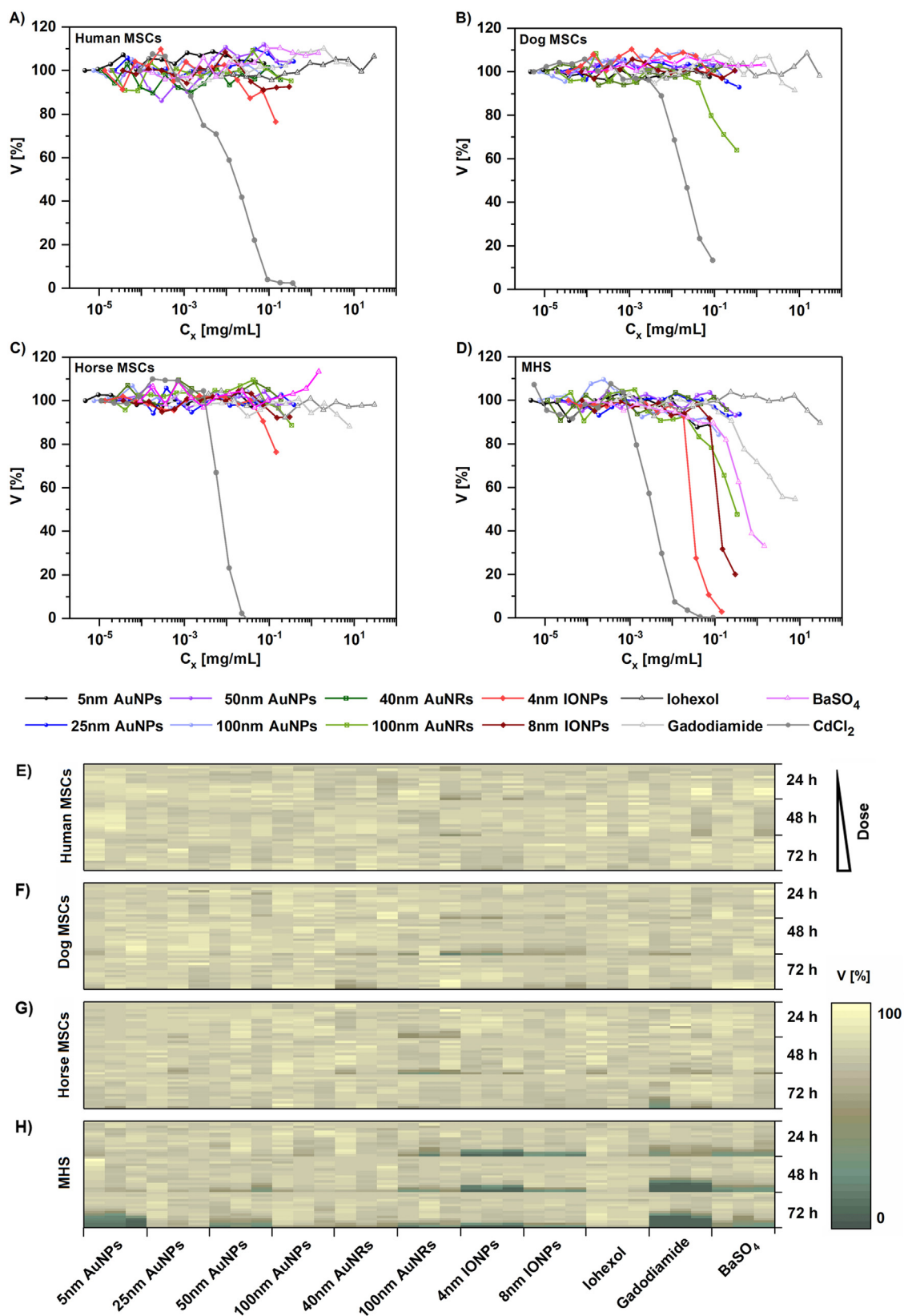


Fig. 6. Cell viability V of MSCs and MHS macrophages after 24 h exposure to AuNPs and IONPs at different Au ($C_x = C_{Au}$) and Fe ($C_x = C_{Fe}$) concentrations, respectively. As control, cells were exposed to Iohexol, Gadodiamide, BaSO₄, and CdCl₂ at different I ($C_x = C_I$), Gd ($C_x = C_{Gd}$), Ba ($C_x = C_{Ba}$), and Cd ($C_x = C_{Cd}$) concentrations, respectively. Cell viability V of (A) human MSCs, (B) dog MSCs, (C) horse MSCs, and (D) MHS macrophages. (E–H) Heat map representing all the cell viability studies conducted at 24 h (data are the same as shown in A–D), 48 h, and 72 h. Results are presented as percent cell viability V [%] as mean from minimum three independent experiments using cells from different donors or different cell passages. Error bars omitted for clarity.

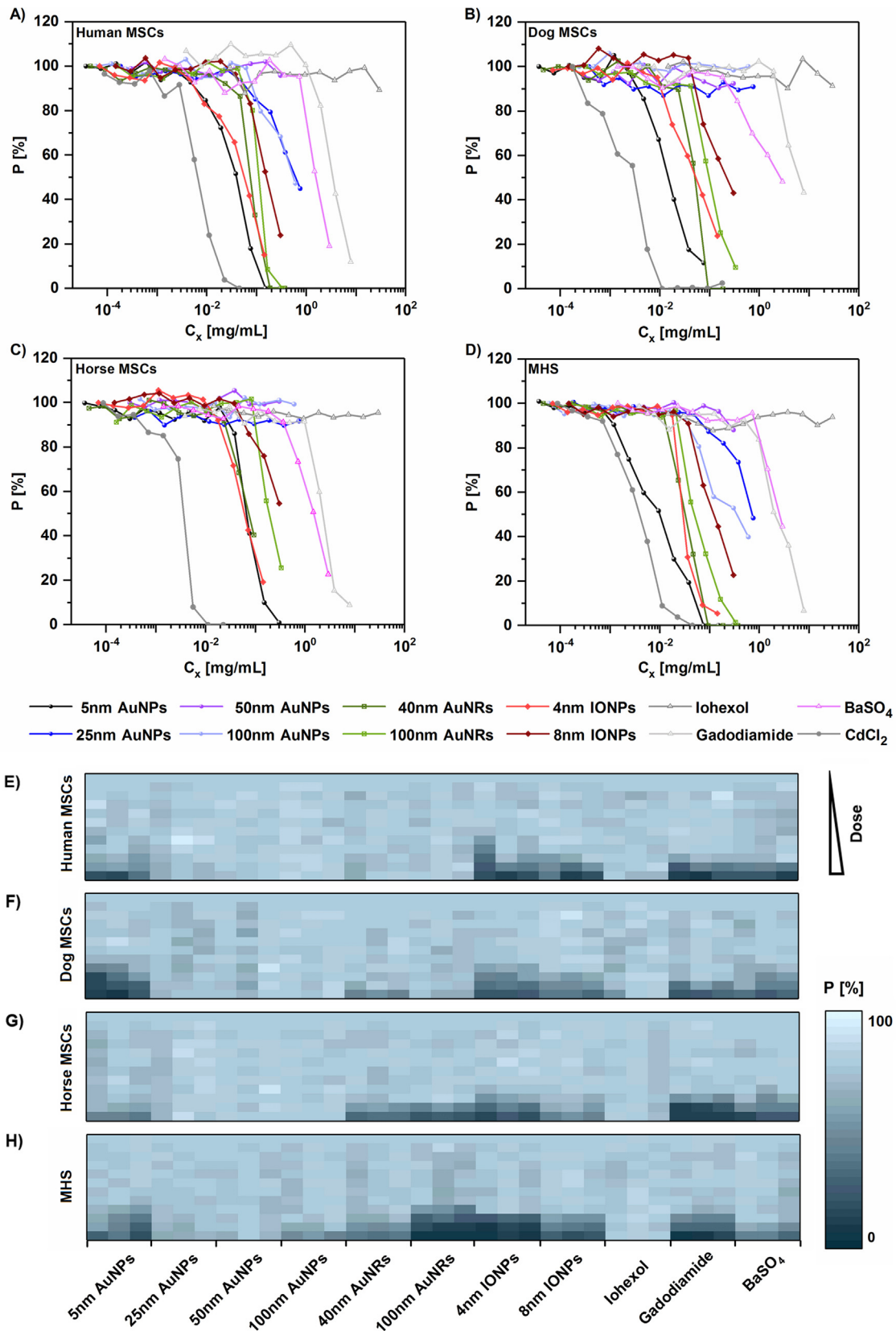


Fig. 7. Cell proliferation P of MSCs and MHS macrophages after 24 h exposure to AuNPs and IONPs at different Au ($C_x = C_{Au}$) and Fe ($C_x = C_{Fe}$) concentrations. As control cells were exposed to Iohexol, Gadodiamide, BaSO₄, and CdCl₂ at different I ($C_x = C_I$), Ba ($C_x = C_{Ba}$), Gd ($C_x = C_{Gd}$), and Cd ($C_x = C_{Cd}$) concentrations, respectively. Cell proliferation P of (A) human MSCs, (B) dog MSCs, (C) horse MSCs, and (D) MHS macrophages. (E–H) Heat map representing all the proliferation studies conducted at 24 h (E), corresponding to the same data as shown in A–D. Results are presented as mean values from a minimum of three independent experiments using cells from different donors or different cell passages. Error bars omitted for clarity.

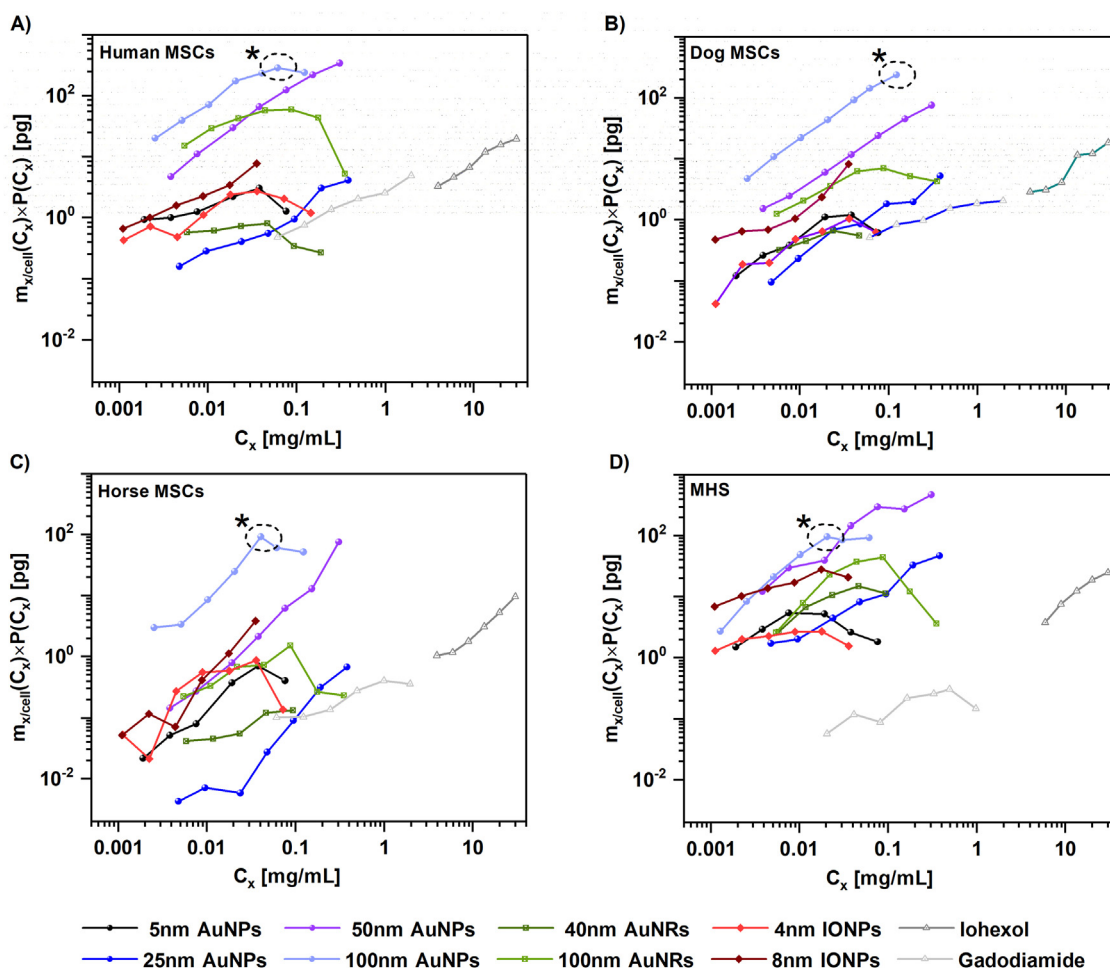


Fig. 8. Amount of incorporated Au, Fe, I, and Gd ($m_{x/cell}(C_x)$ data from Fig. 2) multiplied with the cell proliferation ($P(C_x)$ data from Fig. 7) after 24 h exposure of cells to AuNPs and IONPs at different Au ($C_x = C_{Au}$) and Fe ($C_x = C_{Fe}$) concentrations, respectively. As control cells were exposed to Iohexol and Gadodiamide at different I ($C_x = C_I$) and Gd ($C_x = C_{Gd}$) concentrations, respectively. (A) Human MSCs, (B) dog MSCs, (C) horse MSCs, and (D) MHS macrophages. For the 100 nm AuNPs the optimum exposure concentration C_x^* is indicated with a black star. Results were obtained from a minimum three independent experiments using cells from different donors or different cell passages.

amounts of intracellular Au $m_{x/cell}(C_x)$ as compared with other AuNPs. This result is consistent for all the different MSCs. In the case of MHS cells 50 nm AuNPs yield to the best labeling, because MSC seem to tolerate the 100 nm AuNPs better than the MHS. In terms of IONPs our results indicate that with 8 nm IONPs more Fe can be delivered to cells than with 4 nm IONPs.

With the data provided in Table 2, the maximum contrast which can be achieved with the AuNPs and IONPs used in our study for CT and MRI, respectively, can be predicted by using a calibration curve (see Table 3). In case of CT contrast directly depends on the amount of Au (or I or Gd) and is given in terms of normalized attenuation μ of X-rays measured in Hounsfield units [HU] [32]. For obtaining a calibration curve, the contrast of test solutions with different concentrations of $HAuCl_4$, the different AuNPs, and the CAs was measured in agarose matrixes, see Fig. 9A. The data show that the CT contrast of AuNPs in fact depends on the elemental concentration of gold C_{Au} , as the contrast of all AuNPs follows the calibration curve of $HAuCl_4$. Contrast with CT could then be also observed with cells which have been labeled with AuNPs (cf. Fig. 9B, and SI). Also for the IONPs calibration curves in agarose matrixes were recorded with MRI, see Fig. 9C. Data show the concentration-dependent T_2 MRI contrast. Contrast with MRI could also be observed with cells that have been labeled with IONPs (cf. Fig. 9D and SI).

With this information, the maximum contrast for cellular labeling can be predicted. The maximum mass of internalized Au per

cell divided by the cell volume V_{cell} gives the mean Au concentration inside a cell $m_{x/cell}(C_x^*)/V_{cell}$. The experimental values are listed in Table 2. Using the calibration curve of Fig. 9B, which relates CT contrast with Au concentrations, the CT contrast of the labeled cells μ^* can be calculated, see Table 3. In the case of IONPs the same approach using the calibration curve of Fig. 9D can be used to predict the maximum T_2 MRI contrast I^* for IONP labeled cells, see Table 3. In fact, in both cases (CT and MRI) the contrast recorded with phantoms of labeled cells (star symbols in Fig. 9B and D) match well the predicted values.

3. Conclusions

Here we show that stem cells and macrophages can be successfully labeled with AuNPs and IONPs. We illustrated that the concentration of NPs within a cell depends on the nature of the NPs, their stability in biological media, cell area, cell type, proliferation, exocytosis rate of the cells, etc. We found that bigger AuNPs such as the 100 nm AuNPs (for MSCs) and 50 nm AuNPs (for MHS) used in our study allow for optimizing the amount of intracellular Au at which no significant reduction in cell proliferation occurs. Consequently, higher CT contrast can be achieved by labeling cells with bigger (i.e. 100 nm) AuNPs than with smaller (i.e. 5 nm) AuNPs. Importantly, higher labeling efficiency of cells could be achieved

Table 2

Maximum exposure concentration C_x^* for the different NPs and CAs as taken from Fig. 7, together with the corresponding delivered mass $m_{x/cell}(C_x^*)$ taken from Fig. 2. $X = \text{Au, Fe, I, Gd}$. The NP concentration within the cells is expressed as $m_{x/cell}(C_x^*)/V_{cell}$ [mg/mL]. V_{cell} is taken from Table 1.

Sample	Human MSCs			Dog MSCs		
	C_x^* [mg/mL]	$m_{x/cell}(C_x^*)$ [pg]	$m_{x/cell}(C_x^*)/V_{cell}$ [mg/mL]	C_x^* [mg/mL]	$m_{x/cell}(C_x^*)$ [pg]	$m_{x/cell}(C_x^*)/V_{cell}$ [mg/mL]
5 nm AuNPs	3.80×10^{-2}	5.93	8.91×10^{-4}	3.80×10^{-2}	6.82	1.64×10^{-3}
25 nm AuNPs	0.38	6.79	1.02×10^{-3}	0.38	5.79	1.40×10^{-3}
50 nm AuNPs	0.30	354.11	5.33×10^{-2}	0.30	79.13	1.90×10^{-2}
100 nm AuNPs	0.06	286.28	4.31×10^{-2}	0.06	241.20	5.81×10^{-2}
40 nm AuNRs	0.05	0.94	1.42×10^{-4}	0.05	0.75	1.80×10^{-3}
100 nm AuNRs	0.12	64.85	9.75×10^{-3}	0.12	12.38	2.98×10^{-3}
4 nm IONPs	0.02	4.10	6.17×10^{-4}	0.02	1.72	4.16×10^{-4}
8 nm IONPs	0.03	9.43	1.42×10^{-3}	0.03	11.19	2.70×10^{-3}
Iohexol	30.02	23.06	3.47×10^{-3}	30.02	20.95	5.05×10^{-3}
Gadodiamide	0.98	2.52	3.70×10^{-4}	0.98	1.84	4.40×10^{-3}

Sample	Horse MSCs			MHS		
	C_x^* [mg/mL]	$m_{x/cell}(C_x^*)$ [pg]	$m_{x/cell}(C_x^*)/V_{cell}$ [mg/mL]	C_x^* [mg/mL]	$m_{x/cell}(C_x^*)$ [pg]	$m_{x/cell}(C_x^*)/V_{cell}$ [mg/mL]
5 nm AuNPs	3.80×10^{-2}	0.81	2.44×10^{-4}	1.90×10^{-2}	9.89	6.59×10^{-3}
25 nm AuNPs	0.38	0.72	2.14×10^{-4}	0.38	64.30	4.28×10^{-2}
50 nm AuNPs	0.30	24.39	7.30×10^{-3}	0.30	536.18	0.36
100 nm AuNPs	0.06	62.90	1.88×10^{-2}	0.02	96.33	6.42×10^{-2}
40 nm AuNRs	0.05	0.33	1.00×10^{-4}	0.05	35.26	2.35×10^{-2}
100 nm AuNRs	0.12	6.00	1.80×10^{-3}	0.05	138.32	9.22×10^{-2}
4 nm IONPs	0.02	1.22	3.66×10^{-4}	0.012	4.75	3.17×10^{-3}
8 nm IONPs	0.03	4.54	1.36×10^{-4}	0.03	33.35	2.22×10^{-2}
Iohexol	30.02	10.21	3.06×10^{-3}	30.02	26.92	1.80×10^{-2}
Gadodiamide	0.98	0.44	1.32×10^{-4}	0.49	0.67	4.44×10^{-4}

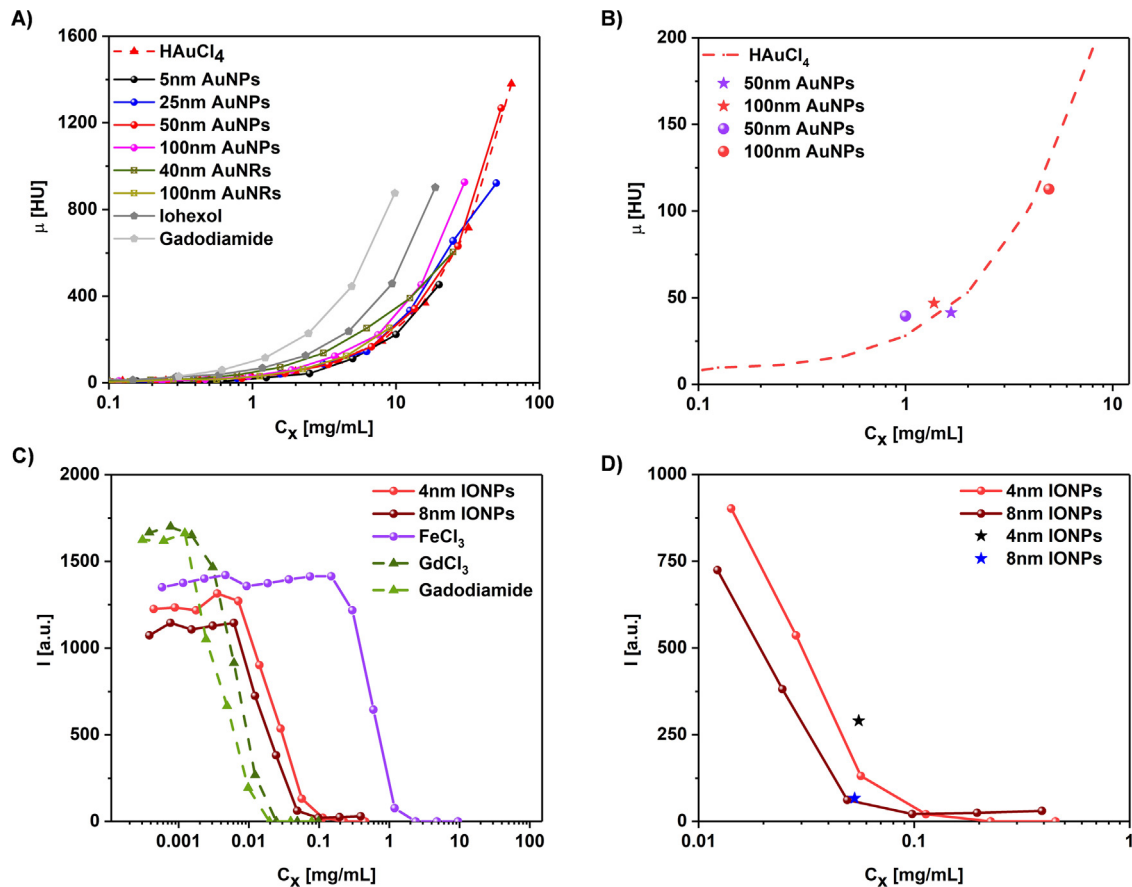


Fig. 9. (A) Normalized attenuation μ versus the concentration of AuNPs in 1% agarose phantoms at different Au ($C_x = C_{Au}$) concentrations. As reference control, HAuCl₄, Iohexol, and Gadodiamide at different Au ($C_x = C_{Au}$), I ($C_x = C_I$), and Gd ($C_x = C_{Gd}$) concentration C_x were used. (B) Zoom into the data shown in (A) were attenuation values μ of label human MSCs (sphere-symbols) and MHS macrophages (star-symbols) labeled with 50 nm and 100 nm AuNPs are also presented. The results indicate that the normalized attenuation directly depends of the concentration of elemental gold, i.e. the values for HAuCl₄ and for AuNPs are on the same calibration curve. (C) T_2 -contrast I of IONPs at different Fe ($C_x = C_{Fe}$) concentrations. As reference control, Gadodiamide, FeCl₃, and GdCl₃ at different Gd ($C_x = C_{Gd}$) and Fe ($C_x = C_{Fe}$) concentrations C_x were used. (D) MRI of labeled human MSCs with 4 nm and 8 nm IONPs are shown and compared with the calibration curve of pure IONPs. See the SI section X–XI for detailed information.

Table 3

Prediction contrast toward CT and MRI. Cells were labeled with AuNPs and IONPs at the maximum exposure concentration C_x^* . Using the values of Table 2 the maximum amount of Au and Fe inside cells then is known. Based on the calibration curves shown in Fig. 9 the normalized attenuation μ^* for CT and the T_2 MRI contrast I^* were calculated for 25,00,000 cells.

Samples	Cell type	μ^* [HU]	I^* [a.u.]
5 nm AuNPs	Human MSCs	9.1	–
25 nm AuNPs	Human MSCs	9.2	–
50 nm AuNPs	Human MSCs	64.5	–
100 nm AuNPs	human MSCs	53.7	–
40 nm AuNRs	Human MSCs	8.2	–
100 nm AuNRs	Human MSCs	18.4	–
4 nm IONPs	Human MSCs	–	429.0
8 nm IONPs	Human MSCs	–	32.8
5 nm AuNPs	Horse MSCs	8.3	–
25 nm AuNPs	Horse MSCs	8.3	–
50 nm AuNPs	Horse MSCs	13.4	–
100 nm AuNPs	Horse MSCs	21.8	–
40 nm AuNRs	Horse MSCs	8.2	–
100 nm AuNRs	Horse MSCs	9.4	–
4 nm IONPs	Horse MSCs	–	1079.2
8 nm IONPs	Horse MSCs	–	178.8
5 nm AuNPs	MHS cells	9.9	–
25 nm AuNPs	MHS cells	19.7	–
50 nm AuNPs	MHS cells	105.2	–
100 nm AuNPs	MHS cells	25.5	–
40 nm AuNRs	MHS cells	14.5	–
100 nm AuNRs	MHS cells	33.2	–
4 nm IONPs	MHS cells	–	319.8
8 nm IONPs	MHS cells	–	27.7

using NPs rather than CA. Our study indicates that for NP labeling for CT, the choice of the size of the AuNPs is crucial factor.

4. Materials and methods

For the full description of the materials and methods we refer to Supporting Information.

Nanoparticles synthesis and characterization: The synthesis of the different AuNPs and IONPs and their characterization was carried out as previously described [35,47]. Full protocols are reported in SI. A similar library was synthesized recently [34], but the data of these study are based on a new, individually synthesized library.

Cell culture: Human, dog, and horse stem cells were extracted and cultured as previously reported [7,19,50]. MSCs were maintained in DMEM medium supplemented with 10% fetal bovine serum (FBS), streptomycin (100 μ g/mL)–penicillin (100 U/mL) (P/S), L-glutamine (2 mM). The MHS cells were maintained in RPMI medium supplemented with 10% FBS, 1 mM Na-pyruvate, P/S, and β -mercaptoethanol (0.05 mM). The cells were cultivated in flasks at 37 °C and 5% CO₂, until they reached confluence.

Determination of cellular parameters: For determining the cross section area the actin network of the cells was fluorescence-stained, and the area of the stained cell surface was recorded from fluorescence images. The time required to duplication of the number of cells due to cell division was determined from the normalized change of cell number per time interval by counting the number of cells on culture substrates at different times after seeding: $[(N_{\text{cell}}(\Delta t) - N_{\text{cell}}(0))/N_{\text{cell}}(0)]/\Delta t$. The average time for cell division $T_{1/2,\text{cell}}$ was then determined as the time in which the cell number doubles: $2 = [(N_{\text{cell}}(T_{1/2,\text{cell}}) - N_{\text{cell}}(0))/N_{\text{cell}}(0)]/T_{1/2,\text{cell}}$.

Cell viability assay: The cell viability V of MSCs and MHS macrophages exposed to different NPs and CAs at different concentrations and time points was evaluated using the resazurin assay as previously reported [45,51].

Cell proliferation assay: The cell proliferation P of MSCs and MHS macrophages exposed to different NPs and CAs at different concentrations and time points was evaluated by directly

measuring DNA synthesis, investigated by the incorporation of the thymidine-analog EdU (5-ethynyl-2'-deoxyuridine) by cells as previously reported [48].

Cellular uptake of NPs: The intracellular concentrations of Au, Fe, I, and Gd were evaluated following incubation of MSCs and macrophages with NPs and CAs at different concentration for 4, 24, and 48 h in serum supplemented medium. The intracellular concentration was evaluated using inductively coupled plasma mass spectrometry (ICP-MS) as previously reported [19].

Exocytosis studies: The amount of exocytosed NPs was evaluated over time after exposure of cells to NPs, followed by removal of NPs from the extracellular medium by rinsing, and then measuring the rise in extracellular NP concentration due to exocytosis [19].

Computer tomography (CT) and magnetic resonance imaging (MRI): In order to evaluate the contrast of different NPs for CT and MIR imaging phantom samples of NPs and CAs at different concentration were prepared and imaged with the respective instruments.

Acknowledgements

We acknowledge Prof. Dr. Frauke Alves and Dr. Christian Dullin for their guidance on MHS cells. We acknowledge Marta Gallego for her contribution to the TEM images. We acknowledge Prof. Dr. Stefan Arnhold for his contribution to the Horse MSCs cultures. This work was supported by the Deutsche Forschungsgemeinschaft (DFG, grant 794/25-1). XS was supported by the Chinese Scholarship Council (CSC). MG was supported by the Fazit Foundation. IC was an Alexander von Humboldt fellow. NF received funding from the Swedish Innovation Agency, Vinnova.

Appendix A. Supplementary data

Supplementary data associated with this article can be found, in the online version, at doi:10.1016/j.apmt.2018.12.006.

References

- [1] S. Wilhelm, A.J. Tavares, Q. Dai, S. Ohta, J. Audet, H.F. Dvorak, W.C.W. Chan, Analysis of nanoparticle delivery to tumours, *Nat. Rev. Mater.* 1 (2016) 16014.
- [2] C. Xie, Z. Yang, Y. Suo, Q. Chen, D. Wei, X. Weng, Z. Gu, X. Wei, Systemically infused mesenchymal stem cells show different homing profiles in healthy and tumor mouse models, *Stem Cells Transl. Med.* 6 (4) (2017) 1120–1131.
- [3] S. Soontararak, L. Chow, V. Johnson, J. Coy, W. Wheat, D. Regan, S. Dow, Mesenchymal stem cells (MSC) derived from induced pluripotent stem cells (iPSC) equivalent to adipose-derived MSC in promoting intestinal healing and microbiome normalization in mouse inflammatory bowel disease model, *Stem Cells Transl. Med.* 7 (6) (2018) 456–467.
- [4] A. Mantovani, F. Marchesi, A. Malesci, L. Laghi, P. Allavena, Tumour-associated macrophages as treatment targets in oncology, *Nat. Rev. Clin. Oncol.* 14 (7) (2017) 399–416.
- [5] P. Tiet, J.M. Berlin, Exploiting homing abilities of cell carriers: targeted delivery of nanoparticles for cancer therapy, *Biochem. Pharmacol.* 145 (2017) 18–26.
- [6] Y. Zhao, S. Tang, J. Guo, M. Alahdal, S. Cao, Z. Yang, F. Zhang, Y. Shen, M. Sun, R. Mo, L. Zong, L. Jin, Targeted delivery of doxorubicin by nano-loaded mesenchymal stem cells for lung melanoma metastases therapy, *Sci. Rep.* 7 (2017) 44758.
- [7] M.A. Kolecka, S. Arnhold, M. Schmidt, C. Reich, M. Kramer, K. Failing, K. von Pückler, Behaviour of adipose-derived canine mesenchymal stem cells after superparamagnetic iron oxide nanoparticles labelling for magnetic resonance imaging, *BMC Vet. Res.* (2017) 13.
- [8] H. Cho, S. Choi, N. Lee, T. Hyeon, H. Kim, W. Moon, Macrophages homing to metastatic lymph nodes can be monitored with ultrasensitive ferromagnetic iron-oxide nanocubes and a 1.5 T clinical MR scanner, *PLoS ONE* 7 (1) (2012) 90–99.
- [9] K. Kirschbaum, J.K. Sonner, M.W. Zeller, K. Deumelandt, J. Bode, R. Sharma, T. Kruwel, M. Fischer, A. Hoffmann, M. Costa da Silva, M.U. Muckenthaler, W. Wick, B. Tewes, J.W. Chen, S. Heiland, M. Bendtszus, M. Platten, M.O. Breckwoldt, In vivo nanoparticle imaging of innate immune cells can serve as a marker of disease severity in a model of multiple sclerosis, *Proc. Natl. Acad. Sci. U. S. A.* 113 (46) (2016) 13227–13232.
- [10] E.T. Ahrens, J.W. Bulte, Tracking immune cells in vivo using magnetic resonance imaging, *Nat. Rev. Immunol.* 13 (10) (2013) 755–763.

- [11] S.S. Moonshi, C. Zhang, H. Peng, S. Puttick, S. Rose, N.M. Fisk, K. Bhakoo, B.W. Stringer, G.G. Qiao, P.A. Gurr, A.K. Whittaker, A unique (19)F MRI agent for the tracking of non phagocytic cells in vivo, *Nanoscale* 10 (17) (2018) 8226–8239.
- [12] L. Liu, L. Tseng, Q. Ye, Y.L. Wu, D.J. Bain, C. Ho, A new method for preparing mesenchymal stem cells and labeling with ferumoxytol for cell tracking by MRI, *Sci. Rep.* 6 (2016) 26271.
- [13] S. Ashraf, A. Taylor, J. Sharkey, M. Barrow, P. Murray, B. Wilm, H. Poptani, M.J. Rosseinsky, D.J. Adamsde, R. Lévy, In vivo fate of free and encapsulated iron oxide nanoparticles after injection of labelled stem cells, *Nanoscale Adv.* (2019), <http://dx.doi.org/10.1039/C8NA00098K> (in press) <https://pubs.rsc.org/en/content/articlelanding/2019/na/c8na00098k#!divAbstract>.
- [14] Y.L. Liu, K.L. Ai, L.H. Lu, Nanoparticulate X-ray computed tomography contrast agents: from design validation to in vivo applications, *Acc. Chem. Res.* 45 (10) (2012) 1817–1827.
- [15] J. Comenge, O. Fraguero, J. Sharkey, A. Taylor, M. Held, N.C. Burton, B.K. Park, B. Wilm, P. Murray, M. Brust, R. Levy, Preventing plasmonic coupling between gold nanorods improves the sensitivity of photoacoustic detection of labeled stem cells in vivo, *ACS Nano* 10 (7) (2016) 7106–7116.
- [16] T. Kim, J.E. Lemaster, F. Chen, J. Li, J.V. Jokerst, Photoacoustic imaging of human mesenchymal stem cells labeled with prussian blue-poly(L-lysine) nanocomplexes, *ACS Nano* 11 (9) (2017) 9022–9032.
- [17] K.D. Wegner, N. Hildebrandt, Quantum dots: bright and versatile in vitro and in vivo fluorescence imaging biosensors, *Chem. Soc. Rev.* 44 (14) (2015) 4792–4834.
- [18] S.M. Kim, C.H. Jeong, J.S. Woo, C.H. Ryu, J.H. Lee, S.S. Jeun, In vivo near-infrared imaging for the tracking of systemically delivered mesenchymal stem cells: tropism for brain tumors and biodistribution, *Int. J. Nanomed.* 11 (2016) 13–23.
- [19] P. Nold, R. Hartmann, N. Feliu, K. Kantner, M. Gamal, B. Pelaz, J. Hühn, X. Sun, P. Jungebluth, P. Pino, d. Hackstein, H. Macchiarini, P. Parak, W.J. Brendel, Optimizing conditions for labeling of mesenchymal stromal cells (MSCs) with gold nanoparticles: a prerequisite for in vivo tracking of MSCs, *J. Bionanotechnol.* 15 (2017) 24.
- [20] J. Choi, H.Y. Kim, E.J. Ju, J. Jung, J. Park, H.K. Chung, J.S. Lee, J.S. Lee, H.J. Park, S.Y. Song, S.Y. Jeong, E.K. Choi, Use of macrophages to deliver therapeutic and imaging contrast agents to tumors, *Biomaterials* 33 (16) (2012) 4195–4203.
- [21] G. von Maltzahn, J.-H. Park, A. Agrawal, N.K. Bandaru, S.K. Das, M.J. Sailor, S.N. Bhatia, Computationally guided photothermal tumor therapy using long-circulating gold nanorod antennas, *Cancer Res.* 69 (9) (2009) 3892–3900.
- [22] Y. Liu, M. Yang, J. Zhang, X. Zhi, C. Li, C. Zhang, F. Pan, K. Wang, Y. Yang, J. Martinez de la Fuentea, D. Cui, Human induced pluripotent stem cells for tumor targeted delivery of gold nanorods and enhanced photothermal therapy, *ACS Nano* 10 (2) (2016) 2375–2385.
- [23] S.S. Lucky, K.C. Soo, Y. Zhang, Nanoparticles in photodynamic therapy, *Chem. Rev.* 115 (4) (2015) 1990–2042.
- [24] A.V. Naumova, M. Modo, A. Moore, C.E. Murry, J.A. Frank, Clinical imaging in regenerative medicine, *Nat. Biotechnol.* 32 (8) (2014) 804–818.
- [25] B. Zhang, W. Yan, Y. Zhu, W. Yang, W. Le, B. Chen, R. Zhu, L. Cheng, Nanomaterials in neural-stem-cell-mediated regenerative medicine: imaging and treatment of neurological diseases, *Adv. Mater.* 30 (17) (2018) e1705694.
- [26] Y. Jin, C. Jia, S.-W. Huang, M. O'Donnell, X. Gao, Multifunctional nanoparticles as coupled contrast agents, *Nat. Commun.* (2010) 1.
- [27] J. Santelli, S. Lechevallier, H. Baaziz, M. Vincent, C. Martinez, R. Mauricot, A. Parini, M. Verelst, D. Cussac, Multimodal gadolinium oxysulfide nanoparticles: a versatile contrast agent for mesenchymal stem cell labeling, *Nanoscale* 10 (35) (2018) 16775–16786.
- [28] B. Pelaz, C. Alexiou, R.A.A. Puebla, F. Alves, A.M. Andrews, S. Ashraf, L.P. Balogh, L. Ballerini, A. Bestetti, C. Brendel, S. Bosi, M. Carril, W.C.W. Chan, C. Chen, X. Chen, X. Chen, Z. Cheng, D. Cui, J. Du, C. Dullin, A. Escudero, N. Feliu, M. Gao, M. George, Y. Gogotsi, A. Grünweller, Z. Gu, N. Halas, N. Hampp, R.K. Hartmann, M.C. Hersam, P. Hunziker, J. Jian, X. Jiang, P. Jungebluth, P. Kadhiresan, K. Kataoka, A. Khademhosseini, J. Kopecek, N.A. Kotov, H.F. Krug, D.S. Lee, C.-M. Lehr, K.W. Leong, X.-J. Liang, M.L. Lim, L.M.L. Marzán, X. Ma, P. Macchiarini, H. Meng, H. Möhwald, P. Mulvaney, A.E. Nel, S. Nie, P. Nordlander, T. Okano, J. Oliveira, T.H. Park, R.M. Penner, M. Prato, V. Puentes, V.M. Rotello, A. Samarakoon, R.E. Schaak, Y. Shen, S. Sjöqvist, A.G. Skirtach, M.G. Soliman, M.M. Stevens, H.-W. Sung, B.Z. Tang, R. Tietze, B.N. Udagama, J.S. VanEpps, T. Weil, P.S. Weiss, I. Willner, Y. Wu, L. Yang, Z. Yue, Q. Zhang, Q. Zhang, X.E. Zhang, Y. Zhao, X. Zhou, W.J. Parak, Diverse applications of nanomedicine, *ACS Nano* 11 (2017) 2313–2381.
- [29] B.D. Chithrani, A.A. Ghazani, W.C.W. Chan, Determining the size and shape dependence of gold nanoparticle uptake into mammalian cells, *Nano Lett.* 6 (4) (2006) 662–668.
- [30] N. Feliu, J. Hühn, M.V. Zyuzin, S. Ashraf, D. Valdeperez, A. Masood, A.H. Said, A. Escudero, B. Pelaz, E. Gonzalez, M.A.C. Duarte, S. Roy, I. Chakraborty, M.L. Lim, S. Sjöqvist, P. Jungebluth, W.J. Parak, Quantitative uptake of colloidal particles by cell cultures, *Sci. Total Environ.* 568 (2016) 819–828.
- [31] P. Sprawls, X-ray image formation and contrast, <http://www.sprawls.org/resources>.
- [32] H. Lusic, M.W. Grinstaff, X-ray-computed tomography contrast agents, *Chem. Rev.* 113 (3) (2013) 1641–1666.
- [33] N. Feliu, B. Pelaz, Q. Zhang, P. del-Pino, A. Nyström, W.J. Parak, Nanoparticle dosage—a nontrivial task of utmost importance for quantitative nanosafety research, *Wiley Interdiscip. Rev. Nanomed. Nanobiotechnol.* 8 (2016) 479–492.
- [34] M. Xu, M.G.M. Soliman, X. Sun, B. Pelaz, N. Feliu, W.J. Parak, S. Liu, Towards the prediction of protein corona formation and in vitro and in vivo interactions of gold nanoparticles based on their physicochemical properties, *ACS Nano* 12 (10) (2018) 10104–10113, <http://dx.doi.org/10.1021/acsnano.8b04906> (in press) Epub 2018 Sep 21.
- [35] J. Hühn, C. Carrillo-Carrion, M.G. Soliman, C. Pfeiffer, D. Valdeperez, A. Masood, I. Chakraborty, L. Zhu, M. Gallego, Y. Zhao, M. Carril, N. Feliu, A. Escudero, A.M. Alkilany, B. Pelaz, P. Pino, W.J. Parak, Selected standard protocols for the synthesis phase transfer, and characterization of inorganic colloidal nanoparticles, *Chem. Mater.* 29 (2017) 399–461.
- [36] N. Feliu, X. Sun, R.A.A. Puebla, W.J. Parak, Quantitative particle–cell interaction: some basic physicochemical pitfalls, *Langmuir* 33 (2017) 6639–6646.
- [37] G.M. DeLoid, J.M. Cohen, G. Pyrgiotakis, P. Demokritou, Preparation, characterization, and in vitro dosimetry of dispersed, engineered nanomaterials, *Nat. Protoc.* 12 (2) (2017) 355–371.
- [38] H.H. Gustafson, D. Holt-Casper, D.W. Grainger, H. Ghandehari, Nanoparticle uptake: the phagocyte problem, *Nano Today* 10 (4) (2015) 487–510.
- [39] W.J. Parak, R. Boudreau, M.L. Gros, D. Gerion, D. Zanchet, C.M. Micheel, S.C. Williams, A.P. Alivisatos, C.A. Larabell, Cell motility and metastatic potential studies based on quantum dot imaging of phagokinetic tracks, *Adv. Mater.* 14 (12) (2002) 882–885.
- [40] E. Panet, T. Mashriki, R. Lahmi, A. Jacob, E. Ozer, M. Vecsler, I. Lazar, A. Tzur, The interface of nanoparticles with proliferating mammalian cells, *Nat. Nanotechnol.* 12 (2017) 598–600.
- [41] M.J. Pittet, F.K. Swirski, R. Reynolds, L. Josephson, R. Weissleder, Labeling of immune cells for in vivo imaging using magnetofluorescent nanoparticles, *Nat. Protoc.* 1 (1) (2006) 73–79.
- [42] D. Bartczak, S. Nitti, T.M. Millar, A.G. Kanaras, Exocytosis of peptide functionalized gold nanoparticles in endothelial cells, *Nanoscale* (2012).
- [43] N. Oh, J.H. Park, Endocytosis and exocytosis of nanoparticles in mammalian cells, *Int. J. Nanomed.* 9 (Suppl. 1) (2014) 51–63.
- [44] N. Oh, J.H. Park, Surface chemistry of gold nanoparticles mediates their exocytosis in macrophages, *ACS Nano* 8 (6) (2014) 6232–6241.
- [45] N. Feliu, P. Kohonen, J. Ji, Y.N. Zhang, H.L. Karlsson, L. Palmberg, A. Nystrom, B. Fadeel, Next-generation sequencing reveals low-dose effects of cationic dendrimers in primary human bronchial epithelial cells, *ACS Nano* 9 (1) (2015) 146–163.
- [46] T.B. Huff, M.N. Hansen, Y. Zhao, J.X. Cheng, A. Wei, Controlling the cellular uptake of gold nanorods, *Langmuir* 23 (4) (2007) 1596–1599.
- [47] M.G. Soliman, B.P. Parak, W.J. Pino, Phase transfer and polymer coating methods toward improving the stability of metallic nanoparticles for biological applications, *Chem. Mater.* 27 (2015) 990–997.
- [48] X. Ma, R. Hartmann, D.J. Aberasturi, d. Yang, F. Soenen, S.J.H. Manshian, B.B. Franz, J. Valdeperez, D. Pelaz, B. Feliu, N. Hampp, N. Riethmüller, C. Vieker, H. Frese, N. Götzhäuser, A. Simonich, M. Tanguay, R.L. Liang, X.-J. Parak, Colloidal gold nanoparticles induce changes in cellular and subcellular morphology, *ACS Nano* 11 (2017) 7807–7820.
- [49] M. Mionic Ebersold, D. Bonvin, H. Hofmann, Neglected nano-effects of nanoparticles in the interpretation of their toxicity, *Analyst* 143 (4) (2018) 837–842.
- [50] P. Nold, C. Brendel, A. Neubauer, G. Bein, H. Hackstein, Good manufacturing practice-compliant animal-free expansion of human bone marrow derived mesenchymal stroma cells in a closed hollow-fiber-based bioreactor, *Biochem. Biophys. Res. Commun.* 430 (1) (2013) 325–330.
- [51] S. Ashraf, J. Park, M. Bichelberger, K. Kantner, R. Hartmann, P. Maffre, A.H. Said, N. Feliu, J. Lee, D. Lee, G.U. Nienhaus, S. Kim, W.J. Parak, Zwitterionic surface coating of quantum dots reduces protein adsorption and cellular uptake, *Nanoscale* 10 (2016) 1318–1328.

Quantitative Particle–Cell Interaction: Some Basic Physicochemical Pitfalls

Neus Feliu,^{†,‡,§} Xing Sun,[†] Ramon A. Alvarez Puebla,^{||,⊥} and Wolfgang J. Parak^{*,†,#}

[†]Fachbereich Physik, Philipps Universität Marburg, Marburg, Germany

[‡]Department of Laboratory Medicine (LABMED), Karolinska Institutet, Stockholm, Sweden

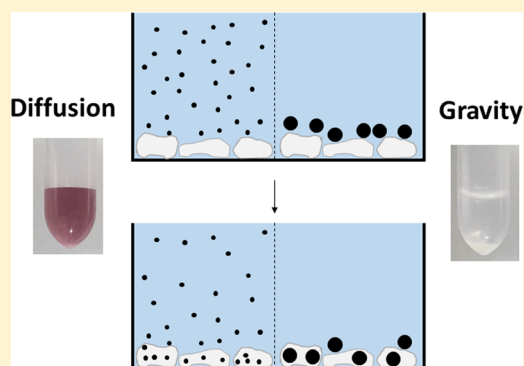
[§]Medcom Advance S.A., Barcelona, Spain

^{||}Departamento de Química Física e Inorgánica and Emas, Universitat Rovira i Virgili, Tarragona, Spain

[⊥]ICREA, Barcelona, Spain

[#]Institute of Nano Biomedicine and Engineering, Key Laboratory for Thin Film and Microfabrication Technology of the Ministry of Education, Department of Instrument Science and Engineering, School of Electronic Information and Electrical Engineering, Shanghai Jiao Tong University, Shanghai, China

ABSTRACT: There are numerous reports about particle–cell interaction studies in the literature. Many of those are performed in two-dimensional cell cultures. While the interpretation of such studies seems trivial at first sight, in fact for quantitative analysis some basic physical and physicochemical bases need to be considered. This starts with the dispersion of the particles, for which gravity, Brownian motion, and interparticle interactions need to be considered. The respective strength of these interactions determines whether the particles will sediment, are dispersed, or are agglomerated. This in turn largely influences their interaction with cells. While in the case of well-dispersed particles only a fraction of them will come into contact with cells in a two-dimensional culture, (agglomeration-induced) sedimentation drives the particles toward the cell surface, resulting in enhanced uptake.



INTRODUCTION

While there are plenty of studies available in literature in which the uptake of colloidal micro- and nanoparticles (NPs) is investigated,^{1–5} many reported findings are not quantitatively described in a way that is based on basic physical and physicochemical properties of NPs.⁶ Though the field moves toward applications, there is still a need for fundamental studies.⁷ Concerning the NPs and their characterization, the field is advanced, and standard protocols are available for synthesizing libraries of NPs with controlled properties,^{8,9} together with corresponding procedures for determining their physicochemical properties.¹⁰ Concerning the actual uptake experiments, in which cells are exposed to NPs and their cellular internalization is quantified, there is no unique established experimental design. Results may depend on how the used NP uptake is quantified,^{11–13} i.e., the way that NP doses are calculated. This is due to the fact that results may depend on the used method of analysis, e.g., on how NPs adherent to the outer plasma membrane can be avoided as false positives.^{14–17} Rigid protocols are required to be able to extract not only qualitative and but only quantitative information on NP–cell interactions.

In fact, several confusing concepts are reported. Let us ask the following fundamental question: when a two-dimensional (2d) cell culture is exposed to 5 and 100 nm gold (Au) NPs, which will be internalized to a higher percentage? Will in both cases most NPs be ultimately internalized, or will the majority of NPs remain

in solution? Intuitively, most of us likely answered these fundamental questions in the wrong way. Thinking about this general question, one has to go through a cascade of well-known classical physics- and physical chemistry-related concepts, and biology comes into play only at the end. In this article, we want to follow the fate of NPs starting from their exposure to the cell culture medium until their contact with cells, which at the end will give an answer to the question raised in the beginning,^{18,19} and to relate those responses to the inner physicochemical properties of the NPs. While most arguments originate from physics/physical chemistry, they are of utmost relevance to biology and need to be considered.

DISPERSION OF NPs

Gravity. Gravity causes a gravitation force F_G on all objects on earth, which is directed toward the center of the earth (cf. Figure 1). This is why an apple falls from the top of a tree straight to the ground. The same is true for a stone that is thrown into a lake: it will fall to the ground. While NPs placed in the solution in a Petri dish are not as heavy as a stone, the laws of gravity still apply to them, and thus they experience a gravitational force toward the

Received: January 2, 2017

Revised: April 2, 2017

Published: April 5, 2017

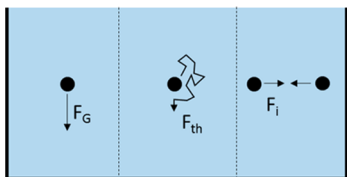


Figure 1. Different forces F acting on a NP in solution: gravity (F_G), thermal motion (F_{th}), and interparticle forces (F_i).

bottom of the Petri dish. In the case of a NP with mass m_{NP} , the gravitational force is

$$F_G = m_{NP} \cdot g = \rho_{NP} \cdot V_{NP} \cdot g \quad (1)$$

with $g = 9.81 \text{ m/s}^2$, ρ_{NP} being the density of the NP, and V_{NP} being the volume of one NP. However, when the density of the NPs is lower than that of water, the NPs would float on top of the solution. This is Archimedes' principle of buoyancy. Only when the density of the NP is higher than that of water will the NP will sink down. However, due to buoyancy it costs less force to lift a stone under water than in air. The buoyancy force F_B than a NP experiences is

$$F_B = -\rho_{H_2O} \cdot V_{NP} \cdot g \quad (2)$$

with $\rho_{H_2O} = 1 \text{ g/cm}^3 = 10^3 \text{ kg/m}^3$ being the density of the medium in which the NPs are dispersed, which in general will be water. Buoyancy directs the NPs toward the surface and thus in an opposite direction than toward the bottom, as indicated by the $-$ sign.

Last but not least, when a NP sinks to the bottom, there is friction. Friction highly depends on the viscosity $\eta_{H_2O} = 8.90 \times 10^{-4} \text{ Pa}\cdot\text{s}$ of the solvent. For slow NP velocities v_G , the friction force F_R of a spherical NP with radius r_{NP} (i.e., $V_{NP} = (4/3) \cdot \pi \cdot r_{NP}^3$) according to Stokes–Einstein is

$$F_R = -6\pi \cdot r_{NP} \cdot \eta_{H_2O} \cdot v_G \quad (3)$$

When the NP is sinking, the friction in the form of viscous drag goes in the opposite direction, so there again needs to be a $-$ sign. At equilibrium, i.e., when the sum of the forces is zero, a NP will sediment with constant velocity:

$$F_G + F_B + F_R = 0 \quad (4)$$

$$\Rightarrow \rho_{NP} \cdot V_{NP} \cdot g - \rho_{H_2O} \cdot V_{NP} \cdot g - 6\pi \cdot r_{NP} \cdot \eta_{H_2O} \cdot v_G = 0$$

$$\Rightarrow (\rho_{NP} - \rho_{H_2O}) \cdot V_{NP} \cdot g = 6\pi \cdot r_{NP} \cdot \eta_{H_2O} \cdot v_G$$

$$\Rightarrow v_G = \frac{(\rho_{NP} - \rho_{H_2O}) \cdot V_{NP} \cdot g}{(6\pi \cdot r_{NP} \cdot \eta_{H_2O})} = \frac{(\rho_{NP} - \rho_{H_2O}) \cdot g \cdot (4/3) \cdot \pi \cdot r_{NP}^3}{(6\pi \cdot r_{NP} \cdot \eta_{H_2O})}$$

$$\Rightarrow v_G = \frac{2 \cdot (\rho_{NP} - \rho_{H_2O}) \cdot g \cdot r_{NP}^2}{9 \cdot \eta_{H_2O}} \quad (5)$$

To summarize, gravity will cause a NP in water to sediment at constant velocity v_G . The major parameters hereby are the density and the size of the NPs.²⁰

Brownian Motion. Any object experiences thermal energy. This energy is kinetic energy, which describes the statistical fluctuations of objects, which are also referred to as Brownian motion. When NaCl is dissolved in water, the sodium ions and chloride ions undergo Brownian motion. The ions move arbitrarily in different directions in a random walklike fashion, i.e., diffusion. Once they scatter, they change their direction.

Therefore, in equilibrium all ions will be equally distributed across the solution. It is not straightforward to describe thermal motion in terms of a force F_{th} as the direction that the thermal kicks statistically change (cf. Figure 1), but one can calculate the mean average velocity v_{th} of a NP. The thermal energy is given as

$$E_{th} = k_B \cdot T \quad (6)$$

with the Boltzmann constant $k_B = 1.4 \times 10^{-23} \text{ J/K}$ and the absolute temperature T . At room temperature $T = 300 \text{ K}$, the thermal energy is around $E_{th} = 1.4 \times 10^{-23} \text{ J/K} \times 300 \text{ K} \approx 5 \times 10^{-21} \text{ J} \approx 25 \text{ meV}$. All thermal energy goes into kinetic energy E'_{kin} .

$$E'_{kin} = (1/2) \cdot m_{NP} \cdot v'_{th}{}^2 \quad (7)$$

The kinetic energy in one direction E_{kin} , for example, vertical to the bottom of the Petri dish, is one-third of the total kinetic energy for diffusion in three dimension. Thus, the average velocity v_{th} of a NP due to Brownian motion in one direction becomes

$$E_{th} = E'_{kin} = 3 \cdot E_{kin} = (3/2) \cdot m_{NP} \cdot v_{th}{}^2$$

$$\Rightarrow v_{th} = \sqrt{\frac{2 \cdot k_B \cdot T}{3 \cdot m_{NP}}} = \sqrt{\frac{2 \cdot k_B \cdot T}{3 \cdot \rho_{NP} \cdot V_{NP}}} = \sqrt{\frac{k_B \cdot T}{2\pi \cdot \rho_{NP} \cdot r_{NP}^3}} \quad (8)$$

To summarize, Brownian motion randomly moves NPs in random-walk-like fashion with an average velocity v_{th} in each of the three spatial directions.

Brownian Motion versus Gravity. From the basic physics above, we know that a stone would sediment to the bottom of a Petri dish based on gravity but that a sodium ion would be homogeneously distributed in solution. Brownian motion and gravity apply to both the stone and the ion. However, in the case of the stone, gravity dominates, whereas in the case of a sodium ion, Brownian motion dominates. In this way, both also have to be considered for NPs. What factor dominates for a NP? The answer lies in the comparison of eqs 5 and 8. When v_G is much bigger than v_{th} , the NP will sediment, driven by gravity. When v_{th} is much bigger than v_G , then thermal kicks will overcome gravity and the NPs will freely diffuse in solution. According to eqs 5 and 8, the relevant parameters of the NPs are their density ρ_{NP} and their radius r_{NP} . Note that hereby the NP is assumed to be a homogeneous entity, though in reality it will have a hybrid nature.²¹ In Figure 2, examples for Au and latex NPs of different radii are given, which represent NPs of high-density ($\rho_{Au} = 19.3 \text{ g/cm}^3$) and low-density ($\rho_{latex} = 1.05 \text{ g/cm}^3$) materials, respectively.

The higher the NP radius, i.e., the heavier the NP, the greater the gravitational force. The smaller the NP radius, i.e., the lighter the NP, the higher the Brownian motion. In this way, for each type of NP material one can determine the range where gravity dominates ($v_G > v_{th}$) or where Brownian motion dominates ($v_G < v_{th}$). In the case of well-dispersed Au NPs, if they are much smaller than $r_{NP} \ll 100 \text{ nm}$, then the NPs will be well dispersed in solution, analogous to sodium ions, and the solution will be homogeneously colored, cf. Figure 3. In the case of gold NPs with $r_{NP} \gg 100 \text{ nm}$, the NPs will sediment and form a pellet on the bottom of the Petri dish/tube, like a stone falling. In case of the latex NPs, which have a much lower density, the NPs will be well dispersed for $r_{NP} \ll 1 \mu\text{m}$. In the case of $r_{NP} \gg 1 \mu\text{m}$, they will sediment, which can be seen by the clear supernatant above the NP pellet, cf. Figure 3. In this way, r_{NP} and ρ_{NP} determine whether NPs will be dispersed or sediment.

Interparticle Forces: Agglomeration versus Brownian Motion. While so far only external forces acting on the NPs

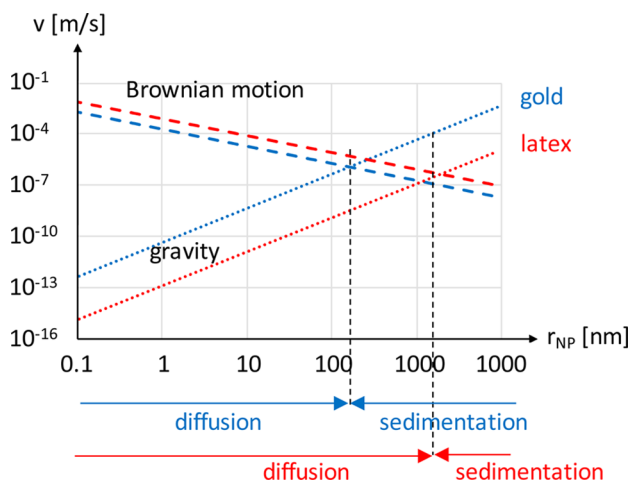


Figure 2. Sedimentation velocity v_G according to eq 5 (dotted lines) and diffusion velocity v_{th} according to eq 8 (dashed lines) for gold (blue) and latex (red) spheres of different NP diameter r_{NP} , with the densities (ρ_{NP}) $\rho_{Au} = 19.3 \text{ g/cm}^3$ and $\rho_{latex} = 1.05 \text{ g/cm}^3$. The following parameters were used: $\rho_{H_2O} = 10^3 \text{ kg/m}^3$, $g = 9.81 \text{ m/s}^2$, $\eta_{H_2O} = 8.90 \times 10^{-4} \text{ Pa}\cdot\text{s}$, $k_B = 1.4 \times 10^{-23} \text{ J/K}$, and $T = 300 \text{ K}$. When $v_G > v_{th}$, the NPs will sediment, and when $v_G < v_{th}$, the NPs will be dispersed.

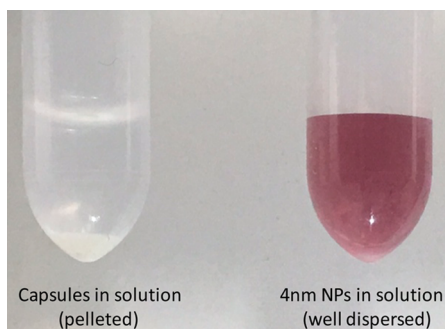


Figure 3. Solutions of polyelectrolyte capsules (similar in density to latex beads) of ca. $3 \mu\text{m}$ diameter (as prepared according to the protocol published by Muñoz Javier et al.²²) and of Au NPs of ca. 4 nm core diameter (as prepared according to the protocol published by Lin et al.²³).

have been considered, there are also interparticle forces F_i . Interparticle forces can be of a different nature, but in general, they are based on electromagnetic interaction. Forces are distance-dependent, i.e., they vary with the interparticle distance, and they can be attractive or repulsive. Between NPs with equal and opposite signs of charge, i.e., two electric monopoles, there will be a repulsive and attractive Coulomb force, respectively. Due to the adsorption of counterions, this force will be partially screened.^{21,24} In the case of magnetic NPs, there will be a magnetic dipole–dipole interaction. Also, van der Waals forces, i.e., induced electric dipole–dipole interaction, as hydration may play a role.²⁵ van der Waals forces are governed by induced electrical dipole–dipole interaction and are attractive.²⁶ However, they play a role only at very short distances of a few nanometers. Also, hydration forces, driven by the interaction of the solvent (water in the described case here), are short-ranged.²⁷ The coordination of water molecules to the NP surface results in adsorption enthalpy (i.e., repulsion between NPs to get the maximum effective NP surface because the formation of a water layer is favored) as well as an entropy decrease (i.e., attraction because water at the NP surface is structured, and thus in order to get maximal entropy, the effective NP surface should be as small

as possible, which would be the case for agglomerated NPs). Nevertheless, in well-dispersed NP solutions the hydrophilic surfaces of NPs usually do not approach each other close enough that short-range interaction is significant, as typically either a diffuse polymer layer (with relatively weak van der Waals forces) provides steric repulsion or bound surface charges provide electrostatic repulsion. However, when there are not enough polymer or net surface charges, aggregation can occur.

In colloidal suspensions, the force between NPs at larger distances is typically repulsive, whereas once the NPs come to close to each other there may be an attractive force and the NPs agglomerate. For calculations²⁸ as well as detailed NPs geometry, as NP interaction with ions and proteins²¹ needs to be considered. A detailed description for analytical calculations would be beyond the scope of this article. We refer the reader here to the Derjaguin, Landau, Verwey, Overbeek (DLVO) theory.^{29–31} Agglomeration thus in fact is not an intrinsic NP property, but it strongly depends on the solution in which the NPs are dispersed. Agglomerates of NPs by definition no longer can be considered to be individual NPs. In fact, instead of having NPs with individual hydrodynamic diameters in solution, in the case of agglomeration the effective NP diameter is the hydrodynamic diameter of the whole agglomerate. Brownian motion counteracts agglomeration, and agglomeration may occur only when attractive interparticle forces are stronger than thermal forces.

Resuming Thoughts about the Dispersion of NPs. We now can summarize the consideration from above. For small NPs, thermal motion outweighs gravity, and the NPs are colloidally stable. They are fully dissolved, i.e., dispersed in the whole (three-dimensional, 3d) medium (Figure 4). In the case of

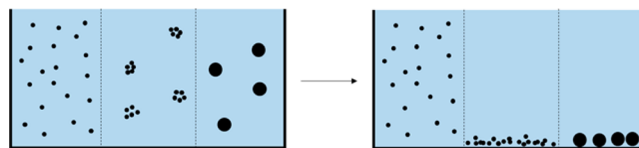


Figure 4. NPs dispersed in solution. Small NPs (left section) remain fully dispersed in solution via thermal energy/Brownian motion. If small NPs agglomerate due to strong attractive interparticle forces (middle section), then gravity acting on the big NP agglomerates causes sedimentation. Also in the case of intrinsically big NPs (right section), sedimentation occurs.

bigger NPs, gravity can play a dominant role in comparison to thermal motion. The NPs then sediment to the bottom of the Petri dish. In this way, there are fewer NPs in the bulk of the solution, but NPs accumulate at the 2d bottom surface. When there is significant agglomeration, the effective size and thus effective mass of the NPs increase, and when gravity acting on the mass of the whole NP agglomerate outweighs the thermal motion, the NP agglomerates sediment.

In the following text, only the effects of size and density will be discussed. Agglomerated NPs can be considered to be NPs with a bigger effective size.

How Many NPs Reach the Cells at the Bottom of a Petri Dish? Knowing the state of dispersion allows us to discuss how many NPs will reach the surfaces of cells that are grown on the bottom of the Petri dish. In case of dispersed NPs, the NPs distribute across the whole (huge, as in 3d) volume of the medium. In this way, only a small fraction of the NPs in solution will reach the surface of the cells by diffusion, and thus only a small fraction of the NPs present in solution may be actually internalized by cells (Figure 5). In fact, by cellular internalization

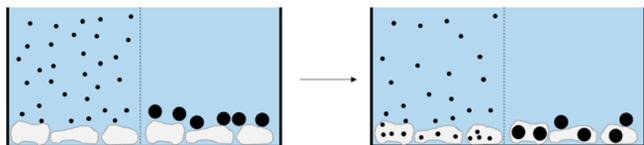


Figure 5. Small NPs are distributed in the huge volume of the medium (left section), and thus most NPs never reach the cells located on the bottom of the Petri dish. Thus, only a small number of NPs in the medium may be incorporated by the cells. Bigger NPs behave differently. They sediment by gravity, and thus there will be an enhanced local NP concentration on top of the cells. Thus, many NPs may be incorporated by the cells.

the local NP concentration close to the cells will be reduced, and thus driven by the concentration gradient, more NPs from the bulk of the solution will diffuse toward the bottom. However, the bulk can be considered to be a big reservoir of NPs, and the total bulk concentration of NPs will be only slightly reduced, as demonstrated by the examples given in Table 1. In contrast, in the case of bigger NPs (or NP agglomerates), gravity causes the NPs to sediment on top of the cells. The chance of a NP encountering a cell is now strongly enhanced from a 3d to a 2d diffusion problem. In this way, a larger fraction of these NPs will be internalized by cells.^{32–34} Note that the actual process of endocytosis itself will be slower in general for the bigger NPs.^{35,36} However, the actual number of internalized NPs will depend on the number of NPs present at the cell surface and the rate of endocytosis. Because there are many more of the bigger NPs locally available, they still will enter the cells to a higher extent despite reduced endocytosis. This is demonstrated by the number of examples in Table 1.

Fraction of Internalized NPs. Obviously, once NPs have reached the surface of cells, biology comes into play. As already pointed out, endocytosis depends on NP size, and there is an optimum size. NPs bigger than this optimum (which is determined, for example, by the mechanical properties of the cell membrane that upon endocytosis wraps around the NPs) are internalized to a lower extent.^{35,36} In fact, uptake has to be deconvoluted into two processes. First, NPs need to reach the surface of the cells. Second, the actual internalization process takes place. With some numbers from experimental data, we can show that for 2d cultures actually the first process, without a dependence on biology but dependent only on basic physicochemical parameters, dominates. To calculate the fraction of NPs actually incorporated by cells in a 2d culture, the

number of internalized NPs (N_{int}) has to be divided by the number of NPs (N_{add}) that have been added to the medium. First, data are shown for small, well-dispersed NPs that were not agglomerated.

In a study by Abdelmonem et al., poly(isobutylene-*alt*-maleic anhydride)-*graft*-dodecyl (PMA)-coated ZnO NPs of 6.8 nm core diameter and 18.4 nm hydrodynamic diameter (in water) were investigated.³⁷ Under the highest exposure condition (NP concentration $c_{\text{NP,medium}} = 1.80 \times 10^{-7}$ M, added to $N_{\text{cell}} = 2 \times 10^5$ cells in $V_{\text{medium}} = 1.5$ mL), $N_{\text{add}}/N_{\text{cell}} = 8.13 \times 10^8$ NPs were added per cell. After $t = 24$ h of exposure, $N_{\text{int}}/N_{\text{cell}} = 3.91 \times 10^6$ NPs were found in each cell.³⁷ Thus, only $N_{\text{int}}/N_{\text{add}} = 4.8 \times 10^{-3}$, i.e., around 5 permille of the added NPs were actually internalized (Table 1). If we assume that the internalized NPs are distributed within the volume of the cell V_{cell} (actually they are located in the much smaller volume of the endosomal/lysosomal compartments), then the intracellular NP concentration $c_{\text{NP,cell}}$ can be calculated. Results show that cells concentrate NPs; i.e., due to internalization, the NP concentration inside cells is higher than the original NP concentration in the medium: $c_{\text{NP,cell}}/c_{\text{NP,medium}} = 7.2$. However, because most NPs never reach the cell, only a small fraction of NPs will be internalized ($N_{\text{int}}/N_{\text{add}} \approx 5 \times 10^{-3}$) and the NP concentration inside the cells is only 1 order of magnitude higher than the extracellular NP concentration ($c_{\text{NP,cell}}/c_{\text{NP,medium}} \approx 7$). Data of another study based on CdSe/CdS/ZnS NPs³⁸ are very similar (Table 1).

For bigger NPs, such as polyelectrolyte capsules with a 5 μm diameter, the situation is different.³⁹ First, due to their size only a lower NP concentration, $c_{\text{NP,medium}}$, can be administered to cells. Because of gravity, the capsules sediment (cf. Figure 3) on top of the cells. Thus, cells come into contact with a large fraction of capsules in solution, and in this way $N_{\text{int}}/N_{\text{add}} = 28\%$ of the added capsules were actually internalized by cells. This is a much larger value than the one obtained for the smaller NPs. For big NPs, the cells also highly concentrate the NPs, as in the case of the polyelectrolyte capsules the intracellular NP concentration is $c_{\text{NP,cell}}/c_{\text{NP,medium}} = 2800$ times higher than the original extracellular NP concentration (Table 1). Obviously, the calculated numbers have to be seen rather as indicators of the order of magnitude than as precise absolute values.

The calculations presented here are based on three previous experimental reports. Unfortunately, in many studies important experimental data, such as the volume of the medium, are not given, and thus it is hard to obtain absolute numbers from those

Table 1. Quantitative Evaluation of NP Uptake by Cells with Numbers Taken from Previous Studies

NP type	d_h [nm]	cell type	t [h]	N_{cell}	V_{medium} [mL]	$c_{\text{NP,medium}}$ [M]		
ZnO ^a	18.4	Hela	24	2×10^5	1.5	1.80×10^{-7}		
CdSe/CdS/ZnS ^b	11.4	Hela	24	2×10^5	1.2	8.0×10^{-8}		
polymer capsules ^c	5000	MDA-MB-435s	19	2×10^4	1.0	1.06×10^{-15}		
NP type	$N_{\text{add}} = V_{\text{medium}} \cdot c_{\text{NP}} \cdot N_A$	$N_{\text{add}}/N_{\text{cell}}$	$N_{\text{int}}/N_{\text{cell}}$	$N_{\text{int}}/N_{\text{add}}$	V_{cell} [mL]	$c_{\text{NP,cell}}$ [M] = $(N_{\text{int}}/N_{\text{cell}})/N_A/V_{\text{cell}}$	$c_{\text{NP,cell}}/c_{\text{NP,medium}}$	ref
ZnO ^a	2.17×10^{14}	8.13×10^8	3.91×10^6	4.8×10^{-3}	5×10^{-9}	1.30×10^{-6}	7.2	37
CdSe/CdS/ZnS ^b	5.78×10^{13}	2.89×10^8	1.1×10^6	3.8×10^{-3}	5×10^{-9}	3.65×10^{-7}	4.6	38
polymer capsules ^c	6.4×10^5	32	9	2.8×10^{-1}	5×10^{-9}	2.99×10^{-12}	2800	39

Avogadro's constant $N_A = 6.02 \times 10^{23} \text{ mol}^{-1}$. d_h = hydrodynamic diameter in water, t = time of incubation of cells with NPs. N_{cell} = number of cells. V_{medium} = volume of the NP solution to which cells were exposed. $c_{\text{NP,medium}}$ = extracellular NP concentration upon incubation. N_{add} = number of NPs that have been added. N_{int} = number of NPs that have been found in all cells. V_{cell} = volume of one cell. $c_{\text{NP,cell}}$ = intracellular NP concentration ^aPMA-coated ZnO NPs;³⁷ hydrodynamic diameter from Table SI–IV.3; $c_{\text{NP,medium}} = 100 \mu\text{g/mL} = 100 \text{ mg/L} = 0.1 \text{ g/L}$ corresponds to $c_{\text{NP,medium}} = 1.80 \times 10^{-7}$ M, cf. Table SI–V.1; for N_{add} and N_{int} cf. Table SI–VI.1 by Abdelmonem et al.;³⁷ V_{cell} (Hela) $\approx 5000 \mu\text{m}^3 = 5000(10^{-4} \text{ cm})^3 = 5 \times 10^{-9}$ mL.⁴⁰ ^bCdSe/CdS/ZnS NPs coated with positively charged ligands;³⁸ for internalization data, cf. Table SI–IV.2 and comments below, data for positively charged NPs with $c_{\text{NP,medium}} = 80 \text{ nM}$, 24 h of incubation; cf. section IV.6 for calculations of intracellular NP concentrations. In contrast, a different cell volume was assumed. ^cPolyelectrolyte capsules made out of poly(styrenesulfonate) (PSS) and poly(allylamine hydrochloride) (PAH);³⁹ number of internalized NPs taken from the peak in Figure 3.

reports. When all parameters are known from quantitative analysis such as to determine the fraction of internalized NPs, $N_{\text{int}}/N_{\text{add}}$ or the concentration factor $c_{\text{NP,cell}}/c_{\text{NP,medium}}$ of NPs in cells versus the exposure medium can be calculated.

DISCUSSION

As pointed out by Cho et al.,¹⁸ sedimentation and diffusion are important physicochemical effects that need to be considered in cellular uptake studies of NPs. This is relevant to ecotoxicology studies in which sedimentation may vary local NP concentrations.^{41,42} For bigger NPs, sedimentation will cause the NPs to precipitate on top of the cells, and thus they can be internalized to a larger amount, which is contrary to the instinctive guess that bigger NPs enter cells less than smaller NPs. In fact, the actual process of endocytosis, which is cell-dependent, is more efficient for smaller NPs (for NPs > 50 nm).^{6,35,36} Still, micrometer-sized NPs are internalized by many cells, even by primary astrocytes.⁴³ However, for a description of the experimental situation two processes need to be carried out. First, the NPs have to reach cells, which is governed by basic physical and physicochemical effects that are generally known from textbook physics. For a diver on the bottom of a lake, it will be different to be hit by falling stones (sedimentation) or by floating dust (diffusion). Only then, in second order, does subtle biology in the form of endocytosis come into play. For instance, these considerations are important for magnetofection.⁴⁴ By pulling down magnetic NPs with a magnetic field gradient to the surface of cells, the local NP concentration around the cells is increased.^{45–47} The actual process of endocytosis is not affected, but due to the enhanced NP concentration around cells, more NPs are internalized.

For small, disperse NPs, most of them actually never come into contact with any cell. Thus, NP uptake will not be limited by the depletion of the medium from NPs. Saturation effects in the case of the cells no longer increasing the number of internalized NPs over time are not due to the lack of NPs in the medium but are due to other effects. When a cell culture is placed upside-down, uptake should be similar to that in cell cultures with the cells located at the bottom. For big NPs, given enough time, most NP sediment on the bottom of the flask will be internalized by cells. When the culture is turned upside-down, most cells would not be able to internalize NPs because they sediment at the bottom and do not reach the cells located on the top.¹⁸ Bigger NP results from 2d culture experiments thus have to be considered with care because they will not fully describe the situation present in real exposure scenarios, such as NP present in the blood. Here, exposure in flow channels would provide a more relevant experimental condition.

Cells can concentrate NPs from solution. In Table 1, the NPs were assumed to be distributed over the whole volume of a cell. However, the internalized NPs will be largely localized in the endosomes/lysosomes and thus have a much smaller volume. This means that the actual local NP concentration in endosomes/lysosomes may be orders of magnitude higher than the extracellular NP concentration upon exposure. This may have important consequences for toxicity analysis.⁴⁸

In addition, the role of agglomeration needs to be stressed. When NPs agglomerate, they will form NP agglomerates, which means that the effective diameter of the NPs will largely increase. Several factors will influence the agglomeration of NPs, including the NP concentration, which will strongly influence their rate of sedimentation.⁴⁹

The effects of NP interactions on agglomeration and sedimentation have been previously addressed, and several analytical tools for its investigation have been proposed.^{50,51} For instance, absorption spectroscopy has been used to investigate the

gravitational sedimentation of spherical Au NPs. Absorbance changes as a function of time were recorded and compared with theoretical values as obtained from the Mason–Weaver sedimentation–diffusion equation. Measurements were performed for a range of NP diameters, with known values of the size, density, and diffusion coefficient.⁵² Furthermore, predictive models have been also developed with the aim of providing information on the NP fate.^{53,54} As an example, Yang et al. evaluated the effects of salt and NP concentration on the agglomeration rate and sedimentation of silica spheres. On the basis of experimental data, the authors developed new models for predicting the relative of agglomeration and sedimentation of monodisperse silica NPs.⁴⁹

As discussed above, agglomeration can facilitate sedimentation and puts the NPs in closer proximity to cells. For a comprehensive cytotoxicity evaluation of NPs, including uptake studies of NPs by cells, the studies should provide information about the state of agglomeration and sedimentation of NPs.

CONCLUSIONS AND FUTURE PROSPECTS

Because of its complexity, the uptake of NPs by cells cannot always be studied directly in vivo. As a first tier, in vitro investigation is helpful, in particular, as under controlled conditions a larger variety of NP libraries can be screened. It is a common agreement that in vitro studies only partially describe real in vivo scenarios. It is important to design and interpret in vitro studies well. The state of dispersion, leading in the case of agglomerated NPs to NPs with an effectively bigger size, plays an important role as shown in this article. Thus, in vitro studies should be carried out at a similar state of dispersion as in vivo. In vivo there are shear forces and a large number of diverse molecules (proteins, lipids, etc.) that may interact with the NPs,⁵⁵ which may change their state of dispersion. Therefore, in vitro studies should attempt to emulate such conditions as well as possible. The use of flow channels may be a good first approach.^{56,57} In addition, new technologies to investigate the state of the dispersion in vivo would be very helpful.⁵⁸

AUTHOR INFORMATION

Corresponding Author

*E-mail: wolfgang.parak@physik.uni-marburg.de

ORCID

Ramon A. Alvarez Puebla: 0000-0003-4770-5756

Wolfgang J. Parak: 0000-0003-1672-6650

Notes

The authors declare no competing financial interest.

Biographies



Neus Feliu graduated in chemistry from Universitat de Barcelona (UB) in 2007 and obtained her Master of Science degree in

biomedical materials from the Royal Institute of Technology (KTH) in Stockholm in 2009. She obtained her Ph.D. in medical science from Karolinska Institutet, Stockholm in the field of engineered nanomaterials for biomedical applications in 2014. She is currently a VINNMER Fellow and a Marie Curie Fellow at the Department of Laboratory Medicine (LABMED), Clinical Research Center, Karolinska Institutet, Stockholm, Sweden. Her research interest is focused on understanding the interactions between nanoparticles and biological systems and exploring their use in the field of medicine.



Xing Sun received his Bachelor's and Master's of Science degrees in chemistry from China University of Petroleum (East China) in 2015. During his Master's degree, he studied drug delivery systems with fluorescent nanoparticles. Afterward, he joined Wolfgang Parak's group at the Philipps University of Marburg, Germany supported by the China Scholarship Council. His research focuses mainly on the interactions between gold nanoparticles and stem cells.



Ramón A. Alvarez-Puebla is currently an ICREA Professor at the Universitat Rovira i Virgili, Tarragona, Spain. He worked as a postdoctoral fellow in the Department of Chemistry and Biochemistry of the University of Windsor, Canada with Prof. Ricardo Aroca, and he was appointed a research officer at the National Institute for Nanotechnology of the National Research Council of Canada. In 2008, he returned Spain. He has coauthored over 140 articles and holds 10 patents. His current interest involves the design and fabrication of plasmonic sensors and their use with surface-enhanced spectroscopies especially in the fields of chemical biology and clinical diagnostics.



Wolfgang J. Parak studied physics at the Technische Universität München and obtained his Ph.D. in Hermann Gaub's group at the Ludwig Maximilians Universität München. After 2.5 years as a postdoctoral researcher in Paul Alivisatos's group at the University of California, Berkeley he started his own group in Munich in the framework of an Emmy Noether fellowship in 2002. Since 2007, he has been a full professor at the Philipps Universität Marburg, and since 2013, he has also been a group leader at CIC biomaGUNE, San Sebastian, Spain. Since 2009, Professor Parak has been an associate editor of *ACS Nano*. He has significantly contributed to the development of new surface chemistries of inorganic nanoparticles and the characterization of their physicochemical properties. In particular, the development of an amphiphilic polymer coating is nowadays used by many different groups worldwide. Nanoparticles with such high colloidal stability are the bases of experimentally correlating their physicochemical properties with their interaction with cells (involving uptake and cytotoxicity), which has been his research topic for the last 17 years, in which he has achieved international recognition. Wolfgang Parak also pioneered the use of polymeric polyelectrolyte capsules fabricated by layer-by-layer assembly in biological applications (for in vitro sensing and delivery).

■ ACKNOWLEDGMENTS

N.F. acknowledges funding from the Swedish Governmental Agency for Innovation Systems (Vinnova). X.S. acknowledges funding from the Chinese Scholarship Council (CSC). W.J.P. acknowledges funding from the Sino-German Center (GZ905) and the German Research Foundation (DFG grant PA 794/21-1).

■ REFERENCES

- (1) Ritz, S.; Schottler, S.; Kotman, N.; Baier, G.; Musyanovych, A.; Kuharev, J.; Landfester, K.; Schild, H.; Jahn, O.; Tenzer, S.; Mailander, V. Protein corona of nanoparticles: distinct proteins regulate the cellular uptake. *Biomacromolecules* **2015**, *16* (4), 1311–21.
- (2) Jiang, Y.; Huo, S. D.; Mizuhara, T.; Das, R.; Lee, Y. W.; Hou, S.; Moyano, D. F.; Duncan, B.; Liang, X. J.; Rotello, V. M. The Interplay of Size and Surface Functionality on the Cellular Uptake of Sub-10 nm Gold Nanoparticles. *ACS Nano* **2015**, *9* (10), 9986–9993.
- (3) Manshian, B. B.; Soenen, S. J.; Al-Ali, A.; Brown, A.; Hondow, N.; Wills, J.; Jenkins, G. J. S.; Doak, S. H. Cell Type-Dependent Changes in CdSe/ZnS Quantum Dot Uptake and Toxic Endpoints. *Toxicol. Sci.* **2015**, *144* (2), 246–258.
- (4) Huefner, A.; Kuan, W. L.; Muller, K. H.; Skepper, J. N.; Barker, R. A.; Mahajan, S. Characterization and Visualization of Vesicles in the Endo-Lysosomal Pathway with Surface-Enhanced Raman Spectroscopy and Chemometrics. *ACS Nano* **2016**, *10* (1), 307–316.
- (5) Beddoes, C. M.; Case, C. P.; Briscoe, W. H. Understanding nanoparticle cellular entry: A physicochemical perspective. *Adv. Colloid Interface Sci.* **2015**, *218*, 48–68.

- (6) Allouni, Z. E.; Hol, P. J.; Cauqui, M. A.; Gjerdet, N. R.; Cimpan, M. R. Role of physicochemical characteristics in the uptake of TiO₂ nanoparticles by fibroblasts. *Toxicol. In Vitro* **2012**, *26* (3), 469–479.
- (7) Tay, C. Y.; Setyawati, M. I.; Xie, J.; Parak, W. J.; Leong, D. T. Back to Basics: Exploiting the Innate Physico-chemical Characteristics of Nanomaterials for Biomedical Applications. *Adv. Funct. Mater.* **2014**, *24*, 5936–5955.
- (8) Pelaz, B.; Del Pino, P.; Maffre, P.; Hartmann, R.; Gallego, M.; Rivera-Fernandez, S.; de la Fuente, J. M.; Nienhaus, G. U.; Parak, W. J. Surface Functionalization of Nanoparticles with Polyethylene Glycol: Effects on Protein Adsorption and Cellular Uptake. *ACS Nano* **2015**, *9* (7), 6996–7008.
- (9) del Pino, P.; Yang, F.; Pelaz, B.; Zhang, Q.; Kantner, K.; Hartmann, R.; Baroja, N. M. d.; Gallego, M.; Möller, M.; Manshian, B. B.; Soenen, S. J.; Riedel, R.; Hampp, N.; Parak, W. J. Basic Physicochemical Properties of Polyethylene Glycol Coated Gold Nanoparticles that Determine Their Interaction with Cells. *Angew. Chem., Int. Ed.* **2016**, *55*, 5483–5487.
- (10) Hühn, J.; Carrillo-Carrion, C.; Soliman, M. G.; Pfeiffer, C.; Valdeperez, D.; Masood, A.; Chakraborty, I.; Zhu, L.; Gallego, M.; Zhao, Y.; Carril, M.; Feliu, N.; Escudero, A.; Alkilany, A. M.; Pelaz, B.; Pino, P. d.; Parak, W. J. Selected Standard Protocols for the Synthesis, Phase Transfer, and Characterization of Inorganic Colloidal Nanoparticles. *Chem. Mater.* **2017**, *29*, 399–461.
- (11) DeLoid, G.; Cohen, J. M.; Darrah, T.; Derk, R.; Rojasasakul, L.; Pyrgiotakis, G.; Wohlleben, W.; Demokritou, P. Estimating the effective density of engineered nanomaterials for in vitro dosimetry. *Nat. Commun.* **2014**, *5*, 3514.
- (12) Parakhonskiy, B.; Zyuzin, M. V.; Yashchenok, A.; Carregal-Romero, S.; Rejman, J.; Mohwald, H.; Parak, W. J.; Skirtach, A. G. The influence of the size and aspect ratio of anisotropic, porous CaCO₃ particles on their uptake by cells. *J. Nanobiotechnol.* **2015**, *13* (1), 53.
- (13) Feliu, N.; Pelaz, B.; Zhang, Q.; del Pino, P.; Nyström, A.; Parak, W. J. Nanoparticle dosage—a nontrivial task of utmost importance for quantitative nanosafety research. *Wiley Interdiscip. Rev. Nanomed. Nanobiotechnol.* **2016**, *8*, 479–492.
- (14) Semmling, M.; Kreft, O.; Muñoz Javier, A.; Sukhorukov, G. B.; Käs, J.; Parak, W. J. A Novel Flow-Cytometry-based Assay for Cellular Uptake Studies of Polyelectrolyte Microcapsules. *Small* **2008**, *4* (10), 1763–1768.
- (15) Hartmann, R.; Weidenbach, M.; Neubauer, M.; Fery, A.; Parak, W. J. Stiffness-dependent in vitro uptake and lysosomal acidification of colloidal particles. *Angew. Chem., Int. Ed.* **2015**, *54* (4), 1365–1368.
- (16) Braun, G. B.; Friman, T.; Pang, H. B.; Pallaoro, A.; de Mendoza, T. H.; Willmore, A. M. A.; Kotamraju, V. R.; Mann, A. P.; She, Z. G.; Sugahara, K. N.; Reich, N. O.; Teesalu, T.; Ruoslahti, E. Etchable plasmonic nanoparticle probes to image and quantify cellular internalization. *Nat. Mater.* **2014**, *13* (9), 904–911.
- (17) Hou, S.; Sikora, K. N.; Tang, R.; Liu, Y. C.; Lee, Y. W.; Kim, S. T.; Jiang, Z. W.; Vachet, R. W.; Rotello, V. M. Quantitative Differentiation of Cell Surface-Bound and Internalized Cationic Gold Nanoparticles Using Mass Spectrometry. *ACS Nano* **2016**, *10* (7), 6731–6736.
- (18) Cho, E. C.; Zhang, Q.; Xia, Y. N. The effect of sedimentation and diffusion on cellular uptake of gold nanoparticles. *Nat. Nanotechnol.* **2011**, *6* (6), 385–391.
- (19) Limbach, L. K.; Li, Y. C.; Grass, R. N.; Brunner, T. J.; Hintermann, M. A.; Muller, M.; Gunther, D.; Stark, W. J. Oxide nanoparticle uptake in human lung fibroblasts: Effects of particle size, agglomeration, and diffusion at low concentrations. *Environ. Sci. Technol.* **2005**, *39* (23), 9370–9376.
- (20) Jamison, J. A.; Krueger, K. M.; Yavuz, C. T.; Mayo, J. T.; LeCrone, D.; Redden, J. J.; Colvin, V. L. Size-Dependent Sedimentation Properties of Nanocrystals. *ACS Nano* **2008**, *2* (2), 311–319.
- (21) Rivera Gil, P.; Jimenez de Aberasturi, D.; Wulf, V.; Pelaz, B.; del Pino, P.; Zhao, Y.; de la Fuente, J.; Ruiz de Larramendi, I.; Rojo, T.; Liang, X.-J.; Parak, W. J. The Challenge to Relate the Physicochemical Properties of Colloidal Nanoparticles to Their Cytotoxicity. *Acc. Chem. Res.* **2013**, *46* (3), 743–749.
- (22) Muñoz Javier, A.; del Pino, P.; Bedard, M. F.; Skirtach, A. G.; Ho, D.; Sukhorukov, G. B.; Plank, C.; Parak, W. J. Photoactivated Release of Cargo from the Cavity of Polyelectrolyte Capsules to the Cytosol of Cells. *Langmuir* **2008**, *24*, 12517–12520.
- (23) Lin, C.-A. J.; Sperling, R. A.; Li, J. K.; Yang, T.-Y.; Li, P.-Y.; Zanella, M.; Chang, W. H.; Parak, W. J. Design of an Amphiphilic Polymer for Nanoparticle Coating and Functionalization. *Small* **2008**, *4* (3), 334–341.
- (24) Zhang, F.; Ali, Z.; Amin, F.; Feltz, A.; Oheim, M.; Parak, W. J. Ion and pH sensing with colloidal nanoparticles: influence of surface charge on sensing and colloidal properties. *ChemPhysChem* **2010**, *11*, 730–735.
- (25) Israelachvili, J. N. *Intermolecular and Surface Forces*, 2nd ed.; Academic Press: London, 1992.
- (26) Hamaker, H. C. The London—van der Waals attraction between spherical particles. *Physica* **1937**, *4* (10), 1058–1072.
- (27) Parsegian, V. A.; Zemb, T. Hydration forces: Observations, explanations, expectations, questions. *Curr. Opin. Colloid Interface Sci.* **2011**, *16* (6), 618–624.
- (28) Schrittwieser, S.; Pelaz, B.; Parak, W. J.; Lentijo-Mozo, S.; Soulantica, K.; Dieckhoff, J.; Ludwig, F.; Altantzis, T.; Bals, S.; Schotter, J. Homogeneous Protein Analysis by Magnetic Core—Shell Nanorod Probes. *ACS Appl. Mater. Interfaces* **2016**, *8*, 8893–8899.
- (29) Derjaguin, B.; Landau, L. Theory of the stability of strongly charged lyophobic sols and of the adhesion of strongly charged particles in solutions of electrolytes. *Prog. Surf. Sci.* **1993**, *43* (1–4), 30–59.
- (30) Levine, S.; Dube, G. P. Interaction between two hydrophobic colloidal particles, using the approximate Debye-Hückel theory. I. General properties. *Trans. Faraday Soc.* **1939**, *35*, 1125–1140.
- (31) Levine, S. Problems of Stability in Hydrophobic Colloidal Solutions. I. On the Interaction of Two Colloidal Metallic Particles. General Discussion and Applications. *Proc. R. Soc. London, Ser. A* **1939**, *170*, 145–164.
- (32) Vranic, S.; Gosens, I.; Jacobsen, N. R.; Jensen, K. A.; Bokkers, B.; Kermandadeh, A.; Stone, V.; Baeza-Squiban, A.; Cassee, F. R.; Tran, L.; Boland, S. Impact of serum as a dispersion agent for in vitro and in vivo toxicological assessments of TiO₂ nanoparticles. *Arch. Toxicol.* **2017**, *91* (1), 353–363.
- (33) Cui, J. W.; Faria, M.; Bjornmalm, M.; Ju, Y.; Suma, T.; Gunawan, S. T.; Richardson, J. J.; Heidar, H.; Bals, S.; Crampin, E. J.; Caruso, F. A Framework to Account for Sedimentation and Diffusion in Particle-Cell Interactions. *Langmuir* **2016**, *32* (47), 12394–12402.
- (34) Spyrogiani, A.; Herrmann, I. K.; Lucas, M. S.; Leroux, J. C.; Sotiriou, G. A. Quantitative analysis of the deposited nanoparticle dose on cell cultures by optical absorption spectroscopy. *Nanomedicine* **2016**, *11* (19), 2483–2496.
- (35) Chithrani, B. D.; Ghazan, A. A.; Chan, C. W. Determining the Size and the Shape dependence of gold nanoparticle uptake into mammalian cells. *Nano Lett.* **2006**, *6* (4), 662–668.
- (36) Chithrani, B. D.; Chan, W. C. W. Elucidating the mechanism of cellular uptake and removal of protein-coated gold nanoparticles of different sizes and shapes. *Nano Lett.* **2007**, *7* (6), 1542–1550.
- (37) Abdelmonem, A. M.; Pelaz, B.; Kantner, K.; Bigall, N. C.; Del Pino, P.; Parak, W. J. Charge and agglomeration dependent in vitro uptake and cytotoxicity of zinc oxide nanoparticles. *J. Inorg. Biochem.* **2015**, *153*, 334–338.
- (38) Ashraf, S.; Park, J.; Bichelberger, M.; Kantner, K.; Hartmann, R.; Maffre, P.; Said, A. H.; Feliu, N.; Lee, J.; Lee, D.; Nienhaus, G. U.; Kim, S.; Parak, W. J. Zwitterionic surface coating of quantum dots reduces protein adsorption and cellular uptake. *Nanoscale* **2016**, *8*, 17994–17999.
- (39) Sukhorukov, G. B.; Rogach, A. L.; Zebli, B.; Liedl, T.; Skirtach, A. G.; Köhler, K.; Antipov, A. A.; Gaponik, N.; Susha, A. S.; Winterhalter, M.; Parak, W. J. Nanoengineered polymer capsules: Tools for detection, controlled delivery and site specific manipulation. *Small* **2005**, *1* (2), 194–200.
- (40) Cohen, L. S.; Studzinski, G. P. Correlation between cell enlargement and nucleic acid and protein content of hela cells in unbalanced growth produced by inhibitors of DNA synthesis. *J. Cell. Physiol.* **1967**, *69* (3), 331–339.

- (41) Xiao, Y.; Ho, K. T.; Burgess, R. M.; Cashman, M. Aggregation, Sedimentation, Dissolution, and Bioavailability of Quantum Dots in Estuarine Systems. *Environ. Sci. Technol.* **2017**, *51* (3), 1357–1363.
- (42) Gupta, G. S.; Kumar, A.; Shanker, R.; Dhawan, A. Assessment of agglomeration, co-sedimentation and trophic transfer of titanium dioxide nanoparticles in a laboratory-scale predator-prey model system. *Sci. Rep.* **2016**, *6*, 10.1038/srep31422.
- (43) Kastl, L.; Sasse, D.; Wulf, V.; Hartmann, R.; Mircheski, J.; Ranke, C.; Carregal-Romero, S.; Martínez-López, J. A.; Fernández-Chacón, R.; Parak, W. J.; Elsaesser, H.-P.; Rivera Gil, P. Multiple internalization pathways of polyelectrolyte multilayer capsules into mammalian cells. *ACS Nano* **2013**, *7* (8), 6605–6618.
- (44) Huth, S.; Lausier, J.; Gersting, S. W.; Rudolph, C.; Plank, C.; Welsch, U.; Rosenecker, J. Insights into the mechanism of magnetofection using PEI-based magnetofectins for gene transfer. *J. Gene Med.* **2004**, *6* (8), 923–936.
- (45) Scherer, F.; Anton, M.; Schillinger, U.; Henke, J.; Bergemann, C.; Kruger, A.; Gansbacher, B.; Plank, C. Magnetofection: enhancing and targeting gene delivery by magnetic force in vitro and in vivo. *Gene Ther.* **2002**, *9* (2), 102–9.
- (46) Mykhaylyk, O.; Vlaskou, D.; Tresilwised, N.; Pithayanukul, P.; Moller, W.; Plank, C. Magnetic nanoparticle formulations for DNA and siRNA delivery. *J. Magn. Magn. Mater.* **2007**, *311* (1), 275–281.
- (47) Zebli, B.; Susha, A. S.; Sukhorukov, G. B.; Rogach, A. L.; Parak, W. J. Magnetic Targeting and Cellular Uptake of Polymer Microcapsules Simultaneously Functionalized with Magnetic and Luminescent Nanocrystals. *Langmuir* **2005**, *21*, 4262–4265.
- (48) Rejman, J.; Nazarenus, M.; Aberasturi, D. J. d.; Said, A. H.; Feliu, N.; Parak, W. J. Some thoughts about the intracellular location of nanoparticles and the resulting consequences. *J. Colloid Interface Sci.* **2016**, *482*, 260–266.
- (49) Yang, Y. J.; Kelkar, A. V.; Corti, D. S.; Franses, E. I. Effect of Interparticle Interactions on Agglomeration and Sedimentation Rates of Colloidal Silica Microspheres. *Langmuir* **2016**, *32* (20), 5111–5123.
- (50) Vikesland, P. J.; Rebodos, R. L.; Bottero, J. Y.; Rose, J.; Masion, A. Aggregation and sedimentation of magnetite nanoparticle clusters. *Environ. Sci.: Nano* **2016**, *3* (3), 567–577.
- (51) Allouni, Z. E.; Cimpan, M. R.; Hol, P. J.; Skodvin, T.; Gjerdet, N. R. Agglomeration and sedimentation of TiO₂ nanoparticles in cell culture medium. *Colloids Surf., B* **2009**, *68* (1), 83–87.
- (52) Alexander, C. M.; Dabrowiak, J. C.; Goodisman, J. Gravitational sedimentation of gold nanoparticles. *J. Colloid Interface Sci.* **2013**, *396*, 53–62.
- (53) Quik, J. T. K.; van de Meent, D.; Koelmans, A. A. Simplifying modeling of nanoparticle aggregation-sedimentation behavior in environmental systems: A theoretical analysis. *Water Res.* **2014**, *62*, 193–201.
- (54) Yang, Y. J.; Kelkar, A. V.; Zhu, X. L.; Bai, G. R.; Ng, H. T.; Corti, D. S.; Franses, E. I. Effect of sodium dodecylsulfate monomers and micelles on the stability of aqueous dispersions of titanium dioxide pigment nanoparticles against agglomeration and sedimentation. *J. Colloid Interface Sci.* **2015**, *450*, 434–445.
- (55) Allouni, Z. E.; Gjerdet, N. R.; Cimpan, M. R.; Hol, P. J. The effect of blood protein adsorption on cellular uptake of anatase TiO₂ nanoparticles. *Int. J. Nanomed.* **2015**, *10*, 687–695.
- (56) Strobl, F. G.; Breyer, D.; Link, P.; Torrano, A. A.; Brauchle, C.; Schneider, M. F.; Wixforth, A. A surface acoustic wave-driven micropump for particle uptake investigation under physiological flow conditions in very small volumes. *Beilstein J. Nanotechnol.* **2015**, *6*, 414–419.
- (57) Samuel, S. P.; Jain, N.; O'Dowd, F.; Paul, T.; Kashanin, D.; Gerard, V. A.; Gun'ko, Y. K.; Prina-Mello, A.; Volkov, Y. Multifactorial determinants that govern nanoparticle uptake by human endothelial cells under flow. *Int. J. Nanomed.* **2012**, *7*, 2943–2956.
- (58) Hadjidemetriou, M.; Al-Ahmady, Z.; Mazza, M.; Collins, R. F.; Dawson, K.; Kostarelou, K. In Vivo Biomolecule Corona around Blood-Circulating, Clinically Used and Antibody-Targeted Lipid Bilayer Nanoscale Vesicles. *ACS Nano* **2015**, *9* (8), 8142–8156.

How Entanglement of Different Physicochemical Properties Complicates the Prediction of *in Vitro* and *in Vivo* Interactions of Gold Nanoparticles

Ming Xu,^{†,‡,⊥} Mahmoud G. Soliman,^{‡,§,#} Xing Sun,^{‡,§} Beatriz Pelaz,^{‡,⊥} Neus Feliu,^{§,||} Wolfgang J. Parak,^{*,‡,§,⊥} and Sijin Liu^{*,†,⊥}

[†]State Key Laboratory of Environmental Chemistry and Ecotoxicology, Research Center for Eco-Environmental Sciences, Chinese Academy of Sciences, Beijing 100085, China

[‡]Fachbereich Physik, Philipps Universität Marburg, Marburg 35032, Germany

[§]Fachbereich Physik und Chemie, CHyN, Universität Hamburg, Hamburg 20148, Germany

^{||}Department of Laboratory Medicine (LABMED), Karolinska Institutet, Stockholm 171 77, Sweden

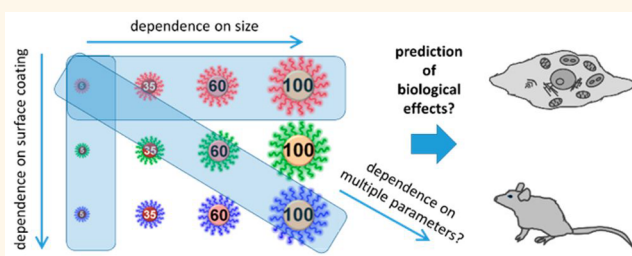
[⊥]University of Chinese Academy of Sciences, Beijing 100049, China

[#]Physics Department, Faculty of Science, Al-Azhar University, Cairo, Egypt

Supporting Information

ABSTRACT: The physicochemical properties of a set of 21 different gold nanoparticles (spherical and rod-shaped nanoparticles (NPs) of different diameters with three different surface coatings) were studied. Protein corona formation, *in vitro* uptake, effect on cell viability and proliferation, and *in vivo* biodistribution of these NPs were determined. The relation of the results of the different NPs was analyzed by hierarchical cluster analysis, which will tell which NPs have the most similar physicochemical properties and biological effects, without having to specify individual physicochemical parameters. The results show that the physicochemical properties of gold nanoparticles (Au NPs) are mainly accounted for by their hydrodynamic diameter and their zeta-potential. The formation of the protein corona is determined by the pH-dependence of their zeta-potential. While several reports found that *in vitro* uptake and *in vivo* biodistribution of NPs are correlated to individual physicochemical parameters, e.g., size, shape, or surface chemistry, such direct dependence in the investigated multidimensional set of NPs was not found in our study. This most likely is due to entanglement of the different parameters, which complicates the prediction of the biological effect of NPs in case multiple physicochemical properties are simultaneously varied. The *in vitro* uptake and *in vivo* biodistribution of NPs seem to be not directly driven by the protein corona, but the physicochemical properties determine as well the corona as they influence *in vitro/in vivo* behaviors, and thus the effect of the protein corona would be rather indirect.

KEYWORDS: gold nanoparticles, physicochemical properties, prediction, hierarchical cluster analysis



Colloidal nanoparticles (NPs) may be valuable tools for *in vivo* diagnosis and therapy in the future.^{1,2} Before they can be safely used in clinics, their interaction with the human body needs to be understood for each individual type of particle.³ This involves for example biodistribution (concerning targeting) as well as toxicity (concerning safety).⁴ In order to avoid testing of each new NP formulation from scratch, predicting the biological effect of any new NP by their physicochemical properties would be ideal.^{5–8} While there are many studies about the impact of certain physicochemical NP properties on the biological effect of NPs,^{9–12} such as size-,

shape-, surface coating-, or band gap-dependence,¹³ a reliable prediction based on the physicochemical properties so far has not been possible. This is largely due to the fact that dependencies of different physicochemical parameters may be strongly entangled. The dilemma can be summarized with the following question: would 5 nm diameter gold NPs (Au NPs)

Received: June 28, 2018

Accepted: September 13, 2018

Published: September 13, 2018

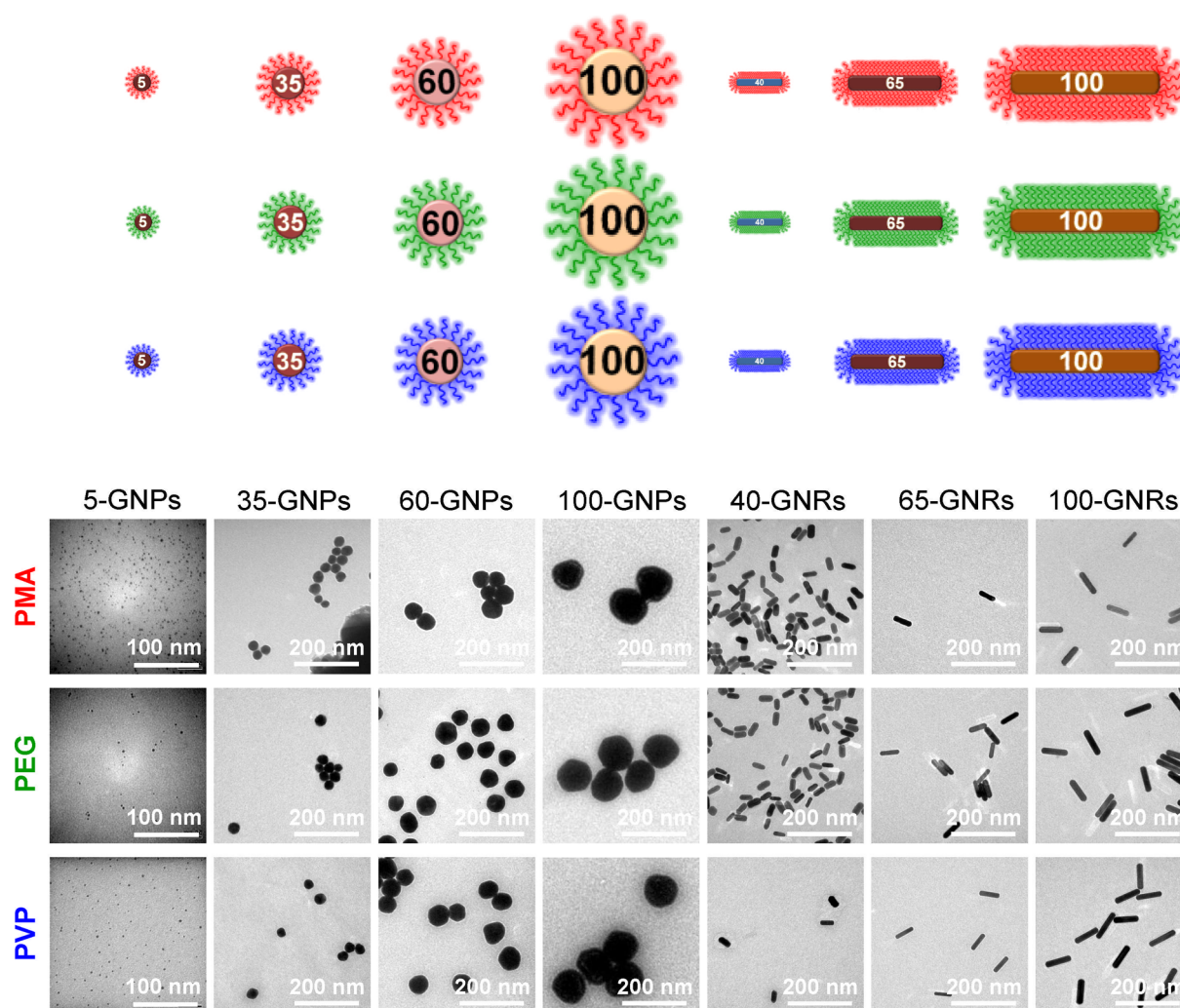


Figure 1. Overview of the NP library, together with corresponding TEM images. Spherical Au NPs with core diameters of 5, 35, 60, and 100 nm, are termed 5-GNPs, 35-GNPs, 60-GNPs, and 100-GNPs, respectively, and rod-shaped Au NPs with core lengths of 40, 65, and 100 nm, are termed 40-GNRs, 65-GNRs, and 100-GNRs, respectively. The color code of the surface coating is as follows: PMA (red), PVP (blue), PEG (green).

with a polyethylene (PEG) coating have a biological response more similar to that of 100 nm diameter Au NPs with a PEG coating or to 5 nm diameter Au NPs with a polyvinylpyrrolidone (PVP) coating? In other words, would the size or the surface chemistry dominate?¹⁴ Given that there are at least tens of important physicochemical parameters, it may be impossible to determine the influence of one isolated physicochemical parameter on the biological effect of NPs. In fact, the effect will depend on an entanglement of all these parameters.

As there are many attempts to predict the biological effect of NPs based on their properties reported in the literature, here first some important findings are summarized. NP uptake and NP-induced toxicity^{15,16} have been related to different individual parameters in various *in vitro* studies,¹⁷ such as size,^{18,19} shape,^{18,20–23} and surface properties,^{19,24–29} e.g., charge.^{30,31} In these studies, the physicochemical parameter subject for analysis (e.g., size) was varied, while the other parameters were kept constant. However, crosstalk between different parameters on the biological effect of NPs was reported, for example, between size and surface coating,¹⁴ and shape and surface coating.³²

Virtually, for any scenario of *in vitro* or *in vivo* application of NPs, the NPs would be exposed to proteins, which eventually will adsorb to the surface of the NPs,³³ and the kinetics depends on the details of the NP–protein interaction.³⁴ The formation of the protein corona has been widely studied.^{35–37} It depends on the physicochemical properties of the underlying NPs.³⁸ Important relevant NP parameters have been identified, such as size,³⁹ shape,^{40,41} and surface chemistry.^{29,42–44} The protein corona is in general not a static entity, but depends on the local environment. It thus may change dynamically in *in vitro* and *in vivo* scenarios along the trajectory of the NPs from administration to their final fate.^{45–47} In addition, the biological effect of the protein corona depends not only on its composition but also on conformation changes^{48,49} of adsorbed proteins.^{50–52} The impact of the protein corona on the biological effect of NPs has been discussed in many reports.^{53–58} It has been reported that the composition of the protein corona may effect cellular uptake^{59–61} and thus also the *in vivo* biodistribution of the NPs.⁵⁹ The enhanced presence of certain proteins on the NP surface may also increase systemic toxicity of the NPs.⁵⁹ In contrast, one study pointed out that the protein corona composition does not

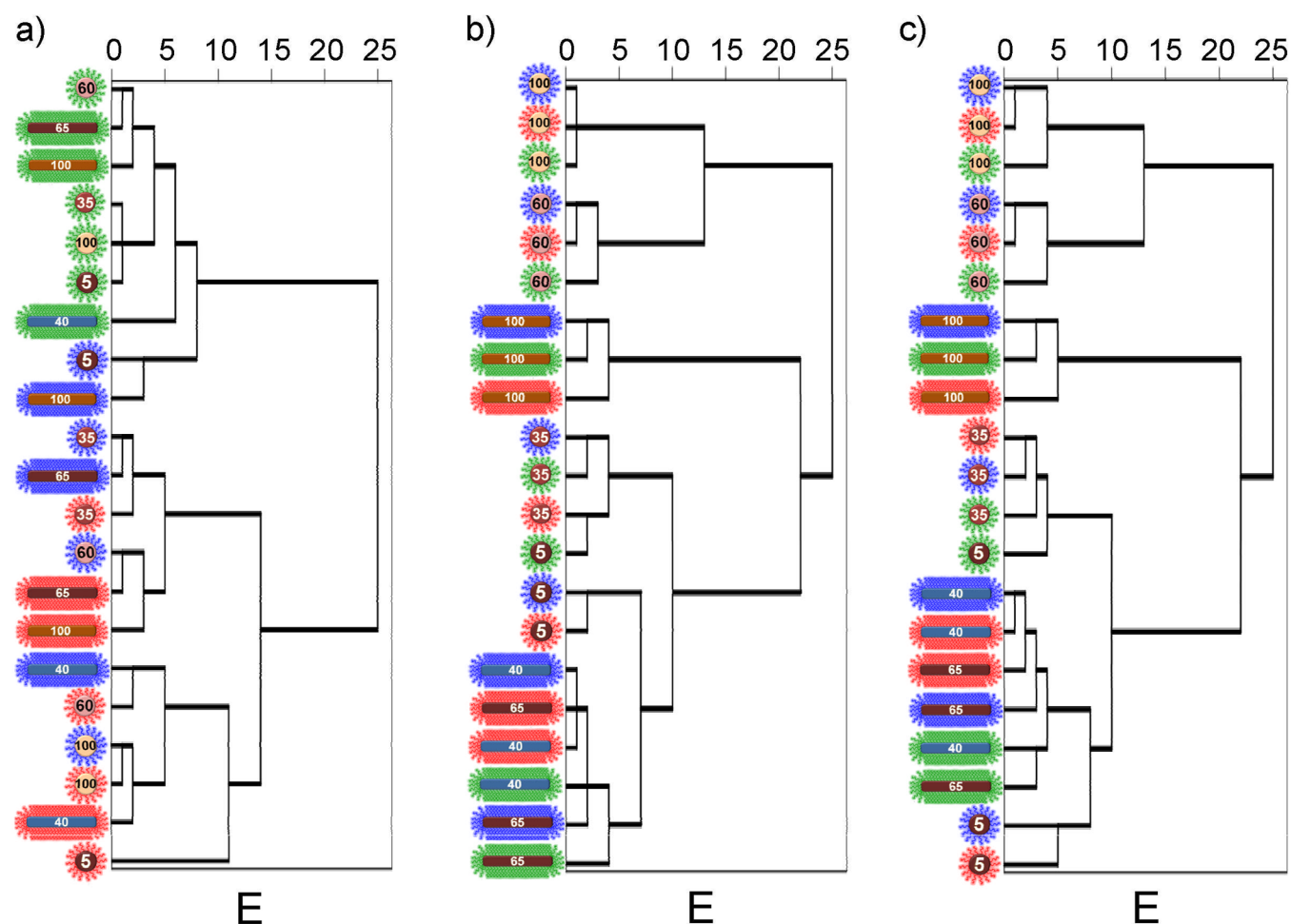


Figure 2. HCA analysis of different subsets of physicochemical properties, shown in terms of Euclidean distance E . The closer two types of NPs are in these “family trees”, the more their properties are related. (a) HCA of zeta-potentials, demonstrating that in particular the PEG coating (green) causes high similarity. (b) HCA of hydrodynamic diameters, resulting in dependence of similarity according to the type of NP core (diameter, shape). (c) HCA of hydrodynamic diameters, zeta-potentials, and electrophoretic mobilities, sorting the NPs remarkably well by their core volume ($V_c(100\text{-GNPs}) > V_c(60\text{-GNPs}) > V_c(100\text{-GNRs}) > V_c(35\text{-GNPs}) > V_c(65\text{-GNRs}) > V_c(40\text{-GNRs}) > V_c(5\text{-GNPs})$).

accurately predict hemocompatibility of the Au NPs.⁶² For an overview about how the protein corona influences the toxicity of NPs, refer to recent reviews.^{63,64} Furthermore, the protein corona may even impact the degradation behavior of NPs.⁶⁵ Despite those reports, which correlate *in vitro* and *in vivo* behavior of NPs to the protein corona, the basic physicochemical properties have been also reported to directly determine the biological effect of NPs,⁶⁶ such as shape-mediated biodistribution⁶⁷ or surface chemistry-mediated immune response.⁶⁸ Apart from the entanglement of physicochemical parameters, the presence of the protein corona also complicates the prediction. Are biological effects due to the basic physicochemical properties or due to the protein corona, which however depends itself on the physicochemical properties?

While the above summarized experiments report the correlations of biological effects to distinct individual physicochemical parameters and the protein corona, as mentioned above, this was in general possible by variation of the relevant parameter when keeping other parameters constant. However, the dependence on parameters would be a linear superposition of the responses to changes in only one parameter; the results could not be extended to studies with multiparameter variation. The above-reported dependencies

thus do not necessarily need to hold true in general, in case NP libraries with multiple variation parameters are investigated.

Given those complications, instead of trying to sort out the biological effect of NPs according to individual physicochemical parameters, in this study we attempted to apply hierarchical cluster analysis (HCA) in order to define which NPs are most closely related. In this way, from a set of many different physicochemical parameters determined for each type of NP, HCA will tell which NPs have the most similar physicochemical properties, without having to specify individual physicochemical parameters. Biological effects of these different types of NPs were then assayed at three different levels. First, the formation of the protein corona upon incubation in mouse serum was measured. Second, the experiments investigating the *in vitro* response, such as NP incorporation by cell lines, cell viability, and proliferation assays, were performed. Third, the *in vivo* biodistribution was measured for all NP types. For each of the different levels, the similarity between the responses to the different NP types was grouped by HCA. In this way, four tiers of HCA groupings were achieved: (i) physicochemical properties, (ii) protein corona, (iii) *in vitro* interaction, and (iv) *in vivo* biodistribution. Within each tier, HCA tells which NPs are more closely related. This was performed for a comprehensive library

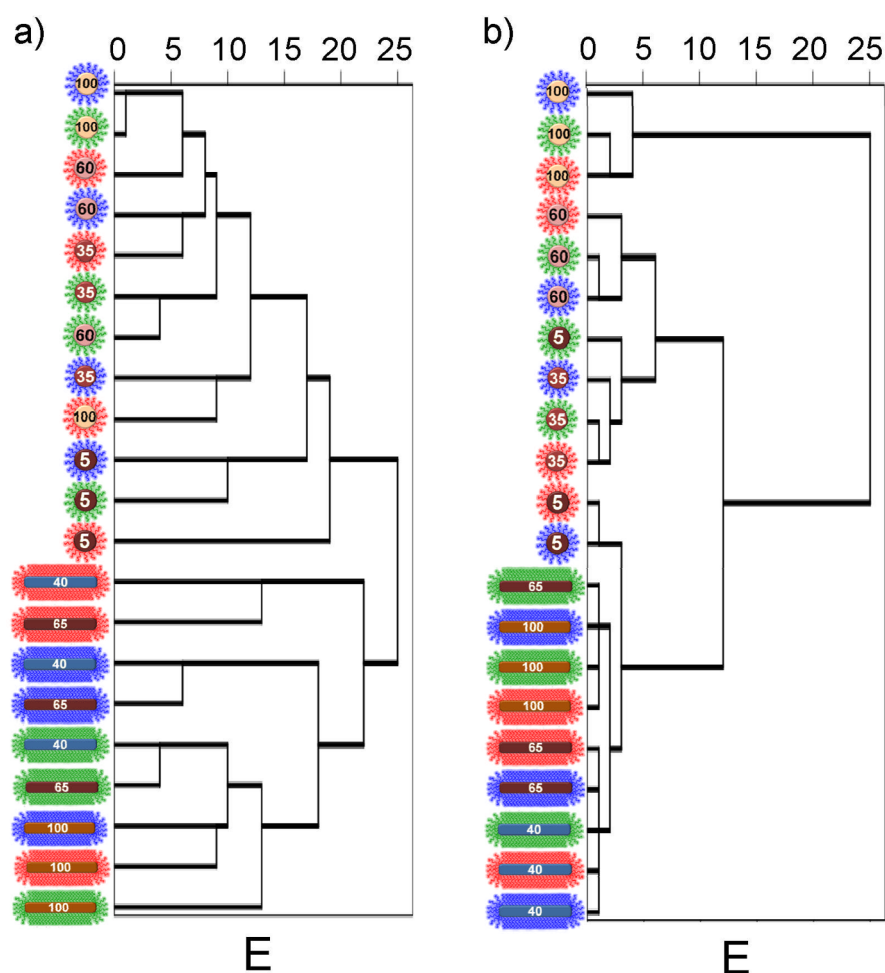


Figure 3. (a) HCA of the protein corona formation around the different NPs, shown in terms of Euclidean distance E . (b) HCA of the pH-dependence of the hydrodynamic diameters.

of 21 different types of NPs, in which size, shape, and surface coating were varied. Comparison of the HCA results between the different tiers might allow for conclusions on how much the protein corona can be predicted from the physicochemical properties, how the *in vitro* interaction might be predicted from the protein corona, *etc.* While these data certainly will not be able to predict how the *in vivo* biodistribution may be determined from the physicochemical properties, still statements about the degree of correlation between the different tiers can be made. In other words, in case a “new” type of NP, according to its physicochemical properties, is closest to one type of NP from the HCA analysis, would the protein corona of this NP also be closest to the reference NP from the HCA analysis, *etc.*?

To this end, our results show that the physicochemical properties of Au NPs are mainly accounted for by their hydrodynamic diameter and their zeta-potential. The formation of the protein corona is influenced by the pH-dependence of their zeta-potential. However, the *in vitro* uptake of NPs and *in vivo* biodistribution of NPs are not directly driven by the protein corona, but the physicochemical properties influence as well the corona as the *in vitro/in vivo* behaviors and thus the effect of the protein corona would be rather indirect. These findings could be boiled down to the entanglement of the different parameters, which in fact complicates the prediction of the biological effects of NPs.

RESULTS AND DISCUSSION

A summary of the 21 NP types is shown in Figure 1. Transmission electron microscopy (TEM) images show that the NPs are homogeneous in size and shape and thus are well suited as a model library. In the TEM images, the controlled variation of size and shape can be observed, whereas the variation in surface coating is demonstrated by TEM employing negative staining (Supporting Information Section III.2) and zeta-potential measurements (*cf.* the Supporting Information Section III.6). This library represents thus a three-dimensional parameter space, including variation in size, shape, and surface coating. The stringent purification protocols of our NPs warrant high purity,⁶⁹ and thus biological effects due to residual impurities from the NP synthesis⁷⁰ should not be significant. The endotoxin contamination may also affect the biological effect of NPs,^{71–73} but endotoxin-free NP solutions are possible.⁷⁴ While in the present study no endotoxin detection assays were employed, the investigation of similar NPs produced under similar conditions did not reveal enhanced endotoxin contamination.

Apart from standard properties such as hydrodynamic diameter and zeta-potential, many other physicochemical properties were determined for each type of NP, which are all summarized in the Supporting Information (Section III.13). Note that in the case of rod-shaped NPs anisotropy was manifested by the presence of two different hydrodynamic

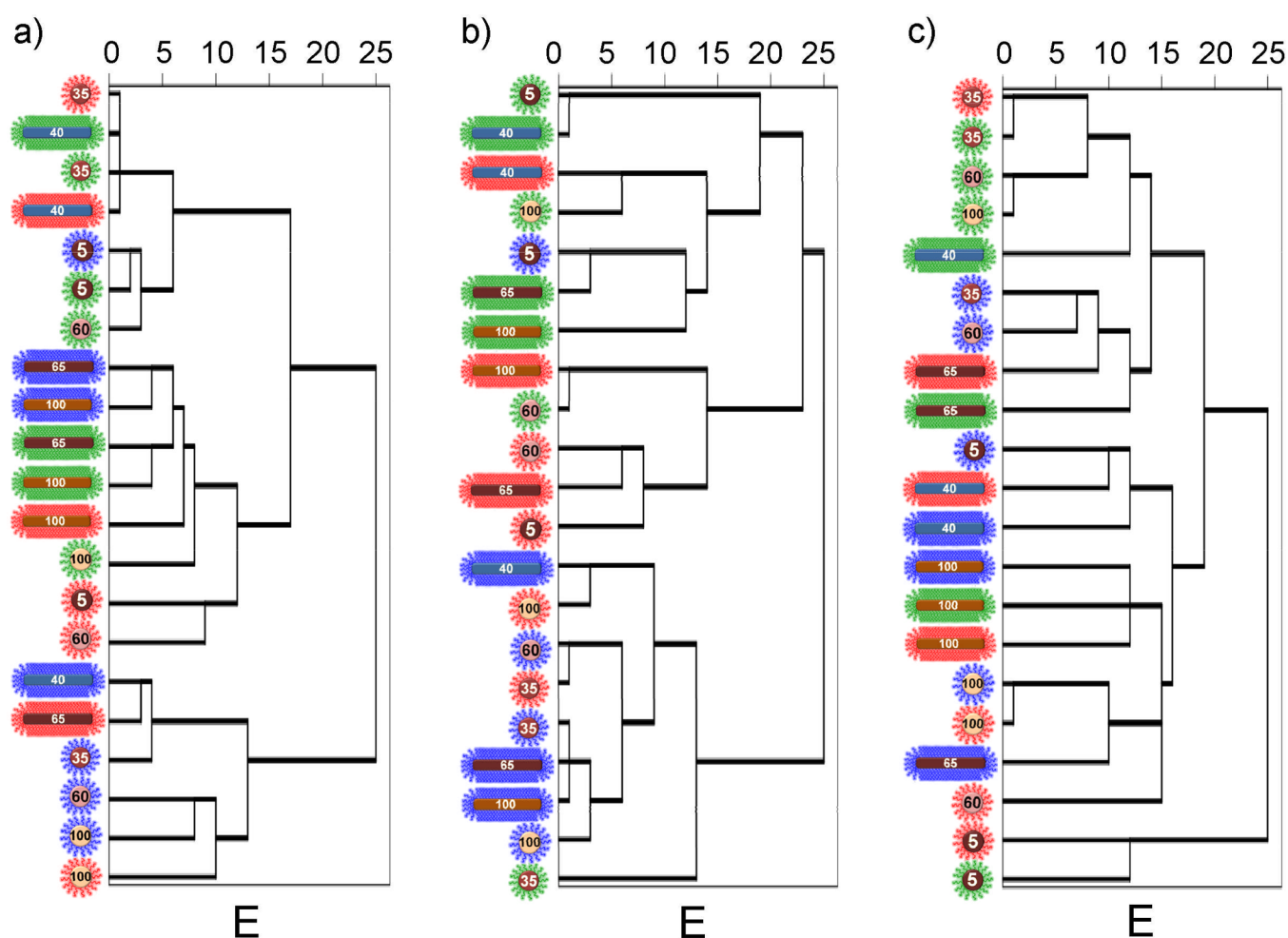


Figure 4. (a) HCA of the NP uptake by cultured cells, shown in terms of Euclidean distance E . (b) HCA of the critical NaCl concentration at which NP agglomeration occurs. (c) HCA of NP-induced reduction in cell viability and proliferation.

diameters; see the [Supporting Information Section III.5](#). Similarities of the different physicochemical properties of the 21 different NP types were probed by HCA, as shown in the [Supporting Information Section VII](#). It is immediately obvious that the physicochemical properties of the NPs can not be reduced to one single parameter. However, two key parameters could be identified. The type of surface coating (PEG, poly(isobutylene-*alt*-maleic anhydride)-graft-dodecyl (PMA), PVP) is highly reflected in the zeta-potential $\zeta_{\text{H}_2\text{O}}$ of the NPs as measured in water ([Figure 2a](#), [Figure SI-VII.2.10](#)). Notably, all PEG-coated NPs are clustered, regardless of their size and shape. The similarity in the type of NP core geometry (different diameters, shapes) largely depends on the hydrodynamic diameter d_h , as probed in water ([Figure 2b](#), [Figure SI-VII.2.13](#)). These data are pronounced, as the determination of hydrodynamic diameters *via* number, Z-average, and intensity distributions, as well as the variation of pH yields similar results (*cf.* [Figures SI-VII.2.12–SI-VI.2.16](#)). A combination of hydrodynamic diameters, zeta-potentials, and electrophoretic mobilities highly relates to the core volume V_c of the NPs ([Figure 2c](#), [Figure SI-VII.2.17](#)). Note that physicochemical characterization was also carried out under different pH's and in the presence of NaCl ([Supporting Information Sections III.8–III.11](#)). Still, the best correlation was obtained to the data measured in water. Basically, shape does not seem to play a dominant role, as closeness of behavior is related to the

overall volume, for example, which in the case of the 60 nm spheres is higher than that of the 100 nm rods, which in turn is higher than that of the 35 nm spheres ([Table SI-II.6.2](#)). Thus, to summarize the physicochemical properties of NPs, their zeta-potential and their hydrodynamic diameter are key parameters, at least in the case where all NPs are composed of the same core material, which in the present case is exclusively gold. The surface coating (as probed by the zeta-potential) will form the interface to biological matter such as proteins or cells. The core volume (as largely probed by the hydrodynamic diameter, in the case of equal core densities) will determine whether an NP is dispersed by diffusion or sediments in solution.⁷⁵

Based on the HCA of the physicochemical properties, now their dependence on the formation of the protein corona and *in vitro* and *in vivo* impact can be investigated. In [Figure 3a](#) ([Figure SI-VII.2.23](#)), the HCA data for the protein corona are shown. Correlation appears to be robust, as HCA data for different data subsets are similar ([Figures SI-VII.2.23–SI-VII.2.25](#)). There is correlation to NP size (in comparison to [Figure 2b](#)), but also to surface chemistry, as often adjacent NPs have similar surface chemistry. This fits a previous analysis of protein corona formation on one type of core with different surface coatings.⁷⁶ The best correlation is found to the HCA of the pH-dependent hydrodynamic diameters ([Figure 3b](#), [Figure SI-VII.2.14](#)). The charge of proteins is highly pH-dependent.

Thus, pH-dependent NP agglomeration as probed by pH-mediated changes in hydrodynamic diameters seems to be an important parameter for the regulation of protein adsorption onto NPs. As the similarities sort rather by shape than by volume, in the data set obtained with the investigated library we could not relate protein adsorption to spherical *versus* rod-like shape of the NPs.

In vitro uptake of NPs by different cell types is linked to both surface chemistry and core volume (Figure 4a, Figure SI-VII.2.26). Due to the nonlinear mix of at least two key properties, no data subset of the physicochemical properties was found to clearly resemble uptake behavior. However, HCA of the critical NaCl concentration at which NPs start to agglomerate (Figure 4b, Figure SI-VII.2.19) shows some similarities to the HCA data of NP uptake. The critical NaCl concentration reflects the colloidal stability of NPs in NaCl-containing medium. The sedimentation of agglomerated NPs is faster, and thus cellular uptake in static two-dimensional cell cultures will be enhanced.⁷⁵ In contrast to reports in the literature, the present data set here shows no direct correlation of the NP uptake behavior (Figure 4a) to the protein corona formation (Figure 3a), different from previous findings based on other (smaller) data sets.⁷⁷ The protein corona as well as NP uptake in this data set rather seem to depend on the underlying physicochemical properties, in particular surface coating and core volume, which has also been speculated before.³¹ There are reports in the literature that related NP-mediated loss in cell viability to the amount of engulfed NPs.³¹ Although some correlation was observed (regarding the HCA of the toxicological data shown in Figure 4c and Figure SI-VII.2.29 with the HCA of the NP uptake in Figure 4a) in the present study, the cytotoxicity is too complex to be described in this way. In the case where one single parameter, such as NP charge, is varied, this variable may be related to NP uptake and NP-induced cytotoxicity. However, in the case of multidimensional parameter sets, these correlations may no longer hold true. Additionally, the direct correlation of cytotoxicity to the catalytic activity of NPs (Figures SI-VII.2.6–SI-VII.2.8), which can be a source of generation of reactive oxygen species (ROS) and thus cytotoxicity, was not possible. Note also that different toxicological end points and different cell cultures varied in their HCA (Figures SI-VII.2.29–SI-VII.2.33). Comparison of the HCA between these data sets helps to understand how robust the significance of one parameter (*e.g.*, viability of one cell line) is.

As last step, HCA of the *in vivo* biodistribution of the NPs after tail vein injection into mice was carried out. It is worth noting that while there are clear differences dependent on the NP type, all investigated NPs are predominantly located in the liver and spleen. Biodistribution relies on surface chemistry, as well as on core volume (Figure 5, Figure SI-VII.2.36). Surprisingly, while zeta-potential measurements cluster all PEG-coated NPs as similar to PVP- and PMA-coated NPs, the *in vivo* biodistribution indicates rather clustering of the PMA-coated NPs with the PEG- and PVP-coated NPs. It also needs to be pointed out that the results depend on whether biodistribution is normalized to the mass of the respective organs or is considered as absolute NP mass in the entire organ (Figures SI-VII.2.35–SI-VII.2.37). Concerning the relevance of the two key physicochemical parameters, surface chemistry and core volume, the surface chemistry seems to be of more relevance for the *in vivo* biodistribution (Figure 5), as compared to the two-dimensional static *in vitro* uptake (Figure

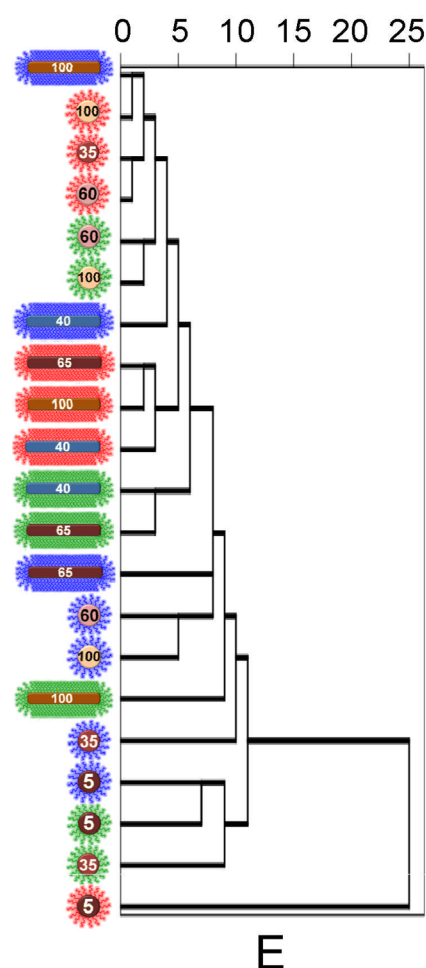


Figure 5. HCA of *in vivo* biodistribution of the NPs.

4a). In the case of static two-dimensional cell cultures, the sedimentation of NPs on the top of cells, as driven by gravity and thus by the core volume, is of importance. Under dynamic flow conditions *in vivo*, this effect has less importance, and thus surface chemistry is more strongly involved. Again, for the present data set, there seems to be no direct correlation of the protein corona (Figure 3a) to the *in vivo* biodistribution (Figure 5), but the importance of the protein corona would rather be an indirect effect, which is related to the underlying physicochemical NP properties.

CONCLUSIONS

The obtained data sets for 21 different types of NPs concerning physicochemical characterization, protein corona formation, and *in vitro* as well as *in vivo* effects of the NPs demonstrate that correlation can not be made on individual parameters, but that effects of different parameters are entangled. With the present HCA data even the envisaged prediction of the protein corona from the physicochemical properties of the NPs was not possible in a straightforward way. Still, important conclusions can be made. There seem to be two main physicochemical parameters: the volume of the NP core (which is, in the case of equal density, proportional to the NP core mass), which can be probed by measurement of the hydrodynamic diameter, and the surface coating around the NP core, which can be probed by measuring the zeta-potential. Formation of the protein corona is influenced by the

pH dependence of the hydrodynamic diameter of the NPs. In our data set, *in vitro* uptake of NPs and *in vivo* biodistribution of NPs are not directly driven by the protein corona, but the physicochemical properties influence as well the corona and the *in vitro/in vivo* behavior, and thus the effect of the protein corona would be rather indirect. Surface properties of the NPs reveal a stronger impact on *in vivo* biodistribution than *in vitro* uptake of NPs in standard two-dimensional static cell cultures. The limitation of *in vitro* models to predict *in vivo* behavior is generally known from the literature.^{78,79} On the negative side, even considering the large data set of measured physicochemical parameters, this study may not provide guidelines toward better design of NPs. It however raises the question of whether guidelines found in studies in which only selected parameters were varied hold true in general.

In the present multiparameter set of data, the dependence of biological effects on individual physicochemical properties could not be found, as reported in other studies in which only the relevant physicochemical parameter has been varied. This points out that findings of limited model libraries may not be possible to be extrapolated in a straightforward way to extended data sets. This emphasizes the need for larger libraries.⁸⁰ Even the present data set only comprises a subspace of relevant NPs. In particular, our study involved gold as the only core material, and sphere *versus* rod-like shape as the only variation in NP shape. Compared to some typical engineered NPs (*e.g.*, iron oxide NPs and silver NPs), Au NPs represent an ideal model for the purposes of the current study, as Au NPs are fairly biologically inert and no major ion dissolution occurs in biological conditions. Nonetheless, the current study might be extended to other NPs with similar physicochemical properties, but of different nature of origin, even though additional parameters should be taken into account under different settings. Also, the surface coatings did not involve bioconjugation with targeting ligands, *etc.* Also this remains a subject for future experiments. Hence, the HCA might be improved through introducing more parameters for better classification and prediction, if multidimension factors are involved in the intricate NPs. In the present approach, each parameter was weighted with the same importance. More sophisticated analysis could give rise to different emphasis on the individual parameters. At any rate, the presented data set is highly comprehensive, and usage for analysis by other groups is encouraged, by providing all raw data in the [Supporting Information](#).

MATERIALS AND METHODS

Au NP Synthesis. Spherical Au NPs with core diameters of 5, 35, 60, and 100 nm, are termed 5-GNPs, 35-GNPs, 60-GNPs, and 100-GNPs, respectively,⁸¹ and rod-shaped Au NPs with core lengths of 40, 65, and 100 nm, are termed 40-GNRs, 65-GNRs, and 100-GNRs, respectively. The above Au NPs were synthesized in the aqueous phase using previously published protocols.⁶⁹ Each type of NP was then modified with three different surface coatings: PVP, PMA, and PMA with an additional 10 kDa of PEG.⁶⁹ In this way, a library of $7 \times 3 = 21$ different types of water-soluble NPs was created. Details on the procedures are described in the [Supporting Information](#).

Characterization of the Physicochemical Properties of the Au NPs. Each type of NP was fully characterized according to previously published protocols,^{69,82} involving the following parameters: core diameter and core length, aspect

ratio, core surface area, core volume, thickness of the organic ligand shell, hydrodynamic diameter in water and at different pH values, zeta-potential in water and at different pH values, critical NaCl concentration at which the NPs start to agglomerate, normalized migration distance upon gel electrophoresis, surface reactivity concerning the reduction of methylene blue, wavelength of surface plasmon resonance, molar extinction coefficient at 450 nm, diameter of the whole NP. Details on the procedures and all experimental results are described in the [Supporting Information](#).

Characterization of the Protein Corona Formation around NPs. NPs were incubated with mouse serum. After incubation, unbound proteins were removed by centrifugation, and then two analysis methods were employed. First, different molecular weight fractions of attached proteins were analyzed by gel electrophoresis. Second, the composition of the protein corona was analyzed by mass spectroscopy. Details on the procedures and all experimental results are described in the [Supporting Information](#).

Characterization of the *in Vitro* Response to Exposure to NPs. The amount of NPs internalized by several cell lines was measured. In addition, cell viability and cell proliferation of several cell lines upon incubation with the NPs were probed. Details on the procedures and all experimental results are described in the [Supporting Information](#).

Characterization of the *in Vivo* Biodistribution of the NPs. The biodistribution of the NPs was determined after intra-tail vein injection of NPs into mice, followed by determination of the NP amount in the different organs by mass spectroscopy. Details on the procedures and all experimental results are described in the [Supporting Information](#).

Statistical Analysis. Briefly, multivariate statistical analyses were used to uncover the hidden relationships in the raw data matrix. HCA is a model-free statistical approach that makes no *a priori* assumptions about the class identification of data. HCA was performed using the IBM SPSS Statistics software (version 22.0). More details on the HCA and related results are provided in the [Supporting Information](#).

ASSOCIATED CONTENT

Supporting Information

The Supporting Information is available free of charge on the ACS Publications website at DOI: 10.1021/acsnano.8b04906.

Detailed description of materials and methods and raw data for selected experiments ([PDF](#))

Full data set provided as an Excel file ([XLSX](#))

AUTHOR INFORMATION

Corresponding Authors

*E-mail: wolfgang.parak@uni-hamburg.de.

*E-mail: sjliu@rcees.ac.cn.

ORCID

Ming Xu: 0000-0002-4499-6116

Beatriz Pelaz: 0000-0002-4626-4576

Neus Feliu: 0000-0002-7886-1711

Wolfgang J. Parak: 0000-0003-1672-6650

Sijin Liu: 0000-0002-5643-0734

Notes

The authors declare no competing financial interest.

ACKNOWLEDGMENTS

The authors are grateful to Mrs. Marta Gallego for TEM measurements and Miss Xue Wang, Dr. Yun Liu, and Dr. Jianqiang Zhu for animal experiments. This research was supported by the National "973" Program (Grant No. 2014CB932000) and the Strategic Priority Research Program of the Chinese Academy of Sciences (Grant No. XDB14000000). X.S. was funded by the Chinese Scholarship Council (CSC). M.G.M.S. was supported by the Fazit Stiftung Germany. N.F. acknowledges funding from the Swedish Governmental Agency for Innovation Systems (Vinnova). This project was funded by the Deutsche Forschungsgemeinschaft (Grant DFG PA 794/25-1). This research was supported by the National Natural Science Foundation of China (Grant Nos. 21425731, 21637004, and 21407169).

REFERENCES

- (1) Choi, H. S.; Frangioni, J. V. Nanoparticles for Biomedical Imaging: Fundamentals of Clinical Translation. *Mol. Imaging* **2010**, *9*, 291–310.
- (2) Croissant, J. G.; Fatieiev, Y.; Almalik, A.; Khashab, N. M. Mesoporous Silica and Organosilica Nanoparticles: Physical Chemistry, Biosafety, Delivery Strategies, and Biomedical Applications. *Adv. Healthcare Mater.* **2018**, *7*, 1700831.
- (3) Meng, H.; Xia, T.; George, S.; Nel, A. E. A Predictive Toxicological Paradigm for the Safety Assessment of Nanomaterials. *ACS Nano* **2009**, *3*, 1620–1627.
- (4) Dobrovolskaia, M. A. Pre-clinical Immunotoxicity Studies of Nanotechnology-formulated Drugs: Challenges, Considerations and Strategy. *J. Controlled Release* **2015**, *220*, 571–583.
- (5) Damoiseaux, R.; George, S.; Li, M.; Pokhrel, S.; Ji, Z.; France, B.; Xia, T.; Suarez, E.; Rallo, R.; Madler, L.; Cohen, Y.; Hoek, E. M. V.; Nel, A. No Time to Lose-high Throughput Screening to Assess Nanomaterial Safety. *Nanoscale* **2011**, *3*, 1345–1360.
- (6) Zhu, M. T.; Nie, G. J.; Meng, H.; Xia, T.; Nel, A.; Zhao, Y. L. Physicochemical Properties Determine Nanomaterial Cellular Uptake, Transport, and Fate. *Acc. Chem. Res.* **2013**, *46*, 622–631.
- (7) Rivera Gil, P.; Jimenez de Aberasturi, D.; Wulf, V.; Pelaz, B.; del Pino, P.; Zhao, Y.; de la Fuente, J.; Ruiz de Larramendi, I.; Rojo, T.; Liang, X.-J.; Parak, W. J. The Challenge to Relate the Physicochemical Properties of Colloidal Nanoparticles to Their Cytotoxicity. *Acc. Chem. Res.* **2013**, *46*, 743–749.
- (8) Di Cristo, L.; Maguire, C. M.; Mc Quillan, K.; Aleardi, M.; Volkov, Y.; Movia, D.; Prina-Mello, A. Towards the Identification of An *in vitro* Tool for Assessing the Biological Behavior of Aerosol Supplied Nanomaterials. *Int. J. Environ. Res. Public Health* **2018**, *15*, 563.
- (9) Lynch, I.; Weiss, C.; Valsami-Jones, E. A Strategy for Grouping of Nanomaterials Based on Key Physico-chemical Descriptors as A Basis for Safer-by-design NMs. *Nano Today* **2014**, *9*, 266–270.
- (10) Liu, R.; Jiang, W.; Walkey, C. D.; Chan, W. C. W.; Cohen, Y. Prediction of Nanoparticles-cell Association Based on Corona Proteins and Physicochemical Properties. *Nanoscale* **2015**, *7*, 9664–9675.
- (11) Moghimi, S. M.; Hunter, A. C.; Andresen, T. L. Factors Controlling Nanoparticle Pharmacokinetics: An Integrated Analysis and Perspective. *Annu. Rev. Pharmacol. Toxicol.* **2012**, *52*, 481–503.
- (12) Albanese, A.; Tang, P. S.; Chan, W. C. W. The Effect of Nanoparticle Size, Shape, and Surface Chemistry on Biological Systems. *Annu. Rev. Biomed. Eng.* **2012**, *14*, 1–16.
- (13) Zhang, H. Y.; Ji, Z. X.; Xia, T.; Meng, H.; Low-Kam, C.; Liu, R.; Pokhrel, S.; Lin, S. J.; Wang, X.; Liao, Y. P.; Wang, M. Y.; Li, L. J.; Rallo, R.; Damoiseaux, R.; Telesca, D.; Madler, L.; Cohen, Y.; Zink, J. I.; Nel, A. E. Use of Metal Oxide Nanoparticle Band Gap To Develop a Predictive Paradigm for Oxidative Stress and Acute Pulmonary Inflammation. *ACS Nano* **2012**, *6*, 4349–4368.
- (14) Jiang, Y.; Huo, S. D.; Mizuhara, T.; Das, R.; Lee, Y. W.; Hou, S.; Moyano, D. F.; Duncan, B.; Liang, X. J.; Rotello, V. M. The Interplay of Size and Surface Functionality on the Cellular Uptake of Sub-10 nm Gold Nanoparticles. *ACS Nano* **2015**, *9*, 9986–9993.
- (15) Juling, S.; Niedzwiecka, A.; Böhmert, L.; Lichtenstein, D.; Selve, S.; Braeuning, A.; Thünemann, A. F.; Krause, E.; Lampen, A. Protein Corona Analysis of Silver Nanoparticles Links to Their Cellular Effects. *J. Proteome Res.* **2017**, *16*, 4020–4034.
- (16) Ma, X.; Hartmann, R.; Aberasturi, D. J. d.; Yang, F.; Soenen, S. J. H.; Manshian, B. B.; Franz, J.; Valdeperez, D.; Pelaz, B.; Feliu, N.; Hampp, N.; Riethmüller, C.; Vieker, H.; Frese, N.; Götzhäuser, A.; Simonich, M.; Tanguay, R. L.; Liang, X.-J.; Parak, W. J. Colloidal Gold Nanoparticles Induce Changes in Cellular and Subcellular Morphology. *ACS Nano* **2017**, *11*, 7807–7820.
- (17) Nazarenus, M.; Zhang, Q.; Soliman, M. G.; del Pino, P.; Pelaz, B.; Carregal-Romero, S.; Rejman, J.; Rothen-Ruthishauser, B.; Clift, M. J. D.; Zellner, R.; Nienhaus, G. U.; Delehanty, J. B.; Medintz, I. L.; Parak, W. J. *In vitro* Interaction of Colloidal Nanoparticles with Mammalian Cells: What Have We Learned Thus Far? *Beilstein J. Nanotechnol.* **2014**, *5*, 1477–1490.
- (18) Yang, H.; Liu, C.; Yang, D.; Zhang, H.; Xi, Z. Comparative Study of Cytotoxicity, Oxidative Stress and Genotoxicity Induced by Four Typical Nanomaterials: the Role of Particle Size, Shape and Composition. *J. Appl. Toxicol.* **2009**, *29*, 69–78.
- (19) Salatin, S.; Dizaj, S. M.; Khosroushahi, A. Y. Effect of the Surface Modification, Size, and Shape on Cellular Uptake of Nanoparticles. *Cell Biol. Int.* **2015**, *39*, 881–890.
- (20) Li, N.; Zhao, P.; Astruc, D. Anisotropic Gold Nanoparticles: Synthesis, Properties, Applications, and Toxicity. *Angew. Chem., Int. Ed.* **2014**, *53*, 1756–1789.
- (21) Herd, H.; Daum, N.; Jones, A. T.; Huwer, H.; Ghandehari, H.; Lehr, C.-M. Nanoparticle Geometry and Surface Orientation Influence Mode of Cellular Uptake. *ACS Nano* **2013**, *7*, 1961–1973.
- (22) Stoehr, L. C.; Gonzalez, E.; Stampfl, A.; Casals, E.; Duschl, A.; Puentes, V.; Oostingh, G. J. Shape Matters: Effects of Silver Nanospheres and Wires on Human Alveolar Epithelial Cells. *Part. Fibre Toxicol.* **2011**, *8*, 3–15.
- (23) Florez, L.; Herrmann, C.; Cramer, J. M.; Hauser, C. P.; Koynov, K.; Landfester, K.; Crespy, D.; Mailander, V. How Shape Influences Uptake: Interactions of Anisotropic Polymer Nanoparticles and Human Mesenchymal Stem Cells. *Small* **2012**, *8*, 2222–2230.
- (24) Qiu, Y.; Liu, Y.; Wang, L. M.; Xu, L. G.; Bai, R.; Ji, Y. L.; Wu, X. C.; Zhao, Y. L.; Li, Y. F.; Chen, C. Y. Surface Chemistry and Aspect Ratio Mediated Cellular Uptake of Au Nanorods. *Biomaterials* **2010**, *31*, 7606–7619.
- (25) Leonov, A. P.; Zheng, J.; Clogston, J. D.; Stern, S. T.; Patri, A. K.; Wei, A. Detoxification of Gold Nanorods by Treatment with Polystyrenesulfonate. *ACS Nano* **2008**, *2*, 2481–2488.
- (26) El Badawy, A. M.; Silva, R. G.; Morris, B.; Scheckel, K. G.; Suidan, M. T.; Tolaymat, T. M. Surface Charge-dependent Toxicity of Silver Nanoparticles. *Environ. Sci. Technol.* **2010**, *45*, 283–287.
- (27) Albanese, A.; Sykes, E. A.; Chan, W. C. Rough Around the Edges: the Inflammatory Response of Microglial Cells to Spiky Nanoparticles. *ACS Nano* **2010**, *4*, 2490–2493.
- (28) Chen, Y.-P.; Wu, S. H.; Chen, I. C.; Chen, C. T. Impacts of Cross-Linkers on Biological Effects of Mesoporous Silica Nanoparticles. *ACS Appl. Mater. Interfaces* **2017**, *9*, 10254–10265.
- (29) Ashraf, S.; Park, J.; Bichelberger, M.; Kantner, K.; Hartmann, R.; Maffre, P.; Said, A. H.; Feliu, N.; Lee, J.; Lee, D.; Nienhaus, G. U.; Kim, S.; Parak, W. J. Zwitterionic Surface Coating of Quantum Dots Reduces Protein Adsorption and Cellular Uptake. *Nanoscale* **2016**, *10*, 1318–1328.
- (30) Breus, V. V.; Pietuch, A.; Tarantola, M.; Basche, T.; Janshoff, A. The Effect of Surface Charge on Nonspecific Uptake and Cytotoxicity of CdSe/ZnS Core/shell Quantum Qots. *Beilstein J. Nanotechnol.* **2015**, *6*, 281–292.
- (31) Hühn, D.; Kantner, K.; Geidel, C.; Brandholt, S.; De Cock, I.; Soenen, S. J. H.; Rivera Gil, P.; Montenegro, J.-M.; Braeckmans, K.; Müllen, K.; Nienhaus, G. U.; Klapper, M.; Parak, W. J. Polymer-

Coated Nanoparticles Interacting with Proteins and Cells: Focusing on the Sign of the Net Charge. *ACS Nano* **2013**, *7*, 3253–3263.

(32) Chakraborty, I.; Feliu, N.; Roy, S.; Dawson, K.; Parak, W. J. Protein-Mediated Shape-Control of Silver Nanoparticles. *Bioconjugate Chem.* **2018**, *29*, 1261–1265.

(33) Cedervall, T.; Lynch, I.; Lindman, S.; Berggård, T.; Thulin, E.; Nilsson, H.; Dawson, K. A.; Linse, S. Understanding the Nanoparticle-Protein Corona Using Methods to Quantify Exchange Rates and Affinities of Proteins for Nanoparticles. *Proc. Natl. Acad. Sci. U. S. A.* **2007**, *104*, 2050–2055.

(34) Vilanova, O.; Mittag, J. J.; Kelly, P. M.; Milani, S.; Dawson, K. A.; Rädler, J. O.; Franzese, G. Understanding the Kinetics of Protein-Nanoparticle Corona Formation. *ACS Nano* **2016**, *10*, 10842–10850.

(35) Kelly, P. M.; Aberg, C.; Polo, E.; O'Connell, A.; Cookman, J.; Fallon, J.; Krpetic, Z.; Dawson, K. A. Mapping Protein Binding Sites on the Biomolecular Corona of Nanoparticles. *Nat. Nanotechnol.* **2015**, *10*, 472–479.

(36) Wan, S.; Kelly, P. M.; Mahon, E.; Stockmann, H.; Rudd, P. M.; Caruso, F.; Dawson, K. A.; Yan, Y.; Monopoli, M. P. The "Sweet" Side of the Protein Corona: Effects of Glycosylation on Nanoparticle-Cell Interactions. *ACS Nano* **2015**, *9*, 2157–2166.

(37) Monopoli, M. P.; Pitek, A. S.; Lynch, I.; Dawson, K. A. Formation and Characterization of the Nanoparticle-protein Corona. *Methods Mol. Biol.* **2013**, *1025*, 137–155.

(38) Walkey, C. D.; Chan, W. C. Understanding and Controlling the Interaction of Nanomaterials with Proteins in A Physiological Environment. *Chem. Soc. Rev.* **2012**, *41*, 2780–2799.

(39) Tenzer, S.; Docter, D.; Rosfa, S.; Wlodarski, A.; Kuharev, J.; Rekić, A.; Knauer, S. K.; Bantz, C.; Nawroth, T.; Bier, C.; Sirirattapan, J.; Mann, W.; Treuel, L.; Zellner, R.; Maskos, M.; Schild, H.; Stauber, R. H. Nanoparticle Size is a Critical Physicochemical Determinant of the Human Blood Plasma Corona: A Comprehensive Quantitative Proteomic Analysis. *ACS Nano* **2011**, *5*, 7155–7167.

(40) Mirsadeghi, S.; Dinarvand, R.; Ghahremani, M. H.; Hormozi-Nezhad, M. R.; Mahmoudi, Z.; Hajipour, M. J.; Atyabi, F.; Ghavami, M.; Mahmoudi, M. Protein Corona Composition of Gold Nanoparticles/nanorods Affects Amyloid Beta Fibrillation Process. *Nanoscale* **2015**, *7*, 5004–5013.

(41) Liu, H. L.; Pierre-Pierre, N.; Huo, Q. Dynamic Light Scattering for Gold Nanorod Size Characterization and Study of Nanorod-protein Interactions. *Gold Bull.* **2012**, *45*, 187–195.

(42) Maiolo, D.; Bergese, P.; Mahon, E.; Dawson, K. A.; Monopoli, M. P. Surfactant Titration of Nanoparticle-Protein Corona. *Anal. Chem.* **2014**, *86*, 12055–12063.

(43) Pelaz, B.; Del Pino, P.; Maffre, P.; Hartmann, R.; Gallego, M.; Rivera-Fernandez, S.; de la Fuente, J. M.; Nienhaus, G. U.; Parak, W. J. Surface Functionalization of Nanoparticles with Polyethylene Glycol: Effects on Protein Adsorption and Cellular Uptake. *ACS Nano* **2015**, *9*, 6996–7008.

(44) Jedlovsky-Hajdu, A.; Bombelli, F. B.; Monopoli, M. P.; Tombacz, E.; Dawson, K. A. Surface Coatings Shape the Protein Corona of SPIONs with Relevance to Their Application *in Vivo*. *Langmuir* **2012**, *28*, 14983–14991.

(45) Tenzer, S.; Docter, D.; Kuharev, J.; Musyanovych, A.; Fetz, V.; Hecht, R.; Schlenk, F.; Fischer, D.; Kiouptsi, K.; Reinhardt, C.; Landfester, K.; Schild, H.; Maskos, M.; Knauer, S. K.; Stauber, R. H. Rapid Formation of Plasma Protein Corona Critically Affects Nanoparticle Pathophysiology. *Nat. Nanotechnol.* **2013**, *8*, 772–781.

(46) Chanana, M.; Rivera Gil, P.; Correa-Duarte, M. A.; Parak, W. J.; Liz-Marzán, L. M. Physicochemical Properties of Protein-coated Gold Nanoparticles in Biological Fluids and Cells Before and After Proteolytic Digestion. *Angew. Chem., Int. Ed.* **2013**, *52*, 4179–4183.

(47) Bertoli, F.; Garry, D.; Monopoli, M. P.; Salvati, A.; Dawson, K. A. The Intracellular Destiny of the Protein Corona: A Study on its Cellular Internalization and Evolution. *ACS Nano* **2016**, *10*, 10471–10479.

(48) Treuel, L.; Malissek, M.; Gebauer, J. S.; Zellner, R. The Influence of Surface Composition of Nanoparticles on their

Interactions with Serum Albumin. *ChemPhysChem* **2010**, *11*, 3093–3099.

(49) Raoufi, M.; Hajipour, M. J.; Kamali Shahri, S. M.; Schoen, I.; Linn, U.; Mahmoudi, M. Probing Fibronectin Conformation on A Protein Corona Layer Around Nanoparticles. *Nanoscale* **2018**, *10*, 1228–1233.

(50) Sukhanova, A.; Poly, S.; Shemetov, A.; Nabiev, I. Quantum Dots Induce Charge-specific Amyloid-like Fibrillation of Insulin under Physiological Conditions. *Proc. SPIE* **2012**, *8548*, 85485F.

(51) Yoo, S. I.; Yang, M.; Brender, J. R.; Subramanian, V.; Sun, K.; Joo, N. E.; Jeong, S. H.; Ramamoorthy, A.; Kotov, N. A. Inhibition of Amyloid Peptide Fibrillation by Inorganic Nanoparticles: Functional Similarities with Proteins. *Angew. Chem., Int. Ed.* **2011**, *50*, 5110–5115.

(52) Linse, S.; Cabaleiro-Lago, C.; Xue, W.-F.; Lynch, I.; Lindman, S.; Thulin, E.; Radford, S. E.; Dawson, K. A. Nucleation of Protein Fibrillation by Nanoparticles. *Proc. Natl. Acad. Sci. U. S. A.* **2007**, *104*, 8691–8696.

(53) Docter, D.; Strieth, S.; Westmeier, D.; Hayden, O.; Gao, M. Y.; Knauer, S. K.; Stauber, R. H. No King without A Crown - Impact of the Nanomaterial-protein Corona on Nanobiomedicine. *Nanomedicine* **2015**, *10*, 503–519.

(54) Konduru, N. V.; Molina, R. M.; Swami, A.; Damiani, F.; Pyrgiotakis, G.; Lin, P.; Andreozzi, P.; Donaghey, T. C.; Demokritou, P.; Krol, S.; Kreyling, W.; Brain, J. D. Protein Corona: Implications for Nanoparticle Interactions with Pulmonary Cells. *Part. Fibre Toxicol.* **2017**, *14*, 42.

(55) Fadeel, B.; Feliu, N.; Vogt, C.; Abdelmonem, A. M.; Parak, W. J. Bridge Over Troubled Waters: Understanding the Synthetic and Biological Identities of Engineered Nanomaterials. *Wiley Interdiscip. Rev. Nanomed. Nanobiotechnol.* **2013**, *5*, 111–129.

(56) Maiolo, D.; Pino, P. d.; Metrangola, P.; Parak, W. J.; Bombelli, F. B. Nanomedicine Delivery: Does Protein Corona Route to the Target or Off Road? *Nanomedicine (London, U. K.)* **2015**, *10*, 3231–3247.

(57) Corbo, C.; Molinaro, R.; Tabatabaei, M.; Farokhzad, O. C.; Mahmoudi, M. Personalized Protein Corona on Nanoparticles and its Clinical Implications. *Biomater. Sci.* **2017**, *5*, 378–387.

(58) Ahsan, S. M.; Rao, C. M.; Ahmad, M. F. Nanoparticle-Protein Interaction: The Significance and Role of Protein Corona. *Adv. Exp. Med. Biol.* **2018**, *1048*, 175–198.

(59) Chen, D.; Ganesh, S.; Wang, W.; Amiji, M. Plasma Protein Adsorption and Biological Identity of Systemically Administered Nanoparticles. *Nanomedicine (London, U. K.)* **2017**, *12*, 2113–2135.

(60) Chinen, A. B.; Guan, C. M.; Ko, C. H.; Mirkin, C. A. The Impact of Protein Corona Formation on the Macrophage Cellular Uptake and Biodistribution of Spherical Nucleic Acids. *Small* **2017**, *13*, 1603847.

(61) Aoyama, M.; Hata, K.; Higashisaka, K.; Nagano, K.; Yoshioka, Y.; Tsutsumi, Y. Clusterin in the Protein Corona Plays A Key Role in the Stealth Effect of Nanoparticles Against Phagocytes. *Biochem. Biophys. Res. Commun.* **2016**, *480*, 690–695.

(62) Dobrovolskaia, M. A.; Neun, B. W.; Man, S.; Ye, X.; Hansen, M.; Patri, A. K.; Crist, R. M.; McNeil, S. E. Protein Corona Composition Does Not Accurately Predict Hematocompatibility of Colloidal Gold Nanoparticles. *Nanomedicine (N. Y., NY, U. S.)* **2014**, *10*, 1453–1463.

(63) Westmeier, D.; Chen, C.; Stauber, R. H.; Docter, D. The Bio-Corona and its Impact on Nanomaterial Toxicity. *Eur. J. Nanomed.* **2016**, *7*, 153–168.

(64) Westmeier, D.; Stauber, R. H.; Docter, D. The Concept of Bio-corona in Modulating the Toxicity of Engineered Nanomaterials (ENM). *Toxicol. Appl. Pharmacol.* **2016**, *299*, 53–57.

(65) Stepien, G.; Moros, M.; Pérez-Hernández, M.; Monge, M.; Gutiérrez, L.; Fratila, R. M.; Las Heras, M.; Menao Guillén, S.; Puente Lanzarote, J. J.; Solans, C.; Pardo, J.; de la Fuente, J. M. Effect of Surface Chemistry and Associated Protein Corona on the Long-Term Biodegradation of Iron Oxide Nanoparticles *In Vivo*. *ACS Appl. Mater. Interfaces* **2018**, *10*, 4548–4560.

- (66) Pant, K.; Pufe, J.; Zarschler, K.; Bergmann, R.; Steinbach, J.; Reimann, S.; Haag, R.; Pietzsch, J.; Stephan, H. Surface Charge and Particle Size Determine the Metabolic Fate of Dendritic Polyglycerols. *Nanoscale* **2017**, *9*, 8723–8739.
- (67) Truong, N. P.; Whittaker, M. R.; Mak, C. W.; Davis, T. P. The Importance of Nanoparticle Shape in Cancer Drug Delivery. *Expert Opin. Drug Delivery* **2015**, *12*, 129–142.
- (68) Moyano, D. F.; Liu, Y. C.; Peer, D.; Rotello, V. M. Modulation of Immune Response Using Engineered Nanoparticle Surfaces. *Small* **2016**, *12*, 76–82.
- (69) Hühn, J.; Carrillo-Carrion, C.; Soliman, M. G.; Pfeiffer, C.; Valdeperez, D.; Masood, A.; Chakraborty, I.; Zhu, L.; Gallego, M.; Zhao, Y.; Carril, M.; Feliu, N.; Escudero, A.; Alkilany, A. M.; Pelaz, B.; Pino, P. d.; Parak, W. J. Selected Standard Protocols for the Synthesis, Phase Transfer, and Characterization of Inorganic Colloidal Nanoparticles. *Chem. Mater.* **2017**, *29*, 399–461.
- (70) Crist, R. M.; Grossman, J. H.; Patri, A. K.; Stern, S. T.; Dobrovolskaia, M. A.; Adisheshaiah, P. P.; Clogston, J. D.; McNeil, S. E. Common Pitfalls in Nanotechnology: Lessons Learned From NCI's Nanotechnology Characterization Laboratory. *Integr. Biol.* **2013**, *5*, 66–73.
- (71) Li, Y.; Fujita, M.; Boraschi, D. Endotoxin Contamination in Nanomaterials Leads to the Misinterpretation of Immunotoxicity Results. *Front. Immunol.* **2017**, *8*, 472.
- (72) Li, Y.; Boraschi, D. Endotoxin Contamination: A Key Element in the Interpretation of Nanotoxicity Studies. *Nanomedicine (London, U. K.)* **2016**, *11*, 269–287.
- (73) Li, Y.; Shi, Z.; Radauer-Preiml, I.; Andosch, A.; Casals, E.; Luetz-Meindl, U.; Cobaleda, M.; Lin, Z.; Jaberi-Douraki, M.; Italiani, P.; Horejs-Hoeck, J.; Himly, M.; Monteiro-Riviere, N. A.; Duschl, A.; Puentes, V. F.; Boraschi, D. Bacterial Endotoxin (lipopolysaccharide) Binds to the Surface of Gold Nanoparticles, Interferes with Biocorona Formation and Induces Human Monocyte Inflammatory Activation. *Nanotoxicology* **2017**, *11*, 1157–1175.
- (74) Talamini, L.; Violatto, M. B.; Cai, Q.; Monopoli, M. P.; Kantner, K.; Krpetić, Z. e.; Perez-Potti, A.; Cookman, J.; Garry, D.; Silveira, C. P.; Boselli, L.; Pelaz, B.; Serchi, T.; Cambier, S. b.; Gutleb, A. C.; Feliu, N.; Yan, Y.; Salmons, M.; Parak, W. J.; Dawson, K. A.; Bigini, P. Influence of Size and Shape on the Anatomical Distribution of Endotoxin-Free Gold Nanoparticles. *ACS Nano* **2017**, *11*, 5519–5529.
- (75) Feliu, N.; Sun, X.; Puebla, R. A. A.; Parak, W. J. Quantitative Particle–Cell Interaction: Some Basic Physicochemical Pitfalls. *Langmuir* **2017**, *33*, 6639–6646.
- (76) Johnston, B. D.; Kreyling, W. G.; Pfeiffer, C.; Schäffler, M.; Sarioglu, H.; Ristig, S.; Hirn, S.; Haberl, N.; Thalhammer, S.; Hauck, S. M.; Semmler-Behnke, M.; Epple, M.; Hühn, J.; Pino, P. d.; Parak, W. J. Colloidal Stability and Surface Chemistry Are Key Factors for the Composition of the Protein Corona of Inorganic Gold Nanoparticles. *Adv. Funct. Mater.* **2017**, *27*, 1701956.
- (77) Walkey, C. D.; Olsen, J. B.; Song, F. Y.; Liu, R.; Guo, H. B.; Olsen, D. W. H.; Cohen, Y.; Emili, A.; Chan, W. C. W. Protein Corona Fingerprinting Predicts the Cellular Interaction of Gold and Silver Nanoparticles. *ACS Nano* **2014**, *8*, 2439–2455.
- (78) Lorian, V. Differences between *in vitro* and *in vivo* Studies. *Antimicrob. Agents Chemother.* **1988**, *32*, 1600–1601.
- (79) Saeidnia, S.; Manayi, A.; Abdollahi, M. From *in vitro* Experiments to *in vivo* and Clinical Studies; Pros and Cons. *Curr. Drug Discovery Technol.* **2015**, *12*, 281–224.
- (80) Alkilany, A. M.; Lohse, S. E.; Murphy, C. J. The Gold Standard: Gold Nanoparticle Libraries To Understand the Nano-Bio Interface. *Acc. Chem. Res.* **2013**, *46*, 650–661.
- (81) Piella, J.; Bastus, N. G.; Puentes, V. Size-Controlled Synthesis of Sub-10-nanometer Citrate-Stabilized Gold Nanoparticles and Related Optical Properties. *Chem. Mater.* **2016**, *28*, 1066–1075.
- (82) del Pino, P.; Yang, F.; Pelaz, B.; Zhang, Q.; Kantner, K.; Hartmann, R.; Baroja, N. M. d.; Gallego, M.; Möller, M.; Manshian, B. B.; Soenen, S. J.; Riedel, R.; Hampp, N.; Parak, W. J. Basic Physicochemical Properties of Polyethylene Glycol Coated Gold Nanoparticles that Determine Their Interaction with Cells. *Angew. Chem., Int. Ed.* **2016**, *55*, 5483–5487.

RESEARCH

Open Access



Optimizing conditions for labeling of mesenchymal stromal cells (MSCs) with gold nanoparticles: a prerequisite for in vivo tracking of MSCs

Philipp Nold^{1†}, Raimo Hartmann^{2†}, Neus Feliu², Karsten Kantner², Mahmoud Gamal², Beatriz Pelaz², Jonas Hühn², Xing Sun², Philipp Jungebluth³, Pablo del Pino², Holger Hackstein⁴, Paolo Macchiarini⁵, Wolfgang J. Parak^{2,6*†} and Cornelia Brendel^{1*†} 

Abstract

Background: Mesenchymal stromal cells (MSCs) have an inherent migratory capacity towards tumor tissue in vivo. With the future objective to quantify the tumor homing efficacy of MSCs, as first step in this direction we investigated the use of inorganic nanoparticles (NPs), in particular ca. 4 nm-sized Au NPs, for MSC labeling. Time dependent uptake efficiencies of NPs at different exposure concentrations and times were determined via inductively coupled plasma mass spectrometry (ICP-MS).

Results: The labeling efficiency of the MSCs was determined in terms of the amount of exocytosed NPs versus the amount of initially endocytosed NPs, demonstrating that at high concentrations the internalized Au NPs were exocytosed over time, leading to continuous exhaustion. While exposure to NPs did not significantly impair cell viability or expression of surface markers, even at high dose levels, MSCs were significantly affected in their proliferation and migration potential. These results demonstrate that proliferation or migration assays are more suitable to evaluate whether labeling of MSCs with certain amounts of NPs exerts distress on cells. However, despite optimized conditions the labeling efficiency varied considerably in MSC lots from different donors, indicating cell specific loading capacities for NPs. Finally, we determined the detection limits of Au NP-labeled MSCs within murine tissue employing ICP-MS and demonstrate the distribution and homing of NP labeled MSCs in vivo.

Conclusion: Although large amounts of NPs improve contrast for imaging, duration and extend of labeling needs to be adjusted carefully to avoid functional deficits in MSCs. We established an optimized labeling strategy for human MSCs with Au NPs that preserves their migratory capacity in vivo.

Keywords: Mesenchymal stromal cells (MSCs), Au nanoparticles (Au NP), labeling, in vivo tracking

*Correspondence: wolfgang.parak@physik.uni-marburg.de; brendelc@staff.uni-marburg.de

[†]Philipp Nold, Raimo Hartmann, Wolfgang J. Parak and Cornelia Brendel equally contributed to this work

¹ Department of Hematology, Oncology and Immunology, Philipps University Marburg, Marburg, Germany

² Department of Physics, Philipps-University of Marburg, Marburg, Germany

Full list of author information is available at the end of the article

Background

Mesenchymal stromal cells (MSCs) exhibit a high ex vivo expansion capacity and have already entered the clinic as cellular products for various applications [1, 2]. They possess anti-inflammatory and regenerative potential, and migrate into sites of inflammation, tissue repair, and neoplasia [3–5]. Due to their properties and safety, they are considered as a promising tool in regenerative medicine and oncology. About 200 clinical phase I/II and III studies revealed no side effects, even in allogenic settings [6]. In oncology, new therapeutic concepts envision e.g. genetically modified MSCs as a vehicle to selectively deliver anti-tumorigenic proteins or compounds to neoplastic tissue [7]. The efficacy of these approaches, as well as the extent of side effects, is directly linked to the potential of MSCs to accumulate in tumors after systemic administration. In the context of regenerative medicine, MSCs are used as a promising therapeutic approach to repopulate extracellular matrixes, with the function to repair and reconstruct complex tissues. Thus, the clinical use of MSCs has overcome its infancy steps [8]. Still, many details remain to be unraveled. This involves for example the mechanisms of homing, and in particular also the in vivo fate of MSCs. This circumstance evokes the necessity for a noninvasive in vivo MSC tracking method that does not influence their biological properties and cellular function, is highly specific to the target cells, is biocompatible, safe and nontoxic, and allows for quantification of low MSC numbers in invaded tissue [9]. Stem cell-tracking methods being currently used rely on labeling the cells with fluorescent molecules for optical imaging, radionuclides for positron or gamma photon emission tomography (PET), or labeling with certain contrast agents, such as exogenous elements, which either allow visualization by magnetic resonance imaging (MRI) or can be detected by mass spectrometry [10–15]. In the first case the application is limited to small animals or intraoperative use, due to light adsorption in thick tissue. The second approach requires extensive preparation of MSCs and handling of radioactive materials. In the third case, when using mass spectrometry as detection method, tissue decomposition prior to measurements is needed. All methods are limited in sensitivity by non-sufficient cell labeling efficiency, or require extensive tissue treatment for further imaging and detection. Combined with low stem cell homing, efficiency revised labeling considerations are needed.

Non-invasive imaging of MSCs after labeling with inorganic colloidal nanoparticles (NPs) is a promising tool that allows for recording distributions and the long-term tracking of the MSCs after systemic application {Huang, 2014 #32200; Skopalik, 2014 #32201; Schmidtke-Schrezenmeier, 2011 #32202; Betzer, 2015 #32883; Meir,

2015 #32885}. In comparison to organic molecules, inorganic NPs may allow for higher contrast in certain imaging techniques, such as magnetic resonance imaging (MRI) and computer tomography (CT). In MRI, FeO_x NPs have been demonstrated to provide good contrast in transverse relaxation time (T₂)-based imaging [16, 17]. In CT, the best contrast is obtained for elements with high atomic number. Thus, Au NPs are good candidates for labeling strategies [18, 19]. For our study we employed 4.25 (±0.88) nm Au NPs coated with the amphiphilic polymer poly (isobutylene-*alt*-maleic anhydride) modified with dodecylamine (PMA). The NPs were purified via gel electrophoresis or ultracentrifugation, and subjected to full characterization as previously reported [20]. This included UV/Vis absorption spectroscopy, transmission electron microscopy (TEM), and dynamic light scattering (DLS). NPs are in general readily endocytosed by cells [21, 22], and thus, labeling of MSCs in principle is straightforward. Upon cell division, the NPs are passed to the two daughter cells [23].

However, while in principle, the concept seems easily to be conducted, labeling of MSCs with NPs has to be performed under a delicate balance. From the imaging point of view, more NPs inside each MSC would relate directly to better contrast in imaging. On the other hand, it is reasonable to reduce the amount of NPs inside each MSC as much as possible, in order to avoid potential cytotoxic effects. Thus, labeling conditions need to be carefully optimized. Au NPs are promising candidates, as their biocompatibility at low doses is well-accepted [24]. Gold has been used for example as clinical therapeutic in patients with severe rheumatologic disorder for many years, with well-known safety profit and limited side effects [25]. Gold is usually not present in living organisms and thus, tracing of Au NPs by mass spectrometry benefits from low background signals, in contrast to FeO_x NPs, as there is a significant level of endogenous/constitutive iron. Recent studies have shown that Au NPs at least partially fulfill basic requirements for efficient long term labeling of MSCs, i.e. long term stability, low cytotoxicity, and most importantly, no interference with cellular functioning. Ricles et al. have demonstrated that lysine coated Au NPs of hydrodynamic diameters of around 50 nm do not interfere with differentiation [26]. Long term tracking for a period of 2 weeks seems feasible, due to high retention times and low cytotoxicity. In contrast with these findings, some studies revealed a negative effect of Au NPs on certain cellular functions such as proliferation [27, 28]. In addition the morphology of subcellular structures seems to be disturbed depending on the applied dose [29].

To further assess the biocompatibility and suitability of Au NPs for MSC tracking, we investigated cellular

responses to Au NP labeling in MSC derived humans (hMSCs), such as uptake, cytotoxicity, proliferation, migration, morphology, immunophenotype, and in vivo biodistribution. For MSC detection via mass spectrometry we elucidated the detection sensitivity by quantifying the required number of labeled cells to be able to prove MSC presence in a population of cancer cells.

Results

Au NPs are readily incorporated by MSCs

We monitored the incorporation of Au NPs into MSCs in a dose- and time-dependent manner, cf. Fig. 1. In the present study, ca. 4 nm core-sized Au NPs and exposure concentrations ranging from $c_{NP} = 1$ to 100 nM were used [30]. The uptake was quantified by determination of elemental Au levels inside cells via ICP-MS (cf. Fig. 1). In general the amount of internalized NPs increased over time, whereby after long exposure times (>24 h) and high NP concentrations saturation effects could be observed, cf. Fig. 1. The data shown in Fig. 1 allow for calculating the average number N_{NP} of Au NPs, which were internalized by each cell as $N_{NP} = (m_{Au}/M_{Au}) \cdot N_A$, with m_{Au} being the mass of elemental Au inside each cell as detected with ICP-MS (cf. Fig. 1), $M_{Au} = 196$ g/mol the molar mass of Au, and Avogadro's constant $N_A = 6.02 \cdot 10^{23}$ /mol. In case of exposure to $c_{NP} = 10$ nM Au NPs for 24 h this results in $N_{NP} \approx 4 \cdot 10^5$ NPs per cell, approximating each NP as a sphere of core diameter $d_c = 4.2$ nm (i.e. ca. 4 nm) and constant density ignoring the extent in volume due to the polymer coating. For comparison, at $c_{NP} = 10$ nM around $6 \cdot 10^{12}$ NPs are contained in 1 mL of growth medium. In fact, only a small fraction of NPs present in the medium was actually incorporated by cells, as known also from previous studies [31]. The classical uptake pathway of

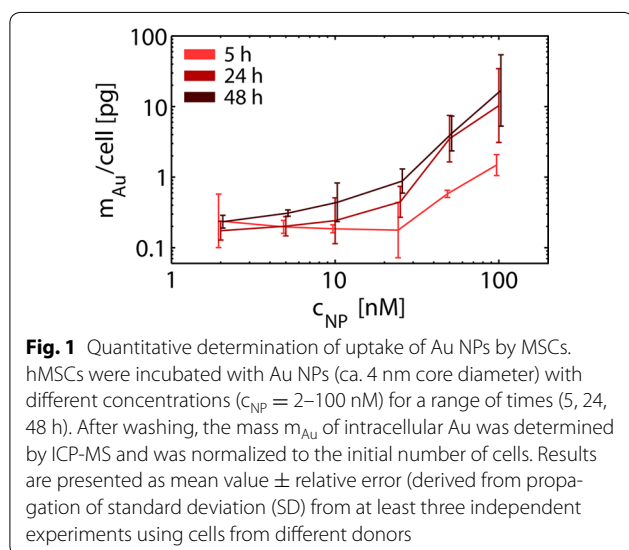


Fig. 1 Quantitative determination of uptake of Au NPs by MSCs. hMSCs were incubated with Au NPs (ca. 4 nm core diameter) with different concentrations ($c_{NP} = 2$ –100 nM) for a range of times (5, 24, 48 h). After washing, the mass m_{Au} of intracellular Au was determined by ICP-MS and was normalized to the initial number of cells. Results are presented as mean value \pm relative error (derived from propagation of standard deviation (SD) from at least three independent experiments using cells from different donors)

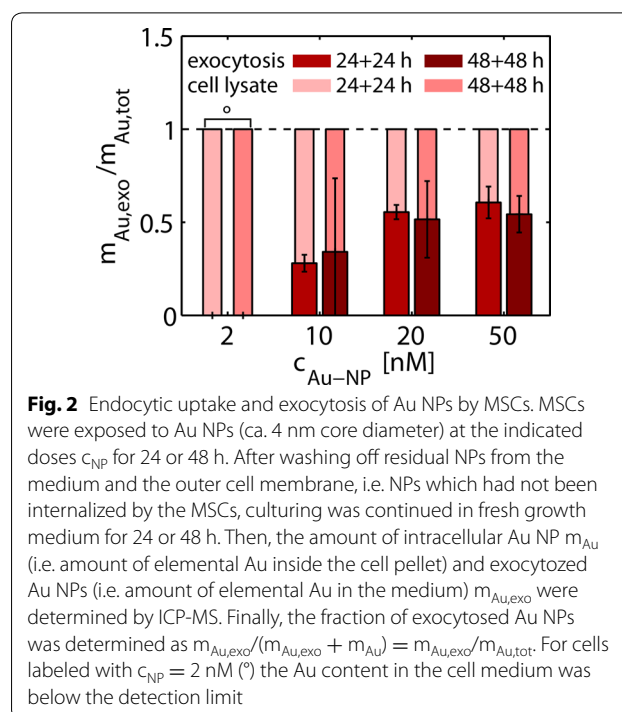
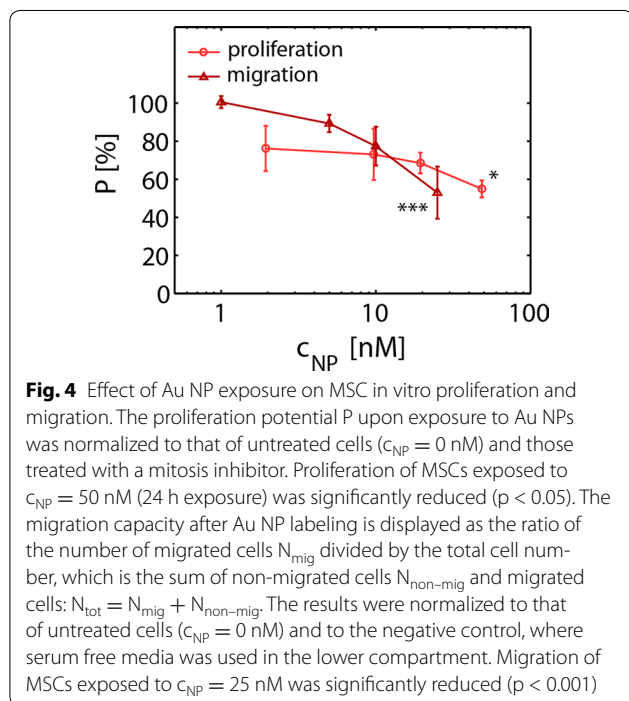
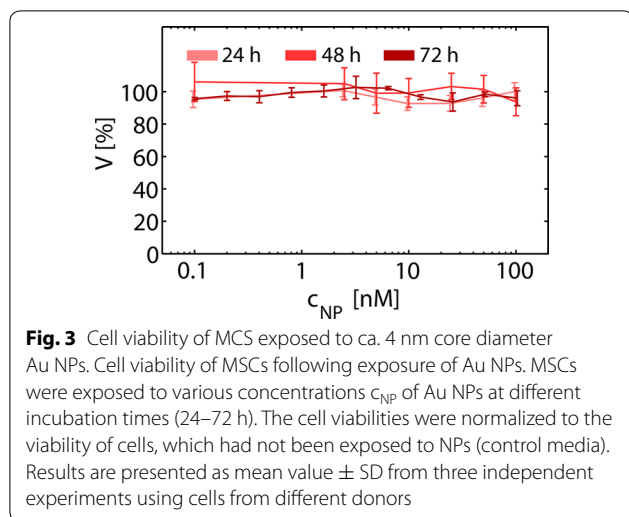


Fig. 2 Endocytic uptake and exocytosis of Au NPs by MSCs. MSCs were exposed to Au NPs (ca. 4 nm core diameter) at the indicated doses c_{NP} for 24 or 48 h. After washing off residual NPs from the medium and the outer cell membrane, i.e. NPs which had not been internalized by the MSCs, culturing was continued in fresh growth medium for 24 or 48 h. Then, the amount of intracellular Au NP m_{Au} (i.e. amount of elemental Au inside the cell pellet) and exocytosed Au NPs (i.e. amount of elemental Au in the medium) $m_{Au,exo}$ were determined by ICP-MS. Finally, the fraction of exocytosed Au NPs was determined as $m_{Au,exo}/(m_{Au,exo} + m_{Au}) = m_{Au,exo}/m_{Au,tot}$. For cells labeled with $c_{NP} = 2$ nM (*) the Au content in the cell medium was below the detection limit

NPs by cells is endocytosis [22], and internalized NPs are enriched in intracellular vesicles. Therefore, NP excretion was investigated by measuring the increasing Au content in the extracellular medium 24 or 48 h after labeling, as depicted in Fig. 2. The data demonstrate that with rising NP concentrations the excretion via exocytosis is also increasing, which takes place largely within the first 24 h. Note that ICP-MS can not distinguish between Au NPs just adherent to the outer cell membrane and Au NPs that have been in fact endocytosed. There are methods available which allow for separating both populations [32, 33]. However, we did not apply this analysis, as it would not be relevant for the in vivo studies, as discussed in the respective paragraph.

Functional impact of Au NP labeling on MSCs

These observations prompted us to investigate the biocompatibility of the ca. 4 nm Au NPs. Cell viability after exposure to Au NPs was assessed employing the resazurin (AlamarBlue) assay [34, 35]. The data shown in Fig. 3 indicate that the cell viability of human MSCs exposed to NPs for 24 and 48 h was not strongly affected. However, a trend for a decrease of cell viability was observed at high NP concentrations ($c_{NP} > 50$ nM) at longer exposure times (72 h). Because cell viability as measured by the resazurin assay has limited sensitivity as indicator for probing effects of NPs on MSCs, we additionally carried out a NP-concentration dependent proliferation assay, cf. Fig. 4. Relative cellular proliferation was



significantly reduced for $c_{NP} = 50$ nM. In fact already at very low NP doses of 2 nM, there is a tendency of concentration-dependent reduction of proliferation. Moreover, migratory functioning is of particular importance for in vivo homing of MSC in tumor tissue. In several studies MSCs were used for homing and tracking experiments [36]. As depicted in Fig. 4 we demonstrate that cellular migration through a porous membrane [37] was affected in case cells have incorporated NPs. Our data suggest a dose dependent inhibitory effect on the migration

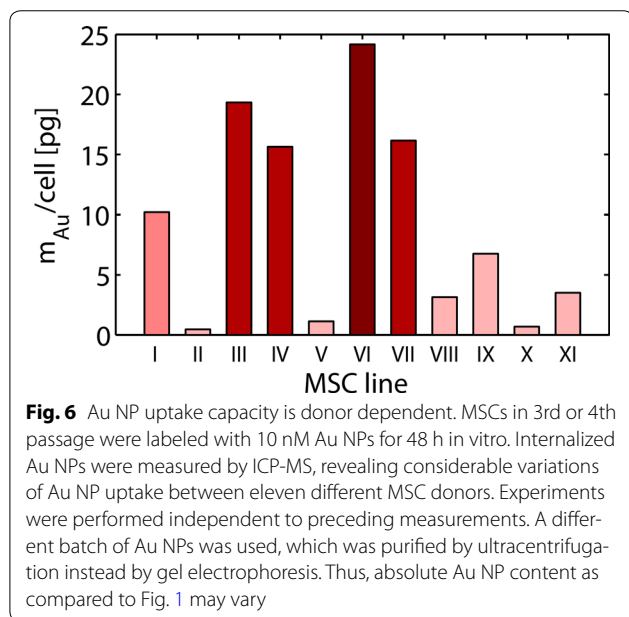
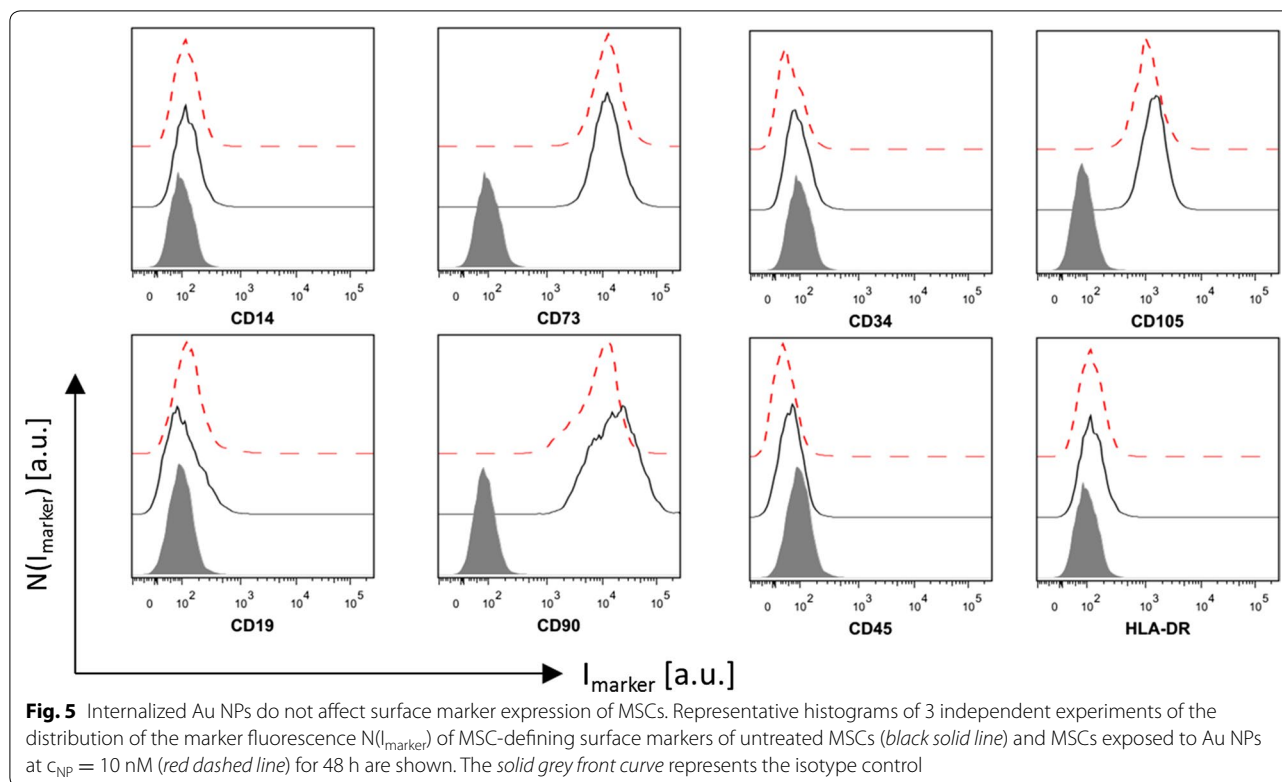
capacity of MSCs labeled with Au NPs. A significant negative effect was already visible for $c_{NP} = 50$ nM. Based on our data, we identified the least tolerable dose of ca. 4 nm diameter Au NPs exposed to MSC for 48 h to be around 10 nM. In order to probe whether labeling of MSCs under these conditions affects the immunophenotype of MSCs, expression of surface markers was determined by flow cytometric analysis upon exposure to NPs. Our results showed that Au NP-labeled MSCs maintained their characteristic immunophenotype, as determined by expression analysis of CD73, CD90 and CD105. MSC did not express CD14, CD19, CD34, CD45, and HLA-DR as shown in Fig. 5. The immunophenotype of MSCs labeled under these conditions is in accordance with the consensus criteria [38]. This is in line with results obtained by Mailänder et al., who showed no impact on lineage markers and differentiation [39] upon NP-labeling of MSCs. In this way, at reasonable Au NP concentrations (i.e. 10 nM for ca. 4 nm Au NPs), the NP labeling does not interfere with the immunophenotype, and does not cause long-term cytotoxicity. However, our data reveal onset of negative effects on proliferation and migration potential already at these concentrations. Taken together the amount of Au NPs which can be reasonably added as label per cell is clearly limited, affecting the maximum contrast which can be obtained.

The Au NP labeling capacity of MSC is donor dependent

In order to determine the efficacy of MSC labeling with Au NPs at an optimized concentration of 10 nM, MSCs from eleven different donors were incubated with Au NP for 48 h. MSCs were all in passage 3 to 4, because many cell doublings may impair cell functioning and differentiation [40]. Although the same optimized labeling strategy and Au NP concentration was applied, uptake of Au NPs varied considerably in MSCs derived from different individuals as shown in Fig. 6. Thus, other parameters apart from size or concentration of Au NPs must be responsible for the biologic variation in NP tolerance of MSCs, and testing of labeling efficiencies is mandatory for subsequent in vivo tracking experiments with NP labeled MSCs.

Linear MSC detection mode with ICP-MS

Using our optimized parameters for NP-labeling of MSCs, we sought to determine whether MSC detection with ICP-MS follows a linear dose response relation. ICP-MS is a frequently used tool for determining bio-distributions, in particular of Au NPs. Upon homing, MSCs actually will only form a small fraction of cells on the target site. For a limiting dilution assay approach we were able to detect as little as 400 labeled MSCs ($c_{NP} = 10$ nM, 24 h) within

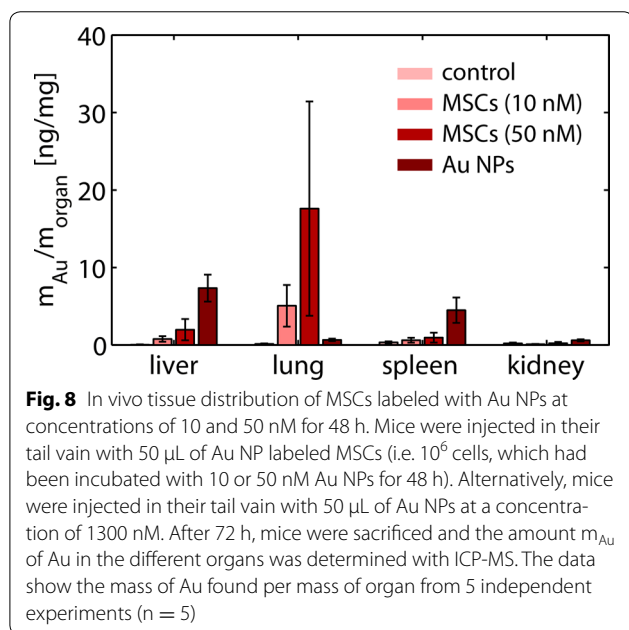
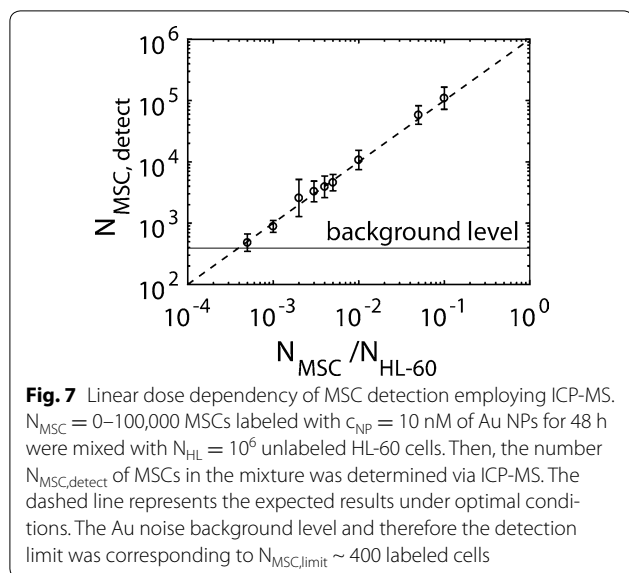


a population of 10^6 acute myeloid leukemia cells (HL-60). Thus, cell numbers down to 400 labeled MSCs/ 10^6 HL-60 cells are resolvable, before signal cannot be discriminated from the background any more. This corresponds to as little as 0.04% cells. The ratio between expected numbers of labeled cell under optimal conditions and detected

MSC via ICP-MS was linear (cf. Fig. 7). This allows for some estimation about the minimum tissue volume V_{min} which could be detected via homing of MSCs. In case one assumes a mean value V_{cell} for the volume of one cell, the tissue volume which can be resolved would be $V_{\text{min}} = V_{\text{cell}} \cdot N_{\text{MSC,limit}} / (N_{\text{MSC}}/N_{\text{cell}})$. Using the experimentally determined value $N_{\text{MSC,limit}} \approx 400$ (cf. Fig. 7) and the numbers $N_{\text{MSC}}/N_{\text{cell}} = 10^{-5}$ and $V_{\text{cell}} = 100\text{--}1000 \mu\text{m}^3$ [41] as example, the smallest structure which can be detected would be between $V_{\text{min}} \approx 0.4$ and 4 mm^3 . This would be the minimum size of a tumor which could be detected with ICP-MS upon MSC homing with our Au NP approach. In summary, optimized Au NP labeling of MSCs and detection via ICP-MS appears suitable for in vivo tracking experiments.

In vivo tracking of Au NP labeled MSC

As high concentrations of Au NPs in MSCs may lead to impaired homing efficiency, we sought to verify whether the migratory capacity of MSC was preserved after Au NP labeling in vivo. One million human MSCs were injected into the tail vein of two mice per condition, respectively. A solution of free Au NPs and phosphate buffered saline (PBS) served as control. 72 h after injection the mice were sacrificed and the amount of Au in liver, lung, spleen, kidney, and blood was determined via ICP-MS. For the control mice, the amount of detected Au was below 1 ppb and



thus below the resolution, cf. Fig. 8. The injected free Au NPs, but not NP labeled MSCs, accumulated predominantly in the liver, as expected from previous studies with similar NPs [42, 43]. The difference was significant as calculated with Student's t test ($p = 0.005$ and 0.04 , respectively). In contrast, in mice injected with Au NP labeled MSCs a higher amount of Au was found inside the lungs. However, due to very high variations ($p < 0.0001$ upon F test for equality of variances) statistical significance was not reached here ($p = 0.2$). This is in agreement with findings by others, which have reported that MSCs get trapped in the pulmonary capillary system first, but then relocate

into the liver or tumor/inflammation sites [44–46]. We conclude that in fact our optimized Au NP labeling protocol for human MSCs allows for proper recording the biodistribution of these cells. Note, that in fact some Au NPs associated to the MSCs could have been just adherent to the MSCs instead of being endocytosed. However, as the biodistribution of Au in case of Au NP labelled MSCs and plain Au NPs is different, the Au NPs must have travelled with the MSCs.

Discussion

On the first glance, the physical properties of Au NPs for MSC labeling seem well suited when looking on the potential perspectives for further applications in cancer diagnostic and therapy. For clinical applications careful monitoring of cellular functions is a vital prerequisite. After thorough testing of biological alterations in NP labeled MSCs we propose an optimized labeling strategy for 4 nm Au NPs and human MSCs, hereby preserving migratory and proliferative capacities in vitro and in vivo. While in this study we demonstrated that exposure of MSCs to Au NPs at non-optimized conditions can have profound effects on the proliferation and migration behavior, the underlying molecular pathways that get disturbed so far are not known. Whether inorganic NP of different size, shape or material require the same or other labeling conditions with regard to MSC biology needs to be determined in further studies. We have previously employed short tandem-repeat (STR) profiling in order to quantify donor cells within recipient tissue. The sensitivity of this assay is about 5% [47]. Another strategy is fluorescent-dye based cell labeling. This method is capable to visualize MSC migration into tumors [48], however, quantification of light intensities in tissues is not always precise with regard to cell numbers. Thus, our approach of MSC quantification via Au NPs that is capable to detect 0.04% labeled MSCs within unstained cells is particularly accurate compared to the other mentioned methods.

We additionally show that there is a remarkable variety in-between individual donors, indicating the need to further elucidate the mechanisms of cellular fitness with regard to Au NP uptake capacity. MSCs administered intravenously initially migrate into the lungs, while intraarterial administration seems to prevent this 'first-pass' effect [44–46]. However, for photothermal tumor ablation intravenous application strategies for Au NP carrying MSCs are preferred [49]. Preservation of migratory capacities of MSC is therefore crucial for all these strategies.

Conclusions

Tumor tropism of MSC has already been used for novel imaging approaches but also for cancer therapy strategies. With regard to the long hike throughout the body

towards tumor tissue and considering future applications in cancer therapy, MSC fitness and migration capabilities appear to be of tremendous importance. We describe a gentle and efficient labeling strategy for human MSCs that is applicable in vivo and paves the way for future clinical applications such as novel tumor detection and destruction strategies.

Methods

Synthesis and characterization of NPs

Polymer-coated Au NPs with a core diameter of $d_c = 4.25 \pm 0.88$ nm (as determined by transmission electron microscopy (TEM), in the following referred to as “ $d_c = 4$ nm”), a hydrodynamic diameter of $d_h = 10.4 \pm 0.7$ (as determined by dynamic light scattering (DLS) in water), and a zeta-potential of $\zeta = -25.1 \pm 0.36$ mV (as determined from laser doppler anemometry (LDA) in water) were prepared according to previously published protocols [30, 50]. The experimental procedure, as well as the effect of salt on the size and colloidal stability of PMA NPs, are described in detail in the Additional file 1. The NPs were overcoated with an amphiphilic polymer, poly(isobutylene-*alt*-maleic anhydride)-*graft*-dodecylamine (PMA) [51, 52]. After synthesis, the NPs were purified by gel electrophoresis and by diafiltration. The concentration of the coated Au NPs was determined by UV/Vis absorption spectroscopy [53]. For detailed characterization of the physicochemical properties of these NPs we refer to previous studies [20, 53–55]. The Au NPs were found to be colloidally stable up to physiological NaCl concentrations (see the Additional file 1).

Isolation, expansion and culture of human mesenchymal stem cells (MSCs)

Mesenchymal stem cells were isolated from bone pieces obtained from hip fragments. Dulbecco's Modified Eagles Medium (DMEM, Sigma-Aldrich, #D5546) was supplemented with 10% fetal bovine serum (FBS), 1% penicillin/streptomycin (P/S, Sigma-Aldrich, #P4333), and 2 mM L-glutamine (Sigma-Aldrich, #G7513). The MSCs were cultivated in flasks at 37 °C and 5% CO₂, until they reached 80% confluence. MSCs were used in passages ≤ 5 due to observed adverse effects on MSC functional capabilities for higher passages as described previously [40].

Quantification of Au NP uptake by MSCs

The labeling efficiency of MSCs with Au NPs (ca. 4 nm core diameter) was examined by inductively coupled plasma mass spectrometry (ICP-MS, Agilent 7700 Series). Cells were seeded into 6-well plates (TPP, Switzerland, #92006) at a density of 10^4 MSCs/cm² and each well with a surface of 9 cm² was filled with $V_{\text{medium}} = 3$ mL of medium. Thus, in each well there

were $N_{\text{cell}} = 9 \cdot 10^4$ cells. After 24 h, the growth medium was replaced with 1.5 mL of Au NP-containing media at different concentrations ($c_{\text{NP}} = 0$ –100 nM) and cells were incubated for 5, 24, or 48 h. After exposure, the cell medium was removed followed by three washing steps with PBS to remove non-internalized NPs. Then, cells were detached with 500 μ L trypsin–EDTA (0.05% trypsin–EDTA, Thermo Fisher Scientific), collected by centrifugation at 280 rcf for 5 min, and washed with PBS, followed by an additional centrifugation step. The recovered cell pellets were treated with 100 μ L of lysis buffer (Luciferase Cell Culture Lysis Buffer, Promega, #E153A) for 30 min. Finally, the samples were prepared for ICP-MS analysis by digestion in aqua regia. Hereby, 50 μ L sample was diluted in 150 μ L aqua regia, consisting of three parts concentrated (35 wt%) HCl (Fisher Chemical, #7647010) and one part of (67 wt%) HNO₃ (Fisher Chemical, #7697372), and left for digestion for at least 3 h. The sample containing acid was diluted 1:10 in 2 wt% HCl prior to measuring the elemental Au concentration in the sample with ICP-MS. The initial cell number was determined by performing a Lowry protein assay (Sigma-Aldrich, #TP0300) with the lysed cell pellets [56].

Assessment of long term labeling efficiency of MSCs with Au NPs by reporting exocytosis versus endocytosis

For evaluation of the long-term labeling efficiency, the fraction of exocytosed NPs was determined after exposure to Au NPs. MSCs (adherent in 25 cm² culture flasks) were exposed to $c_{\text{NP}} = 2$ –100 nM of Au NPs for 24 or 48 h. After labeling, MSCs were detached with trypsin–EDTA, washed with PBS, and plated into new 25 cm² culture flasks. After 24 or 48 h, the Au content remaining inside MSCs (i.e. the remaining endocytosed NPs) and present in growth medium (i.e. the exocytosed NPs) was determined. The intracellular Au was quantified by ICP-MS, as described above for the quantitative uptake analysis of Au NPs by MSCs. The exocytosed fraction of the Au NPs was determined from the Au concentration of the growth medium, which was diluted 1:4 in aqua regia first, followed by 1:10 dilution in 2 wt% HCl prior to ICP-MS measurements. Results are represented as Au mass fractions of intracellular versus the intracellular + extracellular Au.

Viability of MSCs labeled with Au NPs

Mesenchymal stem cells were seeded at a density of 10^4 cells/well into a 96-well plate with each well filled with $V_{\text{medium}} = 0.1$ mL of medium and exposed to Au NPs for 24–72 h. Then, cells were washed once with PBS and AlamarBlue (Thermo Fisher Scientific) was added in each well and incubated for desired time at 37 °C. The fluorescence was measured at 560 nm excitation and

590 nm emission wavelengths using a spectrophotometer (SpectraMax 250, Molecular Devices). Cell viability was assumed to be proportional to the recorded fluorescence intensity. Results are expressed as percentage of cell viability V versus control (i.e. untreated cells). Experiments were performed with MSCs from three independent human/MSC donors in triplicates for each time-point and concentration.

Proliferation of MSCs

The effect of exposure of MSCs to Au NPs on their proliferation rate P was determined with carboxyfluorescein succinimidyl ester (CFSE) and flow cytometry (FCM). Cells were labeled with a certain amount of membrane-impermeable CFSE whose fluorescent intensity decreases upon cell division [57]. $2.5 \cdot 10^5$ cells per sample were labeled with 1 μM CFSE (Molecular Probes, #C34554) for 10 min at 37 °C in 1 mL of PBS. Subsequently, the cells were washed twice with 5 mL of pre-warmed supplemented DMEM and plated in 25 cm^2 culture flasks. After 24 h NPs ($c_{\text{NP}} = 0\text{--}50$ nM) were added, and a negative control was prepared containing 5 μM of the mitosis inhibitor cholchicine (Sigma-Aldrich, #C9754). After subsequent culturing for additional 6 days, cells were detached with trypsin–EDTA, counter-stained with 1 μM propidium iodide (PI, Sigma-Aldrich, #P4170), and signals were acquired with a BD LSR II FCM device with FACS Diva software (BD Biosciences). Data were analyzed with FlowJo version 9.5.3 (TreeStar Inc.) and GraphPad Prism software. CFSE was excited at 488 nm and emission was detected at 521 nm. Living cell were gated after 4',6-diamidino-2-phenylindole (DAPI) (Sigma-Aldrich, #D9542) staining. Results are normalized to the positive ($p = 1$, no Au NPs) and negative control ($p = 0$, cholchicine), and are representing the mean values \pm standard deviations of the median values of the CFSE fluorescent intensity/cell for 3 independent experiments.

Migration of MSCs

The migration potential of MSCs was assessed by analyzing cell migration through membrane inserts by fluorescence microscopy [37]. MSCs were labeled with Au NPs in 25 cm^2 culture flasks filled with 5 mL of medium at $c_{\text{NP}} = 0\text{--}25$ nM for 2 days. Subsequently, cells were detached with trypsin–EDTA and transferred in serum free medium into the upper chamber of membrane inserts (8 μm pore size, Greiner Bio One, #662638), which were placed into the wells of a 24 well plate (Greiner Bio One, #622160). Each insert contained $1 \cdot 10^4$ cells in $V_{\text{medium}} = 0.3$ mL of growth medium. The lower chambers were filled with growth medium containing 10% human platelet lysate (HPL, manufactured

at the Institute for Clinical Immunology and Transfusion Medicine, Giessen, Germany, in a GMP-compliant manner as described in Schallmoser et al. [58]) to stimulate MSC migration from the upper to the bottom side of the membrane inserts. After 16 h, cells were fixed with methanol and nuclei were stained with 50 μM of 4',6-diamidino-2-phenylindole (DAPI, Thermo Fisher Scientific, #D1306) for 5 min. For each sample, migrated and non-migrated MSCs were counted at fixed positions, each comprising an area of 0.38 cm^2 . The counting was based on fluorescent images acquired with a confocal laser scanning microscope (CLSM 510 Meta) from Zeiss using a Plan-Apochromat 20 \times /0.8 M27 objective (pin-hole size: 1 airy unit, lateral sampling rate: 0.6 $\mu\text{m}/\text{pixel}$). DAPI (nuclei) was excited with a 405 nm-laser diode an emission was gated with a 420 nm long-pass filter. For imaging the inserts were placed on a microscope slide in a drop of PBS. For 4–6 randomly chosen positions two images were acquired: Non-migrated cells were captured by acquiring an image at a plane above the membrane, and migrated cells were imaged below the membrane, cf. the Additional file 1 for a sketch of the set-up. For each position (area $A = 0.38$ mm^2) the number of cells above ($N_{\text{non-mig}}$) and below the membrane (N_{mig}) was determined based on their nuclear staining by employing CellProfiler [59] and the ratio $N_{\text{mig}}/(N_{\text{mig}} + N_{\text{non-mig}})$ was calculated. Results are displayed as mean values \pm standard deviations for 3 independent experiments.

Expression of surface markers of MSCs

The immunophenotype of MSCs was analyzed after exposure to 10 nM Au NPs for 48 h. According to the recommendations of the International Society for Cellular Therapy [38] the following surface markers were measured: CD14 (clone M4P9, BD Biosciences, #345785), CD19 (clone SJ25C1, BD, #332780), CD34 (clone 8G12, BD, #345801), CD45 (clone 2D1, BD, #332784), CD73 (clone AD2, BD, #550257), CD90 (clone 5E10, BD, #559869), CD105 (clone 266, BD, #32830) and HLA-DR (clone B8.12.2, Immunotech, #PNIM0463U). In brief, MSCs were stained for 15 min at 4 °C with fluorochrome-labeled monoclonal antibodies, washed with PBS, and resuspended in FACSFlow™ (BD, #342003) with 3% formaldehyde (Merck, #103999). The samples were measured with a LSRII FCM device with CellQuest Pro™ Software (both BD). Isotype-matched antibodies were used as negative controls (BD, #342409, #347221, #345818). FCS data were analyzed with FlowJo™ software version 9.5.3 (TreeStar Inc).

Sensitivity of MSC detection via ICP-MS

In order to prove dose dependency of our assay, dilutions of 10 nM Au NP labeled MSCs within HL-60 cells

were prepared. 10^6 of unlabeled HL-60 were diluted with 10–0.001% labeled MSCs in increments of 10 and measured via ICP-MS. Acute promyelocytic leukemia cells (HL-60) were obtained from the American Type Culture Collection (ATCC, Manassas, VA, USA), and were maintained in RPMI 1640 (Sigma-Aldrich, #R8758) supplemented with 10% FBS, 1% penicillin/streptomycin (P/S, Sigma-Aldrich, #P4333) (complete medium) at 37 °C in 5% CO₂.

Demonstration of recording biodistributions with NP labeled MSCs

To evaluate the *in vivo* biodistribution of NP-labeled MSCs, male BALB/cA_Jic–RAG2–/–IL-2R γ –/– mice (obtained from Prof. Dr. Dorothee von Laer; Georg-Speyer-Haus; Johann Wolfgang Goethe-Universität Frankfurt) at 12–20 weeks of age were used. The experiments were performed in the animal facility of the BMFZ, Marburg, Germany. In brief, 1×10^6 MSCs were seeded in T175 cm² flasks and grown in complete cell culture medium. After 24 h, medium was replaced with NP containing media (10 and 50 nM Au NPs). MSC were incubated with Au NPs for 48 h to ensure cell labeling. After the desired time, the MSCs were washed three times with PBS, dissociated with trypsin, and resuspended in PBS. Subsequently, 50 μ L of 1×10^6 NPs labeled MSCs were injected in a tail vein of mice. Additionally, a group of Mice were injected with 50 μ L of pure Au NPs at a concentration of 1300 nM. Mice injected with PBS were used as control. 72 h post injection, the mice were sacrificed, and the amount of Au in the lung, liver, spleen, kidney, and blood was evaluated by the ICP-MS. For the control mice group, the Au detected was below 1 ppb and thus below the resolution. Data shown represent an average of $n = 5$ independent experiments.

Additional file

Additional file 1. Supplementary information about AuNP synthesis, purification, characteristics and about cell proliferation and migration assays.

Abbreviations

MSCs: mesenchymal stromal cells; NP: nanoparticle; Au: gold; ICP-MS: inductively coupled plasma mass spectrometry; PET: positron or photon emission tomography; MRI: magnetic resonance imaging; FeO_x: iron oxide; PBS: phosphate buffered saline; TEM: transmission electron microscopy; LDA: laser doppler anemometry; PMA: poly(isobutylene-*alt*-maleic anhydride); CFSE: carboxyfluorescein succinimidyl ester; PI: propidium iodide; DAPI: 4',6-diamidino-2-phenylindole; HL-60: human leukemia cell line; FBS: fetal bovine serum.

Authors' contributions

PN, RH, NF, KK, MG, BP, JH, XS, and PdP performed the experiments (all in Marburg), analyzed and interpreted the data, PN; RH, NF, WP and CB contributed in writing the manuscript. PJ and PM consulted part of the initial uptake studies. HH gave substantial careful contributions to the conception and revision of the manuscript. All authors read and approved the final manuscript.

Author details

¹ Department of Hematology, Oncology and Immunology, Philipps University Marburg, Marburg, Germany. ² Department of Physics, Philipps-University of Marburg, Marburg, Germany. ³ Thoraxklinik at Heidelberg University Hospital, Heidelberg, Germany. ⁴ Institute for Clinical Immunology and Transfusion Medicine, Justus-Liebig University Giessen, Giessen, Germany. ⁵ Laboratory of Bioengineering & Regenerative Medicine (BioREM), Kazan Federal University, Kazan, Russia. ⁶ CIC Biomagune, San Sebastián, Spain.

Competing interests

All authors declare that they have no competing interests.

Availability of data and materials

All data generated or analysed during this study are included in this published article and its Additional files.

Consent for publication

All authors have given consent for publication of the manuscript.

Ethics approval

Human cell donations had been approved by the ethics committee of the Philipps-University of Marburg (study no. 64/01 and 25/10) and patients had been given written informed consent. Approval for the described animal experiments was obtained from the local authorities (Regierungspräsidium Giessen, Germany).

Funding

This work was funded in part by the German Research Foundation (DFG Grant PA 794/25-1 to WJP), by the von Behring-Röntgen-Stiftung (Grant 60-0038 to CB and HH) and the RKA Förderpool (Grant FI 38 to CB).

Received: 14 October 2016 Accepted: 20 March 2017

Published online: 29 March 2017

References

- Nold P, Brendel C, Neubauer A, Bein G, Hackstein H. Good manufacturing practice-compliant animal-free expansion of human bone marrow derived mesenchymal stroma cells in a closed hollow-fiber-based bioreactor. *Biochem Biophys Res Commun*. 2013;430:325–30.
- Menard C, Pacelli L, Bassi G, Dulong J, Bifari F, Bezier I, Zanoncello J, Ricciardi M, Latour M, Bourin P. Clinical-grade mesenchymal stromal cells produced under various good manufacturing practice processes differ in their immunomodulatory properties: standardization of immune quality controls. *Stem Cells Dev*. 2013;22:1789–801.
- Chapel A, Bertho JM, Bensidhoum M, Fouillard L, Young RG, Frick J, Demarquay C, Cuvelier FDR, Mathieu E, Trompier FO. Mesenchymal stem cells home to injured tissues when co-infused with hematopoietic cells to treat a radiation-induced multi-organ failure syndrome. *J Gene Med*. 2003;5:1028–38.
- Kidd S, Spaeth E, Dembinski JL, Dietrich M, Watson K, Klopp A, Battula VL, Weil M, Andreeff M, Marini FC. Direct evidence of mesenchymal stem cell tropism for tumor and wounding microenvironments using *in vivo* bioluminescent imaging. *Stem Cells*. 2009;27:2614–23.
- Uchibori R, Tsukahara T, Mizuguchi H, Saga Y, Urabe M, Mizukami H, Kume A, Ozawa K. NF- κ B activity regulates mesenchymal stem cell accumulation at tumor sites. *Cancer Res*. 2012;73:364–72.
- Wang S, Qu X, Zhao RC. Clinical applications of mesenchymal stem cells. *J Hematol Oncol*. 2012;5:19.
- Uchibori R, Tsukahara T, Ohmine K, Ozawa K. Cancer gene therapy using mesenchymal stem cells. *Int J Hematol*. 2014;99:377–82.
- Squillaro T, Peluso G, Galderisi U. Clinical trials with mesenchymal stem cells: an update. *Cell Transplant*. 2015;25(5):829–48.
- Fu Y, Kraitchman DL. Stem cell labeling for noninvasive delivery and tracking in cardiovascular regenerative therapy. *Expert Rev Cardiovasc Ther*. 2010;8:1149.
- Sutton EJ, Henning TD, Pichler BJ, Bremer C, Daldrup-Link HE. Cell tracking with optical imaging. *Eur Radiol*. 2008;18:2021–32.

11. Freyman T, Polin G, Osman H, Crary J, Lu M, Cheng L, Palasis M, Wilensky RL. A quantitative, randomized study evaluating three methods of mesenchymal stem cell delivery following myocardial infarction. *Eur Heart J*. 2006;27:1114–22.
12. Frangioni JV, Hajjar RJ. In vivo tracking of stem cells for clinical trials in cardiovascular disease. *Circulation*. 2004;110:3378–83.
13. Mahmoudi M, Hosseinkhani H, Hosseinkhani M, Boutry S, Simchi A, Journeay WS, Subramani K, Laurent S. Magnetic resonance imaging tracking of stem cells in vivo using iron oxide nanoparticles as a tool for the advancement of clinical regenerative medicine. *Chem Rev*. 2011;111:253–80.
14. Gazeau F, Wilhelm C. Magnetic labeling, imaging and manipulation of endothelial progenitor cells using iron oxide nanoparticles. *Future Med Chem*. 2010;2:397–408.
15. Barrow M, Taylor A, Nieves DJ, Bogart LK, Mandal P, Collins CM, Moore LR, Chalmers JJ, Levy R, Williams SR, et al. Tailoring the surface charge of dextran-based polymer coated SPIONs for modulated stem cell uptake and MRI contrast. *Biomater Sci*. 2015;3:608–16.
16. Jacques V, Desreux JF. New classes of MRI contrast agents. *Top Curr Chem*. 2002;221:123–64.
17. Harisinghani MG, Barentsz J, Hahn PF, Deserno WM, Tabatabaei S, van de Kaa CH, de la Rosette J, Weisleder R. Noninvasive detection of clinically occult lymph-node metastases in prostate cancer. *N Engl J Med*. 2003;348:2491–9.
18. Hainfeld JF, Slatkin DN, Focella TM, Smilowitz HM. Gold nanoparticles: a new X-ray contrast agent. *Br J Radiol*. 2006;79:248–53.
19. Hainfeld JF, O'Connor MJ, Dilmanian FA, Slatkin DN, Adams DJ, Smilowitz HM. Micro-CT enables microlocalisation and quantification of Her2-targeted gold nanoparticles within tumour regions. *Br J Radiol*. 2011;84:526–33.
20. Hühn J, Carrillo-Carrion C, Soliman MG, Pfeiffer C, Valdeperez D, Masood A, Chakraborty I, Zhu L, Gallego M, Zhao Y, et al. Selected standard protocols for the synthesis, phase transfer, and characterization of inorganic colloidal nanoparticles. *Chem Mater*. 2017;29:399–461.
21. Rothen-Rutishauser B, Kuhn DA, Ali Z, Gasser M, Amin F, Parak WJ, Vanhecke D, Fink A, Gehr P, Brandenberger C. Quantification of gold nanoparticle cell uptake under controlled biological conditions and adequate resolution. *Nanomedicine*. 2014;9:607–21.
22. Nazarenus M, Zhang Q, Soliman MG, del Pino P, Pelaz B, Carregal-Romero S, Rejman J, Rothen-Rutishauser B, Clift MJD, Zellner R, et al. In vitro interaction of colloidal nanoparticles with mammalian cells: what have we learned thus far? *Beilstein J Nanotechnol*. 2014;5:1477–90.
23. Parak WJ, Boudreau R, Gros ML, Gerion D, Zanchet D, Micheel CM, Williams SC, Alivisatos AP, Larabell CA. Cell motility and metastatic potential studies based on quantum dot imaging of phagokinetic tracks. *Adv Mater*. 2002;14:882–5.
24. Khlebtsov N, Dykman L. Biodistribution and toxicity of engineered gold nanoparticles: a review of in vitro and in vivo studies. *Chem Soc Rev*. 2011;40:1647–71.
25. Berners-Price SJ, Filipovska A. Gold compounds as therapeutic agents for human diseases. *Metallomics*. 2011;3:863–73.
26. Ricles LM, Nam SY, Sokolov K, Emelianov SY, Suggs LJ. Function of mesenchymal stem cells following loading of gold nanotracer. *Int J Nanomed*. 2011;6:407–16.
27. Jan E, Byrne SJ, Cuddihy M, Davies AM, Volkov Y, Gun'ko YK, Kotov NA. High-content screening as a universal tool for fingerprinting of cytotoxicity of nanoparticles. *ACS Nano*. 2008;2:928–38.
28. Bhattacharya R, Patra CR, Verma R, Kumar S, Greipp PR, Mukherjee P. Gold nanoparticles inhibit the proliferation of multiple myeloma cells. *Adv Mater*. 2007;19:711–6.
29. Soenen SJ, Manshian B, Montenegro JM, Amin F, Meermann B, Thiron T, Cornelissen M, Vanhaecke F, Doak S, Parak WJ, et al. Cytotoxic effects of gold nanoparticles: a multiparametric study. *ACS Nano*. 2012;6:5767–83.
30. Lin CAJ, Sperling RA, Li JK, Yang TY, Li PY, Zanella M, Chang WH, Parak WJ. Design of an amphiphilic polymer for nanoparticle coating and functionalization. *Small*. 2008;4:334–41.
31. Abdelmonem AM, Pelaz B, Kantner K, Bigall NC, Del Pino P, Parak WJ. Charge and agglomeration dependent in vitro uptake and cytotoxicity of zinc oxide nanoparticles. *J Inorg Biochem*. 2015;153:334–8.
32. Braun GB, Friman T, Pang HB, Pallaoro A, de Mendoza TH, Willmore AMA, Kotamraju VR, Mann AP, She ZG, Sugahara KN, et al. Etchable plasmonic nanoparticle probes to image and quantify cellular internalization. *Nat Mater*. 2014;13:904–11.
33. Hou S, Sikora KN, Tang R, Liu YC, Lee YW, Kim ST, Jiang ZW, Vachet RW, Rotello VM. Quantitative differentiation of cell surface-bound and internalized cationic gold nanoparticles using mass spectrometry. *ACS Nano*. 2016;10:6731–6.
34. O'Brien J, Wilson I, Orton T, Pognan FO. Investigation of the Alamar Blue (resazurin) fluorescent dye for the assessment of mammalian cell cytotoxicity. *Eur J Biochem*. 2000;267:5421–6.
35. O'Brien J, Wilson I, Ortaon T, Pognan F. Investigation of the Alamar blue (Resazurin) fluorescent dye for the assessment of mammalian cell cytotoxicity. *Toxicology*. 2001;164:132.
36. Mooney R, Roma L, Zhao DH, Van Haute D, Garcia E, Kim SU, Annala AJ, Aboody KS, Berlin JM. Neural stem cell-mediated intratumoral delivery of gold nanorods improves photothermal therapy. *ACS Nano*. 2014;8:12450–60.
37. Maijenburg MW, Noort WA, Kleijer M, Kompier CJA, Weijer K, Van Buul JD, Der Schoot V, Ellen C, Voermans C. Cell cycle and tissue of origin contribute to the migratory behaviour of human fetal and adult mesenchymal stromal cells. *Br J Haematol*. 2010;148:428–40.
38. Dominici M, Le Blanc K, Mueller I, Slaper-Cortenbach I, Marini FC, Krause DS, Deans RJ, Keating A, Prockop DJ, Horwitz EM. Minimal criteria for defining multipotent mesenchymal stromal cells. The International Society for cellular therapy position statement. *Cytotherapy*. 2006;8:315–7.
39. Brüstle I, Simmet T, Nienhaus GU, Landfester K, Mailänder V. Hematopoietic and mesenchymal stem cells: polymeric nanoparticle uptake and lineage differentiation. *Beilstein J Nanotechnol*. 2015;6:383–95.
40. Nold P, Hackstein H, Riedlinger T, Kasper C, Neumann A, Mernberger M, Fölsch C, Schmitt J, Fuchs-Winkelmann S, Barckhausen C, et al. Immunosuppressive capabilities of mesenchymal stromal cells are maintained under hypoxic growth conditions and after gamma irradiation. *Cytotherapy*. 2015;17:152–62.
41. Del Monte U. Does the cell number 109 still really fit one gram of tumor tissue? *Cell Cycle*. 2009;8:505–6.
42. Lipka M, Semmler-Behnke M, Sperling RA, Wenk A, Takenaka S, Schleh C, Kissel T, Parak WJ, Kreyling WG. Biodistribution of PEG-modified gold nanoparticles following intratracheal instillation and intravenous injection. *Biomaterials*. 2010;31:6574–81.
43. Kreyling WG, Abdelmonem AM, Ali Z, Alves F, Geiser M, Haberl N, Hartmann R, Hirn S, de Aberasturi DJ, Kantner K, et al. In vivo integrity of polymer-coated gold nanoparticles. *Nat Nanotechnol*. 2015;10:619–23.
44. Eggenhofer E, Bensele V, Kroemer A, Popp FC, Geissler EK, Schlitt HJ, Baan CC, Dahlke MH, Hoogduijn MJ. Mesenchymal stem cells are short-lived and do not migrate beyond the lungs after intravenous infusion. *Front Immunol*. 2012;3:297. doi:10.3389/fimmu.2012.00297.
45. Fischer UM, Harting MT, Jimenez F, Monzon-Posadas WO, Xue H, Savitz SI, Laine GA, Cox CS. Pulmonary passage is a major obstacle for intravenous stem cell delivery: the pulmonary first-pass effect. *Stem Cells Dev*. 2009;18:683–92.
46. Nystedt J, Anderson H, Tikkanen J, Pietilä M, Hirvonen T, Takalo R, Heiskanen A, Satomaa T, Natunen S, Lehtonen S. Cell surface structures influence lung clearance rate of systemically infused mesenchymal stromal cells. *Stem Cells*. 2013;31:317–26.
47. Thiede C, Lutterbeck K, Oelschlagel U, Mohr B, Brendel C, Platzbecker U, Neubauer A, Ehninger G, Bornhauser M. Early detection of imminent relapse using quantitative chimerism analysis in peripheral blood CD34+ cells. *Bone Marrow Transplant*. 2001;27:S28–9.
48. Kim SM, Jeong CH, Woo JS, Ryu CH, Lee JH, Jeun SS. In vivo near-infrared imaging for the tracking of systemically delivered mesenchymal stem cells: tropism for brain tumors and biodistribution. *Int J Nanomed*. 2016;11:13–23.
49. Kang S, Bhang SH, Hwang S, Yoon J-K, Song J, Jang H-K, Kim S, Kim B-S. Mesenchymal stem cells aggregate and deliver gold nanoparticles to tumors for photothermal therapy. *ACS Nano*. 2015;9:9678.
50. Zhang F, Lees E, Amin F, Rivera-Gil P, Yang F, Mulvaney P, Parak WJ. Polymer-coated nanoparticles: a universal tool for biolabelling experiments. *Small*. 2011;7:3113–27.
51. Fernández-Argüelles MT, Yakovlev A, Sperling RA, Luccardini C, Gaillard S, Medel AS, Mallet J-M, Brochon J-C, Feltz A, Oheim M, Parak WJ. Synthesis and characterization of polymer-coated quantum dots with integrated acceptor dyes as FRET-based nanoprobes. *Nano Lett*. 2007;7:2613–7.

52. Pellegrino T, Manna L, Kudera S, Liedl T, Koktysh D, Rogach AL, Keller S, Rädler J, Natile G, Parak WJ. Hydrophobic nanocrystals coated with an amphiphilic polymer shell: a general route to water soluble nanocrystals. *Nano Lett.* 2004;4:703–7.
53. Soliman MG, Pelaz B, Parak WJ, Pino P. Phase transfer and polymer coating methods toward improving the stability of metallic nanoparticles for biological applications. *Chem Mater.* 2015;27:990–7.
54. Hühn D, Kantner K, Geidel C, Brandholt S, De Cock I, Soenen SJH, Rivera Gil P, Montenegro J-M, Braeckmans K, Müllen K, et al. Polymer-coated nanoparticles interacting with proteins and cells: focusing on the sign of the net charge. *ACS Nano.* 2013;7:3253–63.
55. Geidel C, Schmachtel S, Riedinger A, Pfeiffer C, Müllen K, Klapper M, Parak WJ. A general synthetic approach for obtaining cationic and anionic inorganic nanoparticles via encapsulation in amphiphilic copolymers. *Small.* 2011;7:2929–34.
56. Lowry OH, Rosebrough NJ, Farr AL, Randall RJ. Protein measurement with the folin phenol reagent. *J Biol Chem.* 1951;193:265–75.
57. Weston SA, Parish CR. New fluorescent dyes for lymphocyte migration studies: analysis by flow cytometry and fluorescence microscopy. *J Immunol Methods.* 1990;133:87.
58. Schallmoser K, Bartmann C, Rohde E, Reinisch A, Kashofer K, Stadelmeyer E, Drexler C, Lanzer G, Linkesch W, Strunk D. Human platelet lysate can replace fetal bovine serum for clinical-scale expansion of functional mesenchymal stromal cells. *Transfusion.* 2007;47:1436–46.
59. Carpenter A, Jones T, Lamprecht M, Clarke C, Kang I, Friman O, Guertin D, Chang J, Lindquist R, Moffat J, et al. Cell profiler: image analysis software for identifying and quantifying cell phenotypes. *Genome Biol.* 2006;7:R100.

Submit your next manuscript to BioMed Central
and we will help you at every step:

- We accept pre-submission inquiries
- Our selector tool helps you to find the most relevant journal
- We provide round the clock customer support
- Convenient online submission
- Thorough peer review
- Inclusion in PubMed and all major indexing services
- Maximum visibility for your research

Submit your manuscript at
www.biomedcentral.com/submit

